ANNUAL REVIEW

INSTITUTE FOR MOLECULAR SCIENCE

OKAZAKI, JAPAN

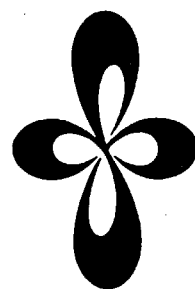## 1978

ERRATA

Page	line	error	correct
i	Figure Caption	AKAMATSU	AKAMATU
3	↓ 15	Adjusnt	Adjunct
4	↑ 14	Koichi	Mitsukazu
58	Caption of Fig. 3	$T_A S_2$	$T_a S_2$
65	left, ↑ 5	11.5 eV	11.8 eV
66	Fig. 2	V_R/V	V_R/V
66	Fig. 1	$h\upsilon$	$h\nu$
66	Captions of Fig. 1,2	$h\upsilon$	$h\nu$
68	right, ↑ 25	HINO	HINO[5]
68	right, ↑ 1	N	N
69	Fig. 2	Current/A	Current/A
69	right, ↑ 8	References	References and notes
69	right, add under the bottom line		5) present address: Chiba University
111	right, ↓ 7	C'	C'
115	22	Kreiner[+]	Kreiner
115	23	Hougen	Hougen[+]
116	left, ↓ 10	$10^{-9} - 10^{-12}$℧ cm	$10^{-9} - 10^{-12}$℧ cm^{-1}
116	left, ↓ 18	10^{-1}℧ cm	10^{-1}℧ cm^{-1}
118	↓ 5	1973	1978
118	↓ 10	1078	1978
118	↓ 22	$n - C_{36} H_{74}$	$n - C_{36} H_{74}$
118	↑ 9	Ortanic	Organic

ANNUAL REVIEW

INSTITUTE FOR MOLECULAR SCIENCE

OKAZAKI, JAPAN

1978

THE FIRST THREE YEARS OF IMS

Foundation

The Institute for Molecular Science was established in April 1975 as an inter-university research institute for theoretical and experimental studies of molecular structures and their functions.

In the years from 1950's to 1960's the industrial recovery after the war made progress, which stimulated the high growth of economy in Japan. Schemes for the promotion of science and technology were pursued at the Government level. Parallel to these efforts, future plans to promote researches were discussed enthusiastically in each branch of science. In the field of chemistry, several plans for establishment of research institutes were proposed. The proposal for a research institute of molecular science was considered as the most relevant and forceful. Here molecular science means a system of disciplines concerned with quantum chemistry, molecular structures, molecular spectroscopy, and molecular solids. It is to provide the most basic methodology to chemistry and to be a driving force to direct chemistry to its proper advancement. As we had many active scholars in this field, the establishment of such an institute would not only encourage the domestic research but would also contribute effectively to the fruitful international collaboration.

In 1965, the Science Council of Japan gave advice to the Government for the establishment of the Institute for Molecular Science. A preparatory period as long as 10 years had been needed, however, before the Government finally decided the foundation of IMS as a national institute in Okazaki. In this period, many scientists

Hideo AKAMATSU, Director

willingly joined to the preparative work for the IMS project, which caused to confirm the solidarity of scholars in this field and to bring up IMS as the nucleus for the center of their joint studies on molecular science. The Preparatory Committee for Establishment of IMS started in due form in 1974; Prof. J. Yamashita, Director of the Institute for Solid-State Physics, Univ. of Tokyo presided as chairman. Preparative details were worked out with sub-committees for organization and operation, for researches and facilities, and for land and buildings; Prof. Y. I'haya, Univ. of Electro-Communications, Prof. I. Tanaka, Tokyo Inst. of Technology, and Prof. S. Seki, Osaka Univ., respectively, presided as the chairman.

IMS as the comprehensive research institute for molecular science has been planned to comprise 15 research laboratories which are grouped into five divisions: theoretical studies, molecular structure, electronic structure, molecular assemblies and applied molecular science. IMS as the inter-university research institute has been planned to be open to universities throughout the country for common use of its research facilities and for joint studies on molecular science. In order to meet this goal, IMS should have well organized research facilities. Instrument Center and Computer Center, in particular, should be well financed and smoothly operated to encourage the use by university scientists. IMS entertains joint studies in collaboration with its members and has some funds to assist meetings held at IMS. In five of 15 research laboratories, the chairs are to be filled with adjunct professors invited from universities. These systems are designed to enhance the cooperation between IMS and universities. IMS has advisory committees to encourage the participation from the outside of IMS. Half or more members of the committees should be invited from universities. Three committees, i.e., Committee for Faculty Selection, Committee for Joint Studies and Committee for Operation are presently in operation.

An inter-university research institute is an unique system. As the center of joint studies among scientists and scholars, it is expected to stimulate the molecular science research in a most direct and comprehensive way which could not be made as the activities of individual universities.

Buildings

The land of IMS is the former site of the Aichi University of Education, and had been left unused after AUE's move to Kariya in 1970. In April 1975, IMS started its first step in the building which used to be the library of AUE. This building was used as the temporary quarter of IMS until January 1977, when the Main Laboratory Building (8855 m²), actually the first half of the building, and the Power Station (854 m²) were constructed. Thereafter, the construction work went on quite favorably; Research Office Building (1850 m²), Instrument Center (1050 m²), Chemical Materials Center (1120 m²) and Development Workshop (1260 m²) were completed in March 1978. Under construction at present and to be completed in the spring of 1979 are Administration Office (2270 m²), Library (2440 m²), Computer Center (1020 m²), Low-Temperature Center (1430 m²) and the remaining half of Main Laboratory Building. IMS has a plan for construction of a seminar house with lodging facilities, which will be used for meetings of a moderate size.

Faculty

IMS made its first two scientific appointments in April 1975. Prof. H. Akamatu of Yokohama National University was named as the Director of the Institute. Prof. H. Inokuchi transferred from the Institute for Solid-State Physics, Univ. of Tokyo and became Professor of Division of Molecular Assemblies. Prof. Inokuchi had been in the Office for Establishment of IMS for a year just before IMS was actually founded.

The most important task for the new Institute was to organize its faculty. Needless to say, the success of IMS lies on the selection of its faculty. The Committee for Faculty Selection preformed its mission in the most deliberate way successfully. Prof. S. Nagakura, Univ. of Tokyo, one of the leading promoters of the IMS project, presided as chairman.

First we succeeded to recruit Prof. E. Hirota and Prof. K. Yoshihara. Prof. Hirota moved to IMS from Kyushu University to head Laboratory of Molecular Structure I in collaboration with Assoc. Prof. S. Saito who came from Sagami Chemical Research Center. Prof. Yoshihara who transferred from the Institute of Physical and Chemical Research started Laboratory of Excited State Chemistry in association with Assoc. Prof. T. Sakata from Osaka University. Prof. Inokuchi collaborated with Assoc. Prof. I. Koyano to get Laboratory of Solid State Chemistry off the ground. In addition, Laboratory of Molecular Structure II was initiated by Prof. K. Kuchitsu, Univ. of Tokyo, and Assoc. Prof. I. Hanazaki, Osaka Univ., as adjunct Professors, and Laboratory of Molecular Assemblies by Prof. H. Chihara, Osaka Univ. and Assoc. Prof. Y. Harada, Univ. of Tokyo, as adjunct Professors. Accordingly five Laboratories were founded in 1975.

In 1976, Prof. K. Morokuma came to IMS from the University of Rochester. He started Laboratory of Theoretical Studies I with Assoc. Prof. M. Tsukada. Laboratory of Theoretical Studies III started with Prof. K. Hijikata, Univ. of Electro-Communications and Assoc. Prof. H. Hosoya, Ochanomizu Women's Univ., as adjunct Professors. Assoc. Prof. H. Takaya transferred to Chemical Materials Center from Nagoya University.

In 1977, Laboratory of Applied Molecular Science II was initiated by Prof. Y. Saito, Univ. of Tokyo and Assoc. Prof. H. Iwamura, Univ. of Tokyo, as adjunct Professors. Prof. Iwamura moved to the chair of Laboratory of Applied Molecular Science I when it started. Computer Center recruited Assoc. Prof. H. Kashiwagi from Hokkaido University.

In April 1978, Assoc. Prof. T. Ito transferred from Hokkaido University to Laboratory of Applied Molecular Science I.

At the end of 1977 nine Laboratories and three Research Facilities, i.e., Instrument Center, Chemical Materials Center and Development Workshop were functioning, and two more Facilities, Computer Center and Low-Temperature Center, had just got off the ground.

In the first three years the following professors took part in the faculty of IMS as adjunct Professors.

H. Chihara,	Prof. (Osaka Univ.)	Dec. 1975 — Mar. 1977
K. Kuchitsu,	Prof. (Univ. of Tokyo)	Dec. 1975 — Mar. 1976;
		Apr. 1977 —
I. Hanazaki,	Assoc. Prof. (Osaka Univ.)	Dec. 1975 — Mar. 1978
Y. Harada,	Assoc. Prof. (Univ. of Tokyo)	Dec. 1975 — Mar. 1976
J. Tanaka,	Prof. (Nagoya Univ.)	Apr. 1976 — Mar. 1977
F. Shimizu,	Assoc. Prof. (Univ. of Tokyo)	Apr. 1976 — Mar. 1978
K. Hijikata,	Prof. (Univ. of Electro-Communications)	Dec. 1976 —
H. Hosoya,	Assoc. Prof. (Ochanomizu Women's Univ.)	Dec. 1976 —
Y. Saito,	Prof. (Univ. of Tokyo)	Apr. 1977 —
I. Tsujikawa,	Prof. (Kyoto Univ.)	Apr. 1977 —
H. Iwamura,	Assoc. Prof. (Univ. of Tokyo)	Apr. 1977 — Dec. 1977

Council

IMS has an advisory board for the Director-General which is composed of 17 Counsellors appointed by the Minister of Education and Science. Two of the counsellors are to be selected among the distinguished foreign scientists. Dr. G. Herzberg, National Research Council of Canada and Prof. H. Gerischer, Fritz-Haber Institut der Max-Planck Gesellschaft, accepted the appointment. This was the first case in Japan in which the door of traditionally closed Government-financed research institutes was internationally opened.

The Council made a start with the following member in January 1976.

Counsellors (1976 – 1978): M. Kotani, Chairman (President, Science Univ. of Tokyo), S. Nagakura, Vice-Chariman (Prof., Univ. of Tokyo), K. Fukui (Prof., Kyoto Univ.), H. Gerischer (Director, Fritz-Haber Institut), G. Herzberg (Distinguished Research Scientist, NRC, Canada), K. Husimi (Vice-President, Science Council of Japan), N. Ishizuka (President, Nagoya Univ.), Y. Morino (Director, Sagami Chem. Res. Center), S. Okamura (Prof., Univ. of Tokyo), S. Seki (Prof., Osaka Univ.), S. Shibata (Prof. Emeritus, Univ. of Tokyo), Y. Tajima (Director, National Inst. of Genetics), N. Tanaka (Prof., Tohoku Univ.), T. Umesao (Director, National Museum of Ethnology), I. Watanabe (Prof., Keio Univ.), T. Yamashita (Prof. Emeritus, Univ. of Tokyo), Y. Yukawa (Prof., Osaka Univ.).

Ex-Officio members: H. Akamatu (Director), S. Okada (Administrative Director).

At the first meeting of Council, Prof. Gerischer made a speech on the system of Max-Planck Gesellschaft and on the common problems of research institutes. At the second meeting Dr. Herzberg talked on his experience in NRC and gave an encouragement at the start of the new institute.

Main Laboratory Building (left) and Research Office Building (right).

Research Activities

IMS set the first step with a small number of staffs. In the first year we were fully occupied with the work of preparing research facilities and for equipping laboratories. However, at the time when we moved from the temporary "library" building in the spring of 1977, we had the newly built Main Laboratory Building ready for research activities.

At the start of IMS, we initiated the following two Special Research Projects which should be carried out in a strong collaboration among staffs.

(1) Investigation of energy conversion process at the molecular level.

(2) Molecular designing for interesting and useful materials.

These projects started in 1975 on a five-year scheme. Several postdoctral research fellows have been appointed for the projects, which are now in progress as is planned on several topics.

IMS has another kind of project which was planned to provide special equipments for general use by university scientists. The equipments to be introduced were expected to be of extremely high quality but too expensive to purchase at universities. Two types of equipments, a system for investigation of high resolution spectroscopy and one for observation of ultra fast spectroscopy, have been developed and put into service in the first three years.

The financial support of the Government increased year by year as the IMS project made a progress:

1975 fiscal year	307,123	thousand yen
1976 fiscal year	637,009	thousand yen
1977 fiscal year	930,954	thousand yen

Salaries and the cost of construction are not included in the figures.

Joint Studies

IMS has national funds to assist joint studies, which encouraged scholars to meet together at IMS. At an early stage of the Institute, even before the research work hardly started, IMS began to function as the center for joint studies on molecular science. The first joint study was in the form of research conference. We had the first small meeting in August 1975 when our first invited scientist, Prof. E. C. Lim of Wayne State Univ. USA came to the newly born Institute in its primitive sate.

"Okazaki Conferences" took the lead as a model for the meetings at IMS. Okazaki Conferences have been held as a part of the Special Research Projects, on subjects related with the projects. The conferences were open only to a limited number, usually 50 or less, of invited participants, including a few invited speakers from abroad. The first Conference was held in January, 1976, on the topics of photoelectrode process with the presence of Prof. H. Gerischer of Fritz-Haber Institut as the invited speaker. In the first three years we had six Okazaki Conferences successfully.

In the first three years, 1975–1977, IMS supported 13 joint studies of research works and 19 research conferences. The proposals for joint studies and the common use of equipments are rapidly increasing in number as the enhancement of research facilities makes a steady progress. IMS is now successfully playing a role of the inter-university research institute.

Prospect

Molecular science has developed itself in the boundary region between physics and chemistry as a discipline which studies the function of molecules on the basis of their structures. Today many fields of science have a keen interest in the investigation at the molecular level and look forward eagerly to the proper advancement of molecular science. The principal role of IMS is to promote basic and exploratory research in molecular science, covering from simple molecules, free radicals and molecular ions to complex molecules such as porphyrin and cytochrome and also molecular assemblies. IMS is expected to exploit new scientific opportunities for chemistry, physics and related fields of science.

In the present decade, the economic and social circumstances around us are being forced to make a large change which will modify our views of values and the way of social life. The change has been caused by the reason directly connected with the basis of material civilization, that is, the rapid increase of energy consumption and the depletion of natural resources. The modern civilization is characterized by a chain of production and consumption of materials in large quantity. In order to continue this chain in a healthy way with our limited natural resources, we should not only practice the effective use of materials but should also actively apply the principle of circulating substances to the flow of materials.

This is also true for energy. The natural world around us is filled with energy which can be used, but it can be stored only in the form of chemical energy in substances, that is, chemical fuels. The hydrogen energy system is a good example for this kind of energy storage and circulation. But it is not necessarily restricted to hydrogen. The demand is extremely high for the development of new science and technology based on the circulation principle. Molecular science is expeted to play a role in such a development.

Chemistry started from being a science of the separation of substances and then proceeded to be a science of the production of substances. At each stage of the progress of chemistry, the concepts of molecules were improved and their new functions were developed. Chemistry is now requested to be a science which pursues the principle of circulation of substances. It will be the coming stage of chemistry. Then one can expect a development and extension of new concepts concerning molecules and their functions.

The molecular science deals with the formation of molecules and their transformation, the elementary processes of chemical reactions and their controls, the interactions between photon and molecules, and the energy transfer and the energy conversion through the molecular process. Studies of these topics will ultimately contribute to overcoming the challenge of long-term problems of world needs.

June, 1978

Hideo AKAMATU

Director

iv

CONTENTS

ORGANIZATION AND STAFF

Organization

The Institute for Molecular Science, upon completion, will comprise 15 research laboratories—each staffed by a professor, an associate professor, two research associates and a few technical associates—and five research facilities. The laboratories are grouped into five divisions as follows:

Division of Theoretical Studies	Theoretical Studies I Theoretical Studies II[1] Theoretical Studies III[2]
Division of Molecular Structure	Molecular Structure I Molecular Structure II[2] Molecular Dynamics[1]
Division of Electric Structure	Excited State Chemistry Excited State Dynamics[3] Electronic Structure[2,3]
Division of Molecular Assemblies	Solid State Chemistry Photochemistry[3] Molecular Assemblies Dynamics[1] Molecular Assemblies[2]
Division of Applied Molecular Science	Applied Molecular Science I Applied Molecular Science II[2]
Five Research Facilities are:	Computer Center Instrument Center Low-Temperature Center Chemical Materials Center Development Workshop

[1] To be established.　[2] Professors and associate professors are adjunct professors from universities.　[3] Established in 1978.

Instrument Center (left) and
Chemical Materials Center (right)

Development Workshop

COUNCIL

Ex-Officio Members

Hideo AKAMATU, Director-General
Misaku MATSUZAWA, Administrative Director

Counsellors

Chairman	Masao KOTANI, President, The Science University of Tokyo
Vice-Chairman	Saburo NAGAKURA, Professor, The University of Tokyo
	Melvin CALVIN, Professor, University of California, U.S.A.
	Kenichi FUKUI, Professor, Kyoto University
	Heinz GERISCHER, Director, Fritz-Haber Institut der Max-Planck-Gesellschaft
	Kodi HUSIMI, President, Japan Science Council
	Naotaka ISHIZUKA, President, Nagoya University
	Keiya KANDA, Professor, Kyushu University
	Yonezo MORINO, Professor Emeritus, The University of Tokyo
	Sogo OKAMURA, Professor Emeritus, The University of Tokyo
	Kazuo SAITO, Professor, Tohoku University
	Shoji SHIBATA, Professor Emeritus, The University of Tokyo
	Yataro TAJIMA, Director-General, National Institute of Genetics
	Yasutada UEMURA, Professor, The University of Tokyo
	Tadao UMESAO, Director-General, National Museum of Ethnology
	Itaru WATANABE, Professor, Keio University
	Yasuhide YUKAWA, Professor Emeritus, Osaka University

The Council is the advisory board for the Director-General. Two of the counsellors are selected among distinguished foreign scientists.

STAFF

Director-General

Hideo AKAMATU

Scientific Staff

Division of Theoretical Studies
    Theoretical Studies I

Keiji MOROKUMA	Professor
Masaru TSUKADA	Associate Professor
Shigeki KATO	Research Associate
Chikatoshi SATOKO	Research Associate
Iwao OHMINE	Research Fellow
Kazuo KITAURA	Research Fellow

    Theoretical Studies II

Katsunori HIJIKATA	Adjunct Professor
(Univ. of Electro-Communications)	
Haruo HOSOYA	Adjunct Associate Professor
(Ochanomizu Women's Univ.)	

2

Division of Molecular Structure
  Molecular Structure I

Eizi HIROTA	Professor
Shuji SAITO	Associate Professor
Chikashi YAMADA	Research Associate
Yasuki ENDO	Research Associate
Kentaro KAWAGUCHI	Technical Associate
Masao KAKIMOTO	Research Fellow
Keiichi NAGAI	Research Fellow
Nobukimi OHASHI	Visiting Scientist
(Kanazawa Univ.)	

  Molecular Structure II

Kozo KUCHITSU	Adjunct Professor
(Univ. of Tokyo)	
Michio TAKAMI	Adjusnt Associate Professor
(Inst. of Chem. Phys. Research)	

Division of Electronic Structure
  Excited State Chemistry

Keitaro YOSHIHARA	Professor
Tadayoshi SAKATA	Associate Professor
Nobuaki NAKASHIMA	Research Associate
Tomoji KAWAI	Research Associate
Minoru SUMITANI	Technical Associate
Akira NAMIKI	Research Fellow
Katsumi TANIMURA	Research Fellow

  Electronic Structure

Mitsuo ITO	Adjunct Professor
(Tohoku Univ.)	
Masahiro MATSUOKA	Adjunct Associate Professor
(Kyoto Univ.)	

Division of Molecular Assemblies
  Solid State Chemistry

Hiroo INOKUCHI	Professor
Inosuke KOYANO	Associate Professor
Kikujiro ISHII	Research Associate*
Kenichiro TANAKA	Research Associate
Naoki SATO	Technical Associate
Kazuhiko SEKI	Research Fellow
Kazumichi NAKAGAWA	Research Fellow

  Molecular Assemblies

Ikuji TSUJIKAWA	Adjunct Professor
(Kyoto Univ.)	
Mizuka SANO	Adjunct Associate Professor
(Univ. of Electro-Communications)	

Division of Applied Molecular Science
  Applied Molecular Science I

Hiizu IWAMURA	Professor
Tasuku ITO	Associate Professor

* Till March 31, 1978. Present address: Department of Chemistry, Gakushuin University.

Tadashi SUGAWARA	Research Associate
Koshiro TORIUMI	Research Associate
Yuzo KAWADA	Technical Associate

Applied Molecular Science II

| Yoshihiko SAITO (Univ. of Tokyo) | Adjunct Professor |
| Teruyoshi SAKATA (Osaka Univ.) | Adjunct Associate Professor |

Research Facilities

Computer Center

| Hiroshi KASHIWAGI | Associate Professor |

Instrument Center

| Keisaku KIMURA | Research Associate |
| Toshiro MURAO | Technical Associate |

Low-Temperature Center

| Toshiaki ENOKI | Research Associate |

Chemical Materials Center

| Hidemasa TAKAYA | Associate Professor |
| Arata YASUDA | Technical Associate |

Development Workshop

| Yoshihiro TAKAGI | Research Associate |

Technical Staff

Shigetoshi TAKAHASHI	Technical Chief
Katsumi KATO	Technician
Kazuo HAYAKAWA	Technician
Masaaki NAGATA	Technician
Norio OKADA	Technician
Koichi SUZUI	Technician
Fumio NISHIMOTO	Technician

Foreign Visiting Staff

Edward C. Lim (Wayne State Univ. USA)	Aug. 3, 1975 — Oct. 9, 1975
Chim-Hsien Wang (Univ. of Utah, USA)	Nov. 27, 1976 — Mar. 11, 1977
Willem Siebrand (NRC, Canada)	Dec. 21, 1976 — Mar. 31, 1977
John M. Morris (Melbourne Univ., Australia)	Feb. 16, 1977 — May 15, 1977
Robert F. Curl (Rice Univ. USA)	May 2, 1977 — Aug. 20, 1977
Frank Willig (Fritz-Haber Inst. der Max-Plank Gesel. Germany)	Dec. 23, 1977 — Mar. 28, 1978
Helmut Tributsch (Fritz-Haber Inst. der Max-Plank Gesel. Germany)	Mar. 1, 1978 — June 30, 1978
James C. Baird (Brown Univ., USA)	May 8, 1978 — Oct. 7, 1978
Jon T. Hougen (NBS, Washington D.C., USA)	July 17, 1978 — Feb. 28, 1979

BUILDINGS AND CAMPUS

The IMS campus covering 62561 m² is located on a low hill in the middle of Okazaki City. The inequality in the surface of the hill and growing trees are preserved as much as possible, and low-storied buildings are adopted for conservation of the environment. The buildings of IMS are separated according to their functions as shown in the map. The Research Office Building and all Research Facilities except for the Computer Center are linked organically to the Main Laboratory Building by corridors. Computer Center, Library, and Administration Buildings are situated between IMS and the neighboring National Institute for Basic Biology and National Institute for Physiological Sciences, because the latter two facilities are common to these three institutes.

The lodging facility of IMS called Yamate Lodge, located within 10 min. walk, has sleeping accommodations for 20 guests. Scientists who visit IMS can make use of this facility. Foreign visiting scientists can also live at this lodge with their families during their stay.

The Institute for Molecular Science
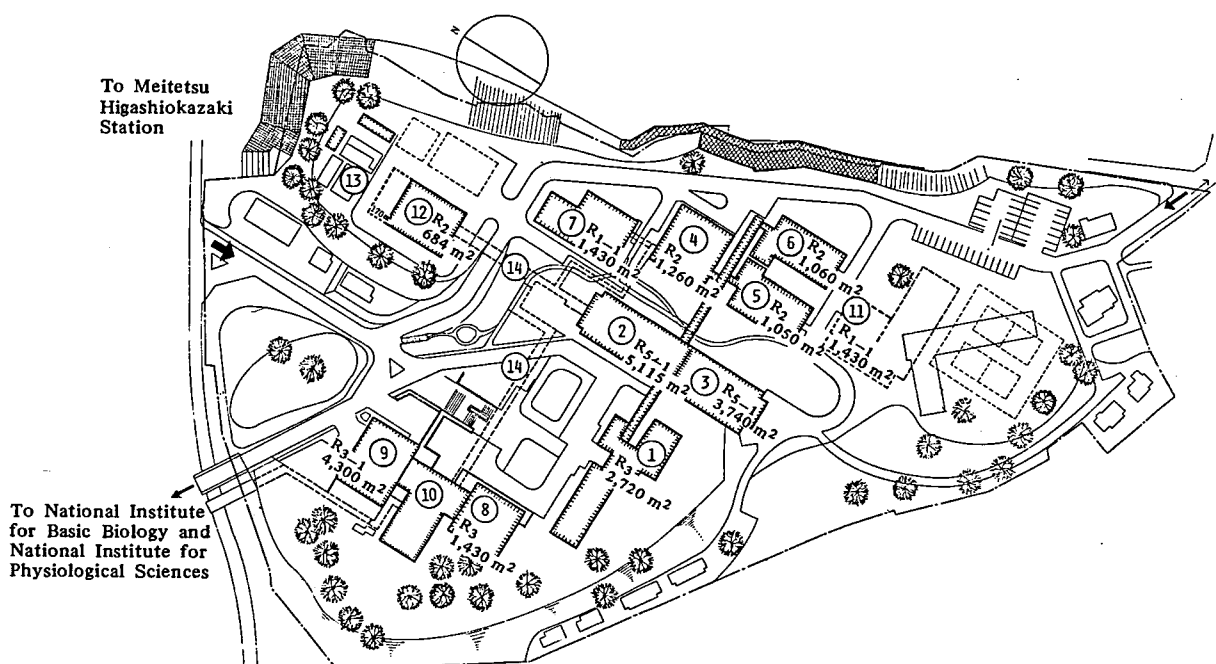
1.	Research Office Building	8.	Computer Center[†]
2.	Main Laboratory Building	9.	Library[†]
3.	Main Laboratory Building[†]	10.	Central Administration[†]
4.	Development Workshop	11.	Special Experiment Building[‡]
5.	Instrument Center	12.	Power Station
6.	Chemical Materials Center	13.	Waste-Water Disposition Facilities
7.	Low-Temperature Center[†]	14.	Service Tunnels

[†] Under construction

[‡] In the planning stage
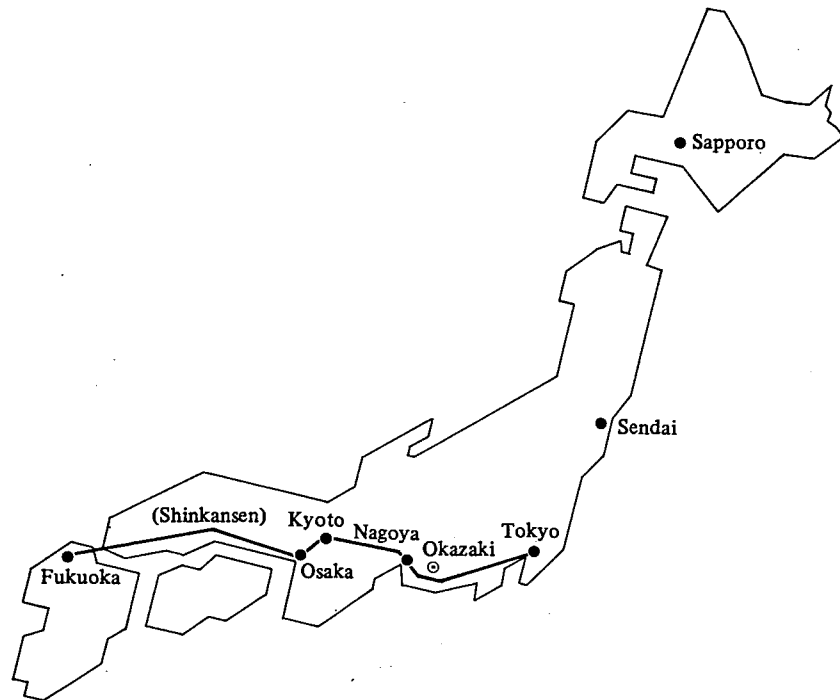
Okazaki (population 250,000) is 260 km south west of Tokyo, and can be reached by train in about 3 hours from Tokyo via New Tokaido Line (Shinkansen) and Meitetsu Line.

The nearest large city is Nagoya, about 40 km west of Okazaki.

RESEARCH ACTIVITIES

I. Division of Theoretical Studies

Research in the Division covers a wide scope of theoretical studies in molecular chemistry and physics, and a strong collaboration with experimental divisions will be emphasized. The projects in which the Division is presently involved can be divided into two groups: one is theoretical investigations of chemical reactions and molecular interactions, and the other is theories of solid surfaces and chemical processes on them.

The main objective purshed in the projects of the first group (I-A~E) is the theoretical understanding of the mechanism of chemical reactions. Potential energy surfaces of various types of reactions are calculated with the use of ab-initio molecular orbital methods. The energy gradient technique is applied to the molecular geometry optimization and the determination of the transition state. The electronic structure of reacting species is analyzed within the framework of molecular interactions. A new methodology of molecular quantum chemistry is also developed to apply to catalytic reactions including transition metal complexes.

The subject carried out in the projects of the second group (I-F, G) is the electronic structure of ideal and real solid surfaces, and their interactions with adsorbates. The current topics include the localized electronic state of surface defects and their role on chemical processes.

I-A LCAO-MO-SCF Scheme with Local Exchange-Correlation Functional Approximation

Kazuo KITAURA, Chikatoshi SATOKO, and Keiji MOROKUMA

The spin-density functional formalism has been presented recently by Gunnarsson and Lundqvist[1] as an extension of the Kohn-Sham scheme[2] to the spin-dependent form. The local-spin-density functional approximation (LSD) to the exchange-correlation energy has been applied to the first row diatomic molecules.[3] The LSD method has been shown to be superior in the calculation of dissociation energy to the Hartree-Fock (HF) method. This is due to the fact that the LSD method takes account of the electron correlation.

The LSD one-electron equation can be solved by the numerical procedures which are used in the $X\alpha$ method.[4] These numerical methods, however, have been mainly applied to the calculation of orbital energies and have practical difficulties in computing the total energy of polyatomic molecules.

We will present the LCAO-MO-SCF scheme, which is familiar in quantum chemistry, to obtain the total energy of molecules in reasonable accuracy. Our scheme will enable one to compare directly the exchange-correlation energy of the LSD method with the exchange energy of the HF method and will shed light on the role of exchange-correlation energy in molecular binding. It should be applicable to transition metal complexes which have large correlation energy and could not be properly described by the HF approximation. It will be also useful for studing chemisorptions of atoms and molecules on solid surfaces.

The LSD one-electron equation in the LCAO-MO scheme is written as,

$$[F_s^{LSD} - \epsilon \cdot S] \cdot C^s = 0 \tag{1}$$

$$F_s^{LSD} = T + V_N + V_C + V_s^{xc} \tag{2}$$

where the subscript s is a spin index. Eq. (1) is a set of simultaneous orbital equations for α and β electrons and is solved self-consistently. S is the overlap matrix, C is the eigenvector corresponding to the eigenvalue ϵ. T and V_N are the kinetic energy and the nuclear attraction energy matrices, respectively. V_C is the two electron Coulomb energy matrix. V_s^{xc} is the exchange-correlation potential matrix and defined as,

$$\left\{V_s^{xc}\right\}_{ij} = \int \phi_i^*(r) V_s^{xc}(\rho(r), \zeta(r)) \phi_j(r) \, dr \tag{3}$$

where ϕ is the basis atomic orbital (AO). The one electron potential $V^{xc}(\rho, \zeta)$ is given elsewhere.[1] The total energy E is written as,

$$E = Tr\left/ D \cdot (T + V_N + \frac{1}{2}V_C + E^{xc})\right\} \tag{4}$$

$$\left\{E^{xc}\right\}_{ij} = \int \phi_i^*(r) E^{xc}(\rho(r), \zeta(r)) \phi_j(r) \, dr \tag{5}$$

$$\left\{D\right\}_{ij} = \left\{D^\alpha\right\}_{ij} + \left\{D^\beta\right\}_{ij} = \sum_{k,s} n_k^s C_{ki}^s C_{kj}^s \tag{6}$$

n_k^s is the occupation number of the k-th spin orbital. $E^{xc}(\rho, \zeta)$ is the exchange-correlation energy per elec-

tron.[1]

We expand the basis AO with Gaussian type orbitals. The one electron integrals ($|T|_{ij}$ and $|V_N|_{ij}$) and the Coulomb integral $|V_C|_{ij}$ are evaluated analytically as they are done in the ab initio LCAO-MO-SCF calculation. The integral $|V_s^{xc}|_{ij}$ is calculated by scaling of the value which is obtained by the numerical integration using random sample points. The integral $|E^{xc}|_{ij}$ is also evaluated by the same manner as $|V_s^{xc}|_{ij}$.

The numerical results of H, He and Li$^+$, whose exact LSD total energies were obtained by Gunnarsson and Lundqvist, are shown in the table to demonstrate the efficiency of the present method. In the calculations, the basis sets which are large enough to remove the error comming from the LCAO approximation are used. The dependence of the total energies on number of sample points is very small. Even in the case of 500 points, the errors are within 0.4 eV. When we use the limited

number of sample points, the absolute value of the error may become large as number of electrons increase in the systems. Even so, the error in difference energy, which is our concern, between the molecule and the constituent atoms will not become so large.

It seems indispensable to introduce the fixed core approximation before applying the present method to molecules containing heavy atoms because of the limitation of the LSD functional approximation itself.[1] Our research is in progress along the line.

References

1) O. Gunnarsson, B. I. Lundqvist, *Phys. Rev.* B13, 4274 (1976).
2) W. Kohn, L. J. Sham, *Phys. Rev.* 140, A1133 (1965).
3) O. Gunnarsson, J. Harris, R. O. Jones, *Phys. Rev.* B15, 3027 (1977).
4) J. C. Slater, Quantum theory of molecules and solids, IV. New York, McGraw-Hill 1974.

Table I. The Dependence of the Total Energy on the Number of Sample Points.[a]

atom	LSD total energy (in eV)					
	500	2000	5000	20000	50000	exact[b]
H (^{2}S)	−13.284	−13.346	−13.357	−13.398	−13.388	−13.39
He (^{1}S)	−77.426	−77.795	−77.818	−77.831	−77.826	−77.8
He (^{3}S)	−58.128	−58.423	−58.422	−58.422	−58.397	−58.4
Li$^+$(^{1}S)	−194.87	−195.51	−195.39	−195.08	−195.20	−195.2

[a] The uncontracted STO-6G basis sets are used. For He, two spherical Gaussians with exponents 0.05 and 0.01 are added.
[b] Ref. 1.

I-B Transition States and Intrinsic Reaction Coordinates

The dynamic properties of chemical reactions are affected by the characteristics of potential energy surfaces of reaction systems. Theoretical investigations on the reaction path and the transition state of chemical reactions are significant to determine the critical factors controlling reaction processes.

In this project, the mechanism of energy disposal along the reaction pathway has been discussed in terms of the aspects of transition state and intrinsic reaction coordinate (IRC). The importance of the shape of IRC is stressed in elucidating such dynamic behaviors. Ab-initio molecular orbital calculations have been performed in an effort to clarify the role of the electronic structure of reaction systems in the reaction dynamics.

I-B-1 Theoretical Characterization of Transition State for $C_2H_4F \rightarrow C_2H_3F + H$ Reaction

Shigeki KATO and Keiji MOROKUMA

The reaction of C_2H_4 + F has received much attention from both experimental and theoretical points of view. The reaction process is characterized by the formation of a long-lived collision complex C_2H_4F and its successive dissociation. Energy partitioning experiments by crossed molecular beam and infrared chemiluminescence have shown a non-statistical translational and vibrational energy distribution in the product.[1] In order to interpret such a non-statistical behavior, an accurate theoretical characterization of the transition state would be significant because previous approaches have been

based on hypothetic transition state geometries and vibrational frequencies.[2]

In the present work, we have performed ab-initio MO calculations with a 4-31G basis set for the reaction path in the dissociative channel. The minimum energy path was determined as a function of the breaking CH bond distance. The gradient method was used for geometry optimizations. The normal mode analyses have been also carried out at the optimized geometries of the reaction complex, the transition state and the product.

Results of our MO calculations can be summarized as follows.

1) The potential energy for the minimum energy path is plotted in Figure 1. The calculated energies of the reaction complex, the transition state and the product are shown in the Table I. The dissociation energy of the

reaction complex C_2H_4F is calculated to be 39.4 kcal/mol., which agrees with an empirical estimation. The height of the reverse activation barrier is experimentally unknown. Our theoretical value is 5.6 kcal/mol.

2) The transition state is located on the later part of the reaction path from the complex to the product. Therefore an enhancement of the translational energy is expected on the basis of an empirical correlation rule between the barrier location and the energy disposal.[3]

3) Several interesting features are observed in the normal mode analysis at the transition state. The reaction coordinate consists mainly of the relative translational motion of two fragments. Among all the vibrational modes, there are three bending vibrations with low frequencies which are related to the velocity vectors pointing to the orbital rotational modes and the deformation mode of the CCF framework of the product. Five vibrational modes are regarded as adiabatic in the process of descending the activation barrier. The CF stretching mode is included in this group.

4) The deformation of C_2H_3F part at the transition state is described by only three vibrational modes of the product, that is the CC stretching, the CH out-of-plane bending and the torsional mode around the CC bond. This suggests that the energy transfer will be accessible between the radial motion and these vibrational modes after passing through the transition state.

References

1. a) J. M. Parson and Y. Y. Lee, *J. Chem. Phys.*, **56**, 4658 (1972).
   J. M. Farrar and Y. T. Lee, *J. Chem. Phys.*, **65**, 1414 (1976).
   b) J. G Moehlmann, J. T. Gleaves, J. W. Hudgens, and J. D. McDonald, *J. Chem. Phys.*, **67**, 2007 (1977).
2. D. Z. Zvijac, S. Mukamel, and J. Ross, *J. Chem. Phys.*, **67**, 2007 (1977).
3. J. C. Polanyi, *Acc. Chem. Res.*, **5**, 161 (1972).

Table I. Calculated Energies of Reaction Complex, Transition State, and Product.

C_2H_4F	eclipsed	0^a
	staggerd	0.19
Transition State		44.96
C_2H_3F + H		39.40

^{a} given in kcal/mol.
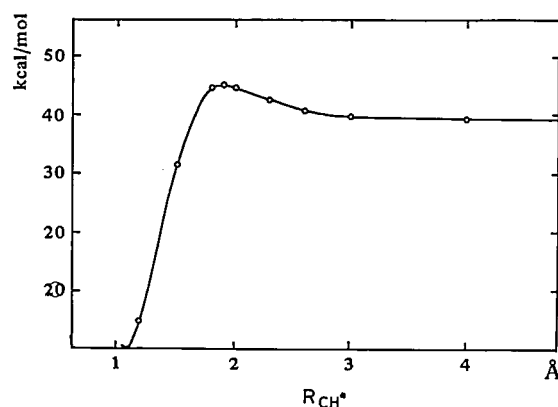
Figure 1. Potential energy along the minimal energy path as the function of CH distance.

I-B-2 A Theoretical Model for the Energy Disposal in Polyatomic Reactions

Shigeki KATO and Keiji MOROKUMA

A detailed description of reaction dynamics of polyatomic systems is one of the ultimate goals of theoretical chemistry. Since chemical reactions are usually associated with complicated modes of nuclear rearrangements along the reaction pathway from the reactant to the product, it is of particular importance to construct an illuminating model in extracting the essential features of reaction processes. The concept of reaction coordinate has been utilized for such a purpose.[1] The intrinsic reaction coordinate (IRC),[2] which is defined as the classical trajectory with an infinitesimal kinetic energy passing through the transition state, has been also applied to describe the nuclear motion of polyatomic systems.[3] The adiabaticity of vibrational motions perpendicular to the reaction coordinate was assumed in the previous approach.

In the present work, we have proposed a theoretical model to treat the energy disposal along the reaction pathway. In this procedure, the dynamic couplings between the motion along the IRC and the vibrational motions perpendicular to it are explicitly included. The final expression of probabilities for energy transfer from the translational motion to the specific vibrational motion is given in terms of with the curvature of IRC and the changes of vibrational frequencies along the IRC.

Qualitative measures of energy transfer are given as follows.

(1) The translation-vibration energy transfer occurs when the condition

$$\Delta E_{mn} + \frac{1}{2}\kappa i(s) \, (\xi_{mi}^2 - \xi_{ni}^2)$$

is satisfied. ΔE_{mn} means the energy difference between the initial (m) and the final (n) vibrational levels of the i-th vibrational mode. $\kappa i(s)$ is the force constant ξ_{mi} and ξ_{ni} are the effective displacements of the origin of vibrational coordinate due to the centrifugal force caused by the curvature of IRC. (2) The transition probability is large when the change of vibrational frequency is large at the point satisfying the above mentioned condition.

We have applied our model to realistic chemical reaction systems. As an example, we have performed molecular orbital calculations for the reaction

$$CH_2OH^+ \rightarrow HCO^+ + H_2.$$
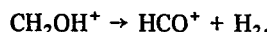
The IRC was calculated by MINDO/3 method. The curvature of IRC is obtained straightforwardly from the definition of IRC. In Figure 1, the projection of principal normal line of IRC to the HH, CH, and CO stretching vibrational modes are shown. The change of vibrational frequencies of these modes are also given in Figure 2. The curvature of IRC has a maximum value at s = 0.6 and the principal normal line is mainly directed to the H_2 stretching coordinate. This result suggests that the H_2 stretching mode will be enhanced at the product. The remarkable change of vibrational frequency of H_2 stretching mode at the region of maximum curvature also supports this suggestion. It is noteworthy that the energy transfer from the reaction coordinate to the vibrational modes seems to occur at a localized region on the reaction coordinate.

References

1) R. A. Marcus, J. Chem. Phys., 49, 2610, 2617 (1968).
2) K. Fukui, J. Phys. Chem., 74, 4161 (1970), K. Fukui, S. Kato, and H. Fujimoto, J. Am. Chem. Soc., 97, 1 (1975).
3) S. Kato, H. Kato and K. Fukui, J. Am. Chem. Soc., 99, 684 (1977).
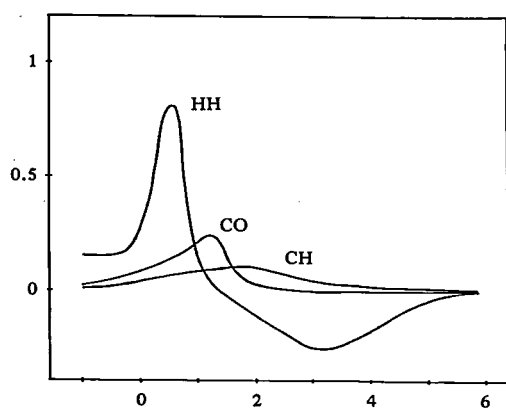
Figure 1. Projection of the principal normal line to IRC to various vibrational coordinates. The reaction coordinate is given in (amu)$^{1/2}$ bohr.
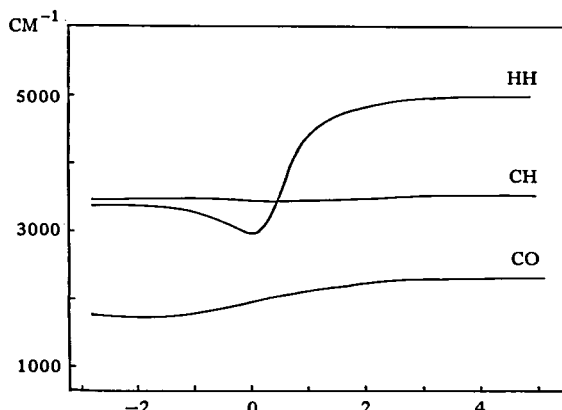
Figure 2. Change of vibrational frequencies along the IRC.

I-B-3 Molecular Orbital Study of the Activation Energy Disposal in $C_2H_5F \rightarrow C_2H_4 +$ HF Reaction

Shigeki KATO and Keiji MOROKUMA

The advance of experimental techniques such as chemiluminescence and mass-spectrometry has revealed the details of chemical reaction processes. The structure of the transition state has been discussed in connection to the energy partitioning data of product species. Since the transition state cannot be isolated experimentally, theoretical approaches would be meaningful to characterize the aspects of transition state and to elucidate the mechanism of energy disposal along the reaction pathway.

In the present work, we have analyzed the potential barrier of reaction to find out how the activation energy is distributed to various modes of product molecules. The energy decomposition analysis along the reaction coordinate gives an intelligible explanation to the mechanism of energy disposal. We have performed ab-initio MO calculation for the reaction

$$C_2H_5F \rightarrow C_2H_4 + HF$$
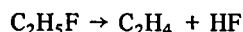
which is a typical example of HX elimination from haloalkanes. The geometry optimizations have been carried out for the reactant, the transition state and the product species with a 4-31G basis set. The normal coordinates have also obtained for the transition state and the products. Finally, the energy decomposition analysis was made for the geometries along the reaction path.

The following results were obtained from our calculations
1) The calculated energies of the reactant, the transition state and the product are summarized in Table I. The calculated barrier height for the reverse association process is 52.2 kcal/mol., which is accord with the experimental value, 50.0 kcal/mol. The fully optimized geo-

metry of the transition state is shown in the Figure 1. The HF bond at the transition state is longer than that at the product (HF) by 0.36 Å. It is noteworthy that the deformation energy of HF at the transition state agrees with the upper limit of the observed vibrational levels, i.e. v = 4, for the analogous reaction $CH_3CF_3 \rightarrow CH_2CF_2 + HF$.[1]

2) The normal mode corresponding to the reaction coordinate at the transition state is localized to the HF stretching mode. This suggests that a large amount of energy will be released to the HF vibration of the product.

3) The results of energy decomposition analysis at the transition state are given in Table II. The activation energy is mainly composed by the deformation energy. The deformation energy of the HF part is larger than that of the C_2H_4 part.

4) The energy decomposition analysis along the reaction path from the transition state to the product shows that the deformation energy is larger than the interaction energy near the transition state and the interaction energy increases rapidly and has a maximum value. The increase of interaction energy is attributed to the reduction of electro-static (ES) and charge transfer (CT) energies along the reaction coordinate. The maximum point of interaction energy corresponds to the point where the main component of reaction coordinate is transformed from the HF stretching to the relative motion of two fragments. Therefore the energy difference between the transition state and this point is expected to be accumulated in the HF vibration in the product.

Reference

1) P. N. Clough, J. C. Polanyi, and R. T. Taguchi, *Can. J. Chem.*, 48, 2920 (1970).

Table I. Calculated Energies of Reactant, Transition State and Product.

CH_3CH_2F	staggerd	0^a
	eclipsed	3.26
Transition State		74.6
$CH_2 = CH_2 + HF$		22.3

^{a} All values are given in kcal/mol.

Table II. Energy Decomposition Analysis of the Reverse Activation Energy^a

Deformation Energy	HF	43.6
	C_2H_4	10.2
Interaction Energy		−1.5
ES		−52.3
EX		156.9
CT		−68.4
PL		−22.7
MIX		−15.0

^{a} All values are in kcal/mol.
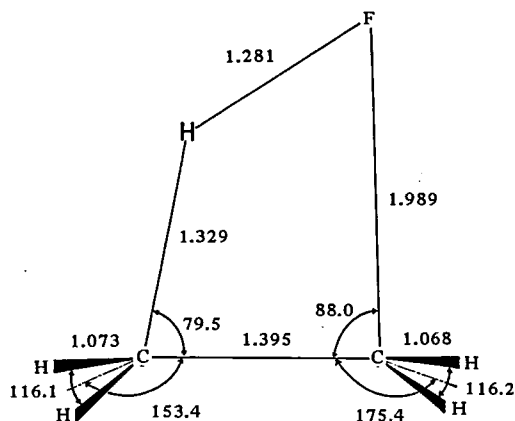
Figure 1. Optimized geometry of the transition state. The bond lengths are given in Å and angles are in degree.

I-C Mechanism of Photochemical Reactions

A complete interpretation of the mechanisms of photochemical reactions is a goal of theoretical chemistry. It requires a detailed knowledge of the ground and excited state potential surfaces as well as of the dynamics on these surfaces, including a crossing from one surface to another. By the development of the ab-initio and semi-empirical methods, it becomes possible to obtain the accurate properties of the potential surfaces.

In this project, the mechanisms of photoisomerization of polyenes and photodissociation of ketene are investigated. In isomerization, it is particularly important to determine the physical properties such as the geometries and the normal modes of the vibronic excitations at the transition region where the transition of the electronic state from one surface to another takes place. The paths of photodissociation of ketene have not been fully elucidated. We examine the orbital and state correlation diagrams for various dissociative paths and carry out ab-initio calculations for the probable paths.

I-C-1 Photoisomerization of Polyenes on Triplet Surface

Iwao OHMINE and Keiji MOROKUMA

For a satisfactory understanding of the photoisomerization process of polyenes, a detail knowledge of their electronic states is necessary. For polyatomic systems with many degrees of freedom, it has been very difficult to determine the accurate properties of potential sur-

faces. Only a few attempts have been made by model calculations.[1] We use a 'gradient method' to calculate the first and second derivatives of the Born Oppenheimer potential with respect to the nuclear coordinates and hence can evaluate the normal modes of vibrations as well as the equibrium and the transition state geometries.[2] Both ab-initio and semi-empirical (MINDO3) methods are applied for ethylene, butadiene, pentadiene, hexatriene and their protonated Shiff basis (PSB) derivatives.

To extract the information concerning the actual course of the isomerization, we determined the intrinsic reaction coordinate (IRC), defined by Fukui and Kato.[3] On the triplet potential surface, the IRC connects the saddle point near the planar configuration and the minimum energy point near the 90°- rotation configuration. On the ground state potential surface, it starts from the transition state of the 90°- rotation configuration and ends at the minimum energy point of the planar configuration. It is found (see Figure 1) that the IRC is consisted of two main components namely, the rotation around the C_1-C_2 bond and the stretchings of all the carbon-carbon bond. Less significant but not negligible is flaping of the H_2, bonded with C_2, against the C_1-C_2-C_3 plane.

To supplement this static approach, we have performed some trajectory studies.[4] We show in Figure 2 the trajectory on the triplet surface of butadiene. The transition state conformation (nearly planar) is chosen as the initial geometry. The trajectory starts with the small velocity to the direction of the lowest normal mode at the transition state. In the early stage of the trajectory (t < 50 a.u.; 1 a.u. of time = 2.42 × 10^{-17} sec), the motions of the carbon-carbon stretchings, of the flaping of the H_2 and of the C_1-C_2 rotation are all coupled as expected from the IRC in Fig. 1a. After this period, these modes interact in a rather complicated manner. The rotational motion of C_1-C_2 is confined in the region of 0° - 180°. A period of this rotation is 120-140 a.u. which is about a third of the C-H vibrational period. The energy redistribution process from this rotational mode to others such as C-H stretchings is very slow, suggesting that many rotational oscillations of C_1-C_2 take place before the system decays to the lowest rotational state on the triplet surface. It is noted that the rotational mode around C_3-C_4 is also strongly coupled with that of C_1-C_2. This indicates that the double rotations around two C-C bonds (C_1-C_2 and C_3-C_4) can occurs if the different initial condition is employed.

The transition from the excited to the ground state potential surface occurs near the 90°- rotation configuration. The physical quantities around this region are very important in the nature of the surface hopping.[5] The minimum energy geometry of the triplet state and the transition state geometry of the ground state are determined in detail. It is found that these two geometries are very similar. This suggests that at the transition region the transition from the excited state takes place, in a nearly equal probability, to the

ground state of the cis-form and to that of the trans-form. The normal modes are calculated. It is found that the corresponding modes of these two states are also very similar except the rotation. Thus only significant accepting mode seems to be the rotation of C_1-C_2.

References

1) W. Warshel and M. Karplus, *J. Am. Chem. Soc.*, **94**, 5612 (1972).
2) J. Gerratt and I. Mills, *J. Chem. Phys.*, **49**, 1719 (1968). J. W. McIver, Jr. and A. Komornicki, *J. Am. Chem. Soc.*, **94**, 2625 (1972).
3) K. Fukui, S. Kato and H. Fuzimoto, *J. Am. Chem. Soc.*, **97**, 1 (1975). S. Kato and K. Fukui, ibid, **98**, 6395 (1976). K. Ishida, K. Morokuma and A. Komornicki, *J. Chem. Phys.*, **66**, 2153 (1977).
4) A. Warshel and M. Karplus, *Chem. Phys. Lett.*, **32**, 11 (1975).
5) W. M. Gelbart, K. Freed and S. A. Rice, *J. Chem. Phys.*, **52**, 2460 (1970). J. N. Kushick and S. A. Rice, *J. Chem. Phys.*, **64**, 1612 (1976).
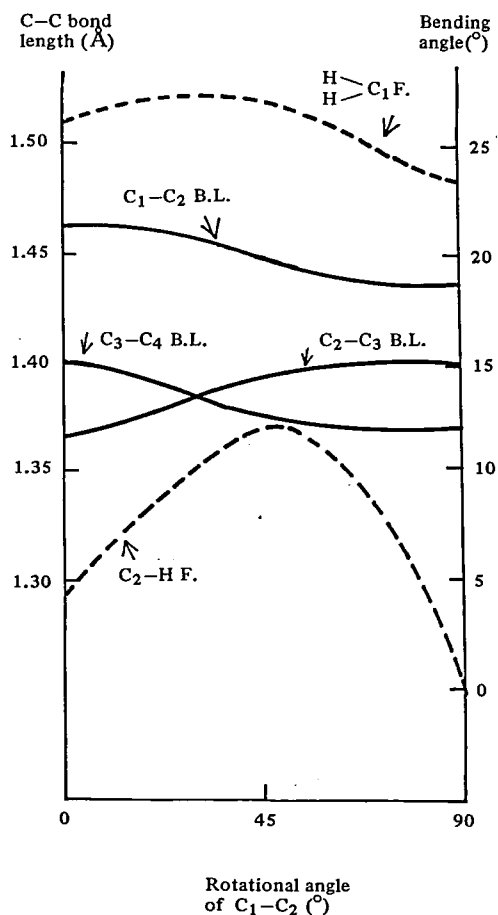
Figure 1a. Intrinsic Reaction Coordinate of the butadiene triplet state. B. L. stands for bond length; F for flaping angle.

C–C Bond
length (Å)

Bending
angle (°)

Rotational angle
of C_1–C_2 (°)

Figure 1b. Intrinsic Reaction Coordinate of the butadiene gound state.

Rotational
angle (°)

Bond
length (Å)

Time (a.u.)
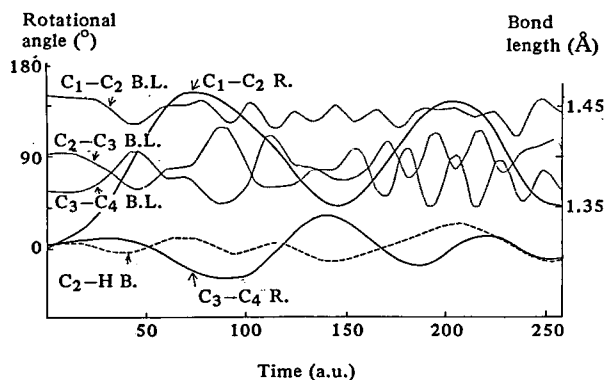
Figure 2. A trajectory of the butadiene triplet states. Initial geometry is the transition state conformation near the planer configuration. Initial velocity is taken to be $T_{kinetic}$ = 0.45 kcal to the direction of the lowest normal mode at the transition state. R stands for rotational angle; B. L. for bond length; B for bending.

I-C-2 Theoretical Study on the Paths of Photodissociation: $CH_2 = C = O \rightarrow CH_2 + CO$

Shinichi YAMABE *(Univ. of Rochester and Nara Univ. of Education)* and Keiji MOROKUMA *(Univ. of Rochester and IMS)*

The mechanism of photochemical dissociation of ketene appears to be rather complicated and is not fully understood. Theoretical studies[1,2] have not elucidated all the paths of the reaction. In the present study we have examined molecular and state correlation diagrams for various dissociation paths for the ground and lower excited states of ketene, and carried out ab initio calculations for probable paths.

Eight high lying "active" electrons are essential in determining the correlation diagrams. In the least motion symmetry C_{2v} they have the configuration $(7a_1)^2$ $(1b_1)^2(2b_2)^2(2b_1)^2$ for ketene and $(2b_2)^2(1b_1)^2(7a_1)^2$ $(8a_1)^2$ for the product. Using the set of numbers of electrons in a_1, b_1, and b_2 representations as an index, one finds that in the $^1A_1$ ground state the reactant (2, 4, 2) has a different set from the product (4, 2, 2) and therefore, the reaction is forbidden. Similarly $^{3,1}A_2$ and $^{3,1}A_1$ excited states are correlated to higher excited states and their C_{2v} reaction paths are forbidden.

As is shown in Figure 1, the path in which ketene is bent in its molecular plane becomes allowed for the $^{3,1}A_2(\pi \rightarrow \pi')$ excited states. The path in which ketene carbonyl is bent out of plane, maintaining the overall C_s symmetry, is allowed for both the $^1A_1$ ground and the $^{3,1}A_1(\pi \rightarrow \pi^*)$ excited states.

Ab initio SCF calculations with a minimal basis set were carried out to optimize the geometry for various values of the C-C interatomic distance. The energy profiles and the geometry changes along the calculated minimum energy paths are shown in Figure 2. Both the triplet bent-in-plane $^3A''$ and the bent-out-of-plane $^3A'$ path have a large barrier, whereas the corresponding singlet paths are simply uphill or would have a small barrier.

References

1) H. Basch, Theo. Chem. Acta, **28**, 151 (1973).
2) P. Pendergast and W. H. Fink, J. Am. Chem. Soc., **98**, 648 (1976).
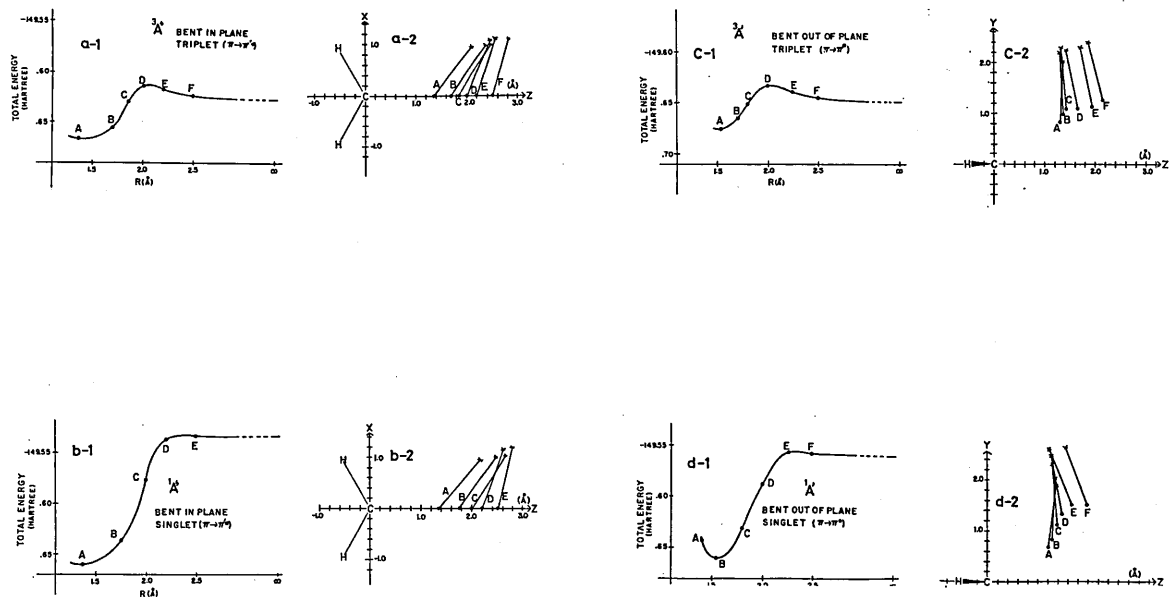
Figure 2.
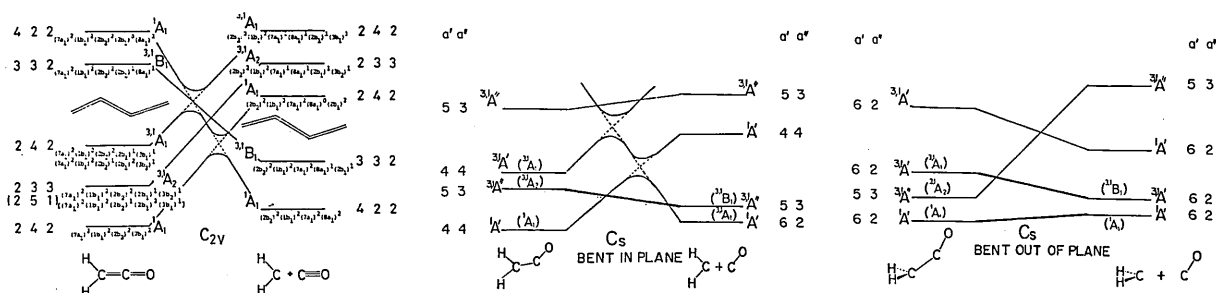
Figure 1.

I-D Energy and Force Analyses of Molecular Interactions

Molecular orbital methods have proved themselves very useful in predicting geometries of molecular interaction complexes. The energy analysis developed by Morokuma and coworkers has provided theoretical tools for elucidating the origin of such molecular interactions, by separating the interaction energy into physically meaningful components. The analysis has been extensively used for studies of hydrogen bonding, electron donor-acceptor complexes and proton affinities. Recently we have extended its application to several other problems, such as the origin of the energy barrier in organic chemical reactions and the stability of perpendicular olefins. We have also found its first application to inorganic chemistry, namely, the origin of the structural stability of a cobalt nitrosyl complex. We expect that the analysis will find a wider applicability in various problems in organic and inorganic chemistry.

I-D-1 The Origin of Electron Donor-Acceptor Complexes, Hydrogen Bonding, and Proton Affinity

Keiji MOROKUMA *(Univ. of Rochester and IMS)*

Atoms and molecules interact with one another. Between the limits of the strong interaction (i.e. chemical bond) and the weak interaction (i.e. van der Waals interaction) there exist various interactions of intermediate strength, including electron donor-acceptor (EDA) complexes and hydrogen bonds. Employing the energy decomposition method developed by the author and his colleagues,[1] we wish to discuss what energy components are essential at the equilibrium geometry of a molecular complex and what components determine the geometry.

EDA complexes:[2] Results of energy analysis for many EDA complexes and shown in Table I. ES is the electrostatic, EX the exchange, PL the polarization, CT the charge transfer and MIX is their coupling energy. ΔE_{SCF} is the sum of these five components. In addition the dispersion energy DISP has to be taken into accounts. A classification for each complex is given in terms of the principal energy components and is meant to be a very qualitative guide to the nature of the interaction. We recognize that these EDA complexes are in general not "charge-transfer" complexes, but rather are a collection of complexes of varying strengths with different origins.

Hydrogen Bonding:[3] Table II summarizes energy components of complexes possessing linear X--H—Y hydrogen bonds. Hydrogen bonds are strongly electrostatic in nature with a small but significant contribution of the charge transfer energy. We define the directionality of a hydrogen bond as the relative orientation of approach of the hydrogen donor Y—H to the acceptor molecule. In $(H_2O)_2$, for instance, the angle between the hydrogen bond axis O--H—O and the bisector T of the proton acceptor's HOH angle is 60°. The analysis indicates that the optimum directionality is dictated by the electrostatic interaction

Table I. Energy Components in kcal/mol at the Optimized Intermolecular Separation R_e and Qualitative Classification of EDA Complexes

Donor-Acceptor	Type	Symmetry	R_e, Å	$\Delta E_{SCF}{}^a$	ES	EX	PL	CT	MIX	DISP^b	Classification
H_3N-BF_3	n-σ*	C_{3v}	1.60	−71.5	−142.3	136.3	−42.7	−52.7	29.9		Strong ES
H_3N-BH_3	n-σ*	C_{3v}	1.70	−44.7	−92.9	86.9	−17.2	−27.1	5.6		Strong ES
OC-BH_3	σ-σ* π*-π	C_{3v}	1.63	−28.5	−60.9	98.9	−61.8	−68.3	63.6		Strong CT-PL-ES
H_3N-ClF	n-σ*	C_{3v}	2.72	−8.2	−11.2	7.4	−1.1	−3.6	0.2		Intermediate ES
H_2O-OC(CN)$_2$	n-π*	C_s	2.70	−8.0	−9.7	4.4	−1.0	−1.8^d		−1.2	Intermediate ES
C_6H_6-OC(CN)$_2$	π-π*	C_s	3.6^c	−4.2	−2.8	1.8	−1.7	−1.6	0.1	−2.6	Intermediate ES-DISP-PL-CT
HF-ClF	n-σ*	C_s	2.74	−3.4	−3.6	1.8	−0.2	−1.4	0.1		Weak ES
H_3N-Cl_2	n-σ*	C_{3v}	2.93^c	−2.9	−4.0	3.9	−0.8	−2.3	0.3		Weak ES-CT
C_6H_6-ClF	π-σ*	C_s	3.6	−1.8	−1.8	0.6	−0.1	−0.8	0.0	−0.5	Weak ES-CT
H_3N-F_2	n-σ*	C_{3v}	3.00	−1.1	−0.8	0.6	−0.3	−0.6	0.0		Weak ES-CT
H_2CO-F_2	n-σ*	C_s	2.91	−0.7	−0.4	0.3	−0.1	−0.5	0.0		Weak CT-ES-DISP
C_2H_4-H_2CO	π-π*	C_s	3.75	−0.7	−0.5	0.4	−0.1	−0.5^d		−0.4	Weak CT-ES-DISP
C_6H_6-Cl_2	π-σ*	C_s	3.6	−0.6	−0.5	0.7	−0.1	−0.8	0.0	−0.7	Weak CT-DISP-ES
C_6H_6-F_2	π-σ*	C_s	3.3	−0.3	−0.2	0.3	−0.0	−0.4	0.0	−0.4	Weak DISP-CT-ES
F_2-F_2	n-σ* π-σ*	C_s	2.7	−0.2	−0.1	0.0	−0.4	−0.4	0.0	−0.2	Weak DISP-CT

^{a} Does not include DISP. ^{b} Estimated by a perturbation calculation. ^{c} Not optimized. ^{d} CT + MIX.

Table II. Energy Components in kcal/mol at the Optimized Intermolecular Geometries^a

Proton acceptor	Proton donor	R_e, Å	θ, deg	ΔE	ES	EX	PL	CT	MIX
H_3N	HF	2.68	0	−16.3	−25.6	16.0	−2.0	−4.1	−0.7
H_2O	HF	2.62	6	−13.4	−18.9	10.5	−1.6	−3.1	−0.4
HF	HF	2.71	60	−7.6	−8.2	4.5	−0.4	−3.2	−0.3
H_3N	HOH	2.93	0^b	−9.0	−14.0	9.0	−1.1	−2.4	−0.4
H_2O	HOH	2.88	60^b	−7.8	−10.5	6.2	−0.6	−2.4	−0.5
H_3N	HNH_2	3.30	0^b	−4.1	−5.7	3.6	−0.6	−1.3	−0.2
H_2O	HNH_2	3.22	60^b	−4.1	−4.6	2.5	−0.3	−1.5	−0.2
H_3N	HCH_3	4.02	0^b	−1.1	−0.6	0.5	−0.3	−0.7	−0.0
H_2O	HCH_3	3.80	60^b	−1.1	−0.5	0.5	−0.1	−0.9	−0.0

^{a} All the complexes are linear, having a linear X–H—Y bond. θ is the between this bond and the molecular axis of the proton acceptor.
^{b} Assumed.

alone. The linearity of the hydrogen bond, the fact that X - - H—Y is nearly linear in most cases, seems to be controlled principally by a balance between changes in the electrostatic attraction and the exchange repulsion upon distortion.

Proton Affinity: The protonated complexes of amines and ethers(alcohols) are 'CT-ES > PL complexes'. However, the alkyl substituent effect is controlled by the change in the polarization interaction.

References

1) K. Morokuma, J. Chem. Phys., 55, 1236 (1971); K. Kitaura and K. Morokuma, Int. J. Quantum Chem., 10, 325 (1976).
2) H. Umeyama and K. Morokuma, J. Am. Chem. Soc., 98, 7208 (1976); H. Umeyama, K. Morokuma and S. Yamabe, J. Am. Chem. Soc., 99, 330 (1977).
3) H. Umeyama and K. Morokuma, J. Am. Chem. Soc., 99, 1316 (1977).

I-D-2 Calorimetric and Molecular Orbital Studies of Hydrogen Bonding between Hydrogen Fluoride and Cyclic Ethers

Mitsunori TSUDA (Kyoto Univ.), Hidekazu TOUHARA (Kyoto Univ.), Koichiro NAKANISHI (Kyoto Univ.), Kazuo KITAURA, and Keiji MOROKUMA

Thermodynamic data for hydrogen bonded complexes are still limited in number and have been so far obtained from infrared study by using the van't Hoff equation. The best values for the thermodynamic functions of complex formation should be obtained by a combined use of calorimetry with spectroscopic measurement.[1,2] The enthalpies of formation of hydrogen bonding complexes ΔH were obtained for hydrogen fluoride (HF)-furan, HF-tetrahydrofuran (THF), HF-2, 5-dimethylfuran(25dmF) and HF-2,5-dimethyltetrahydrofuran(25dmTHF) by precision calorimetry. The frequency shift $\Delta\nu_{HF}$ of H-F stretching vibration due to hydrogen bond formation and the equilibrium constant of complex formation were also obtained by infrared spectra measurement and were used to evaluate free energy and entropy of complex formation. The Badger-Bauer relation was found to exist between ΔH and $\Delta\nu_{HF}$. The ΔH difference between HF-furan (4.8 kcal/mol^{-1}) and HF-25dmF(6.74 kcal/mol^{-1}) was fairly large, while that between HF-THF(7.36 kcal/mol^{-1}) and HF-25 dmTHF(7.41 kcal/mol^{-1}) was almost negligible. ΔH^0 was then corrected for translational, vibrational, vibrational and PV contributions to obtain the electronic contribution ΔE, which is to be compared with the molecular orbital calculation.

Ab initio molecular orbital (MO) caluclations were carried out for HF-furan and HF-THF complexes. The results of energy analysis are summarized in Table I. In both cases HF approaches the oxygen atom on the C_2 axis of the proton acceptor, i.e., $\theta=0$. The energy analysis indicates that θ is determined by the electrostatic interaction. Even for a large acceptor molecule, θ is apparently controlled by the local polarity in the hydrogen bonding rigion.

It has been known that the error in the calculated ΔE is mainly due to the overestimation of the electrostatic interaction.[3] If it is scaled based on values of the dipole moment, a more reliable value of ΔE is obtained.

Table I. Optimum Geometry, Hydrogen Bond Energy and Energy Components in kcal/mol^{-1} for HF - furan and HF -Tetrahydrofuran

	HF - $(CH)_4O$		HF - $(CH_2)_4O$	
Basis set	STO-3G	4-31G	STO-3G	4-31G
Optimum geometry				
R(F-O) (Å)	2.785	2.828[a]	2.644	2.685[a]
θ	0.0	0.0	0.0	0.0
Hydrogen bond energy				
ΔE	−3.63	−8.95	−7.35	−14.40
ΔE_{scaled}		−5.26		−9.89
ΔE_{obs}	−5.0±0.2		−7.17±0.07	
Components				
ES$_{scaled}$		−6.43		−12.83
ES		−10.12		−17.34
EX		4.48		8.39
CT		−1.95		−3.06
CT(B → A)[b]		−1.70		−2.69
CT(A → B)[b]		−0.24		−0.37
PL		−1.15		−1.88
PL(A)[c]		−0.15		−0.41
PL(B)[c]		−0.92		−1.31
MIX		−0.21		−0.51

[a] Estimated from the results of STO-3G. [b] CT(B → A) is the contribution of the charge transfer from proton acceptor to proton donor and CT(A → B) is the contribution of the charge transfer from proton donor to proton acceptor. [c] PL(A) is the polarization of proton donor and PL(B) is the polarization of proton acceptor.

A agreement between ΔE_{scaled} and the observed ΔE_{obs} is satisfactory.

The main difference between HF-furan and HF-THF is due to the electrostatic interaction. The oxygen moiety in furan is less negatively charged than in THF, because electrons on the oxygen atom in furan delocalize through conjugated π-orbitals to decrease the net charges on the oxygen atom. π orbitals do not play a primary role in CT. A small but distinct difference due to conjugated π-electrons can be seen in the polarization of the proton acceptor. However, a much larger effect of π-electrons can be seen in the contribution of PL on the electron redistribution.

References

1) M. D. Joesten and L. J. Schaad, "Hydrogen Bonding", Marcel Dekker, New York, N.Y. 1974.
2) D. V. Fenby and L. G. Hepler, Chem. Soc. Rev., 3, 193 (1974).
3) H. Umeyama and K. Morokuma, J. Am. Chem. Soc., 99, 1316 (1977).

I-D-3 Energy, Charge and Spin Decomposition Analyses at the Transition State and Along the Reaction Pathways of Organic Reactions

S. NAGASE (Univ. of Rochester) and K. MOROKUMA (Univ. of Rochester and IMS)

For a theoretical investigation of reactivities in various organic reactions, it is extremely important to elucidate what types of chemical interactions play essential roles and clarify how effectively the charge and spin redistributions occur during the course of a chemical reaction. In earlier theoretical studies only a portion of interactions are explicitly considered. The static model considers only the electrostatic interaction. The success of Fukui's HOMO-LUMO interaction scheme[1] and the symmetry rule by Woodward and Hoffmann[2] in principle reply on the importance of the charge transfer interaction. It is essential to assess energy components in apparently complicated organic reactions.

We express the reaction energy ΔE as a sum of the intramolecular deformation energy DEF and the intermolecular interaction INT, which in turn is expressed as a sum of physically meaningful terms. Actual calculations were carried out within the framework of the ab initjo SCF theory with a 4-31G basis et. The transition state and the reaction intermediate geometries were taken from published theoretical papers.

Conclusions drawn from the study can be summarized as follows.

1. The deformation energy DEF plays an important role at the transition state and is often the principal source of activation energy. As an example, the variations in INT as well as DEF and $\Delta E=INT+DEF$ are
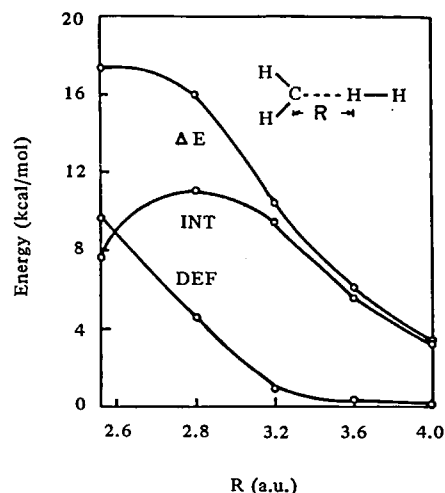
Figure 1. Variations in the intermolecular INT energy, the intramolecular DEF energy, and the reaction barrier ($\Delta E=INT + DEF$) along the reaction pathway of $H_2 + {}^3CH_2$.

Table I. The Relative Importance of the Energy Components at the Transition State, Reaction Intermediate and Stable Complexes

	Ratio[a]	Relative importance %		
		ES	PL	CT
Addition Reaction				
$CH_2 = CH_2 + CH_3^+$	1.60	37	23	40
$CH_2 = CH_2 + Cl^+$	1.58	31	40	29
$CH_2 = CH_2 + HCl$	0.91	46	13	41
$CH_2 = CH_2 + H$	1.39	27	9	64
$CH_2 = CHF + H$	1.41	27	9	64
Addition Reaction				
$CH_4 + H$	0.98	13	6	81
$CH_4 + Cl$	1.01	29	39	32
$H_2 + {}^3CH_2$	0.91	33	13	54
Substitution Reaction				
$CH_4 + H^-$	1.30	48	17	35
$CH_3F + F^-$	1.87	62	9	29
Hydrogen Bond				
$H_2O - H_2O$	2.26	78	4	18
$H_2O - HF$	2.24	80	7	13
$HF - HF$	2.67	70	3	27
EDA Complex				
$H_3N - BH_3$	1.48	12		20
$H_3N - ClF$	1.14	71	7	22
$OC - BH_3$	1.18	32	32	36

[a] The ratio of the attractive and the repulsive INT interaction.

plotted in Fig. 1 along the reaction paths of $H_2+{}^3CH_2$. DEF increases monotonically as the reaction approaches the transition state. INT increases (repulsion) at the early state of reaction and then decreases significantly to reach the transition state. The difference in the activation energy is often determined by the difference in DEF.

2. The nature of interactions vary substantially among various reactive and nonreactive systems. Table I sum-

marizes the relative importance of three attractive energy components for various chemical reactions as well as nonreactive interactions such as hydrogen bonds and electron donor-acceptor complexes. The radical addition and abstraction are dominated by the charge transfer interaction CT. For softer radicals the polarization PL and electrostatic ES interaction becomes increasingly important. In the cationic addition PL as well as CT and ES gives a significant contribution. The nucleophilic substitution is of ES and CT in nature. In general CT interaction plays the most important role in all the reactions and ES and PL becomes significant on the ionic character of the reaction increases. The largest single factor distinguishing reactive system from nonreactive systems is the charge transfer interaction.

References

1) K. Fukui, *Acc. Chem. Res.*, 4, 57 (1971), and earlier references therein.
2) R. B. Woodward and R. Hoffmann, "The Conservation of Orbital Symmetry", Academic Press, New York, 1969 and earlier references therein.

I-D-4 Relative Stability of Planar and Perpendicular Olefins

Shigeru NAGASE *(Univ. of Rochester)* and Keiji MOROKUMA *(Univ. of Rochester and IMS)*

A number of experimental and theoretical investigations have been made on thermal rotational isomerizations about carbon-carbon double bonds as well as photochemical and catalytic isomerizations. The high rotational barrier of ethylene should be lowered significantly by a proper selection of substituents. Their effects are thought to be both steric and electronic in origin. Recently Apeloig *et al* [1] have examined the substituent effects with an ab initio molecular orbital method. It was found that the rotational barrier of 1,1-dilithioethylene not only is very low, but the perpendicular form may actually be more stable than the planar form.

Our purpose here is to analyze and find the origin of the rotational barrier around a double bond from the point of view of intermolecular interactions. The interaction energy between two substituted methylene fragments was analyzed within the framework of the ab initio unrestricted Hartree-Fock theory in terms of electrostatic, exchange repulsion, polarization, charge transfer and their coupling components.[2] The olefins we have investigated are $CX_2=CH_2$(X=H, Li, F, CH_3, CN, BeH and Na), $CX_2=CY_2$(X=Li, CH_3 and Y=F, CN), and polylithioethylene.

The results of energy decomposition analysis are shown in Table I, where $\Delta\Delta E$ is the energy difference between the perpendicular and the planar form, and a positive and a negative value indicates that the planar and the perpendicular form, respectively, is more stable.

Table I. Energy Decomposition Analysis for the Relative Stability of the Planar and Perpendicular $CX_2=CH_2$[a] 4-31G Basis Set

	$CH_2=CH_2$	$CLi_2=CH_2$	$CF_2=CH_2$
Δ ES	−1.0	−0.7	−1.6
Δ EX	23.6	0.6	24.3
Δ PL	0.1	−2.3	−0.6
Δ CT	21.6	2.5	22.9
Δ MIX	2.2	−1.0	4.5
$\Delta\Delta E$[b]	46.5 (46.1)	−0.9 (−1.5)	49.5 (48.8)

[a] Values, given in units of kcal/mol, are the energy of the perpendicular form relative to th planar form. [b] Values in parentheses are obtained by the STO-3G basis set.

ΔES is the electrostatic energy difference, ΔEX is the exchange repulsion difference, ΔPL is the polarization energy difference, the charge transfer energy difference and ΔMIX is their coupling term. In ethylene the perpendicular form is less desirable due to a large increase in the EX repulsion and a large decrease in the CT stabilization. ES and PL change very little during the rotation. The F substitution ($F_2C=CH_2$) increases the barrier ΔE by a small amount due to a small destabilization of CT and EX. The Li substitution ($Li_2C=CH_2$) drastically reduces the CT and Ex destabilization.

An examination of the electron distribution allows us to make the following qualitative description of the bonding between the carbon atoms in the perpendicular form, as is illustrated below.
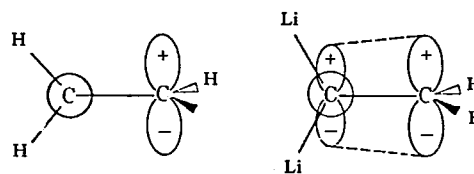
In ethylene a π bond is broken and a nonbonding biradical state is formed. In the case of $CLi_2=CH_2$, however, a bonding orbital is formed within the Li-C-Li plane, but not within the H-C-H plane.

References

1) Y. Apeloig, P. v. R. Schleyer, J. B. Binkley and J. A. Pople, *J. Am. Chem. Soc.*, 98, 4332 (1976).
2) K. Kitaura and Morokuma, *Int. J. Quantum Chem.*, 10, 325 (1976).

I-D-5 Force Decomposition Analysis Along Reaction Coordinate

B. D. JOSHI *(State Univ. College at Geneseo)* and Keiji MOROKUMA *(Univ. of Rochester and IMS)*

The intrinsic reaction coordinate (IRC) is defined as

the classical trajectory, obtained by integration equations of motion, which starts at the saddle point and proceeds "down hill" infinitely slowly.[1] The method of calculating IRC involves at first a search for the saddle point and a subsequent search for the direction of the energy gradient in the mass weighted Cartesian coordinate system.[2] A practical method of the determination and characterization of saddle points by ab initio molecular orbital methods has been established.[3] An IRC within the ab initio SCF framework has been obtained for a model S_N2 reaction[2]: $CH_4 + H^- \rightarrow H^- + CH_4$. (1)

In the present work we have developed an analytical method for the direct calculation of the force contributions (deformation DEF, electrostatic ES, charge transfer CT, exchange EX, polarization PL, and the coupling MIX). Using the similar technique as was used for energy components,[4] one can express the total force (the negative of the energy gradient) as

$$F(TOT) = F(DEF) + F(INT)$$

where the force of interaction can be further separated as

$$F(INT) = F(ES) + F(CT) + F(PL) + F(EX) + F(MIX)$$

If the mass weighted Cartesian coordinates are used, the direction of IRC is defined as the direction of the energy gradient. There, if e is the unit vector in the direction of the IRC, then

$$F_{IRC}(TOT) \equiv e \cdot F(TOT) = F(TOT)$$

That means the total force acts in the direction of IRC. Various force contribution $F(X)$ can be separated to the component $F_{IRC}(X)$ which is parallel to IRC and is therefore responsible for the net movement of reaction along IRC, and $F_\perp(X)$ which determines the inter-

DEF
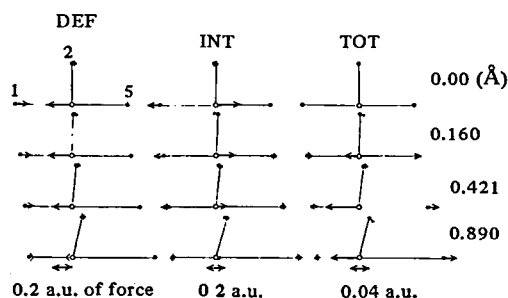
Figure 1. A pictorial representation of DEF, INT, and TOT forces on representative atoms at four selected points on the IRC. The small circles O indicate carbon atoms, and the dots ● indicate hydrogen atoms. The hydrogen atoms in all pictures are numbered as shown in the first one. Here 1 stands for H(1), etc. The atoms shown lie in the XZ plane with the Z axis pointing towards H(5), and the X axis pointing towards H(2). The magnitudes of forces are represented by the lengths of the arrows according to the scales shown. Different size arrows are used for reasons of clarity.
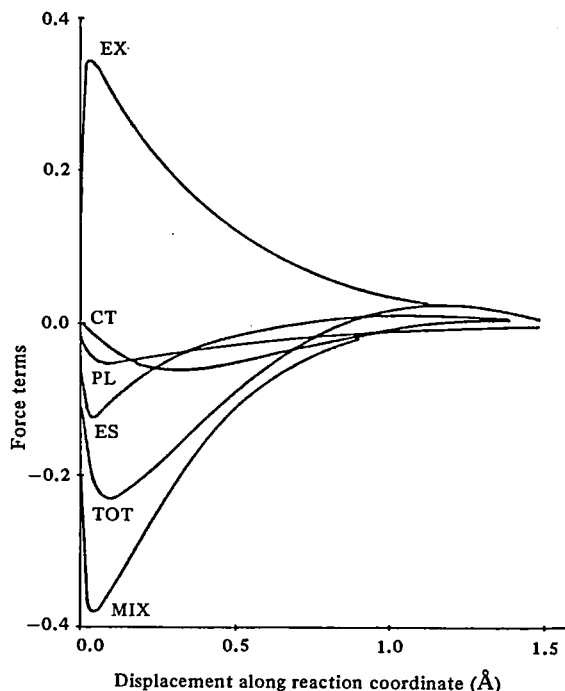
Figure 2. Interaction force and constituent terms as functions of the displacement along the reaction coordinate for the reaction: $CH_4 + H^- \rightarrow H^- + CH_4$. All forces are given in atomic units.

nal coordinate excitations.

$$F(X) = F_{IRC}(X) + F_\perp(X)$$

where X represents ES, CT, EX, PL, MIX or DEF.

An actual calculation of force contributions was carried out for the reaction 1. The total, deformation and interaction forces are shown in Fig. 1 for a few selected points along IRC. Figure 2 shows the interaction force contributions $F_{IRC}(X)$ which are effective for reaction. Near the saddle point the MIX force which is principally the coupling between CT and PL plays the most important role in advancing the reaction.

References

1) K. Fukui, J. Phys. Chem., 74, 4146 (1970).
2) K. Ishida, K. Morokuma and A. Komornicki, J. Chem. Phys., 66, 2153 (1977).
3) A. Komornicki, K. Ishida, K. Morokuma, R. Ditchfield and M. Conrad, Chem. Phys. Lett., 45, 595 (1977).
4) K. Kitarua and K. Morokuma, Int. J. Quantum Chem., 10, 325 (1976).

I-D-6 The Relative Stability of Bent and Linear Coordination of the Nitrosyl Ligand in [CO(NH₃)₅NO]⁺²

I-D-6 The Relative Stability of Bent and Linear Coordination of the Nitrosyl Ligand in [CO(NH₃)₅NO]⁺²

J. O. NOELL *(Univ. of Rochester)* and Keiji MOROKU-MA *(Univ. of Rochester and IMS)*

The coordination of the nitrosyl ligands to metals of the first and second transition series is currently the subject of intense research interest in both structural and interpretive inorganic chemistry. Frenz and Ibers distinguished three classes of complexes:[1] linear nitrosyls in which the M-N-O bond angleϕ is very nearly equal to 180°, bent nitrosyls whose ϕ is in the vicinity of 120°, and intermediates between the two extremes. Walsh-type diagrams have been successfully used to predict the bimodality of the nitrosyl ligand as well as many substituent effects on the nitrosyl coordination.[2,3]

We have chosen to examine in detail, using ab initio MO techniques, the nature of the nitrosyl ligand in a single, well characterized complex, $Co(NH_3)_5NO^{+2}$, an example of the bent class of complexes (ΔM-N-O=ϕ= 119°). The calculation was carried out at two levels. One is the full SCF calculation with a split valence basis set, and the other is a fractional charge model SCF calculation in which only the nitrosyl group and the cobalt atom are explicitly included in the calculation and the ammonia ligands are represented by fractional charges placed on each atom. The energy analysis was carried out mostly by dividing the electrons into the tripositive cobalt pentamine fragment $Co(NH_3)_5^{+3}$ and the nitrosyl anion NO^-, but we also made a comparison of results with a different division $Co(NH_3)_5^+ + NO^+$.

The results are shown in Table I. In agreement with experiment, we find in both calculations that the most stable of the conformations examined is the 119E in which a bent nitrosyl (ϕ=119°) eclipses an equatorial Co-N bond. It is evident from Table I that electrostatic ES and charge transfer CT energies are primarily responsible for the greater stability of the bent modality.

The significance of the electrostatic interaction has be generally neglected in earlier theoretical discussions. NO^-, as well as other diatomic molecules whose π^* orbital is occupied, has an electron distribution which is more dense in the direction perpendicular to the molecular axis than along the axis. The importance of the charge transfer interaction, especially the charge transfer from the π^* orbital of NO^- to the lowest vacant $1a_1(d_z^2)$ orbital of $Co(NH_3)_5^{+3}$, is a confirmation what has been predicted from the orbital symmetry argument.[3] In the linear conformation the σ orbitals of nitrosyl do not mix strongly with the d_z^2 orbital of the cobalt, because their eigenvalues are too widely spaced.

Why is it that the bent nitrosyl eclipses one of the equatorial ligands? One might suspect the staggered conformation to be the more stable, using a steric hindrance argument as a rational. Indeed in Table I, one finds greater exchange repulsion for the eclipsed conformer. More than compensating for this effect, however, is a difference in the electrostatic interaction favoring the eclipsed conformation. The $d_{x^2-y^2}$ orbital is vacant in the complex, and therefore the electron distribution on the cobalt atom is not spherical but is less densely populated on the equatorial Co-N axes than between the axes. Therefore, the negatively charged NO would prefer the eclipsed conformation to maximize the electrostatic attraction.

We have examined also the origin of the large trans influence in the bent nitrosyl complex as well as its longer M-N bond length in comparison with the linear complex.

Reference

1) B. A. Frenz and J. A. Ibers, MTP international Review of Science, *Physical Chemistry* series **11**, 33 (1972).
2) J. H. Enemark and R. D. Fetham, *Coord. Chem. Rev.*, **13**, 339 (1974).
3) R. Hoffmann, M. M. L. Chen, M. Elian, A. R. Rossi and D. M. P. Mingos, *Inog. Chem.*, **13**, 2666 (1974).

Table I. Energy Decomposition for the Interaction: $Co(NH_3)_5^{+3} + NO^- \rightarrow Co(NH_3)_5NO^{+2}$

ϕ (degree)	E/S[a]	ΔE	ES	EX	PL	CT	MIX
Full calculation							
180		−366.5	−367.5	+80.9	−126.9	−26.7	+74.1
119	E[b]	−408.9	−435.6	+130.9	−67.6	−42.1	+5.5
119	S	−402.9	−416.7	+118.2	−75.8	−36.9	+8.3
Fractional charge calculation							
180		−463.6	−421.3	+58.1	−166.6	−57.1	+123.3
150	E	−533.1	−447.5	+67.5	−129.1	−71.0	+47.1
150	S	−530.8	−432.5	+68.0	−144.4	−70.0	+47.6
119	E	−547.7	−493.5	+109.3	−81.7	−106.2	+24.4
119	S	−546.4	−472.1	+98.4	−101.2	−72.3	+0.8

[a] E and S denote eclipsed ($\alpha = 0°$) and staggered ($\alpha = 45°$) conformers, respectively.

[b] The total energy of the complex for this geometry is −1788.664224 hartree, whereas the energy for $Co(HN_3)_5^{+3}$ and NO^- are −1659.080709 and −128.931890, respectively.

I-E Problems in Molecular Structures

Problems of molecular structures always attract interests of theoretical chemists. What is the structure of some unknown compound? Is it stable to the dissociation or the isomerization? Collaboration with experimentalists is extremely enjoyable. We have recently worked on two problems, as shown in the following. We plan to continue work on any problem which may come up in the future.

I-E-1 The Hydrated Electron as Studied by the Fractional Charge MO Model

J. Oakey NOELL *(Univ. of Rochester)* and Keiji MORO-KUMA *(Univ. of Rochester and IMS)*

We wish to examine with ab initio molecular orbital method the binding of the hydrated electron by the two proposed trapping sites. One is a tetrahedral, tetracoordinate, dipole oriented site proposed by Watanabe and Natori[1] and the other is the a hexacoordinate, octahedral bond oriented site of Kevan.[2] In carring out calculations, we explicitly considered the excess electron and the electrons in the first solvation shell into account, while the second and third solvation shell waters were represented by fractional charges.[3] Calculations are at the unrestricted Hartree-Fock level with the 4-31G basis set supplemented by two diffuse s functions situated at the cavity center. The calculated energetics for electron hydration is shown in Table I. The molecules which were treated as fractional charges were represented by lower case letters. The tetrahedral and the octahedral model are very similar in binding characteristics. The energy of solvation by the prepared host is found to increase linearly with the number of shells. The energy required to break hydrogen bonds in bulk water is expected to increase linearly with the number of water molecules. One therefore expects to have the largest number of shells the electron can orient.

Though the present estimates suggestes none of the ordered, anionic clusters are stable with respect to neutral, bulk clusters, a better estimate of the breakage energy or a consideration of electron correlation effects may lead to an actual binding. Important to notice is that there is a sharp break in the overall energy between the second and the third shell. If the first shell has been contructed, it requires little if any energy to orient a second hydration shell. An electron apparently is not capable of orienting the third hydration shell.

The spin density of the first shell proton sites has also been calculated. It is negative, in accord with the Knight shift experiment for the ammonated electron and with Newton's calculations[4] based on tetracoordinate models. But this is in disagreement with Kevan's interpretation of his experiment.

References

1) M. Natori and T. Watanabe, *J. Phys. Soc. Jpn.*, **21**, 1573 (1966); K. Kawabata, *J. Chem. Phys.*, **65**, 2235 (1976).
2) L. Kevan, *J. Phys. Chem.*, **79**, 2846 (1975); S. Schlick, P. A. Narayama and L. Kevan, *J. Chem. Phys.*, **64**, 3153 (1976)..
3) J. O. Noell and K. Morokuma, *J. Phys. Chem.*, **80**, 2675 (1976).
4) M. D. Newton, *J. Phys. Chem.*, **79**, 2795 (1975).

Table I. Energetics of Electron Hydration (in kcal/mole)[a]

Model (R^a)	Tetrahedral (3.0 Å)			Octahedral (3.086 Å)		
Number of shells	1	2	3	1	2	3
1	4	4	4	6	6	6
m	0	8	8	0	12	12
n	0	0	16	0	0	24
Surface Tension of Cavity[b]	11.9	11.9	11.9	10.3	10.3	10.3
Breakage of hydrogen bonds in bulk water[c] $(H_2O)_{1+m+n} \rightarrow (1 + m + n)H_2O$	22.5	90.0	>210	45.0	157.5	>315
Preparation of the host from free molecules $1H_2O + mh_2o + nh_2o \rightarrow (H_2O)_1(h_2o)_m(h_2o)_n$	7.7	−15.5	−48.1	10.9	−9.4	−19.8
Solvation by the prepared host $e^- + (H_2O)_1(h_2o)_m(h_2o)_n \rightarrow e^-(H_2O)_1(h_2o)_m(h_2o)_n$	−10.3	−56.1	−108.5	−10.9	−89.0	−171.7
Overall $e^- + (H_2O)_{1+m+n} \rightarrow e^-(H_2O)_1(h_2o)_m(h_2o)_n$	32	30	>65	55	68	>134

[a] Negative energies denote stabilization. [b] Estimated by the method described by Newton.[4] [c] From the MO calculation for $H_2O + (h_2o)_4 \rightarrow H_2O(h_2o)_4$ in the ice I_h structure, the hydrogen bond energy is assumed to be 7.5 kcal/mol per bond.

I-E-2 Protonation Complexes of R_2CS: R_2HCS^+ or R_2CSH^+?

Keiji MOROKUMA and Tokio YAMABE *(Kyoto Univ.)*

There is no doubt that the protonation of the ketone and aldehyde carbonyl groups takes place on the oxygen atom. There have been discussions as to the position of protonation of thioketones and thioaldehydes. Yamabe et al.[1] interpreted ^1H and ^{13}C NMR as well as electronic absorption spectra as an evidence that protonation of $(RC_6H_4)C=S$ (R=H or CH_3) takes place at the carbon atom, while it occurs at the sulfur atom for $(t-C_4H_9)_2C=$ S. McLafferty et al.[2] uses the collision activation mass spectra to show that in the gas phase both the S-protonated and the C-protonated form can be detected for $R_1R_2CSH^+$ ($R_1=R_2=H$, CH_3 and $R_1=CH_3$, $R_2=C_2H_5$) and that for these thioaldehydes and ketones studied the S-protonated form is more stable than the C-protonated form.

An ab initio calculation has been published for $CH_2=SH^+$ but none for H_3C-S^+.[3] We have carried out geometry optimization for both the triplet and the singlet state of H_3C-S^+ as well as the singlet $CH_2=SH^+$ with the ab initio Hartree-Fock method. With the 4-31G basis set the lowest in energy is the C-protonated triplet in a C_{3v} symmetry with a long C-S bond (1.94Å). The C-protonated singlet has a geometry very similar to that of the triplet, with an energy about 37 kcal/mol above the triplet. The S-protonated singlet of Bernardi et al.[3] lies about 18 kcal/mol higher in energy than the C-protonated triplet. An additional calculation with the polarized basis set (4-31G+a set of d orbitals on S and C and a set of p orbitals on H) changes the trend somewhat: the S-protonated singlet is the lowest and the C-protonated triplet and singlet are 7 and 44 kcal/mol, respectively, above it.

The energy analysis[4] was carried out for $H_2C=SH^+$, H_3C-S^+ (triplet), $H_2C=OH^+$ and H_3C-O^+ (triplet). $H_2C=SH^+$ and $H_2C=OH^+$ have similar energy components. The critical difference in the behavior between H_2CS and H_2CO comes from the energy difference between their C-protonated forms. H_3C-S^+ is much stable than H_3C-O^+ for the two reasons: 1) a smaller energy required to deform H_2CX in the equilibrium geometry to the geometry it takes in the complex, and 2) a larger intermolecular stabilization, mainly due to a less repulsive electrostatic energy and a more attractive polarization energy. The first factor reflects the fact that C=S bond is weaker and does not require as much energy as the C=O bond to stretch. The second factor indicates that the carbon atom in H_2CS has a larger electron density than in the H_2CO and that the C=S bond is more easily polarizable than the C=O bond.

Based on these results, we make the following two proposals. (1) Some thioketones and thioaldehydes may actually have the C-protonated triplet as the ground state. (2) For some thioketones and thioaldehyde the lowest singlet complex may even be a C-protonated form.

References
1) T. Yamabe, S. Nagata, K. Akagi, R. Hashimoto, K. Yamashita, K. Fukui, A. Ohno and K. Nakamura, *J. Chem. Soc. PerkinII*, 1516 (1977).
2) J. D. Dill and F. W. McLafferty, *J. Am. Chem. Soc.*, 100, 2907 (1978); B. Van de Graaf and F. W. McLafferty, *J. Am. Chem. Soc.*, 99, 6806, 6810 (1977).
3) F. Bernardi, I. G. Csizmadia, H. B. Schlegel and S. Wolfe, *Can. J. Chem.*, 53, 1144 (1975); F. Bernardi, I. G. Csizmadia, A. Mangini, H. B. Schlege, M. Whargbo and S. Wolfe, *J. Am. Chem. Soc.*, 97, 2209 (1975).
4) K. Kitaura and K. Morokuma, *Int. J. Quantum Chem.*, 10, 325 (1976).

I-F   Extension of Discrete-Variational $X\alpha$ Cluster Method and Its Application to the Surfaces of Metallic Oxides

Investigation of the electronic structure of solid surfaces, including edge, corner, or various surface defects is the first step towards the elucidation of mechanism of inhomogeneous catalyses, electrode processes and so on. One of the practical and reliable approaches to the study of the surface electronic structure is the discrete-variational (DV) $X\alpha$ cluster method. We extended the applicability of the DV-$X\alpha$ method to the surface of ionic crystals by inventing a scheme to include the Madelung potential of the indented solid.

As typical metallic oxides which are also important from the view point of practical applications, we chose MgO, TiO_2 and $SrTiO_3$ crystals. The surface of these crystals including various defects have been investigated by the extended DV-$X\alpha$ method. A study is in progress on mechanisms of chemisorption on these surfaces.

I-F-1 Surface Electronic Structure of MgO Crystal

Chikatoshi SATOKO, Masaru TSUKADA and Hirohiko ADACHI *(Osaka Univ.)*

Experimental investigations[1~3] by the use of new techniques such as ELS, LEED and ESR have recently been made for the surface of the MgO crystal. There have been some discussions[4] on the surface state of the ionic crystal by the point charge model. They could not explain the surface state energy observed in the LEED. The simple point charge model can not treat subtle composite effects on the partially ionic crystal surface due to the reduction in the Madelung potential,

the polarization of the wave function, ionic charge redistribution. In order to obtain more reliable results, one may want to calculate the surface electronic structure with the ab-initio method or the Xα method. The latter is more practical than the former for cluster calculations because of economical reasons.

The SW-Xα method[5] has been applied to the bulk cluster embedded in ionic crystals. In this procedure, the muffin-tin potential approximation to the Hartree-Fock-Slater (HFS) Hamiltonian becomes more questionable for the calculation of the surface electronic structure which is affected by the potential gradient near the surface. On the contrary, the DV-Xα method is promising for the study of the electronic structure at the surface, where the potential variation is large in the inter-atomic region. The crystal potential can be easily treated by introducing the electronic additive potential.

The electronic structures of the clusters $(MgO_6)^{10-}$ and $(MgO_5)^{8-}$ are calculated with the DV-Xα method, as shown in Figure 1, in which the Coulomb potential for the HFS Hamiltonian is determined from the sum of the spherically averaged atomic potential and the additive potential of ions outsides the clusters.

The external potential along the [100] direction with the central bulk cluster $(MgO_6)^{10-}$ removed is so flat around the cluster that the electronic states of the cluster undergo uniform downward shift. On the other hand, the external potential for the surface cluster is

different from that for the bulk cluster in the following respects. Firstly, an impression of the high electric field along the perpendicular direction to the surface is generated around the surface Mg^{2+} ion due to the absence of the ions outside the surface. Secondly, the Madelung potential on the surface is greatly decreased from that in the bulk. The former effect causes the polarization of the surface Mg^{2+} ion, so that the energy level of the Mg^{2+} $11a_1$ orbital shifts downward into the energy gap. The charge transfer from the anion to the cation occurs by the combined effects of the above two, which reduces the energy gap, as shown in Figure 1. As typically shown in the present model, the surface states of partially ionic crystal is determined as a result of intricately combined effects. The protrusion of the wave function from the surface resulted by the strong polarization effect generally increases the reactivity of the surface.

References

1) Y. Murata and S. Murakami, private communication.
2) K. O. Legg, M. Prutton and C. G. Kinniburgh, J. Phys. C7, 4236 (1974).
3) N. Wong and J. H. Lunsford, J. Chem. Phys. 55, 3007 (1971).
4) J. D. Levene and P. Mark, Phys. Rev. 144, 751 (1966).
5) K. H. Johnson and F. C. Smith, Jr., Phys. Rev. B5, 831 (1972).

I-F-2 Surface Defects of MgO Crystal and Chemisorption

Chikatoshi SATOKO, Masaru TSUKADA, Kazuo KITAURA and Hirohiko ADACHI (Osaka Univ.)

Surface defects such as edge, corner, step and surface vacancy are known experimentally, to be more active in catalytic processes than the clean surface. Shesters and Somorjai have[1] investigated the reactivity of the surface defects. They observed that the nature of the interaction of the stepped surface and the surface vacancies with gas is different from that of the clean surfaces. The surface defects[2] of the TiO$_2$ crystal formed by Ar sputtering raises the reactivity of the photodissociation of the hydroxyle. Lunsford and Jayne[3] have also studied the nature of various types of defects on surface produced by high irradiation. Surface oxygen vacancies of degassed MgO, termed an S centers, are shown to be effective in catalysis of the chemisorbed CO_2, O_2, and NO_2. The corner and the defects on surface of the MgO crystal have been said to be important as reaction sites of the hydrogen-deuterium isotopic exchange.

From a theoretical point of view, there have been some discussions on the correlation between the properties of clean metal surface and reactivity for catalytic processes. The effects of surface defects on catalytic processes, however, have received little attention. This work is to calculate the electronic structure of the surface defects of the typical crystal MgO with
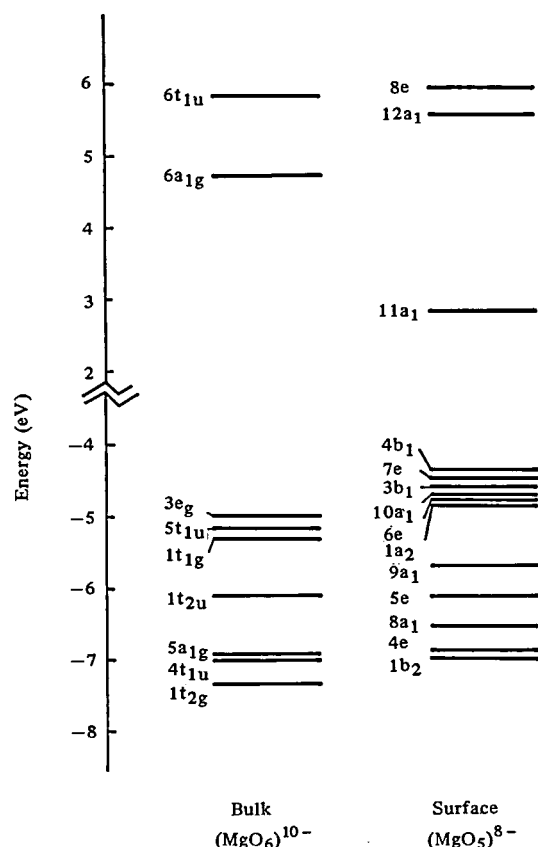
Figure 1. DV-Xα electronic energy levels for bulk $(MgO_6)^{10-}$ cluster and surface $(MgO_5)^{8-}$.

both the DV-Xα method and the ab-initio LCAO–HF method,[4] and to study the effects of surface defects on the catalytic processes.

We choose $(MgO_5)^{8-}$, $(Mg_6O_4)^{2+}$, $(Mg_4O_{3 \text{ or } 4})^{2+ \text{ or } 0}$ and Mg_8O_9 as the model clusters, respectively, for the plane, edge, corner, and surface vacancy. We make theoretical computations of the electronic states of the above clusters taking into account the effect of the indented surface outside the clusters. The ions outsides the clusters are considered as the fixed point charges with the formal valence (Mg^{2+} and O^{2-}). The results of the calculated electronic structure are shown in Figure 1, in which the solid line is obtained from the DV-Xα method in our previous work, and the dotted line from the ab initio HF method with the double zeta basis set.[6] The top of each valence band is scaled to fit the relative energy equal to zero. The orbital energy in the HFS Hamiltonian is the energy per electron required to pull out an infinitesimal amount of electrons from an occupied orbital to vacuum or to put the same from vacuum to an unoccupied orbital. The lowest transition energy is given approximately by the difference between the occupied and unoccupied orbital energies. The hole potential method is used for the calculation of unoccupied levels in ab initio calculations so that a direct comparison can be made of electron energy levels with the DV-Xα method.

The following trends are found in the results of the electronic structure in Figure 1 as the clusters change from bulk to corner: (A) the band gap narrows more and more (B) the surface state mainly composed of the Mg^{2+} 3s orbital shifts into the middle of the band gap (C) the Mulliken charge on the surface Mg ion become more neutral (1.98 for the bulk and 1.08 for the corner) (D) the covalency of the Mg-O bond increases. The above behavior indicates that the corner and edge should interact more actively with gas molecules than the
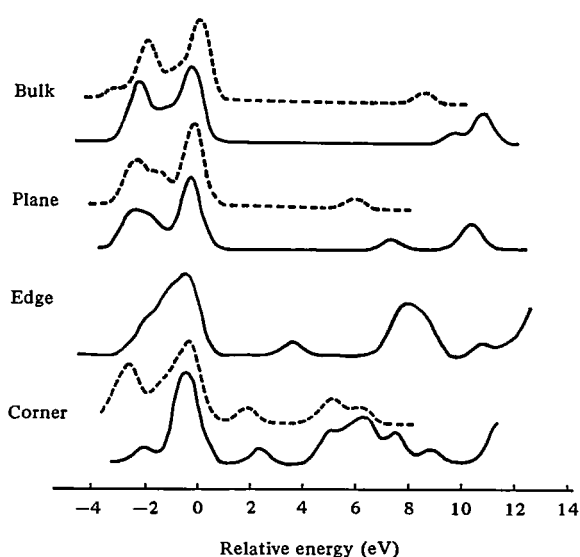
ideal surface, because of the protrusion of the gap state wave functions and their flexibility to the adsorbate perturbations. The role of these states as electron donors or acceptors is also important in redox reactions on the surface. Theoretical studies of radical reactions at the S center on the MgO surface are now in progress.

References

1) M. A. Shesters and G. A. Somorjai, Surf. Sci. 52, 21 (1975).
2) W. J. Lo, Y. W. Chung and G. A. Somorjai, Surf. Sci. 71, 199 (1978).
3) J. H. Lunsford and J. P. Jayne, J. Chem. Phys. 44, 1487 (1966).
4) W. J. Hehre, W. A. Lathan, R. Ditchfield, M. D. Newton and J. A. Pople, GAUSSIAN 70, Program 236, QCPE, Indiana University, 1974.
5) B. Roos and P. Siegbahn, Theoret. Chim. Acta 17, 209 (1970).
6) K. Morokuma and S. Iwata, Chem. Phys. Letters 16, 192 (1972).

I-F-3 Surface Electronic Structure of TiO_2 and $SrTiO_3$

Masaru TSUKADA, Chikatoshi SATOKO, and Hirohiko ADACHI (Osaka Univ.)

The electronic structure of TiO_2 and $SrTiO_3$ surfaces is closely related to their catalytic and photocatalytic activities.

The photo-electrochemical activity of the reduced rutile surface is known to be much stronger than that of the stoichiometric surface. Experimental results suggest that the surface defect states created by the oxygen removal are responsible to the chemical activities of the TiO_2 surface.

To investigate in detail the formation of the surface defect states of the reduced TiO_2 surface, we applied the DV-Xα method to the following clusters embedded in the crystal or the crystal surface; $(TiO_6)^{8-}$ (bulk rutile), $(TiO_5)^{6-}$ (including the five-coordinated Ti site on the (110) surface), $(TiO_6)^{8-}$, $(Ti_2O_{10})^{12-}$ (stoichiometric rutile (110) surface, the six-coordinated Ti site is included), $(TiO_4)^{4-,6-}$, $(Ti_2O_7)^{9-,10-}$, $(Ti_2O_9)^{10-,11-}$ (reduced rutile surface).

Results obtained by the molecular orbital cluster calculations are as follows:

1) For the clusters $(TiO_6)^{8-}$ and $(Ti_2O_{10})^{12-}$ of the stoichiometric rutile surface which contain oxygen atoms sticking out of the surface, the width of the oxygen 2p valence band is about 9 eV, which is much broader than that (5 eV) of the bulk or of the cluster $(TiO_5)^{6-}$ with the five-coordinated Ti site. This is explained by the large potential difference between the outer and the inner oxygen site.

2) The ionicity of oxygen is smallest on the outermost layer, largest on the surface plane, and intermediate for the inner oxygen layer. This suggests that the charge of

Figure 1. Electronic densities of states for various types of surface defects based on Gaussian broadened DV-Xα (—) and ab-initio HF (···) cluster energy levels.

ions approaches the bulk value in an oscillatory way as the distance from the surface increases.

3) When two oxygen atoms sticking out of the surface are removed, the lowest d level of the Ti ion sandwitched between the two eliminated oxygen sites becomes occupied and forms the defect state. The location of the defect level agrees well with the UPS and ELS experiments.[1]

4) If only one of the oxygen atoms sticking out of the surface is removed, no occupied d level is formed on the Ti ions adjacent to the vacant oxygen site. However, empty defect states are induced which are mainly composed of the oxygen 2p states in the outermost layer with a considerable mixing of the Ti d states.

Surface d states of transition-metal perovskites play an important role in heterogeneous catalyses. One of the reasons is the reduction of the symmetry imposed potential barrier along the reaction coordinate by virtue of the localized d level.[2] The level location relative to the conduction band edge and the shape of the wave function are important factors determining the activity of the surface state. As a typical example, we choose $SrTiO_3$ crystal and investigate its surface electronic structure. The comparison of the results with those of TiO_2 surface is also profitable for understanding of the effects of the local atomic configuration on the bulk and the surface electronic structure of these substances. DV-Xα calculations are made for the clusters $(TiO_6)^{8-}$(bulk), $(TiO_5)^{6-}$, $(Ti_2O_{10})^{12-}$(surface) embedded in the $SrTiO_3$ crystal.

A large splitting (about 2.5 eV) is found in the $4e_g$ level composed of Ti d states on the surface, whereas the splitting is negligibly small (about 0.2 eV) for the e_g level of Ti on the third atomic layer. The $2 t_{2g}$ level made of Ti d states on the surface layer slightly splits (about 0.2 eV) and shifts downwards by about 0.6 eV to form a surface state. Thus estimated position of the surface state for the ideal crystal surface is within 0.6 eV below the conduction band. This is consistent

with the recent UPS experiments.[3] Investigations for the surface defect states around the oxygen vacancies and for several chemisorption systems are now in progress.

References

1) V. E. Henrich, G. Dresselhaus and H. J. Zeiger, Phys. Rev. Lett. 36, 1335 (1976).
   Y. W. Chung, W. J. Lo and G. A. Somorjai, Surf. Sci. 64, 588 (1977).
2) T. Wolfram and F. J. Morin, Appl. Phys. 8, 125 (1975).
3) R. A. Powell and W. E. Spicer, Phys. Rev. B13, 2601 (1976).

I-F-4 Chemisorption of Hydroxyl Group and Oxygen onto TiO_2 and $SrTiO_3$ Surfaces

Masaru TSUKADA, Chikatoshi SATOKO, Tomoji KAWAI (Division of Electronic Structure), and Hirohiko ADACHI (Osaka Univ.)

The photodissociation mechanism of water molecules on surfaces of TiO_2 and $SrTiO_3$ has recently attracted a substantial attention. Several gas phase studies of the chemisorption of water molecules onto these surfaces have been made lately with UPS and ELS experiments.

DV-Xα calculations are made for the electronic structure of the surface molecules chemisorbing OH ion or oxygen ion and the character of the chemisorptive bond is investigated. Our interest also extends to the initial process of the photodissociation of the adsorbate.

As the preliminary work, molecular orbitals of the system $OH-TiO_4$ is calculated. The structure of the cluster is modelled on the hydroxyl group chemisorbed on the reduced site on the rutile (110) surface. The molecular axis of OH is assumed to be perpendicular to the surface and the oxygen atom in the OH group is placed on top of the Ti ion. Calculations are made with the charge state $OH^- (TiO_4)^{6-}$ for several values of the distance d between OH and the surface Ti site. The charge 6- of the surface cluster is the same as that of the cluster without OH ion. It has been found that the filled oxygen valence band of the surface becomes too high to be consistent with that of the cluster without OH, when it approaches to the surface. We reduced, therefore, the cluster charge to n in the system $OH^- (TiO_4)^{n-}$, so that the Fermi energy is fixed for all the distances d. This means that the electrons on the defect d level are allowed to flow out of the cluster into the indented bulk by the repulsive potential of the OH^- ion.

The level structure and the cluster charge for several distances are shown in Figure 1. When OH^- ion approaches to the surface, a substantial lowering of the molecular levels of OH^- is induced. This suggests the strong attraction of the hydroxyl ion onto the defect site of the reduced rutile surface. On the other hand, for the case of chemisorption onto the Ti site of the neutral surface, or that of the five-coordinated Ti site, such a large downward shift of the OH^- levels is not
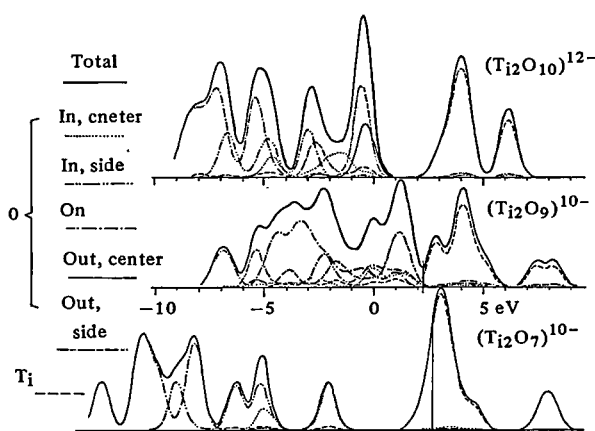
Figure 1. Total and partial state densities of the clusters $(Ti_2O_{10})^{12-}$, $(Ti_2O_9)^{10-}$, $(Ti_2O_7)^{10-}$ including the six-coordinated Ti sites on the (110) rutile surface. The Fermi level is makred by the thin vertical lines.

25
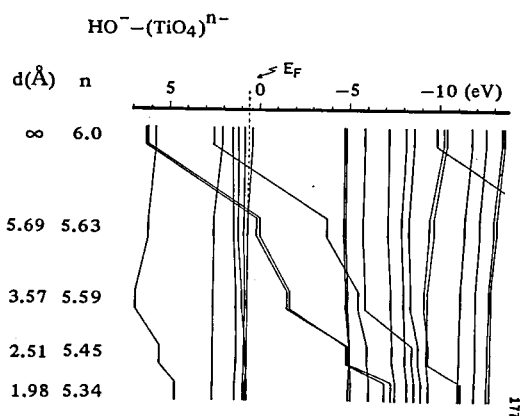
$HO^--(TiO_4)^{n-}$

Figure 1. Level structures of the chemisorption system HO^--$(TiO)^{n-}$ for various distances d of the hydroxyl ion from the surface.

Figure 2. a) The difference of the state densities (full line) between the system $HO^--(TiO_4)^{5.5-}$ (d=2.51A) and $(TiO_4)^{6-}$, and the difference between the UPS spectra (dashed line) before and after exposure to H_2O.
b) The state density of the chemisorption system $HO^--(TiO_4)^{5.5-}$ (full line) and that of the cluster $(TiO_4)^{6-}$ (dashed line).

found. This would explain the reason why the water molecule chemisorbes dissociatively onto the reduced surface, while it chemisorbes onto the neutral surface associatively.[1] The calculated state density for d= 2.51A is shown in Figure 2. The figure also illustrates the state density difference between the systems with and without the chemisorption of OH^-, and the difference in UPS spectra of the argon ion bombarded surface before and after H_2O exposure.[2] A fairly good agreement between the two confirms the reality of the present model for the dissociative chemisorption of water onto the reduced rutile surface. The two peaks in the UPS difference spectrum appeared at about 1.3 and 4.3 eV below the valence band top are assigned to

1π and 3σ bonding level of the OH^- ion, respectively. The third peak at 7.0 eV below the valence band top is due to the upward shift of the oxygen 2p levels caused by the repulsive potential of OH^-.

References

1) W. J. Lo, Y. M. Chung and G. A. Somorjai, Surf. Sci., 71, 199 (1978), V. E. Henrich, G. Dresselhaus and H. J. Zeiger, Solid State Commun., 24, 623 (1977).
2) V. E. Henrich, G. Dresselhaus and H. J. Zeiger, Phys. Rev. Lett., 36, 1335 (1976); Proc. XIII Int. Conf. Phys. Semiconductors, 726 (1976).

I-G   Theory of Two-Dimensional Electron System in MOS Inverstion Layer

In the inversion layer of the MOS (Metal-Oxide-Semiconductor) structure, the electron motion perpendicular to the surface can be quantized by the application of the gate voltage or by the electric field induced by the charged surface states. The electron gas in such system can be regarded as two-dimensional. Since the carrier number can be freely controlled by the gate voltage, the system provides us an interesting material for the study of fundamental problems encountered in many body systems or in disordered systems. Theoretical studies of two-dimensional electron gases are now acquiring an increasing importance in relation to the electronic properties of low dimensional substances.

I-G-1   Two-Dimensional Wigner Crystal in MOS Structures under Strong Magnetic Field

M. TSUKADA

[Proc. 4th Intern. Vac. Cong. and 3rd Intern. Conf. on Solid Surfaces, (Vienna 1977) p403]

The two-dimensional electron systems confined in the MOS inversion layers are important for the study of the many body effects in the electron gas. This is because the electron density can be changed in the wide range by the gate voltage, independent of the impurity concentration. Recently the possibility of the Wigner crystallization[1] in the Si MOS channel under strong magnetic field is suggested by several authors.[2-4] The immobile carriers observed by the Shubnikov-de Haas oscillation in the Si n-channels[2] seems to be an evidence of the Wigner crystallization.

In this work we calculate the phonon dispersion relation of the Wigner lattice under strong magnetic field perpendicular to the surface and investigate the melting curve of the lattice. A special interest is placed on the impurity effect on the sound wave velocity and the melting. By the use of the self-consistent harmonic

approximation for the very strong field region,[4,5] the coupled equation to determine the phonon energy $E(\kappa)$ of the momentum κ associated with the N-th Landau subband is obtained as

$$E(\kappa) = \ell^2 \sqrt{(\sigma + K_t^0(\kappa))(\sigma + K_\ell^0(\kappa))} \qquad (1)$$

where

$$K_{t}^{0}{}_{\ell}(\kappa) = -\frac{e^2}{2\kappa_N}\sum_R \int dx \cdot x^2 \exp\left\{-x^2 L^2(R)/R^2\right\}$$

$$\times \left\{ J_0(x)(1-J_0(\kappa R)) \pm J_2(x)J_2(kR) \right\} \qquad (2)$$

$$L^2(R) = (2N+1)\ell^2 + \frac{q^2\ell^2}{2N_i}\sum_k \frac{K_t^0 + K_\ell^0 + 2\sigma}{\sqrt{(\sigma+K_t^0)(\sigma+K_\ell^0)}}$$

$$\times (1 - J_0(kR)) \coth\left(\frac{E(\kappa)}{2\kappa_B T}\right) \qquad (3)$$

ℓ is the Larmor radius ($\sqrt{c\hbar/eH}$) and $J_n(x)$ is the Bessel function of the order n. The positive parameter σ represents the effective pinning force of the impurities. The lattice melts, when the real solution of $E(k)$ disappears on the increase of the temperature or the electron concentration.

The full lines in Figure 1 show the critical melting curve below which the electrons exist in the crystalline phase. The quantity X is the effective concentration $X = (2N + 1)\ell^2/d^2$, where d is the lattice constant of the triangular lattice. The dashed lines mean the lower approximate critical concentration obtained by $\lim_{k\to 0}$ $K_t^0(k)/k^2 = 0$. The figure is for the case of the lowest Landau subband (N=0). The unit of the temperature T_0 is 208K for the magnetic field of H=140 kG. As shown in the figure the crystalline phase is stabilized considerably by the introduction of only a slight amount of the impurities. This is mainly due to the gap in the phonon dispersion relation caused by the impurities.
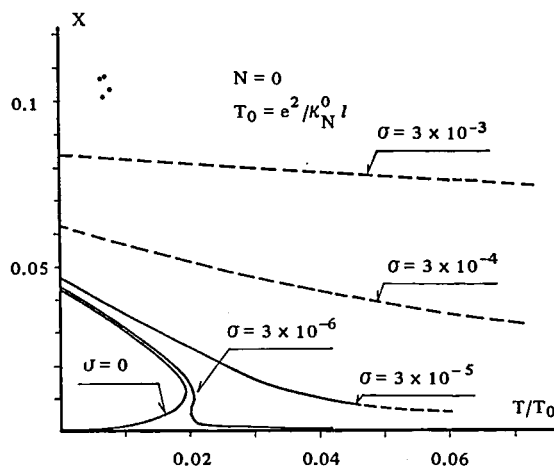
Figure 1. The phase diagram of the Wigner lattice for N=0 and for various pinning force σ. Unit of σ is $e^2/\kappa_N^0 l^3$.

It should be remarked that the random impurity potential pins the Wigner lattice resulting the vanishing of the d.c. conductivity, because the electron system does not respond to the infinitecimal field. The immobile carrier densities experimentally observed through the gap width of the Shubnikov-de Haas oscillation[2] are marked by dots in Figure 1.

The breakdown of the pinning by the finite electric field is studied by the self-consistent harmonic approximation. The very weak breakdown field and its strong magnetic field dependence are predicted, which correspond with the observed source-drain field dependence of the gap width in the Shubnikov-de Haas oscillation.[2]

References

1) E. P. Wigner, Phys. Rev., 46, 1002 (1934).
2) S. Kawaji and J. Wakabayashi, Surf. Sci., 58, 238 (1976).
3) H. Fukuyama, Solid State Commun., 19, 551 (1976).
4) M. Tsukada, J. Phys. Soc. Japan 42, 391 (1977).
5) M. Tsukada, J. Phys. Soc. Japan 41, 166 (1976).

I-H Application of the Graph Theory to Chemistry and Physics

Until very recently little attention has been paid by a majority of researchers to the effectiveness and importance of the graph- and combinatorial theoretical aspects in chemistry and physics, especially in the enumeration of the numbers of isomers, topological characteristics, partition functions, and also in the interpretation of the structure-property relationships.

One of the staffs of the theoretical studies has been working on this problem for years, especially in search of effective counting polynomials for some unsolved problems in chemistry and physics, such as 3-dimensional Ising model and rigorous partition functions for the liquid mixtures, and also for the newer interpretation of old problems, such as aromaticity and bond order. For the latter problem, the Z-counting polynomial, sextet polynomial, and rotational polynomial have been proposed with success. For the former problem, the king and domino polynomials have been proposed as the starting point. Details will be explained below.

I-H-1 King and Domino Poynomials for Polyomino Graphs

Akiko MOTOYAMA *(Ochanomizu Univ.)*, Haruo HOSOYA *(Ochanomizu Univ. and IMS)*

For the purposes of treating several enumeration problems of lattice dynamics, king and domino polynomials are defined for a chessboard, polyomino, or square lattice of arbitrary size and shape. These polynomials are shown to be closely related to the partition function of the dimer statistics, the number of the Kekulé structures, or the maximum matching number. Several recursion formulas are found. Interpretation of these newly proposed quantities is given, and the possibilities of extending them to important physical models is discussed.

A *polyomino* is a graph generated by the stacking of squares (cells) of equal size. A rectangular polyomino graph is denoted as [m, n] having m rows and n columns of squares. For example, graph I is [2, 3]. Polyominoes can be classified into *even* and *odd* ones according to the number of vertices but not that of the cells. An even graph with N-2m vertices is called a *Kekulé graph* if one can choose such a set of m disjoint edges that span all the N vertices as in I, which is called a *Kekulé pattern*. The number of Kekulé pattern for a given graph G is denoted as K(G).
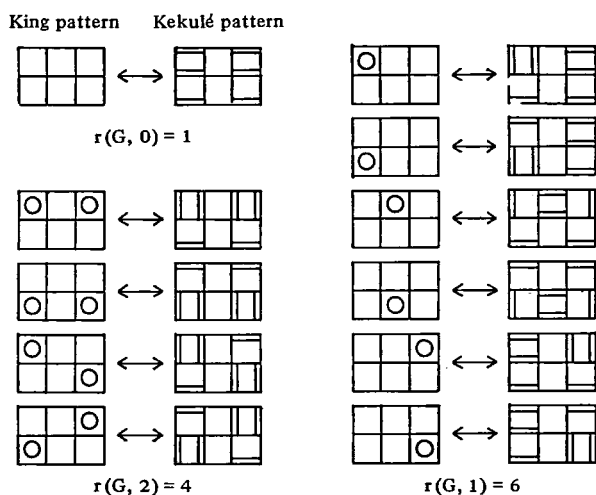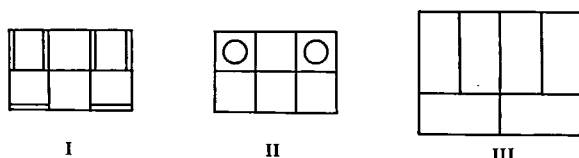
A king can take on any of the eight neighboring cells. Each distinct pattern as II, called as *king pattern*, can be obtained by putting k nontaking kings (circles) for a given graph G.

Define the *nontaking number* r(G, k) as

$$r(G, k) = \binom{\text{number of king patterns with } k}{\text{nontaking kings for graph } G}.$$

For the sake of the later discussion let us define

$$r(G, 0) = 1$$

for all the cases. The *king polynomial* $K_G(X)$ for polyomino G is defined as

$$K_G(X) = \sum_{k=0}^{k_m} r(G, k) \, X^k$$

where k_m is the maximum number for k, which does not exceed N/4. For graph I we have $K_I(X) = 1 + 6X + 4X^2$.

If one puts a 1×2 rectangle (domino) onto each "double bond" of the Kekulé pattern, as I, a *domino pattern*, as III, is obtained. By definition the number of domino patterns for graph G is equal to K(G). Domino polynomial $D_G(X)$ is also defined for G.

The $K_G(X)$ and K(G) for several polyomino graphs are given in Table I. It was found that for graphs without having [3, 3] graph

$$K_G(1) = K(G).$$

This equality is approved by observing the one-to-one correspondence between the king and Kekulé patterns as shown in Figure 1.

For a series of rectangular graphs [m, n] a number of recursive relations are obtained. The weight of each cell with respect to the counting the king and Kekulé patterns is obtained by differentiating $K_G(X)$. Further interesting mathematical relations for $K_G(X)$ and $D_G(X)$ have been found and discussed.

King pattern   Kekulé pattern

r (G, 0) = 1

r (G, 2) = 4   r (G, 1) = 6

Figure 1.

Table I.

G	k= 0	1	2	3	4	$K_G(1)$	K(G)
□	1	1				2	2
▭▭	1	2				3	3
▭▭▭	1	3	1			5	5
▭▭▭▭	1	4	3			8	8
L	1	4	2			7	7
⊞	1	6	4			11	11
⊞	1	9	16	8	1	35	36
⊞	1	4	1			6	5

RESEARCH ACTIVITIES

II. Division of Molecular Structure

The most fundamental problem the Division is interested in is the precise determination of the molecular structures by spectroscopic methods with high resolution and high sensitivity. A special emphasis is placed on the detection and identification of transient molecular species such as free radicals and molecular ions. One of the main tools is a microwave spectrometer, which covers the frequency region up to 180 GHz with a phase-lock system. A CO_2, N_2O, or CO laser source is used with a multiple reflection cell as a laser Stark spectrometer, and with an intracavity cell as a laser Zeeman or LMR spectrometer. Tunable lasers, dye lasers in the visible region and diode lasers in the infrared region, which have been installed as the main facilities of the Large Scale Research Equipments, are also utilized as sources for spectroscopy of unstable molecular species. Fluorescence excited by the dye laser provides a very sensitive method of detecting new free radicals. The diode laser, combined with Zeeman modulation or with a microwave source, provides a new spectroscopic method. For an investigation of unstable species from a more dynamical point of view, highly-excited atoms are produced by the electron bombardment and their reactions with other atoms or molecules are analyzed in detail. In addition to the transient species a few non-polar molecules are being investigated by microwave spectroscopy.

II-A High Resolution Spectroscopy of Transient Molecular Species

Transient species which appear as intermediates in chemical reactions supply an important information on the reaction mechanisms; without the knowledge of such species it is not easy to understand the chemical reaction properly. At present we probably know only a small fraction of such species, because most of them are of short life. We need spectroscopic and other methods which are sensitive enough to detect these species. High resolution spectroscopy not only provides molecular constants at a very high precision, but also allows us to sort out the spectra of unstable species among those of others and thus to unambiguously identify chemical species present in our reaction system. The open-shell electronic structure characterizes many of the unstable species and causes additional complexities in their spectra due to the fine structure and hyperfine structure interactions. Analyses of these structures in the spectra provide us with information on the electronic properties of the molecules, which would not be obtained for molecules without unpaired electrons. Besides these fundamental implications in the field of molecular science and chemical reaction, the present project will be of some significance in related fields such as astrophysics and environmental researches.

II-A-1 Microwave Spectrum, Anharmonic Potential Constants, and Equilibrium Structure of Sulfur Difluoride

Yasuki ENDO, Shuji SAITO, Eizi HIROTA, and Toshio CHIKARAISHI *(Kyushu Univ.)*

The microwave spectra of a bent Y-X-Y type molecule in excited states of the three normal modes allow us to determine not only its equilibrium structure but also all the six anharmonic potential constants. A few molecules of this type have already been investigated,[1] and in the present work we studied an unstable molecule SF_2. Because the spectra in the two stretching excited states are nearly two orders of magnitude weaker than the ground-state spectra, the present investigation also serves as a test of our microwave spectrometer newly constructed at IMS.

Kirchhoff *et al.*[2] have already analyzed the ground-state spectra of SF_2 in detail and have estimated the vibrational frequencies by using the centrifugal distortion constants they determined. It is to be noted that no infrared spectrum has been reported on this molecule.

We generated SF_2 molecules by a reaction of carbonyl sulfide with the fluorine atom produced by a microwave discharge in carbon tetrafluoride, and pumped the reaction products continuously through a cell. The absorption cell was made of gold-plated brass parallel plates of 40 cm length. The system was equipped with a mechanical booster pump (1,800 ℓ/min) followed by two liquid nitrogen traps and a rotary pump (640 ℓ/min). A typical sample pressure was 4-10 and 6-15 mTorr for OCS and CF_4, respectively.

We normally locked mm-wave klystrons to harmonics of the output of an X-13 klystron by a Microwave Systems PLS-60. To measure the line frequency precisely the X-13 was further stabilized by a Microwave Systems MOS-5. The frequency of the X-13 was measured by microwave frequency counter (HP 5340 A).

Table I. Molecular Constants of Sulfur Difluoride

Vibration-rotation constants (MHz)

s	α_s^A	α_s^B	α_s^C
1	4.33	49.851	30.278*
2	−333.778	23.249	26.906
3	186.15	21.118	23.207*

Equilibrium rotational constants (MHz) and equilibrium structure

A_e	26 858.83 (16)	r_e (S−F)	1.587 51(30) Å
B_e	9 259.177 (42)	θ_e (F−S−F)	98.046(20)°
C_e	6 886.130 (38)		

Harmonic force constants (md/Å)

F_{11}	5.128	F_{22}	0.501
F_{12}	0.091	F_{33}	4.395

(1: sym. stretch., 2: bending, 3: antisym. stretch.)

Cubic potential constants (cm^{-1})

k_{111}	−29.0	k_{112}	−15.1	k_{122}	4.1
k_{222}	−10.7	k_{133}	−99.1	k_{233}	−1.8

Third-order anharmonic potential constants

f_{111}, f_{222}	−27.17 md/Å²	f_{123}	−0.39 md/Å
f_{112}, f_{122}	−0.55 md/Å²	f_{133}, f_{233}	−1.57 md
f_{133}, f_{223}	−0.53 md/Å	f_{333}	−3.33 md Å

(1: S−F(1), 2: S−F(2), 3: F−S−F: the coordinates 1 and 2 are taken to be positive when the S−F bonds are stretched and 3 to be positive when the angle is opened.)

We could observe the spectra in all the three fundamental states. To analyze the observed spectra, we used a Hamiltonian which included the centrifugal distortion effects to the first order. The ν_2 satellite was explained by this model, but the ν_1 and ν_3 spectra showed appreciable deviations, which were primarily due to the Coriolis interaction between the two modes. However, the interaction was not large enough to justify a simultaneous analysis of the two sets of satellites based on an effective 2×2 matrix with the Coriolis terms in the off-diagonal block. We analyzed the ν_1 and the ν_3 spectra separately, and derived the effective rotational constants for each state. The vibration-rotation constants α_s thus obtained are listed in Table I. The α_1^{C*} and α_3^{C*} constants denote the values obtained from the observed A and B constants and the calculated inertia defects that do not contain the Coriolis resonance terms. By comparing α_1^{C*} and α_3^{C*} respectively with the effective α_1^C and α_3^C which were obtained from the spectra we calculated $D^2/(\tilde{\nu}_1-\tilde{\nu}_3)$, where D meant the Coriolis coupling term. By assuming the calculated Coriolis coupling constant $\zeta_{13}^c = -0.4248$, we estimated $\tilde{\nu}_1 - \tilde{\nu}_3$ to be 25.8 cm⁻¹, which was to be compared with 31 ± 22 cm⁻¹ reported in Ref. 2).

Table I lists the equilibrium rotational constants and the equilibrium structure. The errors of the structure parameters are mainly due to the neglect of the higher order terms including electronic corrections. We recalculated the harmonic force constants, which were then utilized to calculate the cubic potential constants and the third-order anharmonic potential constants. All these results are summarized in Table I. It is to be noted that the stretch-stretch-stretch terms (f_{111}, f_{222}) are the largest in magnitude and that all the third-order terms are negative, in accordance with the rules mentioned in Ref. 1).

References

1) Y. Morino and E. Hirota, *Ann. Rev. Phys. Chem.*, **20**, 139 (1969).
2) W. H. Kirchhoff, D. R. Johnson, and F. X. Powell, *J. Mol. Spectrosc.*, **48**, 157 (1973).

II-A-2 A New Free Radical FSO Investigated by Microwave Spectroscopy

Yasuki ENDO, Shuji SAITO, and Eizi HIROTA

The hydroperoxy radical HO_2 has recently been investigated in detail by LMR[1,2] and microwave[3,4] spectroscopy, and now its existence has been firmly established. The halogen derivatives of this radical were, however, so far detected only in low-temperature matrices,[5] although the chlorine dioxide O-Cl-O is well known. We planned a systematic study on an analogous series of molecules, XSO with X = H or halogen, by using spectroscopic methods of high resolution and of high sensitivity. We succeeded in detecting the first two members HSO and FSO; the former is described in II-A-6 and the present report will discuss the microwave results on the latter. No papers have been published on the FSO radical.

We generated the FSO radical by the reaction of carbonyl sulfide with products of a microwave discharge in a mixture of oxygen and carbon tetrafluoride. The optimum partial pressures were 20, 20, and 10 mTorr for OCS, O_2, and CF_2. We may replace OCS by carbon disulfide with much less efficiency. The details of the reaction mechanism have not been explored, but the

FSO radical probably derived its three atoms one each from the three reactant gases. If so, this affords an interesting chemical synthesis.

The microwave spectrometer used in the present work is described in II-A-1. Because our reaction system also produced a large amount of other diamagnetic species such as SO_2, SF_2, F_2SO, and CF_2, we discriminated the FSO spectra by applying a D.C. magnetic field of a few Gauss, which we generated by a coil wound on the cell. We also utilized a small permanent magnet to confirm that the radical lasted only in 1/2 - 1/3 length of the cell from the inlet. Because the linear velocity of pumping is about 5 - 10 m/sec, this result means that the lifetime of the radical is about 20 - 40 msec in our cell. In spite of the short lifetime the observed spectrum was strong.

First we assigned the Q branch lines in the 40 GHz region. It was easy to make rotational assignments, but the J and F values were much harder to determine, especially for the low N transitions, because the spin rotation interaction was much smaller than those of lighter molecules such as HO_2 and was comparable with the hyperfine interaction. In addition the off-diagonal terms of the spin rotation and hyperfine interactions made the assignments more difficult. Therefore, we proceeded in a trial-and-error fashion; we calculated the fine as well as hyperfine structures of the spectra by assuming a reasonable set of the coupling constants and improved them one by one by referring to the observed spectra. Finally we set up an energy matrix in a symmetric-top basis and analyzed all the observed line frequencies by a least-squares method. We included the $\Delta N = 0, \pm 1$, $\Delta K = 0, \pm 1, \pm 2$ elements for the spin-rotation interaction with the centrifugal distortion effects on it[6] and the $\Delta N = 0, \pm 1, \pm 2$, $\Delta J = 0, \pm 1$, $\Delta K = 0, \pm 1, \pm 2$ elements for the hyperfine interactions, and thus a matrix for a fixed F value took the following form:

	$N = F\text{-}1$	F	F	$F+1$
	$J = F\text{-}1/2$	$F\text{-}1/2$	$F+1/2$	$F+1/2$
ROT SR HF	SR HF	HF	HF
	ROT SR HF	HF	HF
		ROT SR HF	SR HF
			ROT SR HF

[Note that $J = N + S$, $F = J + I$, $S = 1/2$, and I(fluorine) = 1/2.] The molecular constants thus derived are summarized in Table I. It is worth noting that the off-diagonal terms of the spin-rotation ($|\epsilon_{ab} + \epsilon_{ba}|$) and the hyperfine ($|T_{ab}|$) coupling constants were determined thanks to accidental degeneracies; e.g. that between 5_{14} and 4_{22}, which were separated by about 5,400 MHz. The centrifugal distortion constants which were derived are now being analyzed to estimate the vibrational frequencies. Recently, a partial assignment was achieved for a few transitions of $F^{34}SO$ in natural abundance. The A, B, and C rotational constants of this species may be combined with those of the normal species listed in Table I to calculate the geometry of this radical.

References

1) H. E. Radford, K. M. Evenson, and C. J. Howard, *J. Chem. Phys.*, **60**, 3178 (1974).
2) J. T. Hougen, H. E. Radford, K. M. Evenson, and C. J. Howard, *J. Mol. Spectrosc.*, **56**, 210 (1975).

Table I. Molecular Constants of the FSO Radical (MHz)^a

Rotational parameters		Spin-rotation constants		
A	38 698.187 (13)	ϵ_{aa}	−339.600	(56)
B	9 340.812 (3)	ϵ_{bb}	34.877	(22)
C	7 505.066 (4)	ϵ_{cc}	1.847	(19)
Δ_N	0.009 985 (33)	$|\epsilon_{ab} + \epsilon_{bc}|/2$	207.928	(42)
Δ_{NK}	−0.082 72 (31)	Δ_N^{SR}	−0.002 8	(36)
Δ_K	0.881 81 (36)	$\Delta_{NK}^{SR} + \Delta_{KN}^{SR}$	0.013 8	(23)
δ_N	0.002 900 (13)	Δ_K^{SR}	−0.041 1	(47)
δ_K	0.027 0 (7)			
		Hyperfine constants		
		σ	67.132	(40)
		T_{aa}	−117.95	(14)
		T_{bb}	−117.44	(9)
		$|T_{ab}|$	9.97	(63)

^{a} Values in parentheses denote standard deviations and apply to the last digits of the constants.

3) Y. Beers and C. J. Howard, *J. Chem. Phys.*, 63, 4212 (1975); 64, 1541 (1976).

4) S. Saito, *J. Mol. Spectrosc.*, 65, 229 (1977).

5) For example, F. J. Adrian, E. L. Cochran, and V. S. Bowers, *J. Chem. Phys.*, 56, 6251 (1972).

6) J. M. Brown and T. J. Sears, private communication.

II-A-3 Laser Magnetic Resonance Spectroscopy of SO in the $\tilde{a}^1\Delta$ and the $\tilde{X}^3\Sigma^-$ States with a CO_2 Laser as a Source

Chikashi YAMADA, Kentarou KAWAGUCHI, and Eizi HIROTA

The sulfur monoxide radical is known to be an important intermediate in reactions involving the oxygen and the sulfur atoms. It was also found in the interstellar space by radio telescopes. The microwave, the gas-phase electron-paramagnetic-resonance (EPR), and the electronic spectra of this radical were reported in detail, but few papers have been published on its vibrational spectra. It has been established that the SO molecule has an electron configuration similar to that of the O_2 molecule; the ground state is $^3\Sigma^-$ and the first excited electronic state a metastable $\tilde{a}^1\Delta$ state. The present work aimed at observation of the vibrational transitions of SO, not only in the ground $\tilde{X}^3\Sigma^-$ state but also in the $\tilde{a}^1\Delta$ state, to determine the band origins precisely by the method of laser magnetic resonance (LMR). The high sensitivity of LMR is now fully appreciated, but we wish to test our new LMR spectrometer, by investigating SO as an example. From our microwave studies we know this radical is easily produced by a reaction of carbonyl sulfide with the oxygen atom. Recently S. Saito observed a remarkable increase in intensity of the microwave spectrum of SO in $\tilde{X}^3\Sigma^-$ by adding carbon tetrafluoride to a microwave discharge in the oxygen gas.

We observed two groups of the absorption lines; those belonging to the group A appeared strongly when CF_4 was added to oxygen before discharge, and they remained to be seen even when the partial pressure of the oxygen gas was reduced to 1/5 - 1/6 that of OCS. We assigned these lines to the resonances in the ground state, in accordance with the observation of Saito. On the other hand the lines of the group B were observed only when the oxygen pressure was an order of magnitude larger than the OCS pressure. This observation may be consistent with the following mechanism:

$$O + OCS \rightarrow CO + SO(^3\Sigma^-),$$

$$SO(^3\Sigma^-) + O_2(^1\Delta) \rightarrow SO(^1\Delta) + O_2(^3\Sigma_g^-).$$
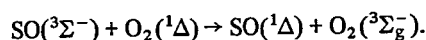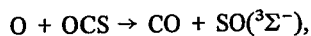
In fact we ascribed the group B spectra to SO in $\tilde{a}^1\Delta$. We needed a fairly low pumping speed of 1 - 6 l/sec. The details of our LMR spectrometer is described in II-A-4.

The results of analysis of the observed spectra are summarized below.

Table I. Molecular Constants of $^{32}S^{16}O$ in the $\tilde{X}^3\Sigma^-$, $v = 1$ State[a]

Constant	Present[b]	Reference[c]
B	21 351.74(24)	21.351.58(4)
λ	159 194.8(50	159 204.7(94)
γ	−170.0(2)	−171.5(12)
D	0.0341(3)	[0.034][d]
λ_D	0.27(3)	[0.305][d]
$g_\perp$	2.0035(3)	
ν_0	1138.0070(10)	1135.95

[a] In MHz, except ν_0 which is given in cm^{-1}.
[b] Values in parentheses denote 2σ
[c] Ref. 6) except ν_0, which is taken from Ref. 11).
[d] Fixed.

(1) $\tilde{X}^3\Sigma^-$. Colin[1] obtained the band origin to be 1135.95 cm^{-1} by analyzing electronic spectra. Because the CO_2 laser covers the wavelength region only up to 1105 cm^{-1}, we could observe the transitions of $\Delta N = -1$ with large N values ($N = 17 \leftarrow 18$ to $26 \leftarrow 27$). For such high N transitions the strongest components, $\Delta J = \Delta N = -1$, are difficult to tune by a magnetic field. In fact we observed only one such transition (eleven Zeeman components), and most others were of $\Delta J \neq \Delta N$ type. Although the latters are weak for
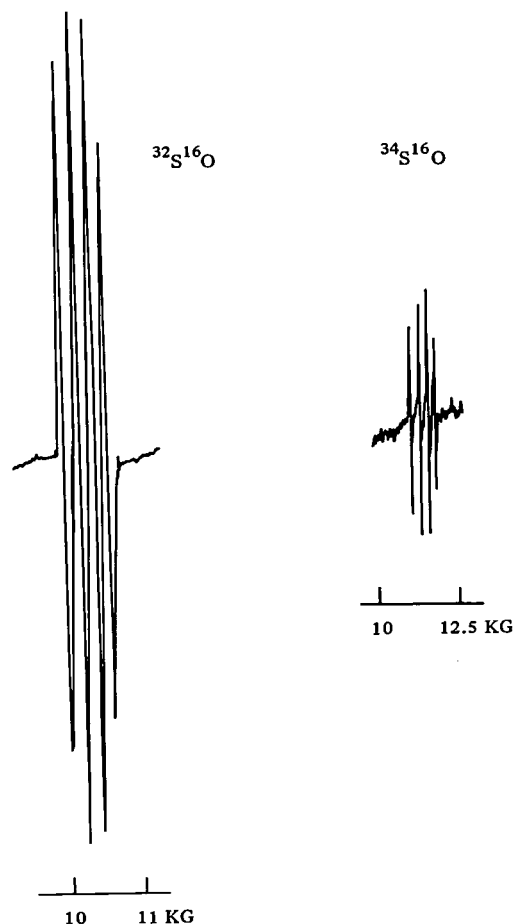
Figure 1. The laser magnetic resonance spectra of the Q(2) transitions of $^{32}S^{16}O$ and $^{34}S^{16}O$ in the $\tilde{a}^1\Delta$ state.

large N values, they have large Zeeman effects which permitted us to bring their Zeeman components into resonance with the laser lines. By fixing the ground state parameters to the microwave and the EPR values and by assuming two minor g factors in $v = 1$ to be the same as those in $v = 0$, we determined the $v = 1$ constants and the band origin as listed in Table I, where the reference values if available are also included for comparison. The band origin of Colin is about $2\ cm^{-1}$ too low.

(2) $\tilde{a}^1\Delta$.   Little is known about the vibrational spectra in this metastable state. Clark and De Lucia[2] estimated the vibrational frequency to be $1108\ cm^{-1}$ from the centrifugal distortion constant which they determined. Because a molecule in the $^1\Delta$ state behaves as a symmetric top in the $K = 2$ level, we could observe only transitions which involve the levels of J less than 5. Figure 1 shows Q(2) of ^{32}SO and ^{34}SO; the signal-to-noise ratio obtained indicates the high sensitivity of our apparatus. From the band origins of the two isotopic species we calculated the harmonic frequency and the vibrational anharmonicity constant to be $\omega_e = 1115.349 \pm 0.081\ cm^{-1}$ and $\omega_e x_e = 6.978 \pm 0.041\ cm^{-1}$ ($\pm 2.5\sigma$), respectively. The equilibrium bond length we obtained, $1.488\ 86 \pm 0.000\ 26$ Å, is larger than that in $\tilde{X}^3\Sigma^-$ by 0.0079 Å. From the observed g factors we estimated the contributions of the excited Π and Φ states.

References
1) R. Colin, Can. J. Phys., 46, 1539 (1968); 47, 979 (1969).
2) W. W. Clark and F. C. de Lucia, J. Mol. Spectrosc., 60, 332 (1976).

II-A-4   Laser Magnetic Resonance Spectroscopy of the v_2 Band of NH_2

Kentarou KAWAGUCHI, Chikashi YAMADA, and Eizi HIROTA

Ramsay and his coworkers[1,2] analyzed the electronic transition $\tilde{A}^2A_1$ - $\tilde{X}^2B_1$ to determine the molecular structure of the NH_2 radical both in the upper and lower states. Recently, Curl and his coworkers[3] applied a high-resolution dye laser to obtain much more detailed information on this free radical. They also succeeded in observing microwave transitions in both $\tilde{A}$ and $\tilde{X}$ states by a microwave-optical double resonance (MODR) technique[4] and to reduce the line-widths less than the Doppler limit by saturation spectroscopy.[5] On the other hand Davies et al.[6] detected NH_2 by a laser magnetic resonance (LMR) method with a far-infrared laser as a source. We initiated the present work to obtain more precise data on the molecular structure in the bending excited state of the ground electronic state. The bending vibration is of particular importance for the XH_2 molecule. We might interpret the two lowest electronic states as derived from an otherwise degenerate state of a hypothetical linear mole-
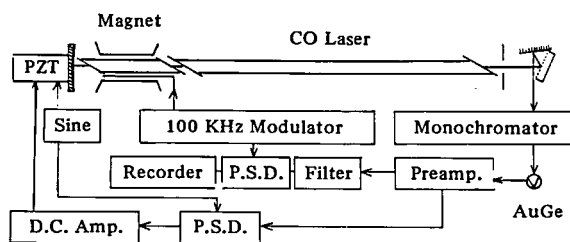
Figure 1. Block diagram of a CO laser magnetic resonance spectrometer.

cule by the Renner-Teller effect. Therefore, the two electronic states might be coupled strongly by the bending mode, as was found by Curl et al.[4] Soon after we started the present work Brown et al.[7] published a short note on the v_2 band of NH_2 by LMR spectroscopy. However, their assignment was not compatible with ours; they assigned the observed resonance fields based on earlier, less accurate molecular constants obtained from the electronic spectra.[1] Furthermore, it is likely that they misassigned their CO laser line.

To produce the NH_2 molecule we tested three reactions: (1) hydrated hydrazine with H, (2) anhydrated hydrazine with H, and (3) ammonia with F, but we did not find substantial differences in efficiency of generating NH_2. Because the first one was easiest to handle and kept the cell clean, we almost exclusively

LMR Spectrum of $NH_2\ v_2$ Band
^{13}CO Laser $1590.55\ cm^{-1}$
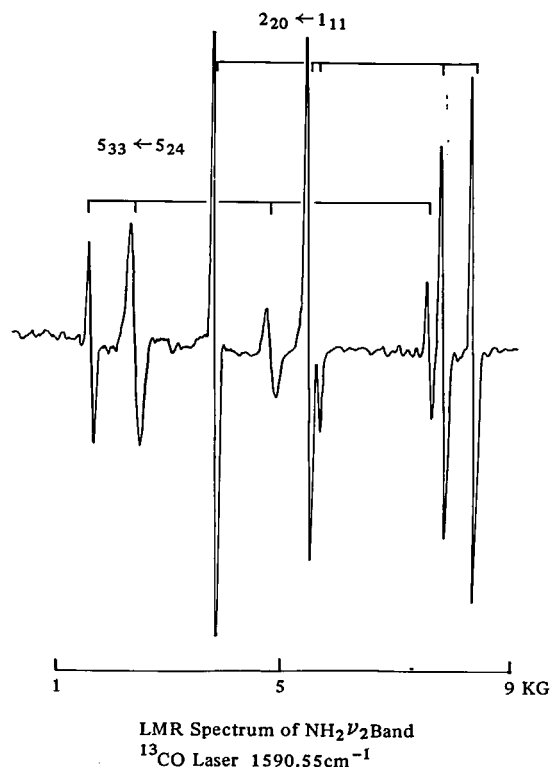
Figure 2. The $2_{20} \leftarrow 1_{11}$ and $5_{33} \leftarrow 5_{24}$ transitions of the v_2 band of NH_2 observed by using a ^{13}CO laser line at $1590.55\ cm^{-1}$ as a source.

Table I. Molecular Constants of NH_2[a]

Constant	Ground state	$v_2 = 1$ state
Rotational parameters (MHz)		
A	710 300(8)	778 450(14)
B	388 275(4)	392 982(12)
C	245 018(3)	240 886(8)
Δ_N	30.9(2)	33.5(2)
Δ_{NK}	−122.5(11)	−158.5(10)
Δ_K	656.0(11)	1 056.3(20)
δ_N	12.77(6)	13.5(1)
δ_K	23.2(11)	60.9(12)
H_{NK}	−0.084(17)	−0.288(25)
H_{KN}	−0.07(9)	0.36(10)
H_{KK}	1.60(10)	3.24(12)
Spin rotation interaction constants (MHz)		
ϵ_{aa}	−9 267.8[b]	−12 141(45)
ϵ_{bb}	−1 353.9[b]	−1 274(57)
ϵ_{cc}	12.0[b]	−87(51)
$\Delta_N{}^{SR}$	−0.312[b]	−1.38(63)
$\Delta_{NK}{}^{SR}$	3.51[b]	17.3(42)
$\Delta_K{}^{SR}$	−33.9[b]	−81.3(78)
$\delta_N{}^{SR}$	−0.155[b]	−0.155[b]
$\delta_K{}^{SR}$	−0.48[b]	−0.48[b]
g-Factors		
$g_s\text{-}T_0{}^0(g_\varrho)/\sqrt{3}$	2.005 07[c]	2.005 5[c]
$T_0{}^2(g_\varrho)$	0.004 6[c]	0.005 7[c]
$T_2{}^2(g_\varrho)$	0.000 88[c]	0.000 78[c]
$T_0{}^0(g_r)$	0.003 8(11)	0.004 2(12)
$T_0{}^2(g_r)$	−0.004 34(97)	0.005 9(21)
$T_2{}^2(g_r)$	−0.000 2(14)	−0.017 1(57)
Band origin ν_0 (cm^{-1})		1497.3200(12)

[a] Values in parentheses denote three standard errors and apply to the last digits of the constants.
[b] Fixed to the values by MODR (Ref. 3).
[c] Fixed to the values calculated by Curl's relation [R. F. Curl, Jr., *Mol. Phys.*, 9, 585 (1965)].

utilized the first reaction. We obtained the H atom by a microwave discharge in the water vapor of 200 mTorr and the partial pressure of $N_2H_4 \cdot H_2O$ was about 100 mTorr. The pumping speed was 10 ℓ/sec at the total pressure of 300 mTorr. Figure 1 shows a block diagram of our LMR spectrometer with a CO laser as a source. A laser cavity 4 m long is formed with a grating and a concave mirror, but the laser tube is only of 2.4 m length, leaving a space for an intracavity cell made of a 20 mmϕ glass tube, which is placed between pole caps of a Varian 15″ electromagnet. The laser tube could be cooled down to −50°C. The typical output power is 100 mW in the 1750 cm^{-1} region, but 5 mW at the lowest end of the region, 1550 cm^{-1}. Figure 2 shows the $2_{20} \leftarrow 1_{11}$ and $5_{33} \leftarrow 5_{24}$ transitions as examples, observed by a ^{13}CO laser line.

The Hamiltonian used to analyze the observed spectra consists of the rotational, the centrifugal distortion, the spin rotation, and the Zeeman terms. We fixed the spin rotation interaction constants in the ground state to accurate values reported by Cook et al.[3] The far-infrared LMR spectra of Davies et al.[6] and the $\Delta K_a = -3$ transitions recently observed by Hills and McKellar[8] by using a CO_2 laser were added to our

spectra in a least-squares analysis. The molecular parameters thus obtained are summarized in Table I. It may be worth noting that $|\epsilon_{aa}|$ increases by about 30 % upon excitation of the ν_2 mode. According to a calculation by Dixon[9] the dominant term of ϵ_{aa} arises from the interaction with the $\tilde{A}^2A_1$ state. It would be interesting to extend this calculation to the large vibrational change of ϵ_{aa} as observed by the present work.

References

1) D. A. Ramsay, *J. Chem. Phys.*, 25, 188 (1956); D. A. Ramsay, *Mem. Soc. Roy. Sci. Liége*, 18, 471 (1957); K. Dressler and D. A. Ramsay, *Phil. Trans. Roy. Soc. London*, A251, 533 (1959).
2) J. W. C. Johns, D. A. Ramsay, and S. C. Ross, *Can. J. Phys.*, 54, 1804 (1976); M. Vervloet, M. F. Merienne-Lafore, and D. A. Ramsay, *Chem. Phys. Lett.*, to be published.
3) J. M. Cook, G. W. Hills, and R. F. Curl, Jr., *J. Chem. Phys.*, 67, 1450 (1977).
4) G. W. Hills, J. M. Cook, R. F. Curl, Jr., and F. K. Tittel, *J. Chem. Phys.*, 65, 823 (1976); G. W. Hills and R. F. Curl, *J. Chem. Phys.*, 66, 1507 (1977).
5) G. W. Hills, D. L. Philen, R. F. Curl, Jr., and F. K. Tittel, *Chem. Phys.*, 12, 107 (1976).
6) P. B. Davies, D. K. Russell, B. A. Thrush, and H. E. Radford, *Proc. Roy. Soc. London*, A353, 299 (1977).
7) J. M. Brown, J. Buttenshaw, A. Carrington, and C. R. Parent, *Mol. Phys.* 33, 589 (1977).
8) G. W. Hills and A. R. W. McKellar, private communication.
9) R. N. Dixon, *Mol. Phys.*, 10, 1 (1965).

II-A-5 Hyperfine Structure in the $\tilde{A}$ State of PH_2 by Intermodulated Fluorescence Spectroscopy

Robert F. CURL *(Rice Univ. and IMS)*, Yasuki ENDO, Masao KAKIMOTO, Shuji SAITO, and Eizi HIROTA

The hyperfine structures provide us with detailed information on the electronic structure of a free radical. However, when we work on the electronic spectra, the Doppler width (typically 1 GHz) prohibits the hyperfine splittings which are an order of magnitude smaller to be resolved. We need thus some special techniques such as saturation spectroscopy and microwave-optical double resonance (MODR) to resolve the hyperfine structures. In the present work we aimed at detecting the PH_2 radical by a high-resolution dye laser with a hope that its hyperfine coupling constants were to be determined with high precision, not only for the ground state but also for the excited electronic state. The 0-0 band of the $\tilde{A}^2A_1 \leftarrow \tilde{X}^2B_1$ system of PH_2 was rotationally analyzed by Dixon et al.[1] In particular, they reported the $0_{00} \leftarrow 1_{10}$ transition at 18 259.49 cm^{-1} with the two components $J = 1/2 \leftarrow 3/2$ and $1/2 \leftarrow 1/2$ unresolved.

We used a Spectra Physics 580 A and a Coherent Radiation 599 dye lasers with Rhodamine 110, operated in single mode. (These dye lasers are described in Large
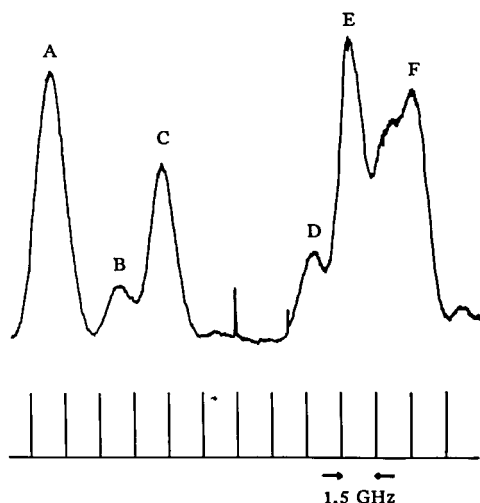
Figure 1. The $0_{00} \leftarrow 1_{10}$ transition of the $\tilde{A}^2A_1 \leftarrow \tilde{X}^2B_1$, (000) $\leftarrow$ (000) band of PH_2, observed by laser excitation spectroscopy.

Scale Research Equipments. We generated the PH_2 radical by passing the hydrogen atoms formed by a microwave discharge in the hydrogen gas over red phosphorus. The linear velocity of pumping was of the order of 10^3 cm/sec at 100 mTorr. Typical laser power was 50 mW with a beam diameter of about 1.5 mm normally employed. The laser light scattered by solid deposits on the inside wall of the cell was cut by two Hoya O-58 edge filters (cut-off wavelength 560 mm) placed in front of a photo-multiplier (Hamamatsu R666S).

We first concentrated ourselves to a region where the $0_{00} \leftarrow 1_{10}$ transition would appear, by using the method of laser excitation spectroscopy. We observed six lines designated by A-F in Figure 1. Saturation behaviors with respect to the laser power were quite different for the two outer lines (A and F) and the remaining four lines were much more easily saturated. We thus presumed that the B-E lines were assigned to $0_{00} \leftarrow 1_{10}$. Further support for this assignment was provided by the LMR result[2] that the spin rotation splitting in the 1_{10} level of $\tilde{X}^2B_1$ was 8.1 ± 0.2 GHz. The B and C lines were thus ascribed to $J = 1/2 \leftarrow 1/2$ and the D and E lines to $J = 1/2 \leftarrow 3/2$ (see Figure 2 for the level structures). Furthermore, because the total nuclear spin of the hydrogen nuclei was zero both for 0_{00} and 1_{10}, we could interpret the splittings between lines B and C (1.83 ± 0.1 GHz) and lines D and E (1.72 ± 0.04 GHz) as arising from the ^{31}P hyperfine structure in the 0_{00} level of the excited state. As Figure 2 indicates, the calculated relative intensities correspond well with the observed values.

According to our present interpretation the C and E lines should further be split into two components. We thus applied intermodulated fluorescence spectroscopy to the two lines. Figure 3 shows the result on the E line, which is resolved in three lines. We may interpret the two outer lines as $F = 1 \leftarrow 2$ (stronger) and $F = 1 \leftarrow 1$ (weaker) and the central line as the so-called "cross-over" transition. The splitting between the two outer lines was 60 MHz. We obtained a similar result for the C line with the splitting of 350 MHz.

Figure 2. The level structures of 0_{00} in $\tilde{A}$ and 1_{10} in $\tilde{X}$ of PH_2.
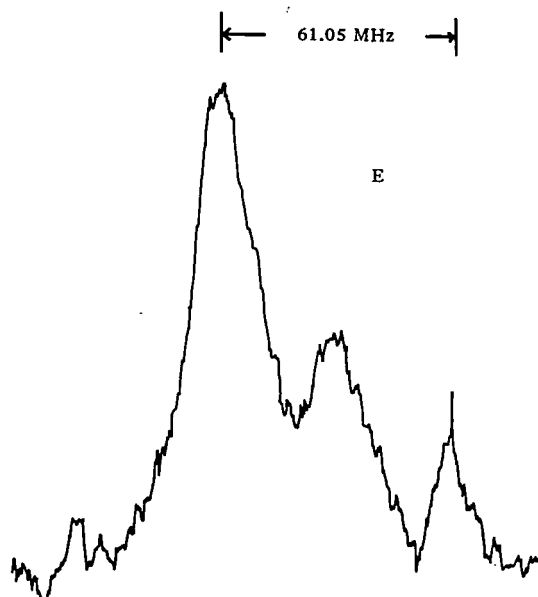
Figure 3. The $N = 0_{00} \leftarrow 1_{10}, J = 1/2 \leftarrow 3/2, F = 1 \leftarrow 2$ and $1 \leftarrow 1$ transition in the $\tilde{A} \leftarrow \tilde{X}$ band of PH_2, recorded by intermodulated fluorescence spectroscopy. The central line is a "cross-over" transition.

35

From the observed spectra as described above we obtain the following results:

$$\widetilde{A}{}^2A_1 \quad (000) \quad \text{Fermi term} \quad \sigma' \;=\; 1.78 \pm 0.03 \text{ GHz}$$
$$\widetilde{A}{}^2B_1 \quad (000) \quad \text{Fermi term} \quad \sigma'' \;=\; 0.23 \pm 0.02 \text{ GHz}$$
$$\text{dipole-dipole interaction constant}$$
$$T_{cc}{}'' \;=\; 0.64 \pm 0.02 \text{ GHz}.$$

The errors are entirely due to instability of a spectrum analyzer. The large Fermi term in the $\widetilde{A}$ state reflects the fact that PH_2 in this state is a σ radical, whereas it is a π radical in the ground state as indicated by the much smaller σ'' value. The 3s character in the upper state may be estimated to be about 18 % by using the pure 3s coupling constant for ^{31}P of 10.2 GHz.[3] We are working on other transitions to determine all the components of the dipole-dipole interaction constant.

References
1) R. N. Dixon, G. Duxbury, and D. A. Ramsay, *Proc. Roy. Soc. London*, A269, 136 (1967).
2) P. B. Davies, D. K. Russell, and B. A. Thrush, *Chem. Phys. Lett.*, 37, 43 (1976).
3) H. J. Bowers, M. C. R. Symons, and D. J. A. Tinling, in "Radical Ions", Ed. by E. T. Kaiser and L. Kevan, Interscience, New York, 1968.

II-A-6 The HSO Radical Studied by Laser Excitation Spectroscopy

Masao KAKIMOTO, Shuji SAITO, Eizi HIROTA, and Nobukimi OHASHI[1]

As mentioned in II-A-2 little is known about molecules of the type XSO with X = H or halogen. Recently, however, Schurath et al.[2] observed chemiluminescence emitted from a system consisting of three reactants, O, H_2S, and O_3. From an analysis of the observed spectra they derived the vibrational frequencies and the molecular structures both in the upper and lower states of the transition, and thus concluded the presence of the HSO radical in the system, which was responsible for chemiluminescence. However, the resolution (about 0.8 cm^{-1}) available allowed them to derive the constants only with moderate precision. We applied laser excitation spectroscopy to this new free radical to determine the molecular constants much more precisely. The dye lasers we used are described in Large Scale Research Equipments.

After a few trials we found that a reaction of the discharge products in the oxygen gas and hydrogen sulfide or methyl mercaptan gave the best signal-to-noise ratio for the fluorescence spectra. The reaction of the O atom and H_2S has been known to produce SO, but the generation of HSO by the same reaction has not been reported before. The typical partial pressures were 25 and 100 mTorr respectively for O_2 and H_2S and 18 and 12 - 22 mTorr respectively for O_2 and CH_3SH. Because the former reaction was easier to handle, we used it for the subsequent observation of the spectra. The lifetime of HSO is probably 10-20 msec in our system. We chopped the laser beam to eliminate chemiluminescence, and also utilized appropriate filters to cut the scattered light.

We searched the spectra in the region of 16 462 - 16 520 cm^{-1}, where according to the assignment of Schurath et al. the (003) ← (000) band would appear. Series of the prominent doublets were observed as shown in Figure 1. We could pick out the Q branch series easily, but the N assignments required careful examination of the spectra. We also found that the K assignments of Schurath et al. were shifted by one, i.e. their $K = 1 \leftarrow 0,\ 2 \leftarrow 1,\ 3 \leftarrow 2$ should be replaced by $K = 0 \leftarrow 1,\ 1 \leftarrow 0,\ 2 \leftarrow 1$. Our assignments are based upon the K splittings, which Schurath et al. could not observe because of insufficient resolution. We assigned 345 transitions in total of $K = 0 \leftarrow 1,\ 1 \leftarrow 0,\ 2 \leftarrow 1$, and $3 \leftarrow 2$.

We assumed a Hamiltonian to analyze the spectra, which comprised the rotational, the centrifugal distortion, and the spin rotation terms. As to the centrifugal distortion we retained only three Δ terms. It was rather difficult to determine the signs of the spin rotation interaction constants. We could eliminate the possibilities that both $\epsilon_{aa}{}'$ and $\epsilon_{aa}{}''$ had the same sign, but
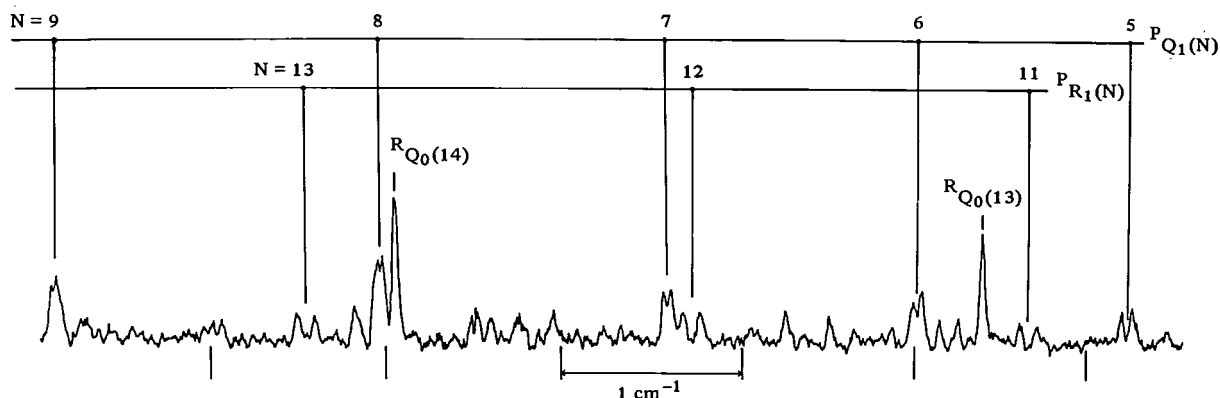
Figure 1. Laser excitation spectrum of HSO in the region of 16 464 - 16 470 cm^{-1}. The Q(5) - Q(9) and R(11) - R(13) transitions of $K = 0 \leftarrow 1$ and the Q(13) and Q(14) transitions of $K = 1 \leftarrow 0$ were identified.

Table I. Molecular Constants of HSO (MHz)[a]

Constant	Ground state	Excited state
A	295 130(120)	288 356(89)
B	20 268(5)	16 725(5)
C	18 917(5)	15 635(5)
Δ_N	0.061(14)	0.059(12)
Δ_{NK}	−0.80(77)	3.49(32)
Δ_K	59(667)	57(223)
ϵ_{aa}	−10 782(575)	17 155(521)
ϵ_{bb}	−396(101)	149(94)
ϵ_{cc}	46(99)	−344(104)

[a] Values in parentheses denote the standard deviations and apply to the last digits of the constants.

the two combinations, (+, −) and (−, +), gave almost equally good fitting to the observed spectra. However, the ground-state constant ϵ_{aa}'' is very likely to be negative, because in the second-order perturbation expression for ϵ_{aa}'' the upper state of the transition under consideration would give the most important contribution. Therefore in Table I we list only the results with a negative ϵ_{aa}''.

We also carried out a preliminary experiment on DSO. Our observation indicated that the band origin of Schurath *et al.* was probably shifted by as large as 40 cm^{-1}.

Reference and Note

1) IMS Visiting Scientist for 1978 − 79.
2) U. Schurath, M. Weber, and K. H. Becker, *J. Chem. Phys.*, **67**, 110 (1977).

II-A-7 Diode Laser Spectrostocpy of Transient Species

Eizi HIROTA, Chikashi YAMADA, Kentarou KAWA-GUCHI, Keiichi NAGAI, Keiji MATSUMURA[1] *(Kyushu Univ.)*, and Michio TAKAMI[2] *(Inst. Phys. Chem. Research)*

A diode laser spectrometer was installed as one of the main facilities of Large Scale Research Equipments. We are developing spectroscopic methods by using the diode laser as a source. A few results we obtained are listed below.

(1) $N_2O\ \nu_1$. First we applied this source to the ν_1 band of N_2O to test resolution and sensitivity of our diode laser spectrometer. In most cases we utilized the source modulation technique with the 2f detection (see Large Scale Research Equipments). It was easy to observe the hot bands from ν_2, ν_1, and $2\nu_2$ and also the ν_1 bands of the three isotopic species, $^{15}N^{14}N^{16}O$, $^{14}N^{15}N^{16}O$, and $^{14}N_2^{18}O$, in natural abundance. Figure 1 shows the spectra in the region of P(14) - P(15) of the main band. The sensitivity was limited by the Fabry-Perot type fringes. The molecular constants we derived are not so accurate as those by

microwave spectroscopy, but are nearly as precise· as those obtained by high-resolution infrared works.

(2) $CH_3F\ \nu_6$. Because many constants involved in this band have already been determined precisely, we derived only four parameters from a least-squares analysis of the five Q subbands, $K = 0 \leftarrow 1$ to $4 \leftarrow 3$. We used the $2\nu_2$ band of N_2O as a reference. The results are summarized in Table I. It may be worth noting that we could determine the sign of the q_6 constant from an analysis of the $^RQ_0$ subband.

(3) $CS\ v = 1 \leftarrow 0$ and $2 \leftarrow 1$ Although CS is an unstable molecule, it is easy to produce it by simply passing CS_2 through a discharge. We thus investigated the vibration-rotation bands of CS with provision for future studies of the transient species. We generated CS by a 60 Hz discharge in the CS_2 vapor (ca. 1 Torr), and pumped it through a single-path cell of 1 m length. We observed the $v = 1 \leftarrow 0$ bands of the four isotopic species, $^{12}C^{32}S$, $^{12}C^{33}S$, $^{12}C^{34}S$, and $^{13}C^{32}S$, and also the $v = 2 \leftarrow 1$ hot band of the main species. The wavelength standards were the ν_1 band of N_2O. By a least-squares analysis we determined the rotational constants, the centrifugal distortion constants, and the band origins. Our B and D constants agree with more accurate microwave values within three standard errors. By assuming the isotopic mass dependences we calculated the harmonic frequency ω_e and the vibrational anharmonicity constant $\omega_e x_e$ from the five observed band origins as follows: $\omega_e = 1285.1392(40)$ cm^{-1} and $\omega_e x_e = 6.4864(20)$ cm^{-1} with the standard deviations in parentheses.

(4) Stark and Zeeman modulation.   Molecular modulation is an ideal technique to sort out the absorption signals, and is expected in our case to eliminate the Fabry-Perot fringes, which limit the sensitivity of source
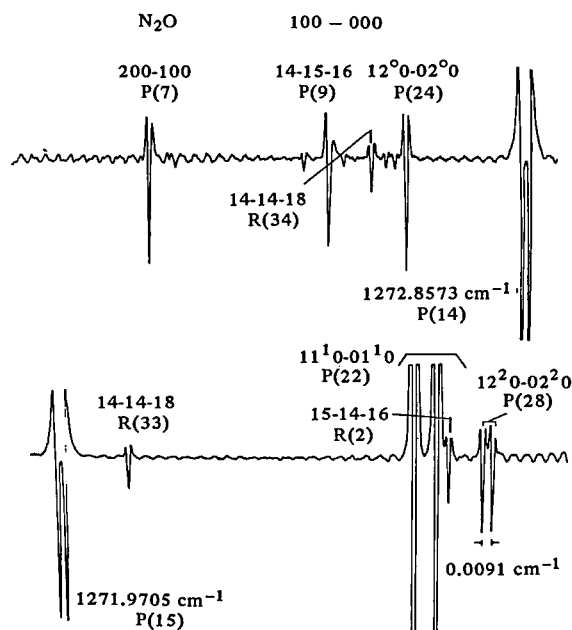
Figure 1. The spectra of the ν_1 band of N_2O, recorded by source modulation.

Table I. Molecular Constants Associated with the v_6 Band of $^{12}CH_3F$ $(cm^{-1})^a$

$\tilde{v}_6$	$1182.676\ 05(80)^b$	$(A\zeta)_6$	$1.543\ 7(11)$
A_6	$5.200\ 6(14)$	$(A\zeta)_6\eta_K$	$1.6(11) \times 10^{-4}$

Assumed:

A_0	$5.182\ 009$	B_6	$0.847\ 883\ 8$
B_0	$0.851\ 794\ 164$	q_6	$+2.902 \times 10^{-4c}$
		$(A\zeta)_6\eta_J$	$-1.87\ \times 10^{-5}$

$D_{J_0} = D_{J_6}$		1.9970×10^{-6}
$D_{JK_0} = D_{JK_6}$		1.4686×10^{-5}
$D_{K_0} = D_{K_6}$		$7.033\ \times 10^{-5}$

^{a} Values in parentheses denote 2.5 times the standard errors and apply to the last digits of the constants.

^{b} The absolute error is probably $0.001 - 0.002$ cm^{-1} because of uncertainties of the wavelength standard.

^{c} The sign was determined by the present work.

moculation. We constructed a Stark cell, which contained two brass plates 50 cm long, 2.5 cm wide, and 3 mm thick supported parallel with a spacing of 10 mm. The transmission of laser light was very good; we did not observe any substantial loss. We could apply an AC (100 KHz) field of up to 500 V/cm superposed on a DC field of up to 100 V/cm. We observed the $^QR_1$ (1) transition of the CH_3F ν_3 and with the S/N ratio of 730. However, we failed to detect the R(3.5) line of NS in the $^2\Pi_{3/2}$ state, which we could observe by source modulation. For Zeeman modulation pick-up was much more serious because of magnetic coupling. We thus first utilized 60 Hz modulation, for which it was eacy to get a high magnetic field. We could observe the two lines of SO in $^3\Sigma^-$ and a few lines of the NO_2 ν_3 band. However, we had to use a long time constant and thus to reduce the sweep rate, to get a good S/N ratio. Recently, we could reduce pick-up

by placing a Zeeman cell apart from the laser source, and could thus increase the modulation frequency as high as 1 KHz.

(5) Laser microwave double resonance. Double resonance spectroscopy is of great use to confirm assignments of vibrational transitions and to determine the molecular constants with high precision. As a first example we carried out an experiment on the ν_4 band of ammonia. The cell is a simple copper tube of 25 mm diameter and 150 cm length with provision for microwave to feed in. We could observe a double resonance signal by pumping the ground-state microwave transition. However, we would need more microwave power density to observe the double resonance signals in the upper vibrational state.

Notes

1) IMS Graduate Student for 1978 –.
2) IMS Adjunct Associate Professor for 1978 –.

II-B Microwave Spectroscopy of Non-polar Molecules

Microwave spectroscopy provides the molecular constants with high precision, but may be applied only to polar molecules. Recent advances in theory and experiment of molecular spectroscopy have made it possible to observe the rotational transitions in molecules which are normally classified as the non-polar molecules. This is of particular importance because most non-polar molecules are of high symmetry and thus play an important role in the theory of molecular structure. Three mechanisms are known, which induce a small dipole moment for a non-polar molecule:
(1) degenerate vibration,
(2) centrifugal distortion,
(3) isotope substitution.
The present project is concerned with the last mechanism. We have already reported the microwave spectra of ethane $(CH_3CD_3,\ ^{13}CH_3\ CD_3,\ CH_3\ ^{13}CD_3)$, allene $(CH_2=C=CD_2)$, and methane (CH_2D_2). Klemperer and his coworkers showed by molecular beam electric resonance that CH_3D was also slightly polar, and Muenter and Laurie observed the $J = 1 \leftarrow 0$ transition of acetylene-d_1 by microwave spectroscopy. At present the origin of the dipole moment induced by isotopic substitution is not completely clear. In polyatomic molecules the intramolecular vibrations probably amplify the induced moment.

II-B-1 Microwave Spectra of Ethylene-1,1-d_2 and Ethylene-d_1

Kazuhiko YOSHIDA[1] *(Sophia Univ.)*, Yasuki ENDO, Shuji SAITO, and Eizi HIROTA

Although it is an asymmetric top, ethylene plays an important role in structural chemistry; its C=C bond length has been taken as a standard for the carbon-carbon double bond. Many papers have already been published on the high-resolution infrared and Raman spectra of this molecule, but we will be able to supply more accurate spectroscopic constants on some of the deuterated species by microwave spectroscopy. It would also be of some interest to determine the dipole moments of these species.

First we investigated ethylene-1,1-d_2 by Stark modulation with a K-band absorption cell 50 cm long, cooled by dry ice. II-A-1 describes the details of our spectrometer. Only two transitions $3_{22} \leftarrow 2_{21}$ and $3_{21} \leftarrow 2_{20}$ were accessible by our spectrometer, which had Stark effects large enough to be modulated. We observed them and measured their Stark effects by using OCS as a standard. The dipole moment we thus determined is 0.0091 ± 0.0004 D.

Other transitions of the 1,1-d_2 species and those of the singly deuterated species, which would appear in the region covered by our spectrometer, have the Stark effects that are too small to be observed by Stark modulation. Therefore, we devised a source modulation technique.[2] The most serious problem with source modulation is distortion of the base line. We corrected a part of distortion by superposing saw tooth on the signal. Our cell was made of a K-band waveguide of 1 m length, which was cooled down to $-120 \sim -130°C$ by liquid nitrogen. We could observe even the $1_{01} \leftarrow 0_{00}$ transition by this technique, which had an absorption coefficient as small as 1.4×10^{-8} cm^{-1} at 150°K. The observed transition frequencies of the 1,1-d_2 species were analyzed by a least-squares method, where the centrifugal distortion constants were fixed to the values calculated by Duncan et al.[3] Table I compares our rotational constants with the infrared values by Speirs et al.[4] The B and C rotational constants were improved in accuracy very much, whereas the A constant was not determined very precisely, because our measurements were limited to the a-type R branches with $\Delta K_{-1} = 0$.

Table II. Rotational Constants and Centrifugal Distortion Constants of Ethylene-d_1 (MHz)

Constant	Present work[a]	Ref. 5
A	$120\ 093.487 \pm 0.045$	$120\ 092.7 \pm 7.5$
B	$27\ 470.540 \pm 0.020$	$27\ 472.4 \pm 2.4$
C	$22\ 297.940 \pm 0.013$	$22\ 301.6 \pm 2.4$
Δ_J	$0.037\ 84 \pm 0.000\ 72$	$0.036\ 9 \pm 0.003\ 6$
Δ_{JK}	$0.188\ 5 \pm 0.002\ 2$	0.183 ± 0.036
Δ_K	$(2.111)^b$	2.111 ± 0.057
δ_J	$0.008\ 47 \pm 0.000\ 10$	$0.006\ 6 \pm 0.001\ 8$
δ_K	$(0.14)^b$	0.14 ± 0.11

[a] Errors are the standard deviations.
[b] Fixed.

Speirs et al. took into account only three centrifugal distortion constants. Therefore, a direct comparison with the present results will need small corrections for the rotational constants.

Ethylene-d_1 belongs to a lower symmetry C_s. In fact we observed both the a-type and b-type transitions. The observed relative intensities corresponded well with those predicted from an assumption that the dipole moment of this species was parallel to the C-D bond. We analyzed the observed transition frequencies by a least-squares method. First we fixed the centrifugal distortion constants to the infrared values,[5] but we found that some of them, in particular δ_J, were to be revised. In the final analysis we included three centrifugal distortion constants, Δ_J, Δ_{JK}, and δ_J, in addition to A, B, and C as adjustable parameters, while Δ_K and δ_K were fixed to the infrared values. Table II compares our constants with those of Ref. 5.

Recent observations of the rotational spectra of a few deuterated species (HDO, N_2D^+, DCO^+, DCN, DNC, NH_2D) in interstellar space suggest that we might be able to observe ethylene by radio telescopes. In that case our data on ethylene-d_1 would be of some use.

References and Notes

1) IMS Graduate Student for 1977 —.
2) E. Hirota and M. Imachi, *Can. J. Phys.*, **53**, 2023 (1975).
3) J. L. Duncan, D. C. McKean, and P. D. Mallinson, *J. Mol. Spectrosc.*, **45**, 221 (1973).
4) G. K. Speirs, J. L. Duncan, and D. Van Lerberghe, *J. Mol. Spectrosc.*, **51**, 524 (1974).
5) Y. Verbist-Scieur, C. P. Courtoy, A. Fayt, and D. Van Lerberghe, *Mol. Phys.*, **33**, 351 (1977).

Table I. Rotational Constants of Ethylene-1, 1-d_2 (MHz)

Constant	Present work[a]	Ref. 4[b]
A	$97\ 512.3 \pm 5.8$	$97\ 501.5 \pm 5.4$
B	$25\ 674.969 \pm 0.029$	$25\ 677.5 \pm 4.8$
C	$20\ 268.949 \pm 0.027$	$20\ 275.0 \pm 6.0$

[a] The τ constants reported in Ref. 2 were fixed in a least-squares analysis. The errors denote the standard deviations.
[b] Three centrifugal distortion constants, D_J, D_{JK}, and D_K, were included as additional parameters.

II-B-2 Microwave Spectra of Acetylene-d in the $v_4 = 1$ and the $v_5 = 1$ States

Keiji MATSUMURA[1] *(Kyushu Univ.)*, Takehiko TANAKA *(Kyushu Univ.)*, Yasuki ENDO, Shuji SAITO, and Eizi HIROTA

Recent investigations on fluoroacetylene[2] and fluoroacetylene-d_1[3] by laser Stark and laser microwave double resonance spectroscopy revealed that the dipole mo-

ments of the two molecules changed by as much as 3 - 9 % on excitation of the normal modes. The change by the v_4 mode (CCH or CCD bending) is particularly large, and the ratio of the changes for the normal and the deuterated species is close to $\sqrt{2}$. It would be of some interest to make a crude estimate of the dipole moment of acetylene-d from those of fluoroacetylenes by assuming an "additivity" of the dipole moments. For example, according to the assumption the dipole moment of acetylene-d_1 in the v_5 = 1 (CCH bending) state is approximately equal to μ (HCCF in v_4 = 1) - μ (DCCF in the ground state), or 0.0772 D. Similarly the dipole moment in the v_4 = 1 (CCD bending) state may be estimated by μ (DCCF in v_4 = 1) - μ (HCCF in the ground state), i.e. 0.0367 D. Although Muenter and Laurie[4] observed the J = 1 ← 0 transition of HCCD in the ground state, they could not determine the dipole moment, because the Stark effect of this transition was too small. However, the ground-state moment is probably of the order of 0.01 D, as inferred from isotope-induced dipole moments determined for other non-polar molecules (Note that the difference between the dipole moments of HCCF and of DCCF in the ground states amounts to 0.0122 D). We might thus presume that the spectra of acetylene-d_1 in the excited states of the bendings are as strong as the ground-state spectra, in spite of unfavorable Boltzmann factors; the factor μ^2 exp($-h\nu/kT$), when normalized to the ground-state value, is 0.7 and 1.3 at 300°K for v_4 = 1 and v_5 = 1 respectively. Furthermore the excited-state spectra will have much larger Stark effects because of the l-type doubling. Baldacci et al.[5] analyzed the high resolution infrared spectra to obtain the rotational and the l-type doubling constants of HCCD in the v_4 = 1 and the v_5 = 1 states. By using the dipole moments estimated above and the l-doubling constants of Ref. 5 we estimated the Stark effects of the J = 2 ← 1 transitions to be 1.8 E^2 MHz and 0.33 E^2 MHz respectively for the v_5 = 1 and v_4 = 1 states, where the Stark field E was given in the unit of kV/cm. These Stark effects are large enough to modulate the absorption lines.

We observed the J = 2 ← 1 transitions of acetylene-d_1 both in the v_4 = 1 and v_5 = 1 states at room temperature by using a Stark modulation spectrometer described in detail in II-A-1. The Stark cell used was the same as in II-B-1. The observed transition frequencies and the rotational constants are listed in Table I, where the values reported in Ref. 5 are also given for comparison. The Stark effects were found to be of the second order for the electric fields of up to 3 kV/cm, and were measured by using OCS as a reference molecule.

Table I. Transition Frequencies and Rotational Constants of Acetylene-d_1 in the v_4 = 1 and the v_5 = 1 States (MHz)[a]

		v_4 = 1	v_5 = 1
J = 2 ← 1	c	118 945.128(10)	118 854.79 (2)
	d	119 477.246 (6)	119 277.505(8)
B_c		29 736.572 (3)	29 713.988(5)
		[29 738.8(9)][b]	[29 717.5(12)][b]
B_d		29 869.554 (2)	29 819.642(2)
		[29 863.8(12)][b]	[29 820.4(15)][b]
μ(D)		0.0231	0.0552

[a] Values in parentheses denote standard errors and apply to the last digits of the values.
[b] Ref. 5.

The dipole moments derived from an analysis of the Stark effects are included in Table I. They are about two thirds of the estimated values, but are certainly larger than isotope-induced dipole moments (0.003 - 0.014 D)[6] already reported.

The dipole moment in a vibrational state may be given by

$$\mu_v = \mu_e - \sum_s (\partial\mu/\partial Q_s) [\sum_{s'} \Phi^{ss'} (v_{s'} + d_{s'}/2)] + \sum_s (\partial^2\mu/\partial Q_s^2) \Omega_s (v_s + d_s/2)$$

$$= \mu_e + \sum_s \delta\mu_s (v_s + d_s/2),$$

where $\Phi^{ss} = (1/2\pi)(h/c\omega_s)^{\frac{1}{2}}(1/\omega_s)3k_{sss}$, $\Phi^{ss'} = (1/2\pi)(h/c\omega_s)^{\frac{1}{2}} (1/\omega_s) k_{ss's'}(s \neq s')$, and $\Omega_s = (h/8\pi^2 c\omega_s)$. The contribution of the s-th mode $\delta\mu_s$ is therefore expressed as follows:

$$\delta\mu_s = -\sum (\partial\mu/\partial Q_{s'}) \Phi^{s's} + (\partial^2\mu/\partial Q_s^2)\Omega_s.$$

The first term may be estimated roughly by using the infrared absorption intensities,[7] and is calculated to be of the order of 4 × 10^{-3}D. Therefore, the large moment in the v_5 state is ascribed to the second term.

Acetylene-d_1 may also be detected by radio telescopes in interstellar space, because acetylene has already been found to be abundant in space.

References and Notes

1) IMS Graduate Student for 1978 –.
2) T. Tanaka, C. Yamada, and E. Hirota, J. Mol. Spectrosc., 63, 142 (1976).
3) K. Matsumura, K. Tanaka, C. Yamada, and T. Tanaka, to be published.
4) J. S. Muenter and V. W. Laurie, J. Am. Chem. Soc., 86, 3901 (1964).
5) A. Baldacci, S. Ghersetti, S. C. Hurlock, and K. N. Rao, J. Mol. Spectrosc., 59, 116 (1976).
6) E. Hirota and M. Imachi, Can. J. Phys., 53, 2023 (1975).
7) D. F. Eggers, Jr., I. C. Hisatsune, and L. Van Alten, J. Phys. Chem., 59, 1124 (1955).

II-C Anharmonic Potential Function and Equilibrium Molecular Structure

Spectroscopy provides us with rotational constants, which we may use to determine the molecular structure precisely. However, at most three rotational constants are available for one species. Obviously the number of independent structural parameters of a molecule exceeds three except for a few simple cases (e.g. diatomic and bent Y-X-Y molecules). Therefore we normally utilize the rotational constants of isotopic species to increase the number of the input data. However, this provides a serious problem for structure determination; the rotational constants usually available are those in the ground vibrational state and are thus contaminated by contributions from the zero-point vibrations. These contributions are unfortunately isotope-dependent, and we need knowledge of the anharmonic potential constants to correct the rotational constants for the contributions of the intramolecular vibrations. In principle we can make the vibrational corrections by observing the rotational spectra in the excited vibrational states and/or the vibration-rotation transitions. It is, however, difficult to determine the rotational constants of a molecule in the first excited states of all the normal modes except for a few simple molecules. Still vibration-rotation constants which are observed only for some of the low-lying excited states are useful to estimate the anharmonic (cubic or third-order) potential constants. Anharmonicity is important not only for structure determination, but also for interpretation of physical constants determined by spectroscopic methods such as the dipole moment. With knowledge of the anharmonic potential function we would certainly be able to understand the intramolecular motions much more in detail than only with the harmonic force field.

II-C-1 Second-Order Coriolis Resonance between ν_2 and ν_5 of $^{13}CH_3F$ by Microwave Spectroscopy

Eizi HIROTA, Shuji SAITO, and Yasuki ENDO

The ν_2 - ν_5 Coriolis interaction in methyl fluoride, which is well known as one of the largest second-order resonances, was recently analyzed in detail by high resolution Raman[1] and microwave[2] spectroscopy. A simultaneous use of the two spectroscopic methods was proved to be very efficient; the band origin and the A constants were determined by Raman spectroscopy, whereas microwave spectroscopy provided accurate values for other constants associated with the two excited states. Recently Hegelund et al.[3] extended a similar analysis to the Raman spectra of $^{13}CH_3F$. The present report will describe the microwave spectra of this molecule in the v_2 and v_5 states.

A sample of methyl fluoride-^{13}C was provided us through the courtesy of Professor Brodersen. The microwave spectrometer used in the present work is described in II-A-1.

First we noticed large isotope shifts of the transition frequencies; for example, the $J = 1 \leftarrow 0$ transitions of $^{12}CH_3F$ in ν_2 and ν_5 appear at -4329 MHz and $+7514$ MHz, respectively, from the ground-state line,[2] while we observed the corresponding transitions at -3371 MHz in the case of $^{13}CH_3F$. These large shifts are mainly due to the isotope effect on the ν_5 - ν_2 frequency difference. In fact, we could explain the ν_2 and ν_5 satellite lines by assuming ν_5 - ν_2 to be about 360 GHz (12.0 cm^{-1}) in $^{13}CH_3F$, which is to be compared with 252 GHz (8.4 cm^{-1}) in $^{12}CH_3F$. Once the ν_5 - ν_2 separation was estimated, we could assign the $J = 2 \leftarrow 1$ transitions quite easily. We observed characteristic Stark effects of the $k = l = \pm 1$ (l-type doublet) transitions. We

Table I. Molecular Constants of $^{13}CH_3F$ in the ν_2 and ν_5 States (MHz)[a]

Constant	Value	Constant	Value
$\nu_5 - \nu_2$	$358.24(87) \times 10^3$	q_5^*	$28.17(96)$
B_5^*	$24\,925.6(18)$	q_5'	$-0.033(39)$
B_2^*	$24\,773.0(10)$	q_5''	$0.000\,6(17)$
D	$21\,276.(35)$	$A\zeta_5\eta_J$	$1.0(13)$
r_5	$87.(55)$		

Assumed:

A_5	$154\,056.7^b$	D_J	$0.056\,6^c$
A_2	$156\,005.4^b$	D_{JK}	0.407^c
$A\zeta_5$	$-38.16(60) \times 10^{3b}$	D_K	2.125^b
$A\zeta_5\eta_K$	$0.$		

[a] Values in parentheses denote 2.5 times standard errors and apply to the last digits of the constants. They include the errors due to the uncertainty of $A\zeta_5$.

[b] Ref. 3.

[c] S. M. Freund, G. Duxbury, M. Römheld, J. T. Tiedje, and T. Oka, J. Mol. Spectrosc., 52, 38 (1974).

could also assign the direct l-doubling transitions of $J = 2 - 6$, some of which showed well resolved Stark components.

We analyzed the observed spectra by using the same Hamiltonian and computer program described in Ref. 4. As in the case of $^{12}CH_3F$[1,2] Hegelund et al.[3] and we performed an "iterated" analysis; we borrowed the A_2 and A_5 constants from the Raman results, which Hegelund et al. derived by fixing most other constants to our microwave values. We compared the transition frequencies calculated from these constants with the observed frequencies. The agreement is much less satisfactory than in the case of $^{12}CH_3F$; the average deviations are about 2.5 times larger. The standard errors of the derived constants are even much larger, in particular for ν_5 - ν_2, $A\zeta_5$, and D. This is primarily due to the fact that the energy difference between the two vibrational states is about 50% larger in the present

case. Hegelund *et al*.[3] determined the $A\zeta_5$ value which was about three times more accurate than ours. We thus carried out an analysis by fixing $A\zeta_5$ to their value. The results are summarized in Table I. We found that the standard deviations of ν_5 - ν_2 and D were very much reduced. The errors given in Table I include those due to the uncertainty of the Raman value of $A\zeta_5$.

We notice that the Coriolis interaction constant D is proportional to the B value; when we multiply the D value of $^{12}CH_3F$ by the ratio of the B constants, we obtain 21 262.5 (±8.0) MHz, which agrees with the D value of Table I. The present results will be of some use for anharmonic potential calculations.[5]

References

1) R. Escribano, I. M. Mills, and S. Brodersen, *J. Mol. Spectrosc.*, 61, 297 (1976).
2) E. Hirota, T. Tanaka, and S. Saito, *J. Mol. Spectrosc.*, 63, 478 (1976).
3) F. Hegelund, S. Brodersen, and I. M. Mills, to be published.
4) T. Tanaka and E. Hirota, *J. Mol. Spectrosc.*, 54, 437 (1975).
5) I. M. Mills, private communication.

II-C-2 Anharmonic Potential Function and Equilibrium Structure of Methylene Fluoride

Eizi HIROTA

For a simple molecule of certain type it may be possible to observe the rotational spectra in the excited states of all the normal modes and to determine its molecular structure at the equilibrium. However, this orthodox approach will not be feasible for a little more complicated molecule, because some of the fundamental states are too high to observe the rotational spectra in these states by microwave spectroscopy. As an example of such a molecule we investigated methylene fluoride in the present work. The following considerations led to the choice of this molecule. Because it is an asymmetric top, we may determine three rotational constants for each vibrational state. Among the asymmetric top molecules it belongs to the highest symmetry C_{2v}. The absence of any nuclei with the quadrupole moments makes the rotational spectrum simple enough to observe weak vibrational satellites. By investigating not only the normal species but also ^{13}C- and D-substituted species, additional information may be obtained.

We have already analyzed the rotational spectra of $^{12}CH_2F_2$[1] and of $^{12}CD_2F_2$[2] in all the fundamental states except for the two C-H or C-D stretching states, which were too high in energy to access by our microwave spectrometer. However, because the two modes are much higher in frequency than others, we might neglect "cross" terms among the anharmonic potential constants, that is, terms which are associated with both C-H(D) stretching and other low-frequency modes. This assumption may allow us to estimate the equilibrium structure as well as anharmonic potential constants concerning with the C-H(D) stretching coordinates.

	r_e	r_z[a]	r_s[c]	r_0[d]
C-H(Å)	1.084(3)	1.097(5)	1.0934(30)	1.092
C-F(Å)	1.3508(5)	1.3601(14)	1.3574(10)	1.358
HCH(°)	112.8(3)	[113.67][b]	113.67(17)	111.87
FCF(°)	108.49 (6)	108.11(16)	108.32(5)	108.28

[a] For $^{12}CH_2F_2$. The difference between r(C-H) in $^{12}CH_2F_2$ and r(C-D) in $^{12}CD_2F_2$ is 0.0025 Å. Other parameters remain the same for the two species within experimental uncertainty.
[b] Assumed.
[c] E. Hirota, T. Tanaka, A. Sakakibara, Y. Ohashi, and Y. Morino, *J. Mol. Spectrosc.*, 34, 222 (1970).
[d] D. R. Lide, *J. Amer. Chem. Soc.*, 74, 3548 (1952).

We analyzed forty two vibration-rotation constants observed for the two species by using a method of Hoy *et al*.[3] We found, however, that our data allowed us to determine only thirteen of the fifty two independent third-order anharmonic potential constants. Furthermore, precision of the derived third-order constants was not high except for f^{333} (37.5 ± 5.0 md/Å²), where 3 meant one of the C-F stretching coordinates. However, we could reproduce the observed vibration-rotation constants with the average deviations of 20.51, 11.25, and 13.83 MHz for α^A, α^B, and α^C. Anharmonic potential constants thus derived were used to calculate the vibration-rotation constants of $^{13}CH_2F_2$, $^{13}CD_2F_2$, and $^{12}CHDF_2$, except the terms in f^{111} (the superscript 1 denotes one of the C-H stretching coordinates). The ground-state rotational constants of the five isotopic species, which were corrected for the vibration-rotation constants thus calculated, were subjected to a least-squares analysis to derive the equilibrium structure listed in Table I and f^{111} of -37 ± 7 md/Å². Table I also shows other structures for comparison, including the r_z structure calculated for $^{12}CH_2F_2$. We obtained an isotope effect r_z(C-H) - r_z(C-D) to be 0.0025 Å.

References

1) E. Hirota, *J. Mol. Spectrosc.*, 69, 409 (1978).
2) E. Hirota and M. Sahara, *J. Mol. Spectrosc.*, 56, 21 (1975).
3) A. R. Hoy, I. M. Mills, and G. Strey, *Mol. Phys.*, 24, 1265 (1972).

II-C-3 Anharmonic Potential Function and Equilibrium Structure of Methane

Eizi HIROTA

The C-H bond length of methane is obviously one of the most important structure parameters. Bartell and and Kuchitsu[1] reanalyzed recently their earlier electron-diffraction data[2] to arrive at r_e(C-H) in CH_4 of 1.086_2 ± 0.0024 Å and at r_e(C-D) in CD_4 of 1.087_5 ± 0.0026 Å. A more recent electron-diffraction experiment by Fink[3] led to r_e(C-H) in CH_4 of 1.087_7 Å. Spectroscopic studies, on the other hand, found it difficult to derive a precise r_e(C-H) distance. This is because CH_4 is a

spherical top and its infrared and Raman spectra are too complicated by the vibration-rotation interactions to derive the equilibrium rotational constant precisely. Fortunately Deroche[4] and Akiyama et al.[5] recently, reported all the vibration-rotation constants of methane-d_2, an asymmetric top species. We may thus derive readily the equilibrium rotational constants and the equilibrium structure. However, we have to be careful in using the observed α constants, especially those in higher excited states, because resonance interactions may often affect the α constants seriously. This holds even in cases where the observed spectra do not exhibit any anomalies.

We thus first analyzed the reported vibration-rotation constants by a method of Hoy et al.[6], where the harmonic force field given in Ref. 7 was used. There are thirteen independent third-order anharmonic constants, but, because of the redundancy, the choice of the independent constants is not unique. We chose a certain set of the constants as independent, and derived relations by which dummy constants might be derived. Deroche[4] analyzed the lowest five bands (ν_3, ν_5, ν_9, ν_7, and ν_4) simultaneously by taking into account the Coriolis interactions explicitly. However, in the present work we calculated the α constants simply by dropping the Coriolis resonance terms from the second-order perturbation expression for α. This assumption will not affect the equilibrium rotational constants very much because of cancellation.

We found that the α_8 and α_2 constants reported by Akiyama et al.[5] were probably perturbed by Fermi interactions; we could not reproduce the large (absolute)

values of the α constants by calculation. The $\alpha_7{}^A$ and $\alpha_4{}^A$ constants of Deroche also did not agree with the calculated values. The discrepancy is probably ascribed to a large Coriolis interaction between the two modes.

Of the thirteen third-order potential constants we could derive only f^{111} to be significant (-27.5 ± 1.4 md/Å^2), while others were determined with large uncertainties. However, they could be used to calculate the contributions of the zero-point vibrations to the ground-state rotational constants. We also applied corrections due to the centrifugal distortion effects and to the electron "slipping" effects. The equilibrium C-H lengths calculated from A_e, B_e, and C_e thus obtained were 1.086 70, 1.087 19, and 1.087 13 Å, and we concluded that

$$r_e(\text{C-H}) = 1.0870 \pm 0.0007 \text{ Å}.$$

This result agrees with those by recent electron-diffraction experiments mentioned above,[1,3] but is more accurate. A recent *ab initio* calculation by Pulay et al.[8] gave 1.086$_2$ Å, in fair agreement with the present result.

References
1) L. S. Bartell and K. Kuchitsu, *J. Chem. Phys.*, **68**, 1213 (1978).
2) K. Kuchitsu and L. S. Bartell, *J. Chem. Phys.*, **36**, 2470 (1962).
3) M. Fink, private communication.
4) J. C. Deroche, Ph. D. thesis, Univ. de Paris-sud, 1977 and earlier referances are cited therein.
5) M. Akiyama, T. Nakagawa, and K. Kuchitsu, *J. Mol. Spectrosc.*, **64**, 109 (1977).
6) A. R. Hoy, I. M. Mills, and G. Strey, *Mol. Phys.*, **24**, 1265 (1972).
7) E. Hirota and M. Imachi, *Can. J. Phys.*, **53**, 2023 (1975).
8) P. Pulay, W. Meyer, and J. E. Boggs, to be published.

II-D Production of Highly Excited Atoms from Molecules

Atoms with very high principal quantum numbers (say $n \lesssim 50$) can be produced in the gas phase by impact of low-energy electrons on atoms or simple molecules. Such "highly excited Rydberg atoms" have long natural radiative lifetimes (from microseconds to milli-seconds depending on their quantum numbers). Therefore, these atoms are metastable species of high electronic energy, i.e., potential sources of novel chemical reactions. The main purpose of the present project is to investigate mechanisms of formation of Rydberg atoms from molecules and their reactions with other neutral atoms or molecules. Since one of the electrons in such an atom is bound to the nucleus only very loosely, their reactions are expected to be a hybrid of an ion-molecule reaction and a free electron-molecule reaction. An apparatus has been designed and constructed to produce Rydberg atoms from molecules by electron impact and to measure the following properties: (a) distribution of their principal quantum numbers, (b) distribution of their kinetic energies, and (c) relative cross sections of ionization by collision with target molecules and, if possible, angular distributions of the resulting ions. Our study is being extended to similar measurements on highly excited hydrogen/deuterium molecules.

II-D-1 Design and Construction of an Apparatus for Production of Highly Excited Atoms and for Measurement of Their Properties

Tamotsu KONDOW *(Univ. of Tokyo)*, Tsutomu FUKUYAMA *(Univ. of Tokyo)*, and Kozo KUCHITSU *(Univ. of Tokyo and IMS)*

The apparatus consists of the following parts: vacuum chamber, source of low-energy electrons for excitation of atoms or molecules, molecular beam source, and a detector system.

1) *Vacuum chamber:* The chamber is composed of four sections, each part being evacuated separately. An atomic or molecular beam is produced in Part I; it is

evacuated by a 1,000 l/s oil diffusion pump to 1×10^{-5} Torr under normal operating conditions. Part II contains a tuning-fork chopper for modulating the beam and is evacuated by another diffusion pump of 600 l/s to 5×10^{-7} Torr. The beam is introduced into Part III and crossed by an electron beam, by which highly excited atoms are produced. Part IV contains a detector system, where the distributions of the principal quantum numbers and kinetic energies of highly excited atoms are determined. Part IV can be rotated about the point of reaction in Part III by ±30°, so that the angular dependence of the product ions can be measured. Parts III and IV are evacuated to $10^{-9} \sim 10^{-10}$ Torr in order to secure stable operation of the electron gun and the detector.

2) *Electron gun:* A gun of modified Simpson-Kuyatt type has been designed so as to cover $5 \sim 500$ eV with a current of $10^{-6} \sim 10^{-4}$ A and an energy spread of $0.5 \sim 1$ eV. The gun is shielded magnetically in order to improve its low-energy characteristics.

3) *Beam sources:* In order to make the beam density as high as possible, a nozzle-beam source has been designed as follows: stagnation pressure at the source, 5,000 Torr maximum; nozzle diamter, 75 μm; skimmer diameter, 0.64 or 0.71 mm, nozzle to skimmer distance, $2 \sim 17$ mm being variable from outside the vacuum; nozzle temperature, 400°C maximum, the nozzle support being water-cooled; precision of the nozzle support, ±0.02 mm; axial precision of the nozzle, ±0.1°. The relative position of the nozzle and the skimmer can be varied within ±1 mm so as to adjust their axes. It is expected to produce a helium beam of Mach number 18 and about 4×10^{19} s^{-1} sr^{-1} at a stagnation pressure of 2,000 Torr. In addition, an effusive beam source has also been designed. A glass plate with capillaries of 0.5 mm long and 2 μm diameter, 50 % transmission, is used. For helium a beam of 2×10^{17} s^{-1} sr^{-1} is expected.

4) *Detector system:* Highly excited atoms are produced by impact of pulsed electrons and ionized by an electrostatic field so that the distributions of their TOF and principal quantum numbers can be measured simultaneously. The product ions are measured by a quadrupole mass spectrometer. Highly excited atoms may also be ionized by radiation of electromagnetic waves or by collision with target molecules in a collision chamber.

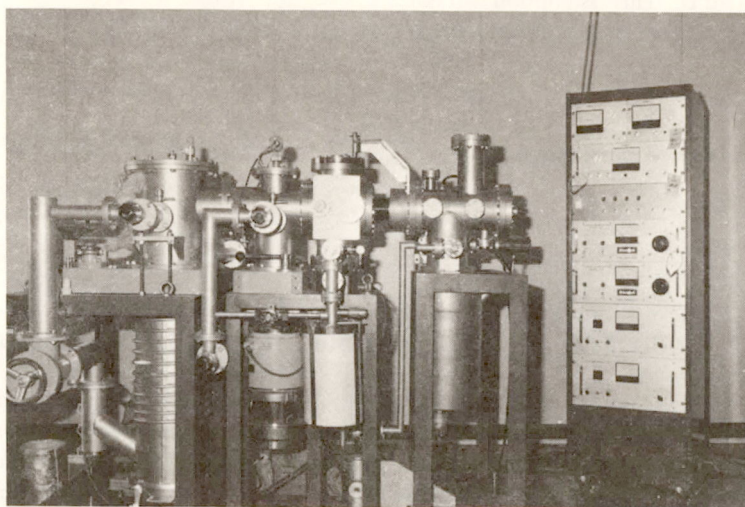Adjustment of the components and a series of test runs are now being made.

Figure 1. Apparatus (left) and power supply (right). The four chambers shown from left to right correspond to Parts I, II, III, and IV.

RESEARCH ACTIVITIES

III. Division of Electronic Structure

The goal of the Division is a development of novel functions of molecules through studies of the electronic structure. To fulfill this goal the basic characters of the electronic spectra are investigated. The emphasis is made on the research of electronically excited states of molecules. The dynamic behavior of fluorescence under various conditions, reactivities of excited molecules, and characteristics of the electron transfer in the excited states are the important feature of molecules. The design of a novel chemical reaction could be made with the intense laser.

Unique properties of the solid-molecule interface are also studied with the emphasis of developing a novel method for solar energy conversion. The fundamental and dynamical processes of photoelectrode and photocatalysis are investigated by measuring transient photocurrents, luminescence of molecules adsorbed on solid surfaces and the photochemical products by a pulsed laser excitation in ultrahigh vacuum. Together with the investigation on the molecular processes of solar energy conversion into electricity and chemical energy, new materials for this purpose are being searched.

III-A Primary Photochemical Reactions of Organic Compounds

The photochemical reactions such as photoisomerization, photosubstitution, photoelimination, photoaddition, and photoionization differ, in many cases, from the thermal reactions and give unique products, since the reaction occurs from the completely different electronic state. The energy of light which is absorbed by molecules are in the same orders of that of a chemical bond, and therefore reactivities are greatly enhanced in excited states. Thus the utilization of the photochemical reactions is important for synthetic chemistry and solar energy conversion. Mechanistic understandigs are very important for the understanding of photobiology and the developments of novel chemical reactions and solar energy conversion.

The cis-trans geometrical isomerization is one of the simplest chemical reactions and has been the object of the research for many decades. We have observed for the first time, the fluorescence lifetime of stilbene at room temperature is about 100 ps and changes enormously with the changing temperature, while the radiative decay lifetime stays constant. Studies are in progress on the direct photoisomerization with picosecond flashphotolysis and its temperature effects.

III-A-1 Temperature Dependence of Fluorescence Lifetimes of *Trans*-Stilbene

Minoru SUMITANI, Nobuaki NAKASHIMA, Keitaro YOSHIHARA, and Saburo NAGAKURA *(Univ. of Tokyo)*

Cis-trans geometrical isomerization of stilbene is one of the most fundamental photochemical reactions. Many workers have attempted to understand the mechanism of the direct photoisomerization of stilbenes.[1] The temperature dependence of fluorescence quantum yields and the quantum yields of *cis-trans* photoisomerization were investigated.[1,2] The quantum yield of fluorescence increases as the temperature decreases, whereas quantum yield of *trans* to *cis* photoisomerization decreases as temperature decreases.

The temperature dependence of the fluorescence lifetimes of *trans*-stilbene was measured with a picosecond laser and a streak camera. We observed a smooth sigmoidal relationship quite similar to the temperature dependence of fluorescence quantum yields. The results have clearly shown that the radiative rate is essentially constant in the temperature range from 77K to 295K.

The 4th harmonic (266 nm) of a passively mode-locked Nd^{3+}: YAG laser (1.06 μm) excited *trans*-stilbene. The fluorescence decay was measured with a Hamamatsu TV streak camera (HTV C979). The streak was digitized by a TV camera/microcomputer system (HTV C1000). The fluorescence lifetimes (τ_f) were obtained from the decay curves by an iterative fitting procedure which simultaneously adjusted pre-exponential factor and τ_f. At least five decay curves were obtained for each measurement, and in each case a good fit to a single exponential was found.

The fluorescence lifetimes (τ_f) are plotted in Figure 1(a) against the temperature. We obtained a smooth sigmoidal relationship quite similar to the temperature dependence of fluorescence quantum yields obtained by Malkin and Fischer[2] which are also shown in the same figure. The S_1 radiative (k_f), radiationless (k_I),
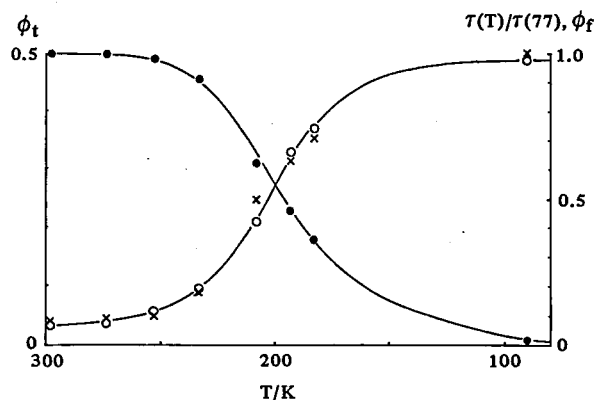
ϕ_t

$T(T)/T(77), \phi_f$

Figure 1(a). The temperature dependence of the observed fluorescence lifetime (—o—), quantum yield of fluorescence (—x—), and quantum yield of isomerization (—●—) in MCH/IH[3]. The fluorescence lifetime is normalized to the fluorescence lifetime at 77K; $T(T)/T(77K)$. The best fit curves are shown in solid lines.
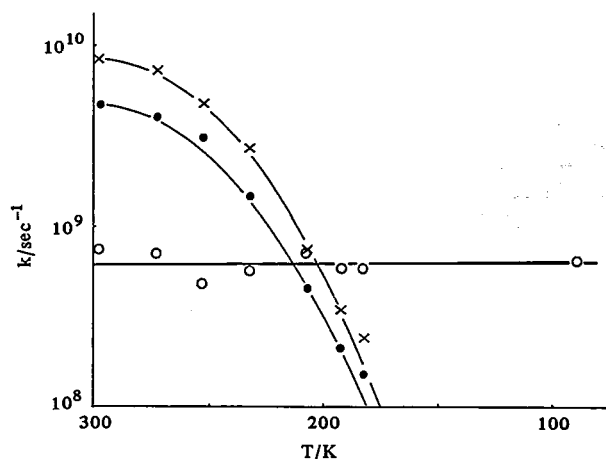
Figure 1(b). The temperature dependence of the radiative (k_f; —o—), radiationless (k_I; —x—), and isomerization (k_t; —●—) rate constant in MCH/IH.

and isomerization (k_t) rates are plotted as a function of temperature in Figure 1(b). As is shown in Figure 1(a), the decrease in T_f is paralleled by a corresponding decrease in ϕ_f. Therefore, as is seen in Figure 1(b),
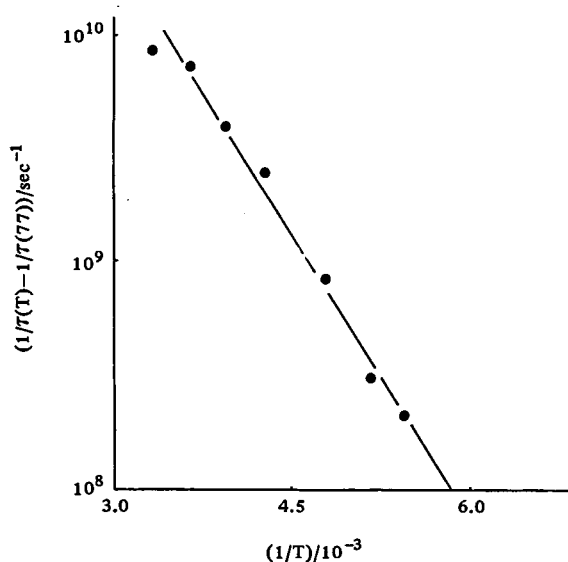
Figure 2. Plots of $1/T(T)-1/T(77K)$ vs. $1/T$. The activation energy (E_a) was calculated by the following equation.[1] Aexp $(-E_a/RT) = 1/T(T)-1/T(77K)$, $E_a = 3.5 \pm 0.5$ kcal/mol a frequency factor $A = (3 \pm 1) \times 10^{12} s^{-1}$.

the radiative rate constant is constant at $6 \times 10^8 s^{-1}$ within experimental error. k_I's and k_t's decrease rapidly paralleling each other with decreasing temperature. From the temperature dependence of the fluorescence lifetimes, the activated decay process from the fluorescent state has an energy barrier of 3.6 ± 0.4 kcal/mol as shown in Figure 2. This is in agreement with measurements of the activation energy from the quantum yield. This is also on good accordance with the energy barrier for trans-cis photoisomerization (4.1 kcal/mol). The observed T_f (108 ps) at room temperature also agreed with the S_1 lifetime estimated by a quenching experiment (100 ps).[3]

References

1) J. Saltiel, J. D'Agostino, E. D. Megarity, L. Metts, K. R. Neuberger, M. Wrighton, and O. C. Zafiriou, Org. Photochem., 3, 1 (1973).
2) S. Malkin and E. Fischer, J. Phys. Chem., 68, 1153 (1964).
3) J. Saltiel and E. D. Megarity, J. Am. Chem. Soc., 94, 2742 (1972).

III-B Electron Transfer Reactions in Ground and Excited States

The electron transfer process is the most critical step in the oxidation and reduction in chemistry and biology. For a detailed investigation of the mechanism the ionization process by solvated electrons has been undertaken. Electron transfer probabilities of solvated electrons were determined in ethanol at 77 K. Large variations in the electron transfer probabilities were found for various kinds of acceptors, being related to the activation energy of the dissociative electron attachments in gases. These variations were ascribed to the effects of the nuclear contributions of the acceptors, namely, the Franck-Condon factors. The actual probability of electron transfer was explained by the electronic exchange mechanism. Theoretical analyses and calculations were made.

The electron transfer from an excited molecule, namely, photoionization can also be treated within the framework of the above theory. The dynamic behaviors of the fluorescence quenching due to the photoionization were studied in rigid matrices at low temperature. A non-exponential decay was observed and explained by the exchange interaction.

It is well known that the rate of electron transfer is very much dependent on the solvent polarity. However, this general concept has not yet proven on the basis of a detailed experimental observation of the electron transfer distance. Analysis of the transient effect in the diffusion-controlled fluorescence quenching reaction gives electron transfer distances for this reaction. We have succeeded in observing the differences in electron transfer distance upon changing the solvent polarity.

The electron transfer reaction from an adsorbed monolayer to a substrate is a most fundamental process for solar energy conversion. Photochemical injection of electron from a monolayer dye to single crystals such as anthracene, phenanthrene, naphthalene was studied by observing decay kinetics of the fluorescence of dye. Non-exponential decay was found in the picosecond region and was ascribed to a fluorescence quenching by an electron transfer.

III-B-1 Transfer of Solvated Electrons to Some Aliphatic Halides in Ethanol at 77K; The Role of Franck-Condon Factors

Akira NAMIKI, Nobuaki NAKASHIMA, Keitaro YOSHIHARA, Yoshiro ITO *(Kyoto Univ.)*, and Takenobu HIGASHIMURA *(Kyoto Univ.)*

Electron transfer probabilities of solvated electrons were determined by optical absorption measurements in ethanol at 77K. The survival probability of e_s^- was found as $P(t) = \exp(-\alpha(t)\,[A])$, where $\alpha(t)$ is the concentration of the acceptor molecule. A large variation in α was found for various solvents as seen in Table 1.

Table 1. Electron Transfer Probabilities, Electron Transfer Distances, Observed $F\tilde{v}$, and Their Relations to the Activation Energies of the Dissociative Electron Attachment in Gases for Various Aliphatic Halides

Compounds	$\alpha(t)$ (M^{-1})	l (A)	$F\tilde{v}$ (s^{-1})	ΔE^b (eV)
CCl_4	32.26	23.4	1.95×10^{13}	-0.026
$CHCl_3$	17.54	19.1	2.46×10^{10}	0.134
CH_2Cl_2	6.94	14.0	9.34×10^6	0.325
CH_2ClCH_2Cl	6.90	14.0	8.96×10^6	0.377
$CH_2ClCH_2CH_2Cl$	5.56	13.0	1.98×10^6	0.334
$(CH_3)_3CCl$	4.05	11.7	2.62×10^5	0.473
CH_2Br_2	24.39	21.3	7.70×10^{11}	0.052
CH_3Br	8.93	15.2	6.23×10^7	0.247
CH_2BrCH_2Br	21.28	20.4	1.77×10^{11}	0.082
$CH_2BrCH_2CH_2Br$	10.64	16.2	2.61×10^8	0.130
CH_3I	20.41	20.1	1.14×10^{11}	0.026
C_6H_5I	20.00^a	20.0	9.27×10^{10}	0.067

Many workers applied the simple tunneling theory[1] to explain the decay of e_s^- as a consequence of electron transfer to solute molecules. This theory was successful in evaluating the magnitude of $\alpha(t)$ to a certain extent, but it failed to explain the variation due to the nature of the acceptors. In this work we used the perturbation theory (Fermi-Golden rule). The dependence of $\alpha(t)$ on acceptors was explained quite well.

Assuming "Condon approximation", the electron transfer rate W_{ab} at donor-acceptor distance R can be written as follows,

$$W_{ab} = \frac{2\pi}{\hbar} |V_{ab}(R)|^2 \sum_\beta |(\chi_\alpha | \chi_\beta)|^2 \delta(E_{a\alpha} - E_{b\beta}),$$
(1)

where $V_{ab}(R)$ is a matrix element between the electronic states of the initial e_s^- and the final anionic states, and $(\chi_\alpha | \chi_\beta)$ is the Franck-Condon vibrational overlap integral. $(\chi_\alpha | \chi_\beta)$ can be evaluated by the same method as in the theory of predissociation[2] and we actually calculated it using Morse potentials. Franck-Condon factor F changes remarkably depending on the bond dissociation energy of each acceptor molecule and on the energy difference between initial and final potential curves. The calculated F's are shown in Figure 1.

Approximating the donor-acceptor exchange integral $V_{ab}(R)$ as
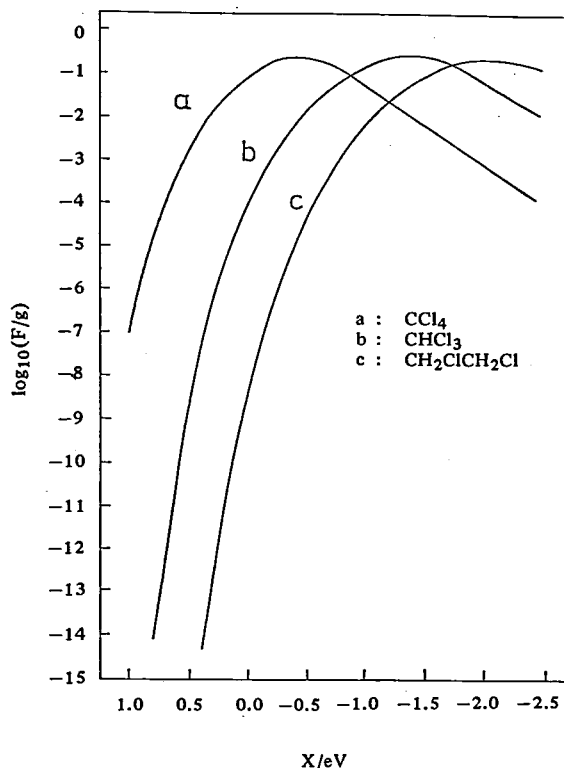
$$V_{ab}(R) = V_{ab}(O) \exp(-R/L).$$
(2)

Figure 1. Calculated Franck-Condon factor (divided by the degeneracy factor g) as a function of the energy difference between the polarization energy of the acceptor anion and the energy of e_s^- ($x = P-E(e_s^-)$).
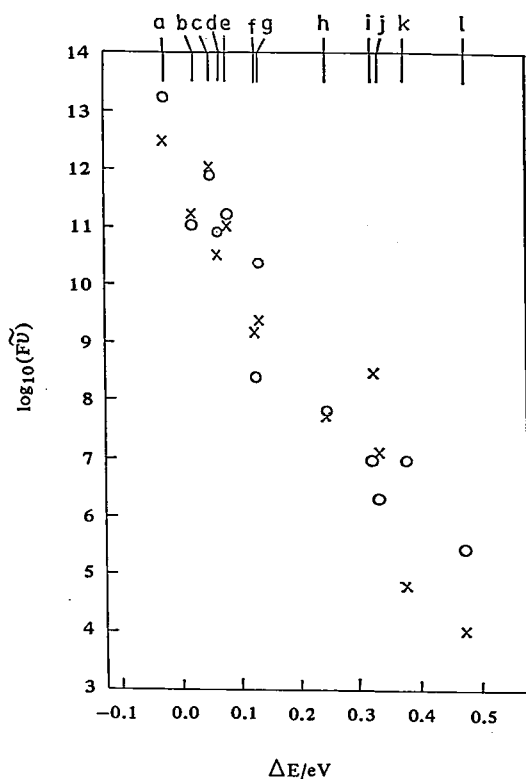
Figure 2. Observed $\widetilde{F\nu}(o)$ and estimated $\widetilde{F\nu}(x)$ for various compounds versus the activation energy (ΔE) of the dissociative electron attachments in gas phase. $CCl_4(a)$, $CH_3I(b)$, CH_2Br_2 (c), $C_6H_5I(d)$, $CH_2BrCH_2Br(e)$, $CH_2BrCH_2CH_2Br(f)$, $CHCl_3(g)$, $CH_3Br(h)$, $CH_2Cl_2(i)$, $CH_2ClCH_2CH_2Cl(j)$, $CH_2ClCH_2Cl(k)$, $(CH_3)_3CCl(l)$.

$\alpha(t)$ can be written in the form

$$\alpha(t) \simeq \frac{4\pi}{3} a^3 \times 6.02 \times 10^{20} (ln\,(\widetilde{F\nu}t))^3 , \qquad (3)$$

where $a = L/2$, L is a Bohr radius of e_s^-,

and $= \dfrac{2\pi |V_{ab}(O)|^2}{\hbar^2 \omega}$, ω is the frequency of the stretch-

ing mode coupled with the transferring electron. Equation (3) was obtained by following the mathematical formulation in the triplet energy transfer by the exchange mechanism.[3]

Experimentally determined $\widetilde{F\nu}$'s are also tabulated in Table 1. The values can be correlated with the activation energy ΔE in the dissociative electron attachment in gases. As the ΔE's increase, $\widetilde{F\nu}$'s decrease exponentially as shown in Figure 2. By taking $\widetilde{\nu} = 10^{13}\,s^{-1}$, a good agreement for $\widetilde{F\nu}$'s between the experiment and theory is obtained.

References

1) For example, J. R. Miller, *J. Phys. Chem.*, 79, 1070 (1975).
2) M. S. Child, *J. Mol. Spectrosc.*, 33, 487 (1970).
3) M. Inokuti and F. Hirayama, *J. Chem. Phys.*, 43, 1978 (1965).

III-B-2 Dynamic Quenching of Fluorescence in Indole-Chloromethane Systems due to Photo-ionization

Akira NAMIKI, Nobuaki NAKASHIMA, and Keitaro YOSHIHARA

The mechanism of the intermolecular electron transfer of excited molecules was studied with indole as an electron donor and chloromethane as electron acceptor in ethanol at a low temperature.

The electron transfer from excited molecules in considered as one of the most important primary processes in ethanol at low temperature.

The electron transfer from excited molecules is confluid media there appeares a serious contribution from the diffusional motion and therefore, it is crucial to extract the net informations on the electron transfer in the fluorescence quenching process. Here, we used the rigid glassy solutions at low temperatures to avoid the effect of the diffusional motion. The fourth harmonic (266 nm) of passively mode-lockd Nd^{3+} : YAG laser excited indole. Fluorescence decays were observed by a high speed channel-plate type photomultiplier connected to a transient digitizer (Tektronix R7912) or by a streak camera (HTV C979). The streak was digitized by a TV camera and a micro-computer system (HTV C1000). These were connected to a mini-computer (Nippon Mini-Computer, NOVA 3) and the raw data were stored in the floppy disk media. The determination of the lifetimes and the curve fitting by a convolution method were made with a mini-computer after recalling these stored data.

The results were summarized as follows:
1) Fluorescence quenching was observed in the presence of CCl_4, $CHCl_3$, CH_2Cl_2 even though the diffusion

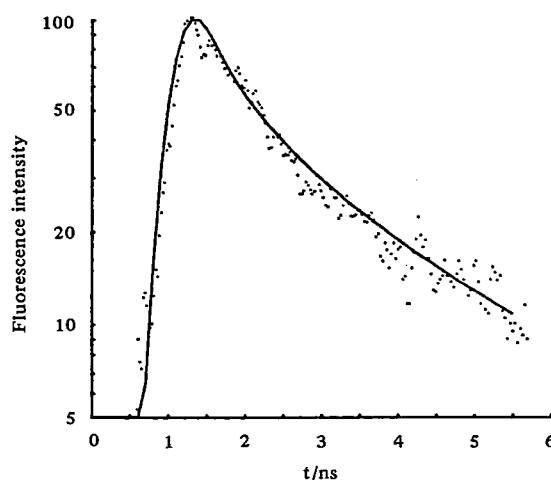Figure 1. Fluorescence decay of indole containing 5.0M $CHCl_3$ in ethanol at 77K. Dotted line is experimental one. Solid line is a convoluted decay function (see text). τ_0 : 6.0 ns, $\widetilde{F\nu}$: $1.5 \times 10^{13}\,s^{-1}$, excitation pulse width : 260 ps (Actual width of the exciting laser is 15 ps, however, the inclusion of the slit function of the streak camera makes the observed pulse width look longer.)

was inhibitted.

2) The order of quenching rates was $CCl_4 > CHCl_3 > CH_2Cl_2$.

3) Decay curves as typically observed in Figure 1 deviated considerably from simple exponentials.

4) In steady state experiments, fluorescence yield decreased in the presence of the quencher at the the concentration $[Q]$ as $I = \exp(-\alpha[Q])$, indicating that the Perrin model is adequate rather than the Stern-Volmer model.

5) Phosphorescence decay was not affected by the presence of any chloromethanes.

6) Fluorescence-phosphorescence intensity ratios were not affected by CCl_4.

Above experimental results are interpreted by the mechanism of non-adiabatic electron transfer. External heavy atom effects in the fluorescence quenching may be negligible, as suggested by the results 5) and 6).

The non-exponential decay can be well fitted by the convoluted decay function with a gaussian shape of the excitation light (solid line in Figure 1). The decay function was recast as,

$$f(t) = \exp\left[-\frac{t}{\tau_0} - \frac{4}{3}\pi a^3 N \left\{ (ln\,(\widetilde{Fv}t))^3 \right.\right.$$

$$+ 1.732\,(ln\,(\widetilde{Fv}t))^2 + 5.934\,ln\,(\widetilde{Fv}t)$$

$$\left.\left. + 5.445 \right\} \right].$$

This result is essentially the same as the one revealed in the electron transfer reaction with solvated electrons.[1]

The main interaction responsible for an electron transfer is the exchange interaction. The triplet-triplet energy transfer in the condensed rigid media[2] shows a non-exponential decay quite similar to the one observed here for the indole fluorescence, suggesting that both electron and energy transfers follow the same mechanism.

References

1) A. Namiki, N. Nakashima, K. Yoshihara, Y. Ito, and T. Higashimura, *J. Phys. Chem.* 82(8), 1901 (1978).

2) H. Kobashi, T. Morita, and N. Mataga, *Chem. Phys. Lett.*, 20, 376 (1973).

III-B-3 Electron Transfer Distances Obtained by Picosecond Study of Fluorescence Dynamic Quenching

Nobuaki NAKASHIMA, Akira NAMIKI, and Keitaro YOSHIHARA

Electron transfer distances have been obtained by analyzing the transient effect in the diffusion-controlled fluorescence quenching reaction of N,N-dimethylaniline (DMA) by acrylonitrile (AN). The value 8.9 ± 0.9A in

acetonitrile should be compared with 6.0 ± 0.8A in cyclohexane. This indicates that a longer range electron transfer occurs in a polar solvent at a range longer than in a non-polar solvent.

It is known that the electron transfer reaction occurs more easily as the solvent polarity increases. However, the radius obtained for anthracene-N,N-diethylaniline is of the order of the sum of van der Waals radii in hexane as well as in acetonitrile.[1] In order to investigate whether the electron transfer distance is really dependent on the solvent polarity, the reaction radii were determined by using a picosecond laser and a streak camera. This technique is very useful for this purpose, since the transient effect is observable only up to 1 ns after the excitation pulse in usual solvents of low viscosity.

The apparatus was the same as described elsewhere[2] with a small improvement. The 4th harmonic (266 nm, 20 ps) of a Nd^{3+}:YAG laser was used as an exciting light source with UV transmitting optics as the relay lens. The distortion of the time base and the virtical intensity of the camera were fully corrected. Fluorescence lifetimes in a few ns region were also measured by a channel plate photomultiplier and a corrected transient digitizer.
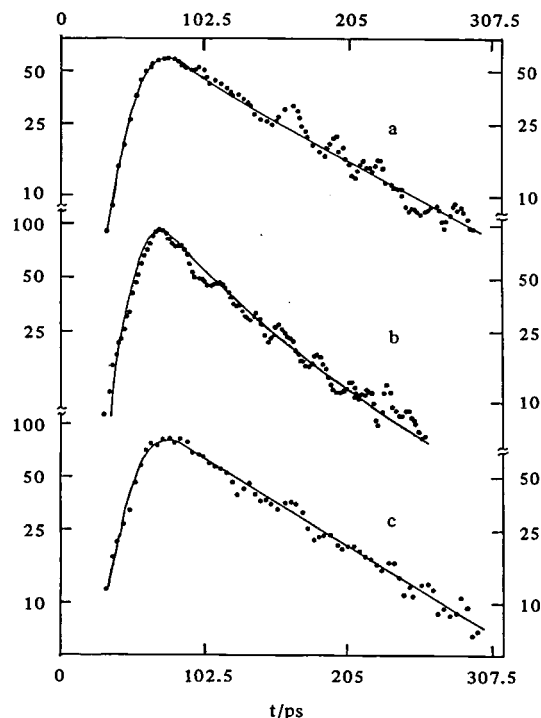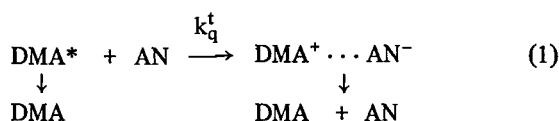
The following quenching mechanism and the decay functions are assumed:

Figure 1. Observed (...) and convoluted (—) typical decay curves. N,N-dimethylaniline (8 x 10^{-5}M), acrylonitrile (0.456 M), a: in cyclohexane, b: in acetonitrile. c: erythrosin (reference) (10^{-4}M in water) shows exponential decay with the lifetime of 90 ps.

$$DMA^* + AN \xrightarrow{k_q^t} DMA^+ \cdots AN^- \quad (1)$$

$$\downarrow \qquad\qquad\qquad \downarrow$$

$$DMA \qquad\qquad\qquad DMA + AN$$

$$I(t) = I_0 \exp\left\{ -\frac{1}{\tau_0} - k_q^o \left(1 + \frac{2R'}{\sqrt{\pi Dt}}\right)[AN]t \right\} \quad (2)$$

$$\lim_{[AN] \to 0} K_{sv} = K_{sv}^o = k_q^o \tau_0 \left(1 + \frac{R'}{\sqrt{\tau_0 D}}\right) \quad (3)$$

$$k_q^o = 4\pi N'R'D, \qquad R' = R/(1 + D/\kappa R). \quad (4)$$

Notations are those of ref. 3. Observed fluorescence decay curves are shown in Figure 1. Small but definite deviations from a single exponential decay could be observed.

The Stern-Volmer constants K_{sv}^o were determined from steady state fluorescence measurements, where the concentrations of AN were below 2.2×10^{-2}M in cyclohexane and 0.75×10^{-2}M in acetonitrile. The fluorescence quenching constants k_q^s ($= K_{sv}^o/\tau_0$) indicate that the reaction is diffusion-controlled. Apparent transient quenching rate constants can be estimated from the average lifetimes τ_{av}. These values are almost same as k_q^t in Table II, and 33% and 63% greater than k_q^s in cyclohexane and acetonitrile, respectively. Intuitively this suggests that the second term $R'/\sqrt{\pi Dt}$ in Eq. 2 is large and contributes to k_q^t more effectively in acetonitrile than in cyclohexane. Fitting the observed decay curves by convolution with Eq. 2 under the conditions of Eq. 3, we obtained R', D, and other parameters are tabulated in Table I and II.

The free energy change of the electron transfer in acetonitrile can be estimated to be $\Delta G \sim -1.0$ eV. If

Table I. Fluorescence Quenching Constants I

Solvent	ϵ^a	τ_0^b	$K_{sv}^{o\ c}$ M^{-1}	k_q^s 10^{10}M^{-1}s^{-1}	τ_{av}^d ps
Cyclohexane	2.023	2.69±0.03^e	44.8±0.2	1.69	91±2
Acetonitrile	37.5	4.46±0.03	85.3±0.2	1.91	69±2

a: dielectric constnat at 20°C, b: fluorescence lifetime of DMA, c: Stern-Volmer constant for low concentration limit of AN, d: obtained by fitting with a single exponential function, $K_q^s = K_{sv}^o/\tau_0$, e: errors in standard deviations.

Table II. Fluorescence Quenching Constants II

Solvent	R'^a A	D^b 10^{-5}cm^{2}s^{-1}	k_q^o 10^{10}M^{-1}s^{-1}	$k_q^t(t=100ps)$ 10^{10}M^{-1}s^{-1}
Cyclohexane	6.0±0.8^c	3.0±0.4	1.37	2.23
Acetonitrile	8.9±0.9	2.2±0.3	1.49	3.09

a: reaction radii, b: diffusion constant, $k_q^o = 4\pi R'N'D$, $k_q^t = k_q^o \left(1 + \frac{R'}{\sqrt{\pi Dt}}\right)$, c: errors in estimated from fitting decay curces.

one assumes that the electron transfer occurs from DMA* to AN in cyclohexane and that induces the formation of a non-fluorescent exciplex which may be more stable than solvated ion pair, the value is estimated to be $\Delta G \sim -0.8$ eV. Therefore, it is safe to assume that the fluorescence quenching is due to the electron transfer. The reaction radius in cyclohexane is 6A and is nearly equal to the encounter distance. In acetonitrile, however, the distance 9A is larger than the sum of the van der Waals radii. The difference cannot be explained in terms of a simple solvent dependent cage effect.

References

1) T. J. Chuang and K. B. Eisenthal, *J. Chem. Phys.*, **62**, 2213 (1975).
2) M. Sumitani, N. Nakashima, K. Yoshihara, and S. Nagakura, *Chem. Phys. Lett.*, **51**, 183 (1977).
3) T. L. Nemzek and W. R. Ware, *J. Chem. Phys.*, **62**, 477 (1975).

III-B-4 Fluorescence Dynamics of a Rhodamine B Monolayer at the Surface of Organic Solids

Frank WILLIG *(Fritz-Haber Institut and IMS)*, Nobuaki NAKASHIMA and Keitaro YOSHIHARA

Rhodamine B molecules have been adsorbed at the surface (ab plane) of a thin anthracene crystal (about 10 μm thickness) from a small droplet (half sphere with about 2 mm diameter) of a 10^{-6}M aqueous solution. About 5 minutes after contact virtually all of the dye molecules in the droplet are adsorbed as monomers at the crystal surface yielding a surface coverage of about 50 per cent.[1] From magnetic field modulation of the reaction kinetics in the system it is known that the first excited singlet state of the adsorbed rhodamine B molecules is quenched with very high efficiency via electron transfer from the surface of the anthracene crystal.[2] We like to report here on the first attempt of determinating directly the decay of the fluorescence of the adsorbed dye monolayer with a streak camera after excitation with a picosecond laser pulse. The apparatus has been described elsewhere.[3]

The decay of the fluorescence in the system is shown in Figure 1. The two signals in Figure 1 correspond to different time scales. The signal obtained for the incident light pulse in the respective time scale is shown for comparison in front of the fluorescence signal. When measuring the fluorescence of the dye monolayer stray light of the incident light beam reflected from the crystal has been completely elliminated with 3 cut off filters. The initial decay of the fluorescence in Figure 1 is very fast with a maximum slope corresponding to a time constant of about 40 ps. The signal is decreasing in a non-exponential fashion but develops an exponential tail with a time constant of 2.8ns. Tentatively, the initial fast decay is attributed to electron transfer from the surface of anthracene to the first excited singlet state of the adsorbed rhodamine B monomer in contact
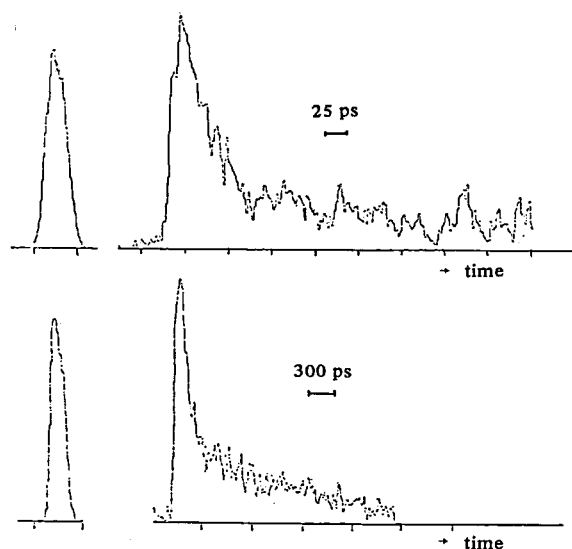
Figure 1. Fluorescence decay curves of the adsorbed rhodamine B on the anthracene crystal in different time scales. The apparent laser pulse widths are shown in the left-hand side and are broadened by a finite slit width (100 μm).

with water. The non-exponential time dependence is ascribed to a series of recombination events taking place between the generated holes and the reduced dye molecules, regenerating thereby with a certain probability the excited singlet state of the dye. The final exponential decay could indicate the lifetime of the generated holes when the concentration of reduced dye molecules and holes becomes fufficiently small.

The fluorescence of an equivalent number of rhodamine B molecules has been measured in a 10^{-6}M aqueous solution. The signal gave an exponential decay with a time constant of 2.5 ns. For further comparison we have recorded the fluorescence of rhodamine B monomers adsorbed via the above procedure at phenanthrene and naphthalene crystals and at polystyrene foil, and finally of rhodamine B dried up with higher concentration at the surface of Teflon. In all cases there was an initial faster non-exponential decay followed by an exponential tail. In the case of dried up rhodamine B on Teflon the fast component had a maximum slope corresponding to a time constant of

about 250 ps and the exponential signal had a time constant of 1.9 ns. The fast portion of the signal became smaller with decreasing light intensity. A second order process may be due to exciton-exciton annihilation. The dye molecules adsorbed at polystyrene in contact with water showed an initial maximum slope corresponding to a time constant of about 700 ps and an exponential decay with a time constant of 1.4 ns. The fluorescence signal of the rhodamine B monomers adsorbed from aqueous solution onto phenanthrene and naphthalene crystals showed an unexpected time dependence. In both cases there was a fast non-exponential decay of the virgin signal with maximum slope corresponding to a time constant of 70 to 100 ps, varying somewhat from place to place at the crystal surface, and an exponential decay with a time constant between 2.5 and 3 ns. The slow exponential component was increasing with the number of shots, and after a series of shots the initial fast decay disappeared completely. Because of the decrease in ionization energy it is expected that the rate constant of electron transfer should decrease by at least a factor of 100 when going from phenanthrene to naphthalene.[1] Therefore, the observed similar fast decay of the dye fluorescence at these different crystals cannot stem from this decay channel. Energetically fast electron transfer is also feasible between two neighbouring rhodamine B molecules in contact with water. Such a reaction has been found e.g. for perylene dissolved in acetonitrile.[4] In this case the slow exponential decay could be due to recombination of trapped charge carriers after being released by the light pulse. The trapped charge carriers have been produced in the dye layer by the preceding light pulse.

Though the interpretation of the above described signals is still very preliminary we consider it interesting and promising that fluorescence quenching of dye monolayers can be resolved on the picosecond time scale.

References

1) H. Gerisher and F. Willig, Topics in Current Chemistry, ed F. L. Boschke, Vol. 61, p. 31, Springer, Berlin 1976.
2) R. P. Groff, R. E. Merrifield, A. Suna, and P. Avakian, Phys. Rev. Lett., 29, 429 (1972).
3) M. Sumitani, N. Nakashima, K. Yoshihara, and S. Nagakura, Chem. Phys. Lett., 51, 183 (1977).
4) K. H. Grellmann and A. R. Watkins, Chem. Phys. Lett., 9, 439 (1971).

III-C Laser Induced Selective Chemical Reactions

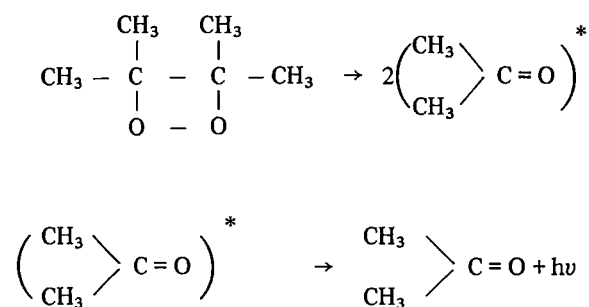Novel properties, such as high intensity, high spectral purity, and the short pulse width of lasers can be applied to increase the rate of reactions or to improve the reaction selectivity. Laser induced isotope separation is one of recent examples.

We have examined induction of vibrational excitations of dimethyl-1,2-dioxetane leading to a bond cleavage reaction, and investigated the effect of vibrational excitation on the reaction.

III-C-1 Effects of Vibrational Excitation on the Bond-cleavage Reaction of Tetramethyl-1,2-dioxetane

Nobuaki NAKASHIMA, Minoru SUMITANI, and Keitaro YOSHIHARA

It is well known that tetramethyl-1,2-dioxetane (TMD) shows a chemiluminescence. The reaction mechanism is described by the following scheme:

$$CH_3 - \underset{\underset{O}{|}}{\overset{\overset{CH_3}{|}}{C}} - \underset{\underset{O}{|}}{\overset{\overset{CH_3}{|}}{C}} - CH_3 \rightarrow 2\left(\begin{matrix} CH_3 \\ CH_3 \end{matrix} C = O\right)^*$$

$$\left(\begin{matrix} CH_3 \\ CH_3 \end{matrix} C = O\right)^* \rightarrow \begin{matrix} CH_3 \\ CH_3 \end{matrix} C = O + h\upsilon$$

In this reaction the bond energy is converted to the electromagnetic energy, i.e., the strain energy within a molecule is released as an energy of light through a chemical reaction.

We have examined the effect of vibrational excitation on this reaction in solution. The material (TMD) was supplied by the Chemical Materials Cneter of IMS. The fundamental (1.064 μm, 30 mJ, 30 ps) from a passively mode-locked YAG laser was introduced to a Raman cell (20 cm) of benzene. About 3% of input energy was converted to a Raman shifted laser (1.189 μm). This wavelength corresponds to the 2nd overtone of the C-H vibration.

It has been known from studies on chemiluminescence that the thermal reaction leads to a 1 : 50 ratio of the singlet and the triplet excited acetone. It is more efficient to observe the fluorescence from dibromoanthracene which is activated by energy transfer from the produced triplet acetone. We actually observed the fluorescence of dibromoanthracene, however, this is more reasonablly explained by the three photon excitation of dibromoanthracene rather than the chemiluminescence. The observation of chemiluminescence with more efficient way is now under investigation.

III-D Studies on Transient Phenomena in Biology

Studies of fluorescence in biopolymers give important informations on their higher order structure. Fluorescence dynamics is related to the energy transfer between fluorescent chromophores. Their distances and mutual orientation are important factors which influence on the fluorescence lifetimes, dynamic behaviors, quantum yields, and the polarization.

Investigations of fluorescence dynamics of coenzyme were performed with a picosecond laser. It has been found that fluorescence decays depend on concentration and this is ascribed to a monomer-dimer interaction in the quaternary structure.

The picosecond fluorescence dynamics were studied with photosynthetic pigments. Fluorescence decays of a spinach chloroplast with a concentrated reaction center and of a bacteriochlorophill (*Rhodopseudomonas spheroidas*) were measured.

III-D-1 Picosecond Analysis of the Fluorescence Lifetime of the Coenzyme in D-amino Acid Oxdase; Evidence for the Difference in the Lifetime between the Monomer and the Dimer

Fumio TANAKA *(Mie Nursing College)*, Nobuaki NA-KASHIMA, Keitaro YOSHIHARA and Kunio YAGI *(Nagoya Univ.)*

The fluorescence lifetime of the coenzyme, FAD, of D-amino acid oxidase [D-amino acid: O_2 oxidoreductase (deaminating), EC 1.4.3.3.] was measured with a picosecond technique at various concentrations of the enzyme. The enzyme was excited by the 3rd harmonic (355 nm) of a passively mode-locked Nd^{3+}:YAG laser (1.06 μm). The fluorescence decays were measured with a Hamamatsu TV streak camera (HTV C979). The streak was digitized by a TV camera/microcomputer

system (HTV C1000). The pulse width was measured as 20 ps. Two different decay components were obtained in the whole range of the enzyme concentration examined (1-100 μM). The longer lifetime was 2.3 ns. The contribution of this component to the maximum intensity increased as the enzyme concentration was lowered. The results indicate that the species with the lifetime of 2.3 ns is free FAD dissociated from the enzyme. On the other hand, the lifetime with a short value depended on the enzyme concentration: 60 ps at 100 μM and 150 ps at 1 μM. At the concentration 100 μM, D-aminoacid oxidase exists mostly as a dimer, while the enzyme is almost in the monomeric form at 1 μM. The change in the lifetime of this phase is considered to be due to the change in the quaternary structure from the dimer to the monomer. The conclusion is coincident with the result obtained by a static analysis based on the measurements of the fluorescence intensity and polarization of the enzyme solution. The

52

fastest decay could represent a dynamic quenching oc-   moiety.
curred in FAD chromophore bound to the protein

III-E Photoelectrochemical Energy Conversion by Thin
Films of Organic Semiconductors

Photoelectrochemical cell is one of the devices for converting solar radiation directly into electrical and chemical energy. It is important to elucidate the processes of the energy conversion at semiconductor/electrolyte interface, not only from the view point of the application but from the pure scientific point of view.

Organic compounds as photoelectrodes are especially interesting, because
1) there are a number of organic compounds which absorb visible light,
2) nature utilizes them as energy convertors, for instance, as seen in photosynthesis, and
3) there are many molecules whose excited states have been investigated well.

This project is aiming to elucidate the mechanism of photoelectrode processes of organic thin films evaporated on various kind of metals and semiconductors and to develop a new method for the solar energy conversion.

III-E-1 Photoelectrochemical Energy Conversion by Thin Films of Metal-Porphines

Tadayoshi SAKATA, Katsumi TANIMURA, and Tomoji KAWAI

Thin porphyrin films on metals were used as electrodes in electrochemical cells and the mechanism of the current and photovoltage generation was investigated by measuring absorption spectra, emission spectra, ultraviolet photoelectron spectra (UPS), current-voltage curves and n-sec pulse laser kinetics. The porphines used in these experiments were various metal-tetraphenylporphines (Figure 1). Among them Zn-tetraphenylporphine (ZnTPP) was found to be a favorable material for photoelectrodes. The photovoltage for the ZnTPP/Pt photoelectrode reached 530 mV and the current efficiency (electron numbers/absorbed photons) was about 2–6%.

The Electronic Structure of the Photoelectrode and Mechanism of Current Generation.

Figure 2 shows the absorption spectrum of ZnTPP

on a quartz plate, the excitation spectrum of the fluorescence and the action spectrum of the photocurrent for the ZnTPP/Pt photoelectrode. The good correspondence between them signifies that the photocurrent is caused by the light absorption of ZnTPP and that the fluorescence state is involved in the charge separation.
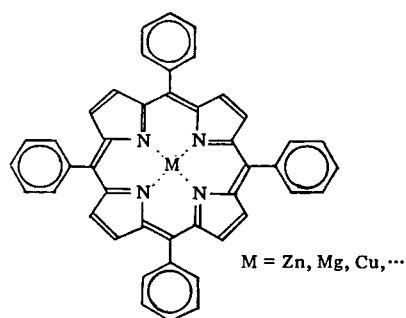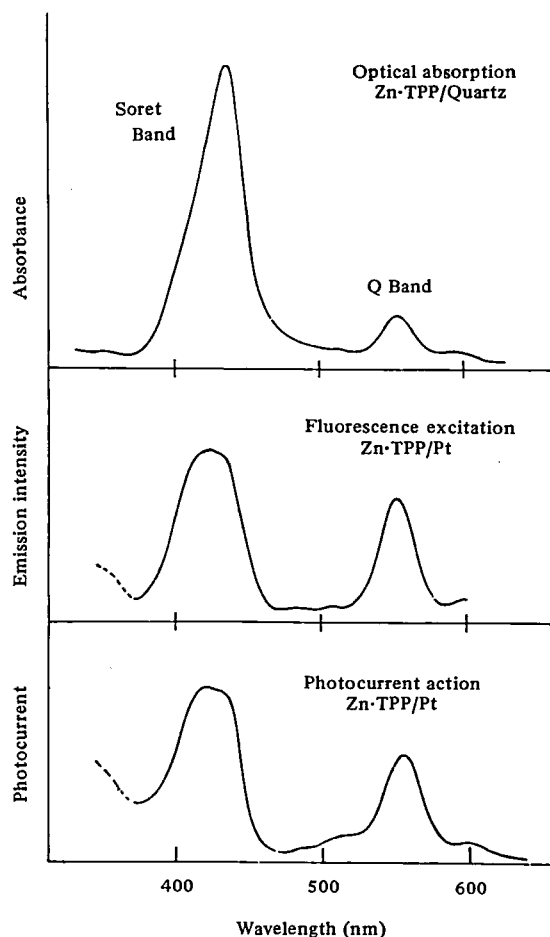

Figure 2.

M = Zn, Mg, Cu, ···

Figure 1.

Table 1.

|	W_F (eV)	I_P (nA)	V_P (mV)
Pt	6.0	300	165
Pd	4.97	250	150
Au	4.76	135	160
Mo	4.29	40	15
Cu	4.29	25	6
Zn	4.25	<5	<1
Al	4.25	<5	<1
Ti	3.92	<5	8

The photocurrent (i_p) and photovoltage (v_p) were found to show a remarkable dependency on the kind of metal substrate on which ZnTPP was evaporated (Table 1). The electronic structure of the photoelectrode, a metal/ZnTPP aqueous solution, was elaborated using the results of UPS of the ZnTPP film and of the electrochemical measurement assuming a Schottky type barrier formed at the interface between ZnTPP (p-type semiconductor) and the metal substrate. This model was found to explain the results well. The detailed mechanism of current generation will be discussed on the basis of the electronic structure of the photoelectrode.

A New Model for Hydrogen Evolution.

The excited ZnTPP was found to reduce well methylviologen (MV^{2+}).

$$MV^{2+} + e^-(ZnTPP\ film) \rightarrow MV^+ \qquad (1)$$

Since the redox potential of MV^{2+}/MV^+ is -0.44 V, the hydrogen evolution from water would, in principle, be possible.

$$MV^+ + H^+ \xrightarrow{k} MV^{2+} + 1/2\ H_2 \qquad (2)$$

$$\Delta G^0 = -0.44\ eV$$
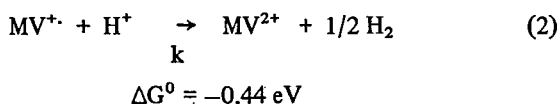
However, this reaction does not proceed due to the small reaction rate even if a large amount of MV^+ is produced.

We succeeded in enhancing the reaction rate by introducing catalysis, for instance, Pd powder dispersed on small alumina particles. At present we have not succeeded in evolving hydrogen at the ZnTPP photoelectrode due to the small photocurrent. But we have
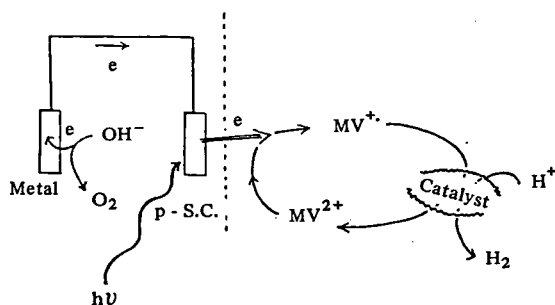
succeeded in the hydrogen evolution using a model photocell, $< TiO_2 | MV^{2+}$ aq.soln.$|$ Au $>$. In this system, the hydrogen evolution was not observed before introducing the catalyst and only MV^{2+} was reduced efficiently. However, when the catalyst was introduced into the system, the blue color of MV^+ disappeared instantly, and simultaneously the bubbles of hydrogen gas were produced vigorously.

This method is considered to be a new one for hydrogen manufacturing and has following advantages:
1) H_2 can be produced easily at pH 7.
2) H_2 can be produced at need by adding the catalyst into the solution of MV^+.
3) Homogeneous catalysts can be used in this system. (The enhancement of the reaction area in the catalyst.)
4) The generality of the method.
   This method can be applicable to various kind of organic compound and for p-type semiconductors which are unstable in the acidic or basic solutions.

Figure 3 shows the schematic diagram of H_2 evolution by using a p-type semiconductor as a photoelectrode.

Reference

T. Kawai, K. Tanimura and T. Sakata, *Chem. Phys. Lett.*, 56, 541 (1978).

III-E-2 Dynamics of Photoelectrode Process Studied by Pulse Laser Technique

Tomoji KAWAI, Katsumi TANIMURA, Tadayoshi SAKATA and Mitsuyuki SOMA (Univ. of Tokyo)

In order to elucidate the dynamic behaviour of photoelectrode processes, we have investigated the time dependence of the photocurrent produced by nitrogen and dye lasers in the nanosecond region. Among the systems investigated were the porphyrine/metal photoelectrode and TiO₂ photoelectrode. Figure 1 shows the experimental apparatus for the optical measurement and for the measurement of the laser induced photocurrent. The pulse widths of the nitrogen and the dye laser (Molectron UV24 and DL14) were 10 and 6 nanosecond, respectively.

Figure 3.

Figure 1.

a)   b)

10 ns/div

(A) : ZnTPP (500A)/Pd
(B) : H$_2$TPP (500A)/Pd

—·—·— : TiO$_2$ in 0.5 KCl   ——— : Incident light
——— : N$_2$ Laser (10 ns)   —·—·— : Photocurrent

Figure 2.

Electron transfer from Zinc-tetraphenylporphine (ZnTPP)/Pd electrode into the solution (cathodic photo-current) was observed after laser excitation of the Soret and Q band in ZnTPP. The action spectrum of photo-current closely resembles the excitation spectrum of fluorescence from ZnTPP photoelectrode. This shows that the electron transfer from ZnTPP does not occur by the direct formation of a charge carrier involving the conduction band, but it occurs through the lowest singlet state or triplet state.
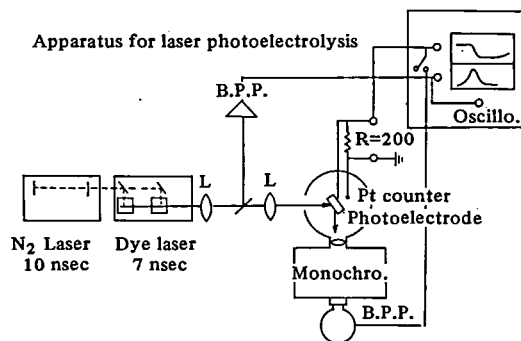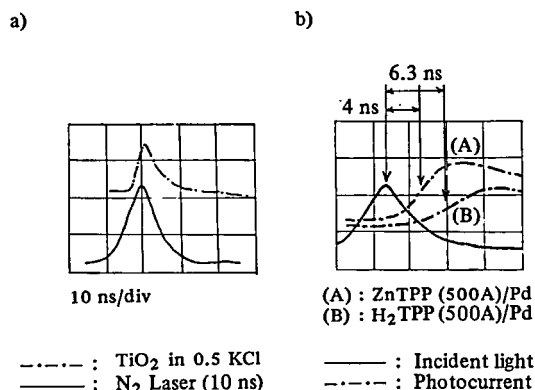
Figure 2 shows the laser induced photocurrent for TiO$_2$(a), ZnTPP/Pd and the H$_2$TPP/Pd electrode(b). For the TiO$_2$ electrode, the displacement current caused by charge separation follows the rise and decay of the incident light except for a small tailing. In the case of the ZnTPP and H$_2$TPP/Pd electrodes, however, the rise profile can be qualitatively expressed as the integral of the rise and decay curve of the fluorescence. The population of the triplet states is expressed by the integral of the change of the lowest singlet when the life time of the triplet state is long enough. The above results seem to indicate the possibility of a large con-tribution of the triplet state to the electron transfer in this condition. For CuTPP/Pd whose triplet lifetime is short, however, a rapid rise and decay of the photo-current was observed. Thus we have succeeded in the measurement of the dynamic changes of photoelectrode processes in the nanosecond-region.

III-E-3 Spectroscopic Study on the Transfer of Energy and Electrons at the Interface between Porphyrin Films and Solid Surface

Katsumi TANIMURA, Tomoji KAWAI, and Tadayoshi SAKATA

Organic dyes in contact with solid (metal and semi-conductor) surfaces show interesting phenomena such as electron transfer and photovoltaic effect at the inter-face. These properties of adsorbed dyes have attracted special attention in the field of solar energy conversion,

and have been studied extensively. Solar cells con-structed with organic dyes involves in general the follow-ing sequence of functions: the capture of photon energy by dyes, and the transfer of the energy to the interfaces where the carrier generation mainly takes place. Thus, an effective energy transfer followed by an effective generation of carriers is crucial for development of a cell with a high efficiency. Nevertheless, detailed mecha-nisms of these functions are far from being well under-stood. This study aims to clarify by means of spectro-scopic measurements the mechanism of electron and/or energy transfer associated with the interface between porphyrin films and metal or semicoundctors.

In Figure 1 is shown the luminescence intensity of the Zn-tetraphenylporphine (ZnTPP) film on Pt relative to that on quartz as a function of film thickness. The strong quenching of the luminescence is evident at the thickness below 400 Å. The solid curve is the calculated result which is derived on following assumptions:

1) Excitation energy is localized at the position where the excitation is made, and no transfer takes place within the porphyrin film.

2) Energy transfer of Förster type is active between the metal and a localized excited molecule, the rate of which depends on d^{-4} where d is the distance between metal surface and an excited ZnTPP.

The spectra in ZnTPP film shows little overlap between Q absorption bands and emission bands. This is due to a large red shift of the latter, which suggests that the excited states responsible for luminescence are localized states. The assumption 1) can be, therefore, justified in the case of ZnTPP. A good agreement between experi-mental and calculated results except in the range below 100 Å, indicates that Förster type energy transfer is taking place in the ZnTPP/Pt system.

In Figure 2, the emission intensity of the H$_2$TPP film evapolated on SnO$_2$ relative to that on quartz (solid circle) is plotted as a function of film thickness. The intensity of the H$_2$TPP film having a thickness of 50 Å spaced from the SnO$_2$ surface by a KCl film (open circle) is also shown as a function of thickness of the
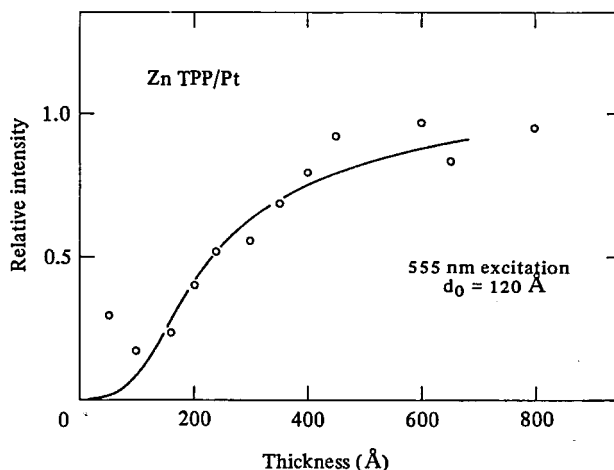

Figure 1. The emission intensity of ZnTPP film on Pt relative to that on Quartz as a function of film thickness. Open circles are experimental results, and the solid curve is calculated result (see text).
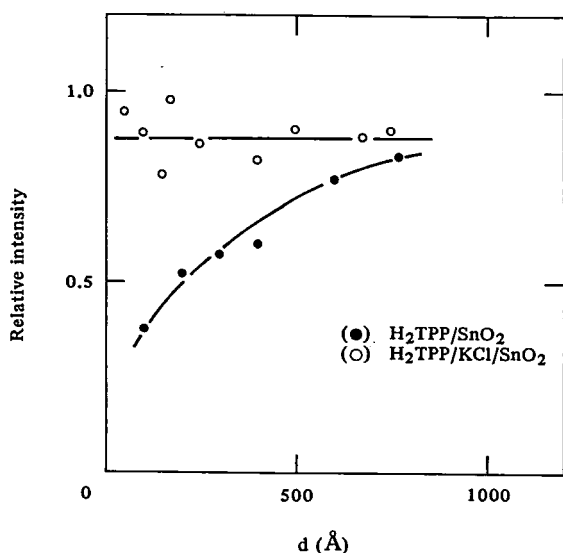
55

Figure 2. The emission intensity of H_2TPP film evapolated on SnO_2 relative to that on Quartz, solid circles, and the intensity of H_2TPP film of 50 Å thickness spaced by KCl film from SnO_2, open circles, respectively.

KCl film. The quenching of fluorescence by SnO_2 is seen only for the former case. H_2TPP spaced by the KCl film does not show a fluorescence quenching even at the film-SnO_2 distance of 50 Å. This finding indicates that no energy transfer takes place between excited H_2TPP and SnO_2, and that the direct contact of H_2TPP with the surface, the very short-range effect, plays an essential role in this type of quenching.

The fluorescence quenching by SnO_2, therefore, can be attributed to the electron transfer of excited H_2 TPP into SnO_2. The effect of a relatively long range seen in Figure 2 can be due to the energy transfer of Förster type within the H_2TPP films to the interface, caused by a large overlap between $Q_x(0-0)$ absorption band and the emission band in H_2TPP films.

III-E-4 Photovoltaic Effect at the Interface between Semiconductor and Electrolyte

Tadayoshi SAKATA, Katsumi TANIMURA and Tomoji KAWAI

The photovoltaic effect generated at the interface between a semicounductor and an electrolyte is one of the possible methods for solar energy conversion. It has some characteristics and advantages compared with other systems, for instance, the solid p-n junction.

The photovoltaic process at the semiconductor-electrolyte(S-E) interface is not well understood. The photovoltages observed experimentally are in most cases proportional to the logarithm of the light intensity in the region of moderately strong light intensity. The gradient dV/dlogI, however, does not show the con-

stant value $2.303.\frac{kT}{e}$ which is expected from the theory of the M-E interface and the p-n junction. It depends greatly on the kind of the electrode material and the electrolyte and is 2 to 9 times greater than $2.303.\frac{kT}{e}$.

In addition, the dependency of photovoltage on the light intensity in the region of the weak light has not been clearly explained.

We measured the dependency of photovoltage for five classical systems in detail and found a new theoretical model which can solve the above mentioned problems. Our new theory is based on the following assumptions.

1) In the dark, cathodic and anodic currents can be expressed by the Tafel equations.

$$i(cath.) = i_0 \exp(\alpha\, eV/kT) \qquad (1)$$

$$i(anod.) = i_0 \exp(\frac{-(1-\alpha)eV}{kT}) \qquad (2)$$

Here, V represents the absolute value of the overpotential i.e. the shift from the equilibrium potential. At the equilibrium potential (V=0), i(cath.) = i(anod.) is satisfied.

2) Under illumination, electrons and holes are separated at the space charge layer and the holes come together to the surface in the case of n-type semiconductors. The photocurrent is proportional to the light intensity for most cases, as far as the light intensity is not too strong. We further assume an exponential dependency of the photocurrent i_p on the voltage. Then the following equation is obtained.

$$i_p = (i_L - i_D) = c_0 I \exp(\frac{\alpha' eV}{kT}) \qquad (3)$$

since the condition of an open circuit is expressed as

$$i(cath.) - i(anod.) - i_p = 0 \qquad (4)$$
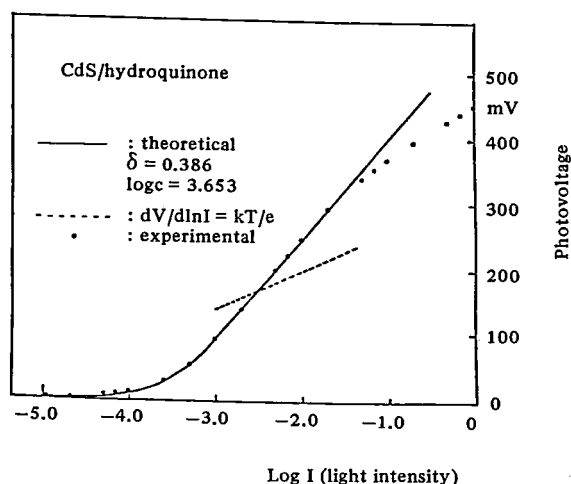

Figure 1.

the final expression for the photovoltage is obtained by substituting eqs. (1) – (3) into the eq. (4).

$$V = \frac{kT}{\delta e} \ln(1-e^{-\frac{eV}{kT}})^{-1} \cdot cI \qquad (5)$$

Here, $c = c_0/i_0$, $\delta = \alpha + \alpha'$.

The procedure for p-type semiconductors is quite similar and the same equation as eq. (5) is obtained. Eq. (5) is simplified under the condition of the strong illumination, i.e. $eV \gg kT$.

$$V = \frac{kT}{\delta e} \ln I + \frac{kT}{\delta e} \ln c \qquad (6)$$

This equation predicts a logarithmic dependency of photovoltage on the light intensity. In Figure 1, a comparison between the theory and the experiment is shown for CdS electrode. The agreement is quite good. Similar good agreements were observed for other 4 electrode systems.

The validity of this theory was confirmed from another point of view. The sum of α and α' obtained from current-voltage curve (see eqs. (1) and (3)) shows a good agreement with the value of δ obtained from the V-logI curve.

III-F Energy Storage and Solar Energy Conversion by "Layer Compound Electrode"

The layer compound is a relatively new substance for the study of electrochemistry, in paticular of photochemistry. This compound has the following interesting features.
1) It intercalates molecules between the layers.
2) A variety of electrical properties can be obtianed.
   [insulator (H_fS_2), semiconductor (MoS_2, $MoSe_2$), semimetals (TaS_2, WTe_2) and metals (NbS_2)]
We are interested in the following phenomena.
1) Energy storage utilizing the intercalation.
2) Solar energy conversion by using the semiconductive $MoSe_2$, and MoS_2 electrodes.

III-F-1 Energy Storage by Layer Compound Electrode

Tomoji KAWAI, Katsumi TAMINURA, Tadayoshi SA-KATA and Tamotsu KONDOW (Univ. of Tokyo)

In any system for solar energy conversion, it is very important how one stores the energy rich materials obtained. In the case of a hydrogen energy system, several methods have been proposed for the storage of the produced hydrogen, such as the liquefication and as a metal hydride. We have been interested in the fact that the "layer type compounds" often intercalate materials between the layers, and have started to study the electrochemical intercalation and the energy storage taking advantage of the intercalation. Here we report that the electrode potential is changed by several hundred mV after the electrochemical intercalation of hydrogen or potassium into TaS_2 or MoS_2 (Figure 1), and that these electrode can be used as a battery element. Furthermore, we found that the electrochemical behaviour of the TaS_2 electrode is strongly dependent on the crystal faces and on the kind of electrolytes used.

As an energy conversion system, this electrochemical intercalation method has following advantages. Hydrogen or other molecules can be stored directly into the electrode which serves as an energy resorvoir and the electricity can be derived directly from the electrode. This is in contrast to the complexity of a common

method in which the following procedures are combined: the decomposition of water into the hydrogen, the liquefaction of the hydrogen for the storage, the vaporization into the hydrogen gas and finally the conversion into the electricity by fuel cells.
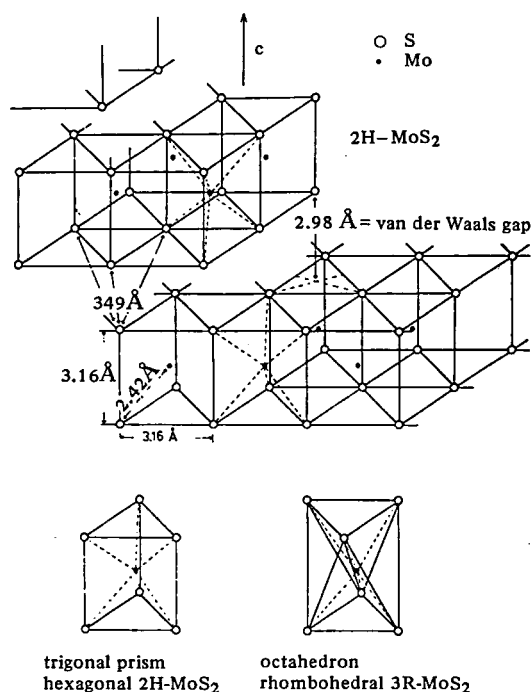

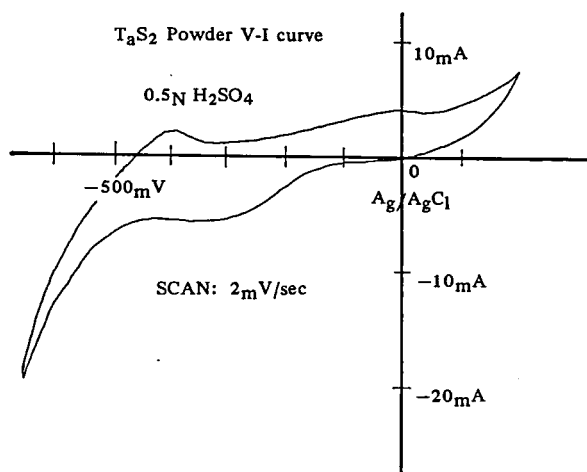Figure 1. Structure of MoS_2 layer crystals.

57

Figure 2.

(I) TaS₂ powder electrode

The current voltage curve by TaS_2 powder electrode in an acidic solution ($0.5N$ H_2SO_4), is shown in Figure 2. The reference electrode is Ag/AgCl. A large cathodic current was observed when the bias voltage was over −400 mV vs AgAgCl. The cathodic current observed around this range usually corresponds to the hydrogen evolution which results in the production of hydrogen bubbles when the electrode is a metal such as Pt. The evolution of the hydrogen, however, was not observed on the TaS_2 electrode, but rather the electrode became expanded after several minutes on application of the bias voltage of 500 mV vs Ag/AgCl. On the Pt counter electrode, the oxygen was vigorously evolved. These phenomena seem to indicate that the hydrogen is absorbed in the TaS_2 electrode in this electrochemical procedure.

(II) Battery effect of TaS₂ electrode

The above process was monitored by the changes of current. The cathodic charging current decreases in time, in contrast to the constant current of the Pt electrode at a cathodic bias condition. When the electrode was charged up after the current flow tapered off, the voltage was measured versus Ag/AgCl. The electrode potential changed from the rest potential of −70 mV to −430 mV. A current began to flow between the TaS_2 and the counter electrode upon a connection. This indicates that a battery can be constructed by the sorption of the hydrogen into TaS_2 electrode. An elemental analysis made after charging the electrode for 24 hours in $0.1N$ HCl showed the stoichiometry of $TaS_2H_{0.8}$. We also have found that MoS_2 single crystal intercalates potassium between the layers and makes a battery of −380 mV vs Ag/AgCl.

(III) Electrochemical behaviour of TaS₂ single crystal

A clean single crystal surface of TaS_2 was obtained by mechanically peeling the surface layers. A van der Waals surface appeared. When this surface was exposed to the KCl solution, an anomalous behaviour was observed. Figure 4(a) shows the V-I curve of the electrode in $0.5N$ H_2SO_4. The gradual increase of cathodic current was observed at about −400 mV, which is the normal electrochemical behaviour on this van der Waals surface. When the KCl solution is substituted as the electrolyte, the appearance of a steep and high cathodic current above −600 mV referred to the potential of the Ag/AgCl electrode was observed. The appearance voltage changed when this procedure was repeated. An addition of KCl into the acid solution during the measurement caused a steep increase of the cathodic current, superimposed on the normal V-I curve of the acid solution. The amount of the steep cathodic current was nearly equal to that of the anodic counter peak at −520 mV and was proportional to the concentration of the K^+ ion, indicating that this phenomenon was due to the strong interaction between K^+ and the TaS_2 surface.

This drastic change of current is not predicted by the usual Tafel equation, but rather it seems to correspond to the formation of a new compound. The direct reduction of K^+ should require a more negative
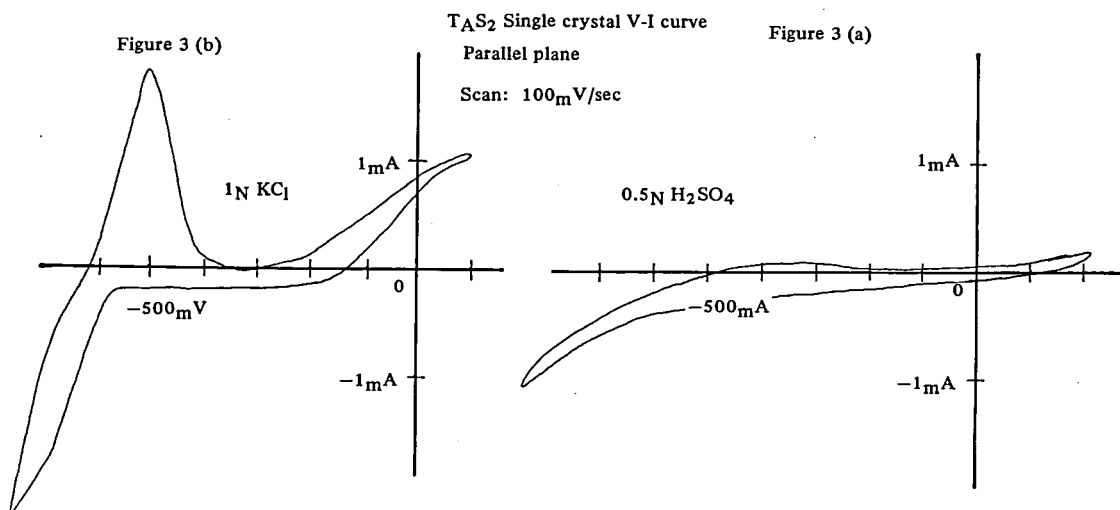

Figure 3.

TₐS₂ Single crystal V-I curve
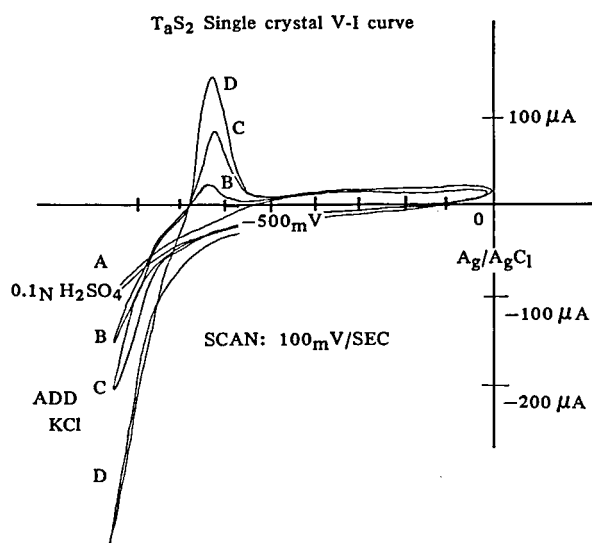
SCAN: 100ₘV/SEC

0.1ₙ H₂SO₄

ADD KCl

Figure 4.

electrode potential. Judging from the well known fact that TaS_2 intercalates alkali metals, it seems plausible that the K^+ ion has penetrated into all over the van der waals face at the bias voltage of about -600 mV to produce a TaS_2K compound. The height of the counter peak is proportional to that of the steep cathodic current, and then the counter peak would correspond to the ejection of K^+ ion from the TaS_2K into the solution.

III-F-2 Interface Phenomena Controlling the Efficiency of Electrochemical $MoSe_2$: I^-/I_2 Solar Cell

Helmut TRIBUTSCH, Tomoji KAWAI, and Tadayoshi SAKATA

A serious problem concerning semiconducting materials used in electrochemical solar cells (CdS, CdSe, CdTe, GaP, GaAs) is their gradual anodic photocorrosion as a consequence of breaking chemical bonds on the electrode surface. Various stabilizing electrolytes have been suggested, the most efficient up to date being those containing polyselenides and polytellurides. In a recent publication by one of the authors (H. Tributsch),[1] it has been proposed that d→d phototransitions in transition metal dichalcogenide layer compounds, which do not break existing chemical bonds, may favourably be utilized for energy conversion in regenerative electrochemical solar cells. It has been shown that stable photoelements can actually be obtained with the p-conducting MoS_2 as a photocathode and with a suitable redox couple (e.g. Fe^{2+}/Fe^{3+}) in the electrolyte.

Another interesting property of layer type compounds is its easy regeneration of the clean surface, being favorable for getting reliable electrochemical data.

The basic structural unit of $MoSe_2$ is a sandwich of three planes: Se-Mo-Se, and sandwiches are loosely bound together. The band gap is approximately 1.4 eV. The $MoSe_2$ crystals used in this experiment had all n-type character.

One of the authors (H. Tributsch)[1] already reported the fundamental features of the $MoSe_2$ electrochemical solar cell. He observed the following interesting phenomena which remain still unexplained.

1. In the presence of I^-, the electrode surface of $MoSe_2$ changes its metallic color reversibly into brown one under illumination. Corresponding to this color change of the $MoSe_2$ surface, its reflectivity changes drastically and there appears a sharp dip on the current-voltage curve.

2. I^-/I_2 reagents show the specific effect on the improvement of the $MoSe_2$ solar cell together with the stabilization of the electrode surface.

These results imply a light induced specific interaction between the surface of $MoSe_2$ and iodine. To clarify the mechanism, the dependency of the reflectivity on the wavelength was measured controlling the electrode potential. For the precise measurement of reflectivity, $NbSe_2$ was used as an electrode, because this layer compound is a metal and shows a similar surface change in the KI solution in the anodic potential region without illumination. In Fiugre 1 the results of the reflectivity measurement are shown. The result shows rather uniform change of the absorption in the whole wavelength region of the measurment, $\lambda = 500 - 900$ nm. Since a similar phenomenon was observed at the Pt electrode in the KI solution, it was concluded that the surface change is due to the thin film formation of iodine. This thin film was supposed to be composed

$\log \dfrac{I_0}{I_s}$

NbSe₂

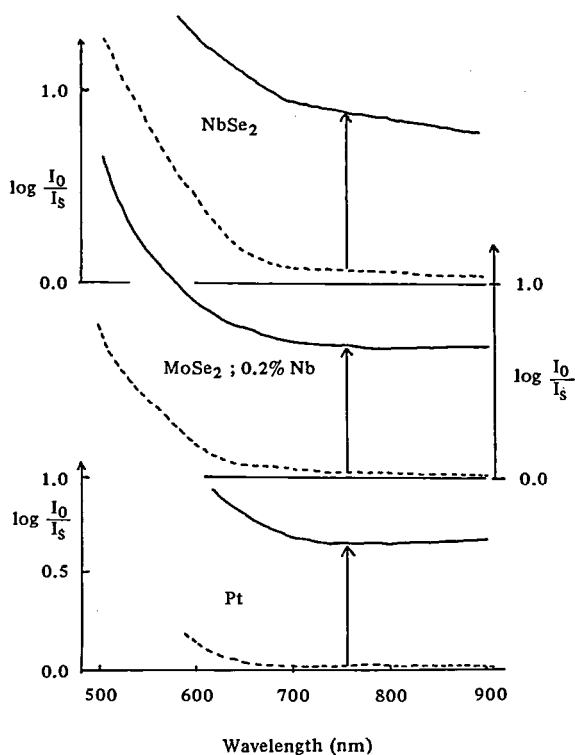$MoSe_2$; 0.2% Nb

$\log \dfrac{I_0}{I_s}$

Pt

Wavelength (nm)

Figure 1.

of many fine particles of iodine, because the reflectivity change is quite enormous, being more than 90% in the wavelength region where iodine does not have any absorption (Maxwell-Garnett theory).

Along with the film formation of iodine, the surface of $MoSe_2$ was presumed to have changed. The surface change was seen clearly with eyes in the case of $NbSe_2$ when the $NbSe_2$ electrode was kept for several hours at the anodic potential where a film formation takes place. The x ray diffraction pattern is consistent with the intercalation of iodine. For $MoSe_2$, the light induced interaction of iodine was assumed, since its electronic structure is similar to that of $NbSe_2$. From the above findings, the improvement of the efficiency of MoS_2 solar cell by I^-/I_2 redox reagents is considered to be due to this photointercalation accompanied by the thin film formation of iodine.

Reference

1) H. Tributsch, Ber. Bunsenges. Phys. Chem., 82, 169 (1978).

III-G Photocatalytic Effects of Semiconductors

Essential roles are played by semiconductors in the photocatalytic effects to which a particular attention has been paid in connection to the solar energy conversion through such processes as photolysis of water and photoreduction of N_2. In order to elucidate the mechanism of these effects, we need detailed knowledges of the characteristics of adsorbed molecules on the surface as well as of the correlation between reactivities and structural and electronic conditions of the surface. Work on the following topics is in progress with the purpose of clarifying the photocatalytic effects of semiconductors from the view point of solar energy conversion.

1) Dynamics of photocatalytic reactions of semiconductros.

2) New artificial surfaces modified by the molecular beam epitaxial (MBE) method and their reactivity.

3) Electronic structures of semiconductor surfaces and adsorbed molecules as studied by theoretical calcualtions.

III-G-1 Dynamics of Photocatalytic Reactions on Semiconductor Surface

Katsumi TANIMURA, Tomoji KAWAI, and Tadayoshi SAKATA

The absorption of light by a semiconductor which is interacting with molecules on its surface causes various effects in adsorbed molecules. It affects the adsorption capacity of a semiconductor, accelerates (and sometimes retards) catalytic reactions which are taking place, and results in some new reactions such as photolysis of water and photoreduction of nitrogen.[1,2] Extensive studies have recently been made on these phenomena, the

Figure 1. Schematic representation of experimental blocks. A UHV system has a basic pressure of 1×10^{-10} torr and includes following apparatus; MBE, oven for molecular beam epitaxy, GBG, generator of gas beam, SG, Ar^+ ion sputter gun, LAO, the LEED-Auger Optics, QMS, quadrupole mass spectrometer, LS, the He-1 light source for UPS, EA, hemispherical electron analyser, and VP, viewing port. S is the sample on a manipulater which enables rotational and three-dimensional motions.

photocatalytic effects, on which a particular interest has been focused in connection to conversion of the light energy into the electronic power and/or chemical energy. The aim of our research is to make clear the fundamental mechanism of these photocatalytic reactions on a semiconductor surface.

Characteristics of the methods we use are the following.

1) Experiments in an ultra high vacuum (UHV) system

It is of great advantage to make use of the well defined structural and electrical conditions of semiconductor surfaces, since catalytic reacitons are in general strongly sensitive to surface conditions. A UHV system including a proper apparatus for surface analysis enables us to characterize the solid surface concerned, and hence to simplify situations we must take account of.

2) Observation of dynamics in reactions

An investigation of dynamical aspects of photocatalytic reactions, caused by a pulse light, reveals important quantities which cannot be obtained by conventional stational measurements. For instance an application of time-of-flight method into the detection of reacted species provides us with such an information as the rate of the reaction, the nature of interaction of the reacted substances with the surface and the initial distribution of energy.

We describe briefly experimental procedures, and show some preliminary results of the photo-induced decomposition of CH_3OH on the clean [001] surface of the ZnO single crystal.

Our UHV system, called "Koku I", consists of a Ar^+ ion sputter gun, LEED-Auger optics, and He-1 UPS analyser, a molecular beam generator, and a quadropole
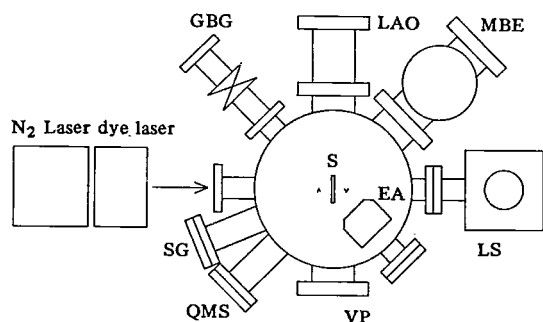
Figure 2. Oscilloscope display of the time dependent change in concentration of CO_2 decomposed photocatalytically from CH_3OH on ZnO [001] surface.

mass filter, and has a basic pressure of 1.0×10^{-10} torr. An N_2 laser, having a peak power of 600 kW and a half-width of 10 ns is used as the light source. A ZnO single crystal placed on a holder of a manipulater was cleaned by the Ar^+ ion gun and annealed to establish the ordered [001] surface. The CH_3OH gas was guided onto the ZnO surface, and then it was excited by the 3371 Å light of the laser. Reacted species was detected selectively by the mass analyser, output signal of which was put into a oscilloscope, and was recorded on a poraloid film.

Figure 2 is the oscilloscope trace of the time-dependent change in the concentration of CO_2 which is photocatalytically formed from CH_3OH on ZnO. This curve should contain an information concerning the rate of the decomposition reaction of CH_3OH, the stay of CO_2 on the surface, and the time of flight. Our efforts are in progress in analysing these experimental data to obtain a crucial information of the reaction.

References

1) A. Fujishima and K. Honda, Nature, 238, 37 (1972); Bull. Chem. Soc. Jpn., 44, 1148 (1971).
2) G. N. Schrauzer and T. D. Guth, J. Am. Chem. Soc., 99, 7189 (1977).

III-G-2 Studies of Silver Surface Made by Molecular Beam Epitaxy

Tomoji KAWAI, Katsumi TANIMURA and Tadayoshi SAKATA

The solid surface phenomenon is one of the most rapidly developping research subjects in the field of catalysis, electrochemistry, metallurgy as well as pure surface physics. The clean surface of single crystal has

gtrigonal prism   octahedron
hexagonal 2H-MoS₂   rhombohedral 3R-MoS₂
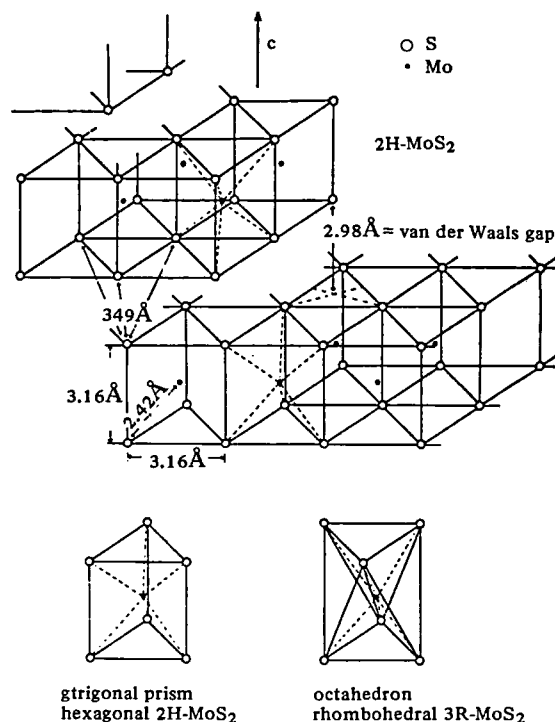
Figure 1. Structure of MoS_2 layer crystals.

been treated essentially as a well defined surface. It is often difficult, however, to separate surface effect from the bulk effect. The molecular beam epitaxy (MBE) makes it possible to create a very thin artificial surface on the substrate. The MBE technique has often been applied to make electronic devices, and it would also be very useful to make well defined artificial surfaces, which we desire to create. We are now studying chemical and physical properties of this controlled artificial surface by using the electron and the optical spectroscopy, and are also trying to clarity the mechanism of photocatalytic reactions on the surface by a pulse laser technique. We are also studying the surface properties of "layer compounds", such as MoS_2, TaS_2 and $MoSe_2$ because layer compounds themselves have a strong two dimensional character. Here we report on studies of the silver surface made by the molecular beam
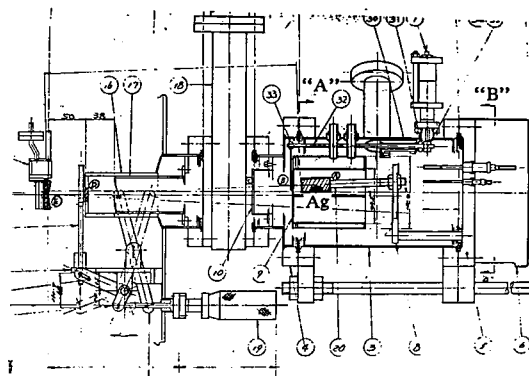
Figure 2. Oven for molecular beam epitaxy.
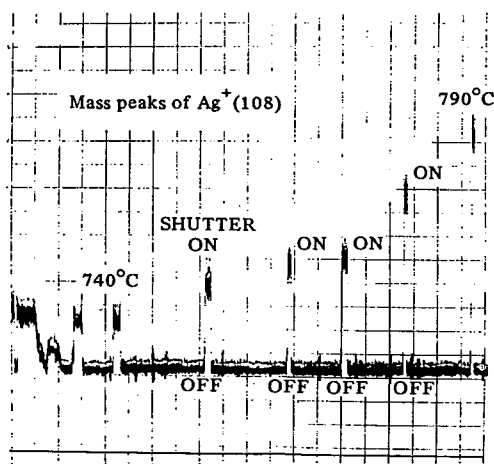
Figure 3. Mass peaks of Ag^+ (m/e = 108).

epitaxy. An atomic beam of silver was produced in the ultrahigh vacuum and was depositted on the clean MoS_2 surface. The two dimensional van der Waals plane (Figure 1) was exposed by mechanically peeling the surface layers. This surface is inactive as the outermost layer was covered with sulfur, and can be regarded as a surface matrix.

The ultrahigh vacuum system used for the experiment consists of:

1) a manipulator on which the sample can be cooled down to the liquid nitrogen temperature and heated up to $500°C$.

2) an Ar^+ sputtering gun for cleaning up the surface.

3) a LEED-AES apparatus for characterization of the surface structure and surface composition.

4) a Ultraviolet photoelectron spectrometer for the study of electronic structure.

5) a molecular beam epitaxy oven for making an artificial surface.

6) a gas beam inlet for the catalytic surface reaction.

7) a Q-pole mass filter for the detection of the reaction products.

8) a quartz window for the laser inlet. Nano-second N_2 and dye lasers are used for the excitation of the surface.

9) a vacuum chamber (10^{-10} torr).

An Ag atomic beam produced by heating the oven at a constant temperature (Figure 2), was collimated through the slits onto the surface of the specimen, and was monitored for its intensity by mass spectrometry. Figure 3 shows the height of mass peak of m/e = 108 (Ag^+) when the shutter was operated. Mass peaks corresponding to Ag^+ was detected but not those of Ag_2^+ or Ag_3^+. This result shows that only the atomic silver exists in the beam.

The AES on the MoS_2 surface was examined. The deposition of silver atoms onto the MoS_2 surface resulted in an increase of Ag (MNN) Auger peak as shown in Figure 4. The LEED spot of this silver surface
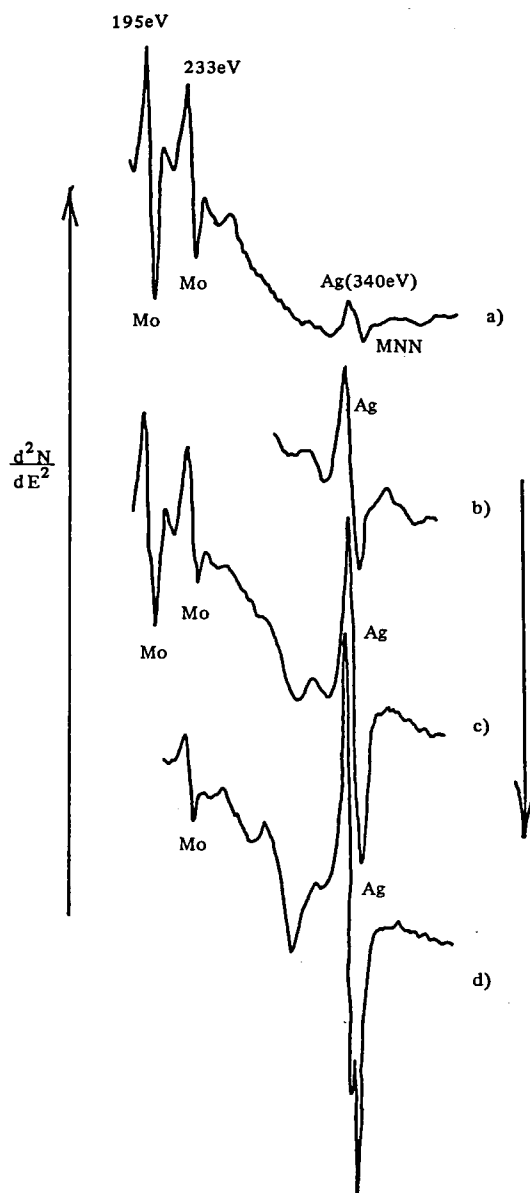
Figure 4. Auger peak of Ag on MoS_2 surface.

showed the same pattern as that of the original trigonal prismic hexagonal structure of MoS_2. The ELS of this surface was dependent on the amount of Ag, and a new peak at 4 eV of the loss energy appeared which would be due to the two dimensional character of the Ag surface.

III-G-3 On the Mechanism of Photoelectrolysis of Water on TiO_2

Tadayoshi SAKATA, Katsumi TANIMURA, and Tomoji KAWAI

Since Fujishima and Honda discovered the photolysis of water on a TiO_2 electrode in 1972,[1] several semi-

conductors such as SnO_2, $SrTiO_3$, $KaTaO_3$, WO_3 and $BaTiO_3$ have been discovered to work as stable photo-anodes for the decomposition of water. Its detailed mechanism is, however, not well understood well. In many published papers, the redox potential of water has been used as the sole basis to judge whether the photolysis is possible or not. We propose a simple model for the photodecomposition of water on n-type semiconductors from the view point of elementary reactions and of the energetical relationship between the semiconductor and molecules to be oxidized.

As to the photodecomposition of a water molecule on a stable photoanode, the following reaction is usually considered:

$$2H_2O + 4p^+ \rightarrow 4H^+ + O_2 \qquad (1)$$

This equation, however, does not show what elementary reactions are. As suggested in eq. (1), several electron transfer reactions are involved in the process of the oxygen evolution from water. Since the electron transfer is too fast to be followed by the rearrangement of the solvent molecules, it is better to apply a quantum mechanical theory of the vertical transition to the oxidation processes rather than to discuss them on the basis of the thermodynamical consideration.

We propose th efollowing molecular model for the oxygen evolution at the semiconductor/water interface. As the first step of the oxidation of water, two kind of reactions are considered. One is the reaction of a water molecule with a hole (p^+).

$$H_2O + p^+ \rightarrow H_2O^+ \qquad (2)$$

$$H_2O^+ \rightarrow H^+ + \cdot OH \qquad (3)$$
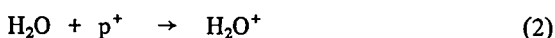
another is the reaction of OH^- with a hole.

$$OH^- + p^+ \rightarrow \cdot OH \qquad (4)$$

The oxidation of $\cdot OH$ is the second step.

$$\cdot OH + p^+ \rightarrow OH^+ \qquad (5)$$

$$OH^+ \rightarrow \cdot O + H^+ \qquad (6)$$
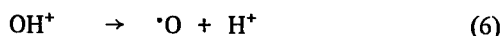
The final reaction is the recombination of atomic oxygens.

$$O \cdot + \cdot O \rightarrow O_2 \qquad (7)$$

As seen from the above equations, the reactions with holes in the valence band of the semiconductor are (2), (4) and (5). It is critical to find out whether any of these reactions is difficult. We estimated the energy of electrons in the hightest occupied level relative to the vacuum level by considering the following vertical transition.

$$M \xrightarrow{\text{vertical}} M^+ + e^-(\text{vacuum}) \qquad (8)$$
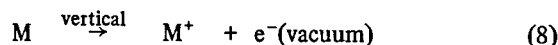
$$\Delta W = I_p^{gas}(M) + P^{adiab}(M) - P^{elect}(M^+) \qquad (9)$$

Here ΔW is the vertical ionization energy for the process (8), and $I_p^{gas}(M)$ is the ionization potential of a molecule M in the gas phase. $P^{elect}(M^+)$ is the electronic polarization energy for a molecule M^+ in the medium under consideration and $P^{adiab}(M)$ the adiabatic polarization energy for a molecule M. The electronic polarization energys were estimated with the Born's equation by replacing the dielectric constant with the square of the index of refraction of the medium.

The result is shown in Figure 1. In this figure, the distribution function of the electrons in the highest occupied orbital, in which the Franck Condon factor of the vertical transition for the electron transfer is taken into consideration, is shown for three molecules, H_2O, $\cdot OH$, OH^-. For the physical adsorption, the contribution of the polarization energy from TiO_2 medium is also taken into account.

From the above energetical consideration, the following conclusions are obtained.

1) The reaction of H_2O with a hole in TiO_2 is difficult, while the reaction of OH^- with the hole is easy. Therefore, as a first step of the oxidation of water, the reaction of OH^- with p^+ is considered to be the most probable except in the acidic region.

2) The level of $\cdot OH$ is located near or below the valence band of TiO_2. However, this level is possibly lifted up by the interaction of TiO_2 surface (charge transfer from TiO_2 to $\cdot OH$), as is suggested by the theoretical calculation of the cluster model. Therefore, the interaction of $\cdot OH$ with the TiO_2 surface would play an important role in the second step of the oxidation of water. On
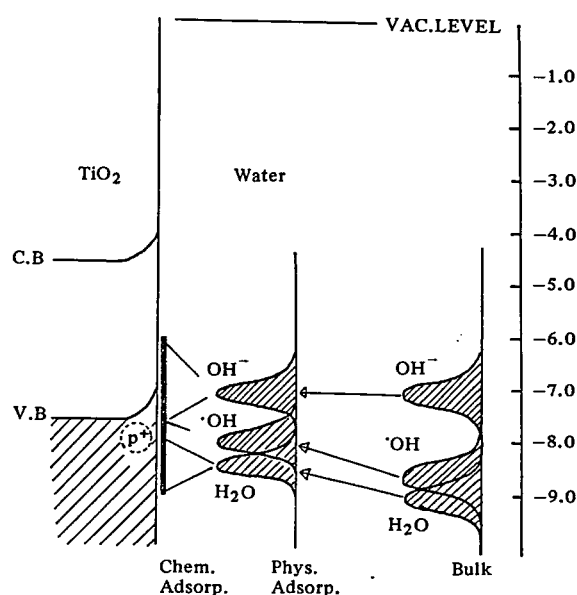
Figure 1.

the whole, for a better understanding of the mechanism of photooxidation on semiconductor surfaces, it is quite important to investigate what kind of interaction between their surfaces and reacting species exists and works. Such problems remain to be investigated experimentally and theoretically in the future.

Reference

1) A. Fujishima and K. Honda, Nature, 238, 37 (1972).

The projects of "Molecular Approaches to Solar Energy Conversion" (IIIE - IIIG) are summarized schematically in the following Figure.

Nanosec Laser
N₂, dye Lasers

Polarization System
for Electrochemical
Measurement

Xe, W, D₂ Lamp.
Monochromator.
Optical Apparatus.

Evaporation System
for Thin Solid
Films

Ultra-high Vacuum
System for Surface
Analysis and Photo-
catalysis

Photon Counting System
for Surface Analysis
and Measurement of
Life Time

PHOTOELECTRODE PROCESS

PHOTOCATALYSIS

Photoelectro-chemical energy conversion by thin films of organic semiconductor

Energy storage and solar energy conversion by layer compound electrode

Photocatalytic effect of semiconductros

Photoelectrochemical energy conversion by thin films of metal porphines, and its application to hydrogen evolution.

Dynamics on photoelectrode process studied by pulse laser technique.

Spectroscopic study on the transfer of energy and electrons at the interface between porphyrin film and solid surfaces.

The photovoltaic effect at the interface between semiconductor and electrolyte.

Energy storage by layer compound electrode.

Interface phenomena controlling the efficiency of electrochemical $MoSe_2 : I^-/I_2$ solar cell.

Dynamics of photocatalytic reactions on semiconductor surface.

Studies of silver surface made by molecular beam epitaxy.

On the mechanism of photoelectrolysis of water on TiO_2.

Synthesis of ammonia from water, nitrogen and solar energy.

Figure 1. Scheme of the projects of "Solar Energy Conversion".

RESEARCH ACTIVITIES

IV. Division of Molecular Assemblies

In this Division, studies on electronic structures and electrical properties of aromatic solids are being carried out using as a probe their photoelectric phenomena such as photoconduction and photoemission. A new photoelectron spectrometer, in which we were able to control a wide range of the specimen temperature, was prepared. We are also carrying out an experimental research on physico-chemical and also electrochemical properties of hydrogenase and its electron carrier, cytochrome c_3; these properties might be related to its enzymatic activities.

The photoionization processes of simple molecules, such as diatomics and triatomics, are being studied by using both mass spectrometric and photoelectron spectroscopic techniques. In particular, measurements of threshold electron spectra are possible with our apparatus which is equipped with a helium Hopfield continuum light source.

In an application of the photoionization technique, the internal energy dependence of ion-moelcule reactions is being studied intensively. A new technique which utilizes the threshold electron-secondary ion coincidence has been developed for this purpose.

The intercalation compounds of graphite with alkali metals and also ferric chloride are also being investigated.

IV-A Photoelectric and Optical Properties of Organic Solids in Vacuum Ultraviolet Region

Since research on organic semiconductors has been started, a large number of studies have been reported to analyse their conduction mechanism. Its quantitative investigation, however, still remains ambiguous. Application of the photoelectron spectroscopical me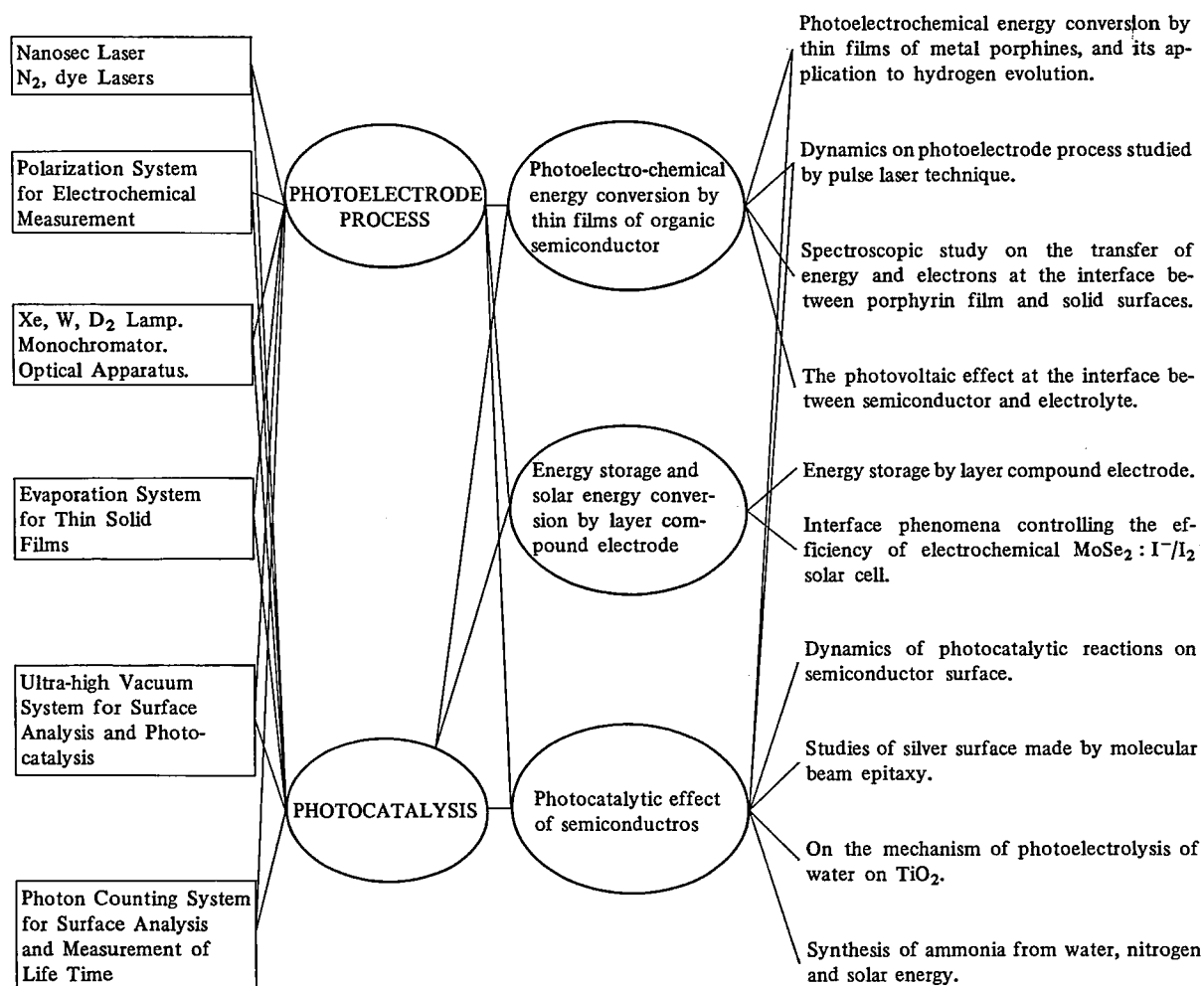thod gives much information about the electronic properties of the organic semiconductors. After an introduction of high-vacuum technique and repeated improvements, we constructed a new photoelectron spectrometer equipped with a temperature control.

IV-A-1 Instrumentations of Photoelectron Spectroscopical Studies on Organic Solids

Kazuhiko SEKI, Naoki SATO, and Hiroo INOKUCHI

Study of the photoelectron emission of solids, in particular of the photoelectron spectroscopy, gives much information about the electronic properties such as the density of states of occupied and unoccupied states, the work function, and the behavior of quasi-free electrons in the solid. We have applied this technique for the investigations of electronic properties of organic solids, particularly of the condensed polycyclic aromatic hydrocarbons.[1]

At present we can use two light sources and three photoelectron spectrometers. One of the light source is the combination of a Hinteregger type hydrogen discharge lamp and a 0.5 m Seya-Namioka type vacuum uv monochromator with a LiF window at the exit slit. It emits light of $4\,\mathrm{eV} \leq h\nu \leq 11.5\,\mathrm{eV}$. This continuous light source is useful for the precise determination of the photoemission threshold by the measurement of the $h\nu$ dependence of the quantum yield (the number of electrons emitted per incident photon). This is a com-

plementary method to photoelectron spectroscopy. In this method, the light intensity is measured by a photomultiplier with a fluorescent wavelength converter.[2] Another light source is a differentially pumped rare gas resonance line lamp (Figure 1). This emits almost
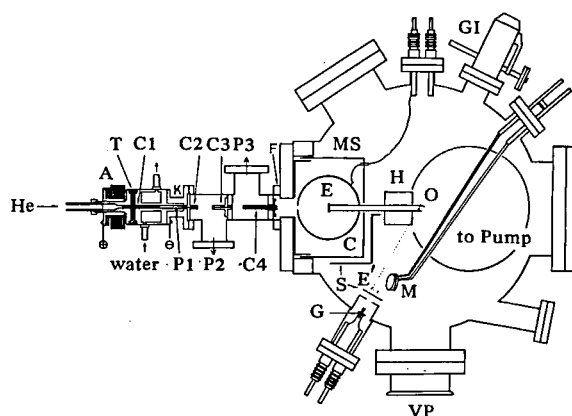

Figure 1. Combination of the rare gas resonance line light source and a photoelectron spectrometer.
A: lamp anode, K: lamp cathode, P1 ~P3: differential pumping ports, G: sample evaporation source, E: substrate, M: thickness monitor, C: photoelectron collector.

monochromatic light of $h\nu$ = 11.7, 16.8 and 21.2 eV for the discharge gas Ar, Ne, and He, respectively.

The sample and the photoelectron spectrometer must be kept in vacuum to avoid the scattering of electrons and the contamination of the surface. The vacuum condition for organic solids is generally not so critical as for metals or inorganic semiconductors because of their inactive surfaces. However, ultrahigh vacuum is necessary in some cases, for instance when one wants to cool the sample. Depending on the subject, we choose one of the three sample/energy analyzer chambers of the attainable vacuum of (i) 10^{-3} Pa (by an oil diffusion pump), (ii) 10^{-6} Pa to 10^{-7} Pa (by an ion pump and a Ti sublimation pump), and (iii) 10^{-8} Pa (by an ion pump, a Ti sublimation pump). As an example, the combination of the resonance line lamp and (ii) is shown in Figure 1.

The sample is usually evaporated onto metal substrates *in situ* under vacuum. The film thickness (usually several tens nm) is monitored with a quartz crystal oscillator. For the measurement of the spectra, the sample is moved to the position surrounded by a spherical collector and is irradiated by light. The number of photoelectrons is measured as a photoelectric current by a Cary 401 vibrating reed electrometer. The energy of electrons is analyzed with applying a retarding potential V_R between the sample and the collector. When V_R is very large, the photocurrent I_P = 0. When V_R is decreased, I_P increases and finally becomes saturated. The photoelectron spectrum is obtained by differentiating this V_R - I_P curve with the ac modulation technique.[3] As an example, the results for dibenzotetrathiafulvalene at $h\nu$ = 7.75 eV are shown in Figure 2.

References

1) K. Seki, T. Hirooka, Y. Kamura, and H. Inokuchi, *Bull.*

Chem. Soc. Jpn., **49**, 904 (1976).

S. Hino, N. Sato, and H. Inokuchi, *Chem. Phys. Lett.*, **37**, 494 (1976), and references in these.

2) F. Masuda, M. Kochi, S. Iwashima, and H. Inokuchi, *Jap. J. Appl. Phys.*, **6**, 1423 (1967).

H. Inokuchi, Y. Harada, and T. Kondow, *J. Opt. Soc. Am.*, **54**, 842 (1964).

3) R. C. Eden, *Rev. Sci. Instr.*, **41**, 252 (1970).

IV-A-2 Vacuum-ultraviolet Photoelectron Spectroscopy of Polyethylene and n-$C_{36}H_{74}$ in Solid and Gaseous Phases

Kazuhiko SEKI, Shimpei HASHIMOTO *(Japan Synthetic Rubber Co.)* Naoki SATO, Yoshiya HARADA *(Univ. of Tokyo)*, Kikujiro ISHII,[1] Hiroo INOKUCHI, and Junichiro KANBE *(Kyoiku Univ.)*

The electronic structure of polyethylene is interesting as this polymer is (1) one of the simplest organic polymers and (2) the long chain limit of n-alkanes. X-ray photoelectron spectroscopy revealed the valence band (occupied states) features and fairly good correspondence was found with theoretical calculations.[2] However, the conduction band (unoccupied states) structures have not been clarified experimentally.

We measured the ultraviolet photoelectron spectra of the evaporated films of polyethylene and its model compound hexatriacontane n-$C_{36}H_{74}$ at 11.7 eV $\leq h\nu$ $\leq$ 21.2 eV (region I) and found three or four features of the conduction band for the first time. We also measured the spectra at $h\nu$ = 40.8 eV for both solid and gaseous n-$C_{36}H_{74}$, which permitted a comparison of the valence bands in solid and gas phases.

Solid phase photoelectron spectra in the region I were measured by the instrument shown in Figure 1 of IV-A-1 and the combination of similar photoelectron spectrometer with a light source of condensed discharge
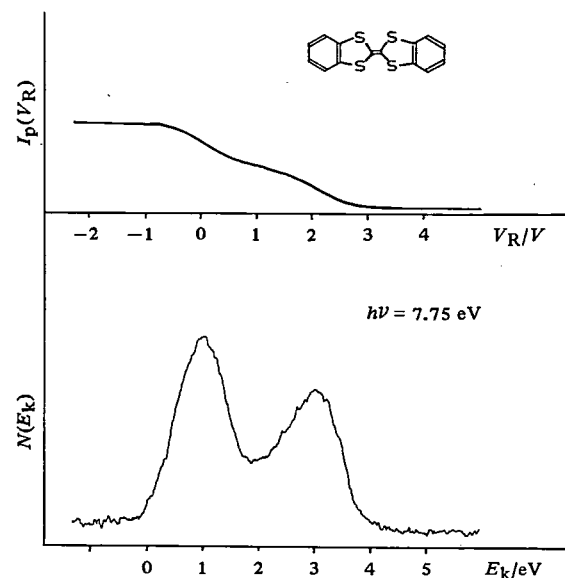

Figure 2. Retarding potential (V_R) - photocurrent (I_P) curve (a) and photoelectron spectrum (b) of dibenzotetrathiafulvalene at $h\nu$ = 7.75 eV.
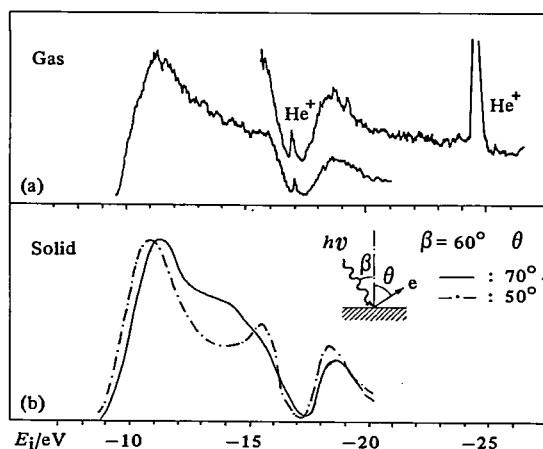

Figure 1. Valence band photoelectron spectra ($h\nu$ = 40.8 eV) of n-$C_{36}H_{74}$ in gas (a) and solid (b) phases.

of air monochromatized by a 0.5 m Johnson-Onaka type vacuum-uv monochromator. Photoelectron spectra at $h\nu$ = 40.8 eV were measured with a Perkin-Elmer PS-18 photoelectron spectrometer with some modifications for solid phase measurements. Polyethylene and n-$C_{36}H_{74}$ gave essentially the same results.

In region I, the spectra were dominated by severely scattered secondary electrons. They are accumulated to the parts of the conduction band where density-of-states is large. These parts are revealed as features in the photoelectron spectra which have constant kinetic energy E_k independent of the photon energy $h\nu$. The location of these high-density-of-states parts was obtained from the measured E_k values.

At $h\nu$ = 40.8 eV, the high-E_k part of the spectra reflects the features of the valence bands. Figure 1 shows the valence band photoelectron spectra of gaseous and solid phases n-$C_{36}H_{74}$. An interesting finding was the observation of a strong dependence of the photoelectron spectra of solid on the emission angle of electrons, as shown in Figure 1(b). Although its origin is not yet clear, such measurements may give an information about the photoemission mechanism of organic solids. Hexatriacontane molecules crystallize in extended regular zig-zag chains, while in gas phase they take a random coil form. We previously found a good correspondecne between these states for rigid molecules.[4] The fairly good overall correspondence of the spectra between gas and solid phases except for some details suggests that the change in the gross valence bend structure is small, as was previously shown between the C_{13} gas and the C_{36} solid by XPS.[5]

In Figure 2, features in the density of states of solid polyethylene are shown with measured UPS spectra and reported XPS spectra[6] (Figure 2a), and are compared with the theoretical calculations for an isolated chain. More refined calculations for the whole crystal may be more useful particulary for the discussion of the conduction bands.

References and Notes

1) Present address: Gakushuin University.
2) M. H. Wood, M. Barber, I. H. Hieller and J. M. Thomas, *J. Chem. Phys.*, **56**, 1788 (1972).
   J. Delhalle, J. -M. André, S. Delhalle, J. J. Pireaux, R. Caudano and J. Verbist, *J. Chem. Phys.*, **60**, 595 (1974).
3) See Ref. 5 of IV-A-3.
4) K. Seki, H. Inokuchi and Y. Harada, *Chem. Phys. Lett.*, **20**, 197 (1973).
5) J. J. Pireaux, R. Caudano and J. Verbist, *J. Elec. Spectrosc.*, **5**, 267 (1974).
6) J. J. Pireaux, S. Svensson, E. Basilier, P-Å Malmqvist, U. Gelius, R. Caudano and K. Siegbahn, *Phys. Rev.* **A14**, 2133 (1976).
7) W. L. McCubbin and R. Manne, *Chem. Phys. Lett.*, **2**, 230 (1968).
8) J. E. Falk and R. J. Fleming, *J. Phys.*, **C6**, 2954 (1974).

IV-A-3 Anisotropic Vacuum-uv Absorption Spectra of Elongated Thin Polyethylene Films Near the Absorption Edge

Shimpei HASHIMOTO *(Japan Synthetic Rubber Co.)*, Kazuhiko SEKI, Naoki SATO, and Hiroo INOKUCHI

As a part of the studies of the electronic properties of polyethylene, we studied the photoabsorption process which occurs in the band structure investigated in IV-A-2. The fundamental electronic absorption spectrum of polyethylene is interesting, not only because polyethylene is one of the simplest organic polymers but also because the spectra can serve as the experimental check of the theories for the absorption spectra of shorter alkanes. Although several experimental reports have been published about the absorption spectra of polyethylene,[1,2] its interpretation has not been settled, partly because of the lack of detailed experimental data. In particular reliable data of anisotropic absorption spectra with the polarized light have been watned.

In the uniaxially elongated film of polyethylene, the chains are known to orient in the direction of elongation. We have for the first time succeeded to prepare

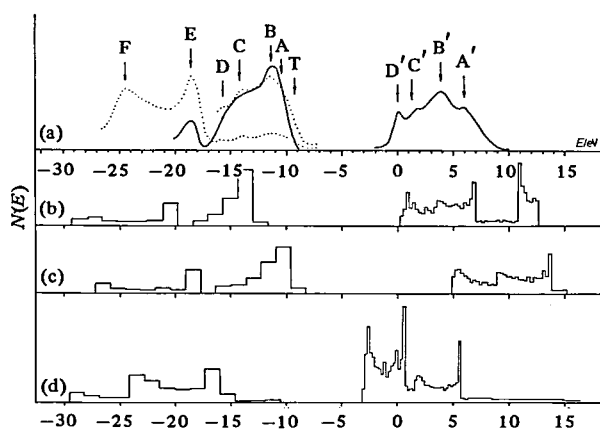Figure 2. Features in the density of states shown by the measured photoelectron spectra (a) and the calculated density of states (b-d). — in (a) are measured for $h\nu$ = 18.1 eV ($E >$ 0 eV), and 40.8 eV ($E < 0$ eV) respectively. · · · in (a) is the XPS spectra reported in Ref. 6. (b) and (c) is read from Ref. 7 and (d) is read from Ref. 8.
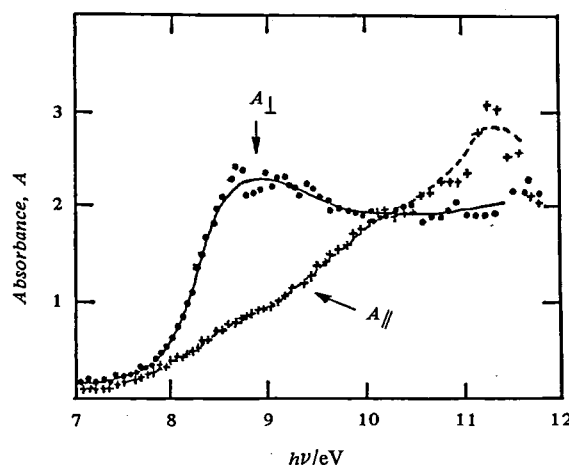

Figure 1. Anisotropic absorption spectra of 5 times elongated oriented polyethylene.

ultrathin elongated films and measured the anisotropic absorption spectra of polyethylene by direct transmission.

Methods of sample preparation was reported elsewhere.[3] Polarized light was produced either (i) by the reflection of the concave grating of the Seya-Namioka type monochromator described in IV-A-1 or (ii) by a Brewster angle reflection of a LiF polarizer attached to a McPherson 225 normal incidence monochromator. In case (i), the transmission was measured point to point and the polarized spectra were obtained after the calibration with the degree of polarization measured with the polarizer of (ii). In case (ii), the spectra were measured by the double beam attachment of the monochromator. Both gave essentially the same results. Typical anisotropic absorption spectra for a film elongated 5 times (average thickness 50 nm) are shown in Figure 1. Weyland[2] reported anisotropic absorption spectra of polyethylene obtained by the Kramers-Kronig conversion of reflection spectra. Although he reported a shoulder at $h\nu \sim 8$ eV in the $E//c$ spectrum (E is the electric vector of the incident light and c is the c axis of the crystal which corresponds to the direction of molecular chains), it was not found in the present result. Other features agree fairly well with his, and the spectra are similar to those of $n\text{-}C_{23}H_{48}$ single crystal reported by him.

Partridge[1] applied the exciton theory of Raymonda and Simpson[4] for the interpretation of the spectra of small alkanes to polyethylene, and predicted the lowest absorption band to be polarized parallel to the molecular chain. This does not agree with the present result. A simple interpretation based on available band calculations for isolated chain[5] does not readily explain the experimental results well either, and a further refinement of theory seems to be necessary.

The obtained anisotropic absorption spectra showed a very good correspondence with the anisotropy of the photon energy dependence of the photoemission yield by the polarized light,[6] as shown in Figure 2. This can be explained if we assume a very short escape depth of photoelectrons, as confirmed by photoemission experiments (see IV-A-2).

References

1) R. H. Partridge, *J. Chem. Phys.*, **49**, 3656 (1968).
2) J. P. Weyland, Thesis, Univ. of London, (1974) and references therein.
3) S. Hashimoto and H. Inokuchi, *Polymer J.*, **8**, 467 (1976).
4) J. W. Raymonda and W. T. Simpson, *J. Chem. Phys.*, **47**, 430 (1967).
5) For a review, see J. -M. André, in "Electronic Structure of Polymers and Molecular Crystals", ed. by J. -M. André and J. Ladik (Plenum, N. Y., 1975).
6) S. Hashimoto, S. Hino, K. Seki, and H. Inokuchi, *Chem. Phys. Lett.*, **40**, 279 (1976).

IV-A-4 Low Energy Electron Escape Depths in Organic Solids

Shojun HINO *(Josai Univ.)*, Naoki SATO, and Hiroo INOKUCHI

We have tried to determine directly the escape depths of electrons in organic solids excited by the vacuum ultraviolet light. Few workers have ever carried out similar studies,[1,2] though for metals or inorganic semiconductors a lot of investigations have been carried out by the X-ray photoelectron spectroscopy.[3]

Figure 1 illustrates the experimental apparatus. In the vacuum chamber ($\sim 1.5 \times 10^{-4}$ Pa) a LiF substrate is situated at the symbol A, on which we deposit CuI (a highly photoemissive material for 160 nm light operates as the electron injector to the organic layer) and an organic compound from evaporating furnaces F_1 and F_2, while monitoring their thickness by a quartz oscillator B. C is an electron collector applied with +100V, which is connected to a vibrating reed electrometer. In this experiment CuI layer was irradiated with a monochromatized light ($\lambda = 160$ nm; $h\nu = 7.75$ eV) and we observed the electron current through the sample film which varied with the successive changes of its thickness. The electron energy distribution curve of CuI obtained with the 160 nm light was nearly Gaussian notated $N(1.5 \text{ eV}, (0.5 \text{ eV})^2)$ above the vacuum level of
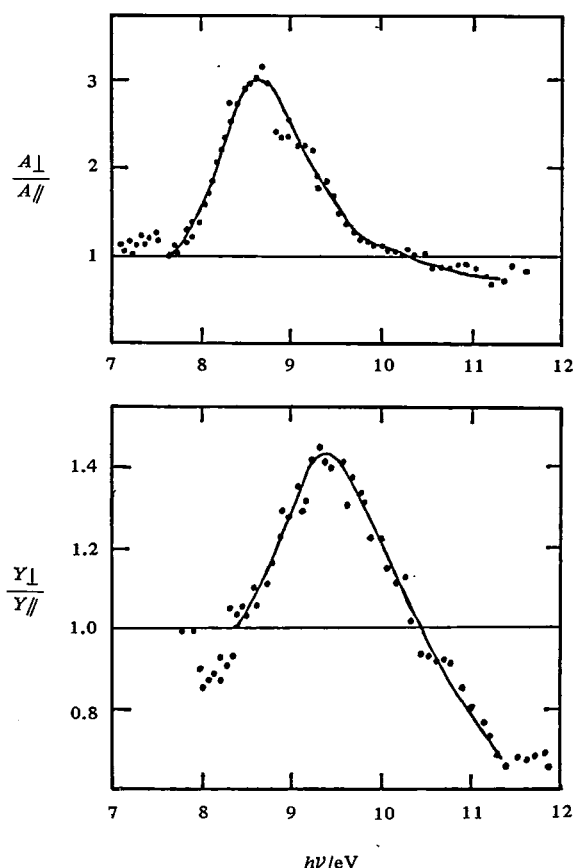

Figure 2. Comparison of the anisotropic ratio of the electronic absorption coefficient (upper) and the quantum yield of photoelectric emission (lower) or oriented polyethylene.
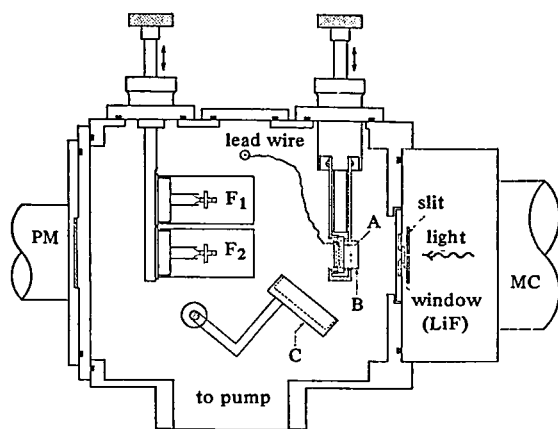
Figure 1. Apparatus for the measurement. Details are written in the text.

CuI.

When an electron moves with a finite kinetic energy toward a solid-vacuum interface, the electron loses its energy by collisions with various scattering centres and it might end up being trapped in the solid. The transport probability S of electrons in a solid is given by

$$S(E, x) = \exp\left[-x/L(E)\right], \tag{1}$$

where E is the initial kinetic energy, x is the distance from the surface to the point of electron generation, and $L(E)$ is defined as the electron escape depth. We use the above equation to calculate the photoemission yield[3] as a function of film thickness t.

In experiments we have observed the total photoelectric current I_{tot} of the lamellar specimen which is expressed as

$$I_{tot} = I_{CuI} \, S(E, t) + I_{org}, \tag{2}$$

where I_{CuI} is the photoemitted current from the CuI film and I_{org} is the photocurrent emitted from the organic film due to the light penetrating through the lamellar specimen.

In the thin film region of organic compounds where the first term of Eq. (2) is dominant in I_{tot}, the value of L can be obtained from Eq. (1) applied to the experimental plots. In the thick film region, however, the second term may dominate I_{tot}, when we can apply the calculated photoemission yield to experimental results. Then we can obtain L values and absorption coefficients directly.

We obtained the dependence of the photoelectric current on the light transmittance for six compounds as a function of film thickness in a semilogarithm plot. The result for violanthrene A is shown in Figure 2. The observed L values shown in Table I vary widely
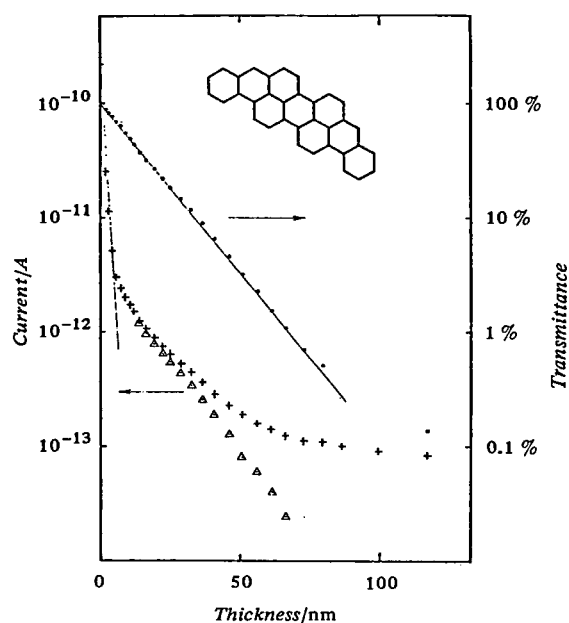
Figure 2. Thickness dependence of the emitted electron current (+) and the light transmittance (•) of the violanthrene A evaporated film, and also the electron current (△) subtracted by the electron current of 100 nm thick film.

Table I. Electron Escape Depths and Absorption Coefficients of the Organic Solids

	L/nm	$\alpha/10^7\text{m}^{-1}$
Naphthacene	7.5	9.2
	14[a]	
Pentacene[b]	7.5	4.9
Perylene[b]	80	2.0
Coronene	25	2.4
	61	0.98
Violanthrene A	1.3	6.9
Cu-phthalocyanine	2.7	4.2
	1.1[c]	

[a] Reported in Reference 2).
[b] Reported in Reference 3).
[c] Reported in Reference 1).

among the compounds. Our present result on Cu-phthalocyanine agrees with the experiment by Pong and Smith and the calculation by Schechtman.[4] In order to find an interpretation of the observed variation, we are continuing our study, including the characterization of film structures, the energy distribution of transmitted electrons, and the dependence on the light energy.

References
1) W. Pong and J. A. Smith, J. Appl. Phys., 44, 174 (1973).
2) A. I. Belkind, S. B. Aleksandrov, V. V. Aleksandrov, and V. V. Grechov, Electrical Properties of Organic Solids Conference, Karpacz, 1974.
3) S. Hino, N. Sato, and H. Inokuchi, Chem. Phys. Lett., 37, 494 (1976).
4) B. H. Schechtman, Thesis, Standord University, 1968.

IV-B Photoconduction in Organic Solids

The electric conduction in organic solids is one of the subjects which have led physical chemists to the study of molecular assemblies. Details of the conduction phenomena in organic solids, however, have not been clearly understood yet. Excited states of molecular crystals have recently been studied extensively. Photoconduction in a molecular solid has been shown to be a phenomenon which involves the generation of highly excited states of molecules, their conversion to ionized states and the migration of these states. These processes can be studied individually by using techniques of photoconduction measurement.

In the Division of Molecular Assemblies, photoconduction of some organic solids is studied to elucidate the mechanism of conduction in molecular solids. A great deal of effort has been also made to find substances with novel electrical properties. Since electrical properties of a solid strongly depend on its purity and crystallinity, the study of techniques of purification and crystal-growth is an important part of this project.

IV-B-1 Synthesis and Purification of Tetrabenzo [a, cd, j, lm]-Perylene (TBP)

Hiroo INOKUCHI, Junji AOKI (Toho Univ.), Satoshi IWASHIMA (Meisei Univ.), Kikujiro ISHII,[1] Naoki SATO and Mizuka SANO (Univ. of Electrocommunications)

As a technique of obtaining aromatic hydrocarbons with large molecular weight, the alkali fusion method has been employed. When this reaction is applied to benzanthrone [1], one obtains violanthrone A and some other byproducts, reduction of which leads to violanthrene A [2] and its isomers. On the other hand, Aoki[2] has found that the reaction of benzanthrone with copper powder and fused zinc chloride selectively gives tetrabenzo[a, cd, j, lm]perylene (TBP) [3], violanthrene B (VEB) [4] and iso-violanthrene B (iso-VEB) [5], which are hard to obtain by the method described above. It has been recently found that TBP has novel molecular and crystal structures[3] and shows a large photoelectric response.[4] Therefore, methods of preparation and purification of TBP were examined again on a large scale, since a large amount of the material is necessary for a refined study of photoconduction using single crystals.

A mixture of 0.5 kg of benzanthrone, 0.5 kg of copper powder, 2.5 kg of zinc chloride, 0.5 kg of sodium

chloride and 100 ml of water was maintained at 230°C for 30 min in a stainless steel vessel. After washing the content with water, 1.06 kg of the crude product was obtained including residual copper powder. From 909 g of the crude product, organic components were extracted four times by refluxing with chloroform of the total volume of 6 1. The first and second extracts were rich with TBP, while other extracts were found to contain large amounts of VEB, iso-VEB and benzanthrone. From several parts of the first and second extracts, crude samples of TBP (ca. 99 %) were obtained by sequential recrystallizations from xylene or o-dichlorobenzene, and pyridine. Further purifications were carried out by (i) a treatment with maleic anhydride, (ii) a treatment with sodium and (iii) chromatography on active alumina and active charcoal. The crude TBP contains VEB and iso-VEB as well as an unknown impurity which has absorption bands in the enrgy region lower than 2×10^4 cm^{-1}. Purification of other parts of the extracts is in progress.

The purity of the samples obtained by the above treatments was examined by fluorescence spectra of thin evaporated films. The best sample which was obtained after the three treatments in the above sequence shows a clear peak of fluorescence at 2.05 X
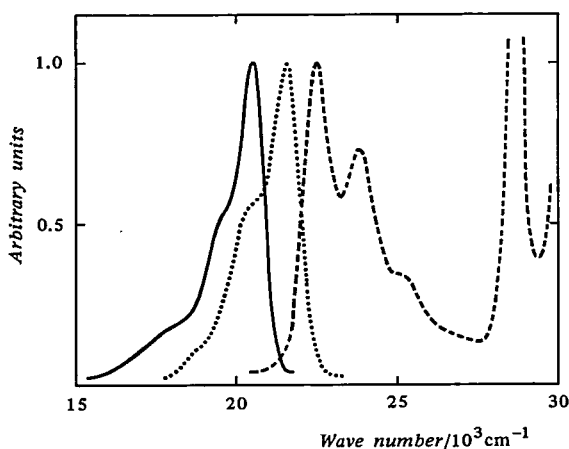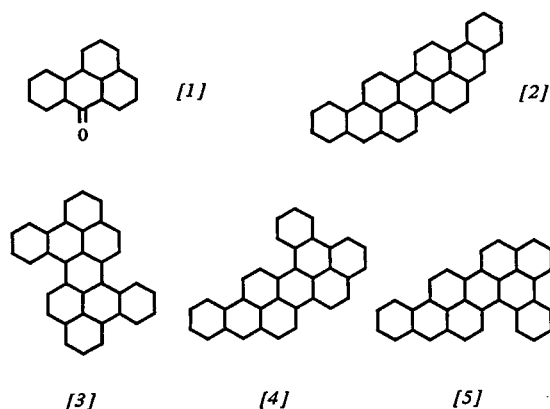

Figure 1. Fluorescence and Absorption Spectra of TBP: Fluorescence of a thin-evaporated film (full line), fluorescence of a solution of benzene (dotted line) and absorption spectrum of a solution of benzene (dashed line).

$10^4 cm^{-1}$ (life time: 17 ns) which is not accompanied with prominent bands in the region lower than $1.8 \times 10^4 cm^{-1}$ (Figure 1). The peak-position and the shape of the fluorescence spectrum were sensitive to the grade of the sample. These are important observations for choosing a method of purification and judging the quality of a sample.

We have not yet obtained a single crystal of TBP with a size large enough for photoconduction measurements. Techniques to grow large crystals as well as to measure the carrier mobility using small crystals are now being developed.

References and Notes

1) Present address: Gakushuin University.
2) J. Aoki, *Bull. Chem. Soc. Jpn.*, 37, 1079 (1963). J. Aoki, M. Takekawa, S. Fujisawa and S. Iwashima, *ibid.*, 50, 1017 (1977).
3) Y. Kohno, M. Konno, Y. Saito and H. Inokuchi, *Acta Cryst.*, B31, 2076 (1975).
4) Y. Kamura, H. Inokuchi, J. Aoki and S. Fujisawa, *Chem. Phys. Letts.*, 46, 356 (1977).

IV-B-2 Carrier Generation in Solid Molecular Complexes

Kikujiro ISHII[1] and Hiroo INOKUCHI

Charge-transfer complexes between aromatic hydrocarbons and π-electron acceptors belong to a class of complexes in which the interaction between the molecules is of a moderate strength. Molecules in this class of complexes can be assumed to be neutral in the ground state and largely ionic in the excited states.[2] It is interesting in this sense to compare the electric properties of such complexes with those of usual one-com-ponent crystals. Can electric carriers be efficiently generated from the lowest charge-transfer state?

To begin with, threshold energies of the photoelectric response of crystals were measured and compared with their absorption spectra. We studied a series of complexes in which pyromellitic dianhydride (PMDA) was the electron acceptor. It has been known that spectral response of photoconduction is sometimes deformed due to detrapping of trapped carriers by excitons in the bulk of a crystal.[3] Spectral responses of the above complexes obtained by recrystallization from the solution showed the characteristic behavior of detrapping, while some crystals obtained by sublimation in the vacuum showed responses similar to the absorption spectra.[4] These results imply that charge-carriers are efficiently generated in those complexes from charge-transfer states. This speculation is supported by a consideration of energies for the carrier generation based on the data of photoelectron emission.[5]

Perylene and 7,7,8,8-tetracyanoquinodimethane (TCNQ) have recently been found to form a 3:1-complex as well as a 1:1-complex.[6] The phase diagram of the binary system of perylene and TCNQ was studied by using a differential scanning calorimeter, and a 3:1-complex was found also to be a stable phase (Figure 1). The crystal structure of this 3:1-complex[7] is different from that of most of charge-transfer complexes, such as perylene-TCNQ 1:1-complex, in which the donor and the acceptor molecules stack alternately making columns.[2] The photoconduction and electronic spectra of these two modifications were studied for the purpose of comparing the mechanism of carrier generation. In Figure 2, results of the 3:1-complex are shown. The lower-energy portion of these spectra resembles that of the 1:1-complex. Therefore, the initial mechanism of carrier generation is inferred to be similar in these two modifications.

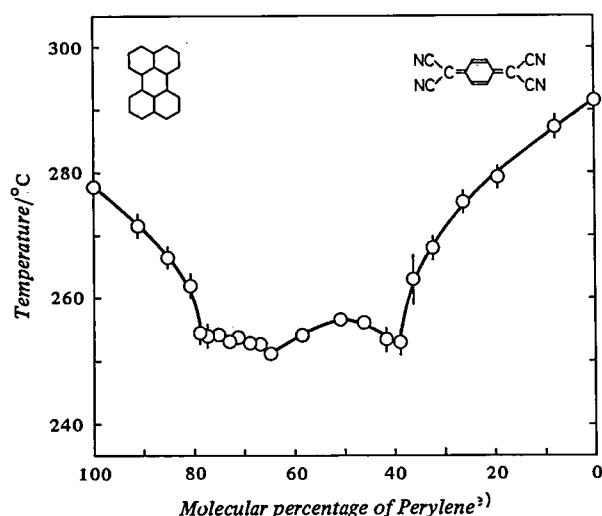Figure 1. Phase-Diagram of Perylene-TCNQ Systems: Two humps whose maxima are seen around 50 and 75 % of perylene show that 1:1 and 3:1-mixtures compose stable complexes.
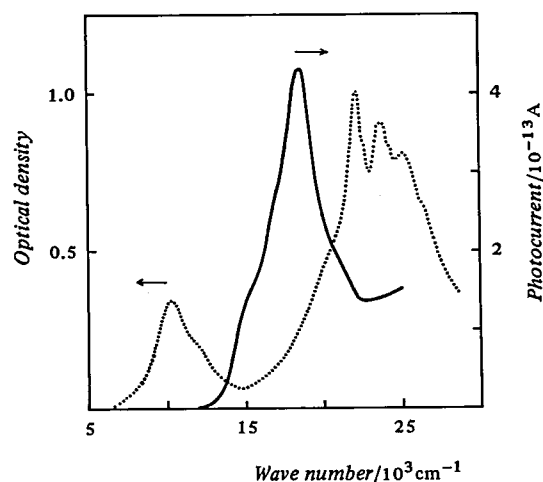

Figure 2. Photoconduction and Absorption Spectra of Perylene-TCNQ 3:1-Complex: Photoconduction spectral response of a single crystal (full line) and absorption spectrum obtained of powder sample dispersed in KBr (dotted line).

71

It should be noted here that carriers in perylene-TCNQ complexes seem to be generated through some highly excited states but not through the lowest charge-transfer state. On the other hand, a consideration of the energy similar to that described above infers that the carriers are generated at an energy as low as that of the lowest charge-transfer state. Why are not the carriers generated from the lowest charge-transfer state? What kind of state is the highly excited state if the carriers are generated through it? These are questions open to further investigations.

References and Notes
1) Present address: Gakushuin University.
2) See for example, R. Foster, "Organic Charge-Transfer Complexes," Academic Press Inc., New York (1969),
   R. S. Mulliken and W. B. Person, "Molecular Complexes," Wiley-Interscience, New York (1969).
3) H. Akamatu and H. Kuroda, J. Chem. Phys., 39, 3364 (1963).
4) K. Ishii and H. Inokuchi, unpublished data.
5) K. Ishii, K. Sakamoto, K. Seki, N. Sato and H. Inokuchi, Chem. Phys. Letts., 41, 154 (1976).
6) K. D. Truong and A. D. Bandrauk, Chem. Phys. Letts., 44, 232 (1976).
7) A. W. Hanson, Private communication.

IV-C Reaction Mechanism of Hydrogenase and Electron Transport Properties of Cytochrome

Hydrogenase, a bacterial enzyme, is a bio-catalysis of the hydrogen cleavage reaction. The ferredoxin type Fe-S clusters are a reaction center in this enzyme. Optical absorption spectra and Mössbauer spectra of hydrogenase were found to be somewhat different from those of the clostridium 8Fe-8S cluster which did not catalyse the H_2-D_2 exchange reaction. These differences might be related to the catalytic activities of hydrogenase.

Cytochrome c_3, the electron carrier linked with hydrogenase, has four hemes in the molecule. In order to analyse its carrier transport mechanism, the electrical conduction of a film of the cytochrome c_3 and its related compounds has been observed. The electrochemical techniques are also applied to the cytochromes in order to clarify the electron transfer character of heme on the electrode surface. (See the section VII-A and VII-B)

IV-D Application of Photoelectron Spectroscopy to the Study of Photochemical Reaction of Solid

Yoshiya HARADA (Univ. of Tokyo and IMS) and Hiroo INOKUCHI

Although extensive studies have been performed on reactions on solid surfaces, solid-state photochemical reactions have not been investigated by the electron spectroscopy. In the present work with an intension to study photochemical reactions of organic solids we designed an ultra-high-vacuum photoelectron spectrometer with which changes in the photoelectron spectrum during a photochemical reaction can be recorded. Some experiments have been carried out on the photooxidation of aromatic compounds.

IV-E Studies of Ion-Molecule Reactions by a Threshold Electron-Secondary Ion Coincidence Technique

One of the final objectives of the experimental studies of an elementary reaction

$$A + B \rightarrow C + D$$
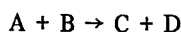
is to obtain the most detailed information on this system. That is, given a molecule A in internal state i passing by a molecule B in internal state j with a relative velocity v and at a distance b, the probability $p(i,j,v,b|i',j', v_C, v_D)$, with which the reaction takes place to give a molecule C in state i' and D in state j' with velocities v_C and v_D, respectively. Toward this end, we are studying state-selected ion-molecule reactions by the use of a new technique which we have developed.

This technique, which utilizes the threshold electron-secondary ion coincidence, allows direct measurements of $p(i, v)$, namely, the internal and translational energy dependence of ion-molecule reaction rates. Distinct from previous methods for studying state-selected reactions, this technique has versatility which promises a wide variety of future studies to be made.

IV-E-1 Construction and Performance of the IMS-TEPSICO: A Threshold Electron-Secondary Ion Coincidence Apparatus

Kenichiro TANAKA and Inosuke KOYANO

Although considerable efforts have been devoted in recent years to the determination of state-selected reaction cross sections or rate constants, most techniques employed so far in such experiments, in both neutral-neutral and ion-molecule reactions, remain to be indirect. We have designed and constructed an apparatus which enables us to determine the state-selected ion-molecule reaction cross sections directly.

This apparatus, which utilizes the threshold electron-secondary ion coincidence (TESICO), is shown schematically in Figure 1. Vacuum ultraviolet radiation from a helium Hopfield continuum source (L.S.), dispersed by an 1 m Seya-Namioka monochromator (M), ionizes the sample gas A in the ionization chamber (I) to produce primary (reactant) ions A^+ and electrons. The ions and photoelectrons are repelled out of the ionization chamber to directions opposite to each other. A hemispherical electron energy analizer (E.A.), together with the straight section between I and E.A. (which serves as a steradiancy analyzer), selects the threshold electrons from electrons with kinetic energies and registers them to a channeltron. The ions, on the other hand, are formed into a beam of a desired velocity and led into the reaction chamber (R), where they react with the second sample gas B. The secondary (product) ions C^+ produced, together with unreacted primary ions, are extracted from the chamber to the forward direction, mass-analyzed by a quadrupole mass spectrometer (Q), and detected by a second channeltron. These ion signals are then counted in coincidence with the threshold electron signals. The whole system is pumped by a six-stage differential pumping system, keeping each section at an appropriate pressure.

When the wavelength of the incident radiation corresponds to the threshold energy of the ith internal state of the A^+ ion (A^+ (i)), the ions produced are A^+(i),
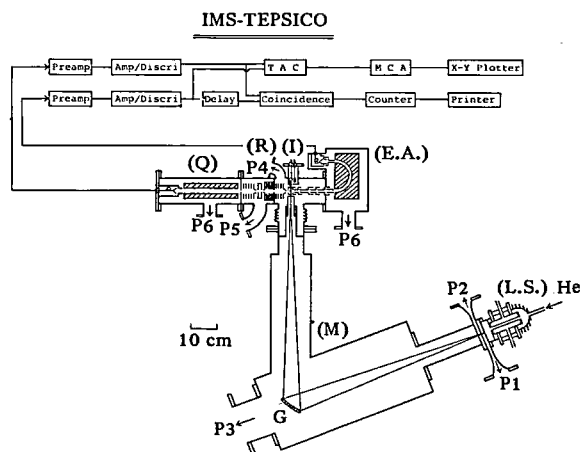
IMS-TEPSICO

Figure 1. Schematic diagram of the IMS-TEPSICO apparatus.
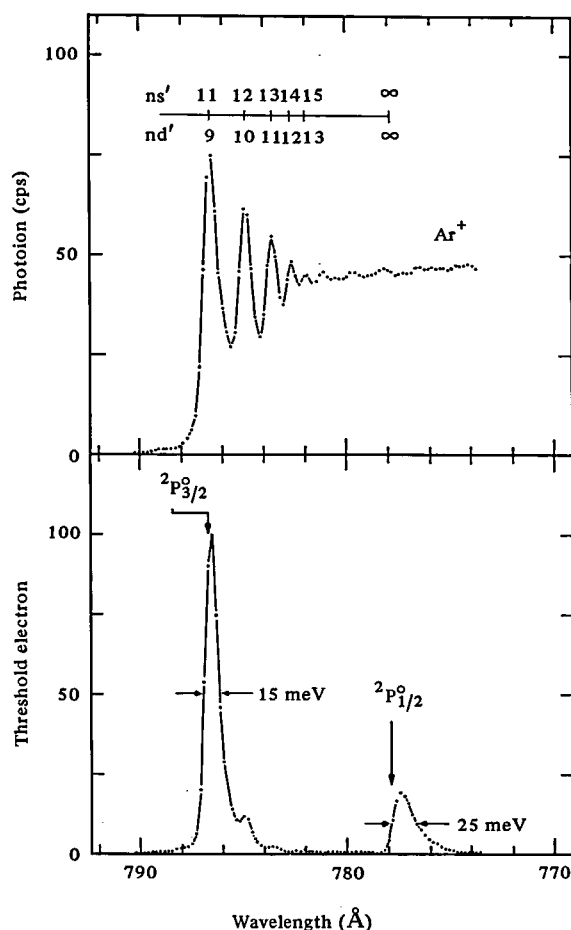
Figure 2. Photoionization efficiency curve (top) and threshold electron spectrum (bottom) of Ar obtained with a resolution bandwidth of 0.52 Å (FWHM). Known spectroscopic term positions are indicated above the spectra.

A^+(i−1), - - - - -, A^+(0), among which only A^+(i) gives threshold electrons. Thus, although all of the above ions react with B to produce C^+, we can observe the reactions of A^+(i) selectively by measuring C^+ in coincidence with threshold electrons. The first application of this technique to the study of ion-molecule reactions is described in Section IV-E-2.

In Figure 2, shown are a photoionization efficiency curve and a threshold electron spectrum of Ar, just to give a brief idea of the performance of the apparatus. Both spectra were taken at 10^{-3} torr of the sample pressure and with 0.52 Å (FWHM) bandwidth of the incident radiation. Under these conditions, the count rates of ions and threshold electrons indicated on the ordinate were obtianed with a mass spectral resolution of about 350. The resolution of the threshold electron analyzer (FWHM) is indicated in the figure. These data indicated the feasibility of the coincident measurements.

IV-E-2 Vibrational Energy Dependence of the Cross Section of the Reaction $H_2^+ + H_2 \rightarrow H_3^+ + H$

Inosuke KOYANO and Kenichiro TANAKA

The Threshold Electron-Secondary Ion Coincidence technique described in the preceeding section was first applied to the study of the vibrational energy dependence of the cross section of the reaction

$$H_2^+ + H_2 \rightarrow H_3^+ + H . \tag{1}$$
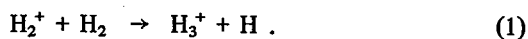
Results obtained for an average collision energy of 0.38 eV (LAB) are shown in Figure 1, where the numbers of coincidence counts are plotted vs the delay time between the electron and the ion signals for four incident wavelengths indicated (corresponding to the $v = 0 - 3$ peaks of our threshold electron spectrum). Sample pressure was kept constant throughout the experiment using an automatic pressure controller. It may be noted that the total accumulation times T (shown in the figure) required to obtain the same S/N ratios are quite different for different wavelengths.

Two peaks clearly appear at delay times corresponding to the times-of-flight (TOF) of the H_2^+ and H_3^+ ions from the ionization chamber to the detector (the electron TOF can be neglected compared with the ion TOF). Of course, ions of only one m/e are collected

at a time when a quadrupole mass spectrometer is used. The two-ion TOF spectra in Figure 1 were obtained by repetitively switching, during the accumulation time, the rf voltage of the quadrupoles on the values corresponding to the H_2^+ and H_3^+ ions. This was accomplished by the use of a mass programmer, with the residence time on each mass position being 1 second each time.

The relative reaction cross sections σ (v) for the vibrational states $v = 0 - 3$ were obtained from the figure by dividing the area of the H_3^+ peak by the sum of the areas of the H_2^+ and H_3^+ peaks in each spectrum. Results are shown in Figure 2 (upper curve). It is clearly seen that the cross section of reaction (1) at this low translational energy decreases with an increasing vibrational energy from $v = 0$ to 3.

Coincidence spectra similar to those in Figure 1 were also obtained at the average translational energy of 1.66 eV (LAB). At this energy, even longer accumulation times were necessary because of the lower reaction cross sections. The relative cross sections obtained are also shown in Figure 2 (lower curve). Comparing two curves, it can be seen that a substantial change in the vibrational energy dependence of the cross section has occurred in going from 0.38 eV to 1.66 eV of translational energy; the cross sections are much less steeply decreasing or almost constant at the latter energy. The vibrational energy dependence, at both energies, is in good agreement with the result of Chupka et al.[1] who utilized the vibrational autoionization to prepare the
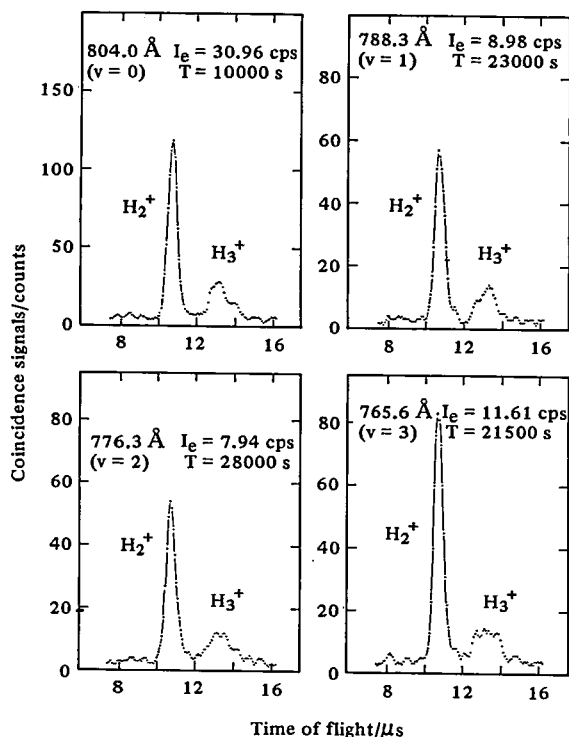
Figure 1. Signals of the primary and secondary ions of the reaction $H_2^+ + H_2 \rightarrow H_3^+ + H$ taken in coincidence with threshold electrons at four wavelengths indicated. I_e and T represent the threshold electron count rate and data accumulation time, respectively.
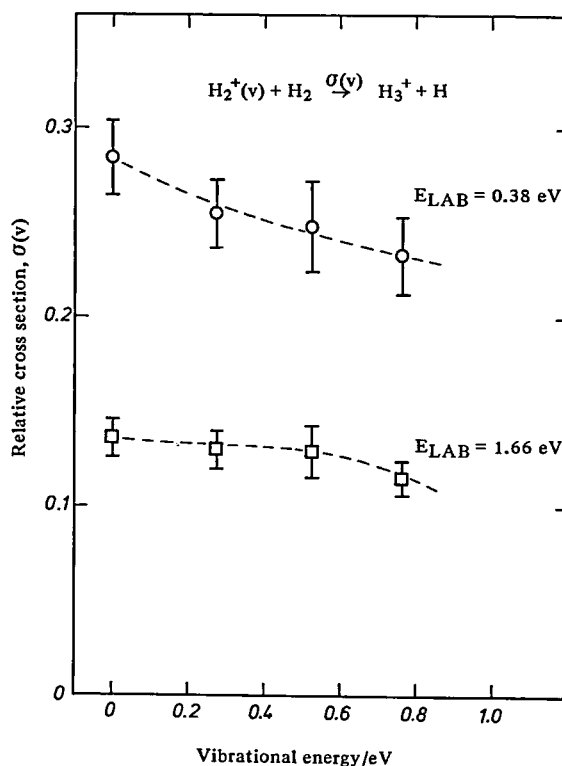

Figure 2. Vibrational energy dependence of the cross section for the reaction $H_2^+ + H_2 \rightarrow H_3^+ + H$ at two different collision energies.

reactant H_2^+ ions in specific vibrational states.

The decrease in the reaction cross section with an increasing vibrational energy at the low collision energy would suggest that the reaction proceeds via an intermediate complex at this energy, since the probability of decay back of the intermediate complex (if exists) to the reactants is expected to increase with the vibrational energy, thus decreasing the probability of the

forward decay (product channel). A theoretical investigation of the H_4^+ intermediate is in progress in collaboration with the group of the Division of Theoretical Studies.

Reference

1) W. A. Chupka, M. E Russell, and K. Refaey, *J. Chem. Phys.*, 48, 1518 (1968).

IV-F Photoionization Processes in Small Molecules

Two techniques have generally been used for the study of molecular photoionization processes, i.e., measurements of photoionization efficiency curves and photoelectron spectra. While photoionization efficiency curves yield valuable information on the ionization processes and energy levels of ions and neutral molecules, a difficulty is often encountered with this technique when autoionization obscures the step structure of the curve. This is especially so with simple molecules, such as diatomic molecules, in which autoionization predominates near the first ionization threshold. The photoelectron spectroscopy is thus essential in determining precise locations of ionic states and the transition probabilities to these states. In addition, the photoelectron spectroscopy provides a deeper insight into the ionization mechanism through such measurements as the angular distribution or the wavelength dependence of electron energy distribution.

Thus for a complete study of photoionization process it is necessary to have an apparatus which allows measurements of both photoions and photoelectrons. We have constructed such an apparatus and are carrying out an extensive study of photoionization processes in small molecules. In particular, measurement of threshold electron spectra is possible with this apparatus.

IV-F-1 Photoionization Efficiency Curve and Threshold Electron Spectrum of N_2 in the 800 — 650 Å Region

Kenichiro TANAKA and Inosuke KOYANO

The absorption spectra, photoelectron spectra, and photoionization efficiency (PIE) curves of N_2 have been studied by a number of investigators. Recently, Chutjian and Ajello[1] reported for the first time the threshold electron spectrum (TES) of N_2, together with a PIE curve, obtained by the technique of threshold electron attachment to SF_6 followed by the detection of the SF_6^-. More recently, Peatman et al.[2] reported the TES of N_2 together with the absorption spectrum obtained using the synchrotron radiation. The results and interpretations of the two TES measurements are in slight disagreement with each other.

Here we present a PIE curve and a TES of N_2 measured with our photoionization apparatus and compare them with these previous results. The apparatus used is the same as described in Section IV - E - 1. It consists of a helium Hopfield continuum light source, an 1 - m Seya - Namioka monochromator (bandwidth: 0.52 Å FWHM), a quadrupole mass filter, and a threshold electron analyzer (resolution: 25 meV FWHM). Mass-analyzed photoions and threshold photoelectrons were measured simultaneously using a dual counting system. By scanning the wavelength of the incident photons continuously at a rate of 0.5 Å/min, the numbers of counts of both signals obtained during every

20 seconds were recorded.

The TES and PIE curve of N_2 in the 800 - 650 Å wavelength region are shown in Figure 1, where the threshold electron and photoion signal intensities, normalized to the transmitted photon intensity, are plotted against the wavelength. Also indicated in Figure 1 are the locations of vibrational levels in the $X^2\Sigma_g^+$, $A^2\Pi_u$, and $B^2\Sigma_u^+$ states of N_2^+ and of Rydberg states converging to several vibrational levels in the $A^2\Pi_u$ and $B^2\Sigma_u^+$ states of N_2^+, which were taken from the spectroscopic data.[3] The general structure of the PIE curve is similar to that of the absorption curve reported by Huffman et al.[4] and the PIE curve of Cook et al.[5] When both curves are compared quantitatively, however, an interesting feature is revealed; the ratio of the PIE intensity to the absorption coefficient varies considerably from wavelength to wavelength. Especially, the ratio is reduced by a factor of two at some autoionizing peaks, e.g., at 789.4, 778.7, 771.7, 761.3, and 757.1 Å. This is not unexpected since molecules excited to autoionizing states generally undergo two major competing processes, autoionization and predissociation, and the ionization yields at autoionization peaks are largely dependent on the relative rates of these processes. Thus the detailed analysis of these ratio is expected to yield an information on the predissociation of autoionizing states.

The shape of the TES in Figure 1 (b) is in fairly good agreement with that of the high resolution TES reported by Peatman et al.[2] In both TESs, the threshold electron peaks corresponding to the higher vibrational members ($v' \geq 2$) of the $X^2\Sigma_g^+$ state, which
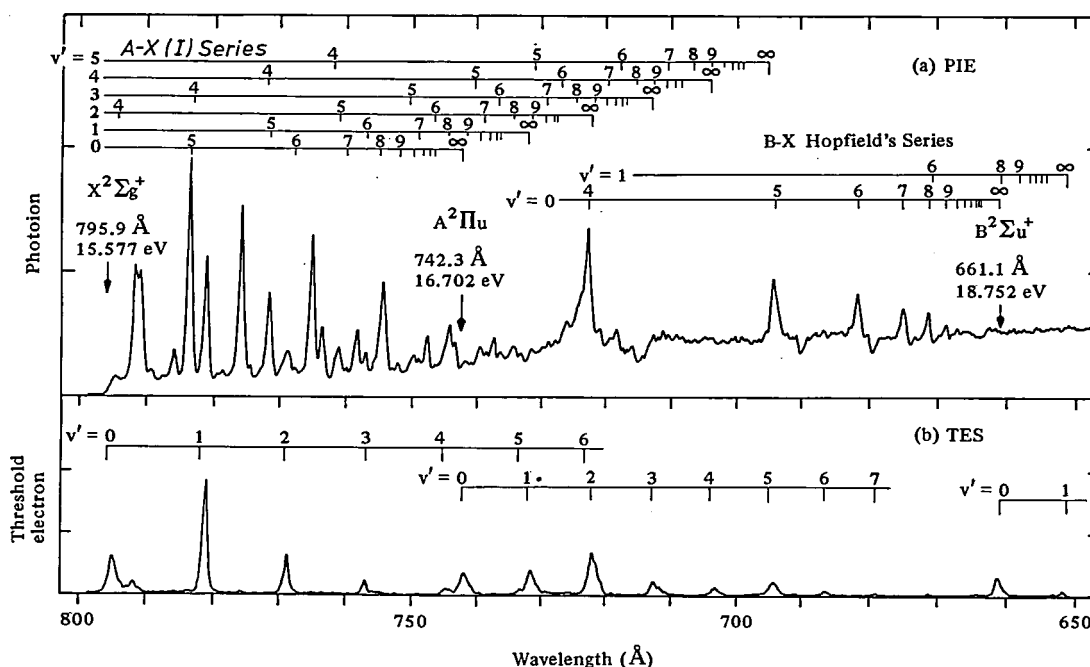
Figure 1. (a) PIE curve of N_2. Identified Rydberg series are shown above the curve. (b) TES of N_2 together with their identification. Bandwidth of the monochromatic radiation in each spectrum is 0.52 Å (FWHM).

have not been observed in He I photoelectron spectra, are observed at positions predicted by spectroscopic data. The detailed positions and intensity distributions in the two TESs are, however, in a significant disagreement with each other. In this connection, it should be emphasized that the observed position and intensity of a threshold electron peak are strongly dependent on the bandwidth of the incident radiation and the resolution of the threshold electron analyzer. When an autoionization state is lying just above the threshold for a certain vibrational state of the ion, the electrons ejected when this state autoionize to the nearby ionic state have a very small kinetic energy and often can not be discriminated by the threshold electron analyzer with a finite resolution. A small peak appearing just above

the $v' = 0$ peak and the major part of the highest peak at $v' = 1$ of the $X^2\Sigma_g^+$ state in Figure 1 (b) seem to be due to such an autoionization. Thus a special care is needed to interprete TES correctly, even when the measurement is carried out with a very high resolution technique.

References

1) A. Chutjian and J. M. Ajello, *J. Chem. Phys.*, **66**, 4544 (1977).
2) W. B. Peatman, B. Gotchev, P. Gürtler, E. E. Koch, and V. Saile, DESY SR-78/01 Feb. 1978.
3) A. Lofthus and P. H. Krupenie, *J. Phys. Chem. Ref. Data*, **6**, 113 (1977).
4) R. E. Huffman, Y. Tanaka, and J. C. Larrabee, *J. Chem. Phys.*, **39**, 910 (1963).
5) G. R. Cook and P. M. Metzger, *J. Chem. Phys.*, **41**, 321 (1964).

IV-G Studies of Formation and Destruction Mechanisms of Interstellar Molecules

Recent discoveries of a large variety of molecules, including complex organic compounds, in interstellar space of our galaxy stimulated not only astrophysicists but also chemists to wonder and investigate how these molecules were formed under the physical conditions prevailing in interstellar space. Among several mechanisms which have been proposed, the gas phase and grain surface molecular synthesis models are most intriguing to chemists. The only promising gas phase models are those involving ion-molecule reactions, since rates of most neutral reactions are not sufficiently large at interstellar temperatures because of activation energies required.

We are carrying out non-steady-state calculations of the abundance of these molecules based on an ion-molecule reaction model. Included in these calculations are 72 molecular species and 202 relevant reactions. Emphasis is placed on the extension of previous calculations to include molecules with more than five atoms and to predict abundance of molecules which have not yet been detected because of the lack of the dipole moment.

IV-G-1 Molecular Evolution in Dense Interstellar Clouds by Ion-Molecule Reactions

Inosuke KOYANO, Kenichiro TANAKA, and Hideo YAMAZAKI (Tokyo Institute of Technology)

As stated in the introductory section, io. -molecule reactions are essential in formulating a gas-phase molecular synthesis model for molecular formation in dense interstellar clouds. Although there have been several proposals of ion-molecule reaction models and extensive calculations based on them,[1~5] some utilized the steady-state approximation to calculate abundances of various species and some were quite limited in the numbers of molecular species and reactions considered. So far, molecules with more than five atoms have not been included in the calculation.

We are studying the chemical evolution of dense $(10^4 - 10^6 cm^{-3})$ molecular clouds based on an ion-molecule reaction model which involves 72 chemical species with up to eight atoms. Coupled differential equations were solved numerically for up to 10^{14} seconds which is comparable to the lifetime of interstellar clouds of gas density $10^4 - 10^6 cm^{-3}$.

A feature of our model is the inclusion of molecules which have not yet been detected in interstellar clouds because of the lack of the dipole moment but are undoubtedly believed to exist, such as CH_4 and C_2H_2. The molecule with the highest number of atoms included in the model is $C_3H_5^+$, and seven- and six-atom molecules included are C_3H_4, $C_2H_5^+$, C_2H_4, $CH_2NH_2^+$, CH_3CO^+, and CH_5^+.

A careful examination was made on the large number of chemical reactions which are likely to be relevant to the formation and destruction of these 72 species, and a set of 202 reactions, involving ion-molecule reactions, atom-radical reactions, and ion-electron recombination reactions, was adopted. Experimental rate constants were critically chosen from the literature as long as such are available. When there is no experimental determination, calculated rate constants by the Langevin and the ADO theories were used with appropriate branching ratios.

A part of our reaction scheme which is pertinent to the formation of acetylene is shown in Figure 1. Destruction reactions for each species are of course included in the whole scheme but are omitted in the

Formation of Interstellar Acetylene

$C^+ + CH_2 \rightarrow C_2H^+ + H$
$\quad\quad CH_3 \quad\quad\quad\quad H_2$

$C_2H^+ + H_2 \rightarrow C_2H_2^+ + H$
$C^+ + CH_4 \rightarrow C_2H_2^+ + H_2$

$C_2H_2^+ + H_2 \rightarrow C_2H_3^+ + H$
$C^+ + CH_4 \rightarrow C_2H_3^+ + H$

$C_2H_3^+ + e \rightarrow C_2H_2 + H$
$C_2H_3^+ + M \rightarrow C_2H_2 + MH^+$

$M = NH_3, H_2O, HCN, H_2CO$
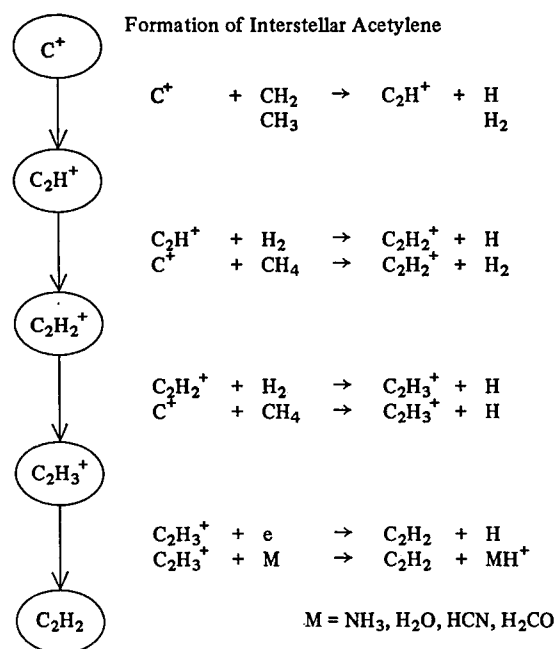
Figure 1. Chemical reaction scheme relevant to the formation of neutral acetylene.

Table I. Initial Conditions

H_2	1×10^5	cm^{-3}
He	2.8×10^4	
CO	75	
N	15.7	
O	11.7	
N_2	0.87	
O_2	0.65	
ζ^a	10^{-17}	s^{-1}

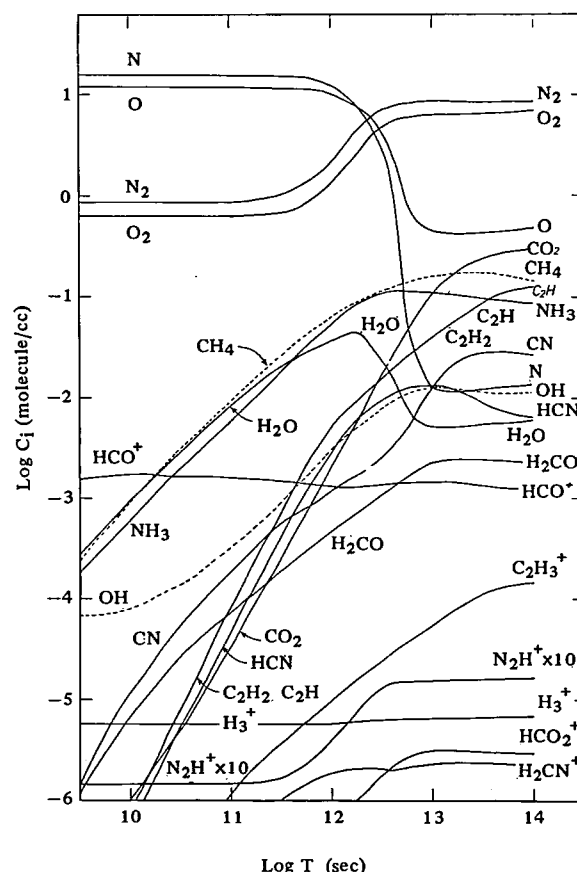[a] ζ is the ionization rate of H_2 and He by cosmic ray.

Figure 2. Chemical evolution of a dense molecular cloud characterized by the initial conditions shown in Table I. Only some representative neutral and ionic species are shown.

figure for simplicity. Among the reactions shown in the figure, the reaction $C_2H_2^+ + H_2 \rightarrow C_2H_3^+ + H$ is almost thermoneutral and has a rate constant as low as $3 \times 10^{-13} cm^3 \cdot sec^{-1}$, but is still considered to be important because of the high density of hydrogen.

Results of the calculation are shown in Figure 2 for some representative ionic and neutral species. Initial conditions used are listed in Table I. It can be seen that for almost all neutral species the chemical equilibrium time scale is about 10^{13} sec or 10^6 yr, while for most ionic species it is much shorter ($\lesssim 10^9$ sec). While equilibrium abundances of some polar molecules such as, H_2CO, NH_3, and HCN are in reasonable agreement with those observed in typical molecular clouds, it is predicted that unobserved species such as CH_4 and C_2H_2 should exist in those clouds in even higher densities than HCN or NH_3.

References

1) E. Herbst and W. Klemperer, *Astrophys. J.*, **185**, 505 (1973).
2) H. Suzuki, S. Miki, K. Sato, M. Kiguchi, and Y. Nakagawa, *Prog. Theor. Phys.*, **56**, 1111 (1976).
3) E. Iglesias, *Astrophys. J.*, **218**, 697 (1977).
4) W. D. Watson, *Astrophys. J.*, **188**, 35 (1974).
5) M. Oppenheimer and A. Dalgano, *Astrophys. J.*, **187**, 231 (1974); A. Dalgano, T. de Jong, M. Oppenheimer, and J. H. Black, *ibid.*, **192**, L37 (1974); J. Turner and A. Dalgano, *ibid.*, **213**, 386 (1977).

IV-H Effect of Vibrational Energy Transfer and Reactant Vibrational Excitation on the Cross Section of the Vapor-Phase Chemical Reaction

It has been known recently that the excitation of the reactant vibrational-rotational state by a strong infrared laser beam leads in some cases to an appreciable enhancement of the chemical reaction cross section. The purpose of this project is to develop a strong tunable infrared light source and to study the detailed mechanisms of the enhancement. The vibrational-rotational energy transfer must also play an important role during the process. As a final goal of the project, we hope to find and develop a means of controlling chemical reactions.

IV-H-1 Development of Strong, Tunable Infrared Light Source

Ichiro HANAZAKI *(Osaka Univ. and IMS)*

(See Special Research Project I-1-b)

IV-H-2 Vibrational Energy Transfer in Gaseous Molecules

Ichiro HANAZAKI *(Osaka Univ. and IMS)*

A number of studies have been performed on the vibrational energy transfer of the gaseous molecules. In most of the studies, however, the wavelengths of the excitation are restricted by the availability of the infrared laser source (a CO_2 laser has been used in most cases). With a tunable infrared laser it seems possible to excite any desired vibrational transition. This means that the energy transfer cross section from any vibrational state can be studied with a direct excitation to the desired excited state. Hence a rapid V-V transfer process from any vibrationally excited state is expected to be observed. The infrared laser mentioned above has a high output power and is tunable from the mid infrared down to the near infrared region. This might make it possible to excite highly excited vibrational states directly, providing a possibility to study the energy transfer among highly excited states. It would provide a useful knowledge about the vibrational excitation leading to the bond cleavage.

IV-H-3 Effect of the Vibrational Excitation on the Chemical Reaction Rate

Ichiro HANAZAKI *(Osaka Univ. and IMS)*

In some elementary reaction systems, it has been known that the vibrational excitation of the reactant molecule enhances the reaction rate appreciably. In the other cases, however, the effect is not observed. Although the reason for the difference has partly been understood, the mechanism of the effect has not been clear especially for larger molecules. The purpose of the present study is to examine the effect of the excitation of various vibrational states on the reaction cross section. As an example, we are planning to study the system:

$$R - H + Cl \rightarrow R + HCl.$$

The nanosecond pulse of the third harmonics of the Nd:YAG laser produces Cl atom instantaneously from Cl_2. At the same time, tunable infrared output of the optical parametric oscillator excites one of the vibrational modes of the R-H molecule. By monitoring the emission from the product (HCl) or absorption, with and without the infrared light, one can obtain an information about the effect of the vibrational excitation on the reaction cross section.

IV-I Chemistry and Physics of Intercalation Compounds of Graphite

Mizuka SANO *(Univ. of Electro-Communications and IMS)*, Ikuji TSUJIKAWA *(Kyoto Univ. and IMS)*, Kentaro O-HASHI *(Kyoto College of Pharmacy)*, and Hiroo INO-KUCHI

Metallic solids are known to be synthesized by the intercalation of suitable species between the hexagon sheets of carbon atoms in graphite. The addition of third component to the metallic solids thus obtained is expected to form what is called mixed valency, which shows a wide diversity of electronic characteristics, such as superconductivity. Electronic properties of these ternary compounds are being studied in relation to their electronic sturctures by the measurements of the conductivity, the magnetic susceptibility, NMR, and the Raman scattering.

RESEARCH ACTIVITIES

V. Division of Applied Molecular Science

The division has two research objectives. It aims at developing the new findings and methodologies in molecular science to be adapted for researches in the adjoining fields of science. At the same time, new materials and reactions of interest to theoreticians, spectroscopists and solid state physicists have to be introduced.

The division is made up of two laboratories, Applied Molecular Sciences I and II. The Applied Molecular Science I Laboratory is only one year old and the researches being carried out are yet more or less continuation of the works performed by the staff members when they were in the previous affiliations.

Physical organic chemistry is one of the main themes of this laboratory. Syntheses of molecules of theoretical interest, photochemistry of aromatic compounds, and dynamical studies by multi-nuclear nmr are typical examples. Chemistry of coordination compounds is another subject of this laboratory. The determination not only of the location of atoms in coordination compounds but also of the electron density distribution by the X-ray crystallographic study is being carried out.

V-A Syntheses and Physico-chemical Properties of Bridged Aromatic Compounds

We are interested in elucidating the structural and electronic factors necessary and sufficient for development of particular solid state physical properties such as photoconductivity and superconductivity in order to design such properties at molecular levels. One of possible approaches is to simulate the crystal and electronic structures of the known compounds which exhibit such properties. Attempts are being made of the syntheses of a series of compounds which incorporate aromatic rings in the three dimensional framework.

Triptycene and cyclophane derivatives made of the donor and acceptor rings are a couple of the examples. We have come across an intramolecular triptycene quinhydrone which exhibits an interesting charge-transfer and electrochemical behavior. Excited state chemistry of triptycenes has been studied and unique structural features of the triptycene skeleton have been analyzed.

V-A-1 9,10-Dihydro-9,10[1′,2′]-benzenoanthracene-5,8-diol-1,4-dione. An Intramolecular Triptycene Quinhydrone

Hiizu IWAMURA (Univ. of Tokyo and IMS) and Katsumi MAKINO (Univ. of Tokyo)

The title compound 1 has now been prepared to disclose the strength and mechanism of the transannular interaction between the π-donor and acceptor groups incorporated into the apparently unfavorable triptycene framework.

The Diels-Alder reaction of 1,4-dimethoxyanthracene with p-benzoquinone gave the 9,10-adduct in 86 % yield. Isomerization to dimethoxyhydroquinone 2, m.p. > 200°C (decomp.), took place quantitatively on treatment with KOH in aq. dioxan. Oxidation with Ag_2O in acetone gave dimethoxyquinone 3 which was then treated with ceric ammonium nitrate to effect oxidative demethylation. Bisquinone 4 thus obtained in 85 % yield was hydrogenated over Pd/C to give bishydroquinone 5. Partial oxidation of the latter with the cal-

culated ammount of DDQ gave the intramolecular quinhydrone 1 as black violet crystalline solid: m.p. >250°C; nmr (DMSO-d_6) δ 6.01(s, 2H), 6.33(s, 2H), 6.70(s, 2H), 6.9–7.1(m, 2H), 7.3–7.5(m, 2H) and 8.99 (s, 2H). Most intriguing was the spontaneous formation of 1 when the acetone solutions of 4 and 5 in an equimolar amount were mixed and warmed briefly.

Quinhydrone 1 is slightly dissociated into 4 and 5 in DMSO and its enthalpy of formation from 4 and 5 is 2.3 kcal/mol. The charge-transfer band of 1 has the maximum at 430 nm (ϵ_{max} 425) in DMSO, extending as far as to 550 nm and is almost comparable to that of quinhydrone itself (λ_{max} 440 nm; ϵ_{max} 890 in 0.05 M HCl). Note also 3: λ_{max} 411 nm; ϵ_{max} 450 in CH_3CN vs. p-benzoquinone – 1,4-dimethoxybenzene: λ_{max} 413 nm; ϵ_{max} 370 in cyclohexane.

The first and second half-wave potentials of 4 in DMF with n-$Bu_4N^+ClO_4^-$ as a supporting electrolyte are −0.23 and −0.48 V with respect to SCE, respectively. One can conclude that the second quinonoid ring in 4 has the electron-attracting effect on the electrolytic reduction of the first quinonoid ring and that the intermediate semiquinone ring has the electron-donating effect on the reduction of the remaining quinone ring.

All the results clearly indicate that the electron

donor-acceptor interaction between the hydroquinone and p-benzoquinone chromophores incorporated in the apparently unfavorable triptycene skeleton is almost as strong as that of genuine quinhydrone, namely, the complex of the free component molecules. We propose a through-bond homoconjugative interaction between the donor and acceptor rings, since a simple through-space interaction between the rings held at 120° to each other cannot be strong enough to explain the observed strong interaction.

Effects of geometry and conformation on the charge transfer and exciplex interactions have been the subject of extensive studies. Efforts have so far been directed towards the design of most favorable situations. A series of [2.2]-paracyclophane quinhydrones by Staab, et al.[1] are one of the most successful examples. Our work presented here offers the other extreme case. The π-donor and acceptor rings are apparently under unfavorable circumstances, and yet show a surprisingly strong interaction.

1 R = H
3 R = CH₃

2 R = CH₃
5 R = H

4
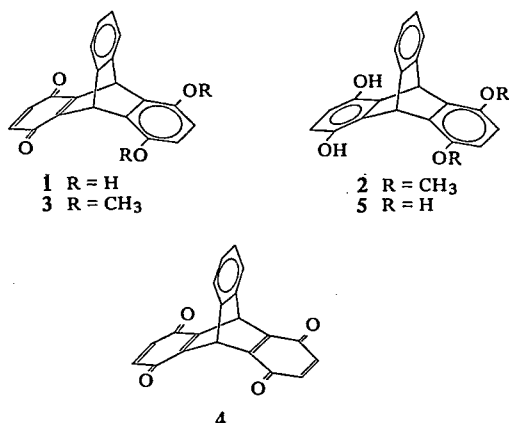
A JEOL D-300 GC-Mass spectrometer newly installed in Chemical Materials Center was instrumental in determining the elemental composition of all the new compounds prepared in this work.

Reference

1) W. Rebafka and H. A. Staab, Angew. Chem., Internat. Ed., 12, 776 (1973); 13, 203 (1974).

V-A-2 The "Wittig Rearrangement" of α-Alkoxycarbenes Formed by Photorearrangement of 1-Alkoxytriptycenes

Hiizu IWAMURA and Hideyuki TUKADA (Univ. of Tokyo)

Photochemistry of triptycenes has a number of unique features. First of all, it is a typical example of deviation from the di-π-methane mechanism through which photochemistry of the lower benzologs, i.e., barrelene, benzobarrelene, and dibenzobarrelene takes place.[1] Only a limited number of examples for the non-di-π-methane rearrangement has yet been documented, and elucidation of the mechanism itself claims the merit of further studies. Another facet of triptycene photochemistry is its unambiguous generation of arylcarbene species under chemically mild conditions.

When a 1–5 mM solution of 1-alkoxytriptycenes **1** in an alcohol was irradiated for 1.5 hr with a Vycor filtered Hg source, a smooth conversion to the corresponding acetals **2** was achieved. The intermediary formation of alkoxycarbenes **3** followed by OH insertion is thus confirmed. In inert solvents, the reactions are just as efficient as in alcohols. The photoproducts isolated in good yield (Table 1) were, however, not the expected norcaradienes **5**. Aldehyde **4a** was obtained almost exclusively from 1-methoxytriptycene **1b**. The corresponding ketones **4d-4g** were the main photoproducts from 1-allyloxy- and 1-benzyloxytriptycenes **1d-1g**. 1-Phenoxytriptycene **1h** formed the exception to the foregoing reaction pattern; benz[a]aceanthrylene **7** together with diphenylacetal **2** (R = R' = Ph) were obtained.

These reactions in inert solvents are rationalized as the homolysis and rearrangement of α-alkoxytriptycenes **3**. Aldehyde **4a** appears to be formed by the homolysis of the O-CH₃ bond to give the acyl radical followed by abstraction of a hydrogen atom from solvent molecules. The migratory aptitude of the alkyl groups in the above reactions is very reminiscent of the Wittig rearrangement of α-metallated ethers.[3] Thus various allyl and benzyl groups migrate, but the simple alkyl and aryl groups are reluctant to the [1, 2] shift in consonant with the diminishing ease of ordinary nucleophilic substitution on group R. Reduced electrophilic reactivity of the α-alkoxycarbenes as predicted by a canonical structure Ar-C⁻=O⁺-R of the resonance hybrid is considered to be responsible for the occurrence of the Wittig type rearrangement in these carbenes **3** which otherwise might have been intercepted internally by the double bond of the aromatic ring to give normal photoisomers **5**.
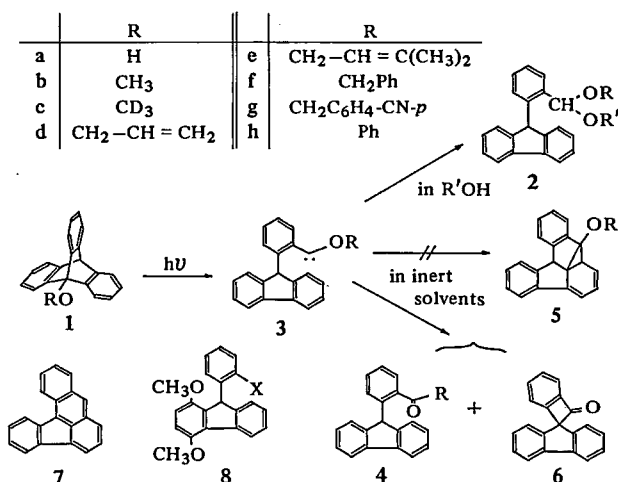
	R			R
a	H	e		CH₂-CH = C(CH₃)₂
b	CH₃	f		CH₂Ph
c	CD₃	g		CH₂C₆H₄-CN-p
d	CH₂-CH = CH₂	h		Ph

Table 1. Photoproducts of 1-Alkoxytriptycenes

Triptycene	Solvent and/or additive	Photoproducts isolated yields (%)^a
1b	CH$_3$OH	2 (R = R$'$ = CH$_3$) 62
1b	t-C$_4$H$_9$OH	2 (R = CH$_3$, R$'$ = t-C$_4$H$_9$) 43^a
1b	cyclohexane	4a 73; 6 ≤5; 4b^c
1b	cyclohexane + dimethyl fumarate^d	4a 98
1c	cyclohexane	4a 73; 6 ≤5; 4b^c
1d	n-pentane	4d 62; 4a 4; 6^c
1e	n-pentane	4e 78; 4a 15; 6^c
1f	CH$_3$OH	2 (R = CH$_2$Ph, R$'$ = CH$_3$) 29^b
1f	n-pentane	4f 66; 4a^c; 6^c
1g	n-pentane	4g 36; 6 16; 4a^c
1h	cyclohexane	7 31; 2 (R = R$'$ = Ph) 29; 4a ≃ 1
1,2,5-(OCH$_3$)$_3$	CH$_3$OH	8 (X = CH(OCH$_3$)$_2$) 29; 8(X = CO$_2$CH$_3$) 41
1,2,5-(OCH$_3$)$_3$	n-pentane + ether	8 (X = CHO) 30^b

^{a} By layer chromatography on silica gel. ^{b} Although the isolated yield was not necessarily high, no significant n.m.r. signal left unidentified. ^{c} Not detected. ^{d} 35 mM in added dimethyl fumarate.

We conclude that, in contrast to alkylcarbenes in which the hydrogen atom or a group aligned with the vacant pπ-orbital of the ambident carbene center migrates preferentially to give olefins and thus the [1, 2] shifts have the character of the Wagner-Meerwein rearrangement,[4] the migration in alkoxycarbenes resembles the Wittig rearrangement.

References

1) S. S. Hixon, P. S. Mariano, and H. E. Zimmerman, Chem. Rev., 73, 531 (1973).
2) H. Iwamura and K. Yoshimura, J. Am. Chem. Soc., 96, 2652 (1974).
3) T. S. Stevens in "Progress in Organic Chemistry", vol. 7, J. Cook and W. Carruthers, Ed., Butterworths, London, 1968. p.48.
4) R. Hoffmann, G. D. Zeiss, and G. W. Van Dine, J. Am. Chem. Soc., 90, 1485 (1968); H. E. Zimmerman, Accounts Chem. Res., 5, 393 (1972); A. Nickon, F. Huang, R. Weglein, K. Matsuo, and H. Yogi, J. Am. Chem. Soc., 96, 5264 (1974).

V-A-3 The Unique Structural Features of the Triptycene Molecules. The CNDO/2 MO, ^{13}C NMR, and Photoelectron Spectral Studies of Parent Triptycene

Hiizu IWAMURA and Tadashi SUGAWARA

Triptycene is a unique molecule in a number of spectroscopic, structural and chemical aspects and thus has been the subject of active studies in physical organic chemistry, since it was first prepared by Bartlett et al. almost four decades ago.[1] The molecule is characterized by the presence of three benzene rings tightly held together at 120° angles to each other by two tetrahedral carbon atoms so that no conjugative interaction between the benzene rings may be possible.

Bond hybridization of the carbon atomic orbitals at the bridgehead of triptycene has now been shown by the CNDO/2 MO calculations to be unsymmetric in that the exocyclic bond is sp$^{2.5}$ and the endocyclic bonds are sp$^{3.2}$ hybridized. The latter orbitals are energetically high-lying and mix thoroughly with π-orbitals to effect through-bond homoconjugative interaction between the benzene rings. The one-bond ^{13}C-H coupling at the bridgehead is 141.5 Hz and is consistent with the theoretical bond hybridization. Not only the proton shift[2] but also ^{13}C shift due to the bridgehead appear at the higher field than the methine group of triphenylmethane. The orbital interactions as above have been confirmed by the unexpectedly low ionization potential of 7.84 eV as revealed by the He I photoelectron spectrum.

Structural features disclosed by the X-ray crystallographic analyses, the presence of an extremely high (40 - 50 kcal/mol) barrier to rotation around the bond extending out of the bridgehead[3] the chemical reactivity, and spectral data have been interpreted consistently in terms of the unsymmetrical hybridization at the bridgehead and the through-bond π-interaction between the benzene rings.
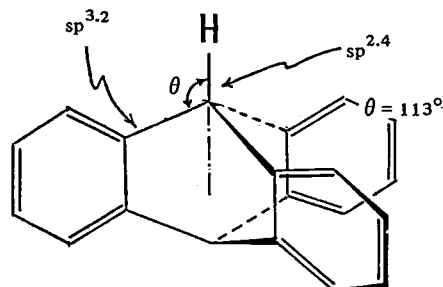
References

1) P. D. Bartlett, M. J. Ryan, and S. G. Cohen, J. Am. Chem. Soc., 64, 2649 (1942).
2) W. B. Smith and B. A. Shoulders, J. Phys. Chem., 69, 2022 (1965); K. G. Kidd, G. Kotowycz, and T. Schaefer, Can. J. Chem., 45, 2155 (1967).
3) H. Iwamura, J. Chem. Soc., Chem. Comm., 232 (1973); L. H. Schwartz, C. Koukotas, and C. -S. Yu, J. Am. Chem. Soc., 99, 7711 (1977).

V-B Structural and Kinetic Studies by Means of NMR of Other Nuclei

Hiizu IWAMURA, Tadashi SUGAWARA, and Yuzo KAWADA

Recent development in a tunable probehead, a frequency synthesizer, and a broad-band preamplifier made multinuclear nmr experiments easily accessible. Such exotic nuclei as ^{29}Si, ^{77}Se, ^{117,119}Sn, ^{195}Pt, ^{199}Hg, ^{203,205}Tl and ^{207}Pd have nuclear spin of 1/2 and can now be used for the structural study with a high resolution nmr as well as usual ^{1}H, ^{13}C, ^{15}N, ^{19}F and ^{31}P. Although some broadening of resonance lines cannot be avoided due to an efficient spin lattice relaxation by the interaction of nuclear quadrupole moments with the fluctuating electric field gradients, nmr for ^{7}Li, ^{11}B, ^{14}N, ^{17}O and ^{33}S is also promising. Structural analyses of complex organic compounds, the detection of reaction intermediates of organo-metallic and metalloid compounds, and the observation of CIDNP phenomena are being actively carried out by the use of a Varian FT-80A multinuclear spectrometer.

V-C Spin-state Variations among Nickel(II) Complexes Containing Macrocyclic Ligands

Tasuku ITO (Hokkaido Univ. and IMS) and Koshiro TORIUMI (Univ. of Tokyo and IMS)

Nickel(II) ion forms with macrocyclic tetradentate ligands (mac) a number of complexes of the type Ni (mac)X_2, X = an anion or solvent, which either are diamagnetic or have a triplet ground state. Changes from paramagnetism to diamagnetism and vice versa are often brought about by apparently trivial changes in the macrocyclic ligands, anions, and/or solvents. In some cases, the paramagnetic and diamagnetic forms of the same compound can be isolated. We are investigating the behavior of such systems in solution and in solid states with the following techniques: electronic spectral measurements for the solution equilibria; kinetic measurements by a temperature-jump method; calorimetric measurements for the spin-state transitions in solid state; X-ray crystallographic analyses of the isolated complexes.

V-D Electron-density Distribution in Transition Metal Compounds

Yoshihiko SAITO (Univ. of Tokyo and IMS)

The effective charge localized on each atom was estimated by direct integration of the observed electron-density in an appropriate volume allocated for each atom and also by the electron-population analysis. Both methods generally gave consistent results. In Werner complexes such as $[Co(NH_3)_6]^{3+}$ and $[Co(NO_2)_6]^{3-}$, the central metal atom is largely neutralized by donation of electrons from the ligating atoms. For example, the effective charge on the cobalt atom in $[Co(NH_3)_6]^{3+}$ was estimated to be + 0.7(3) e. Thus the positive charge is distributed on the surface atoms of the complex ion. Accordingly Pauling's electroneutrality rule was indeed verified for the transition metal complexes.

The charge distribution around the transition metal atoms placed in the ligand field was found to be aspherical. Such distribution can be reasonably accounted for by the ligand field theory. In fact, the asphericity of the d electron distribution in an octahedral complex was shown to be contrary to that observed for a tetrahedral complex.

A cooling device for crystal specimens set on a four circle diffractometer was constructed as preliminary to the one to be installed in IMS. The crystal specimen was cooled by a flow of the cold nitrogen gas surrounded by a jacket of the dry nitrogen gas at the room temperature, both delivered from an evaporation vessel containing the liquid nitrogen. The transfer tube was made of stainless steel and other metals. The lowest attainable temperature was 90 K.

RESEARCH ACTIVITIES

VI. Computer Center

The research activity at the IMS Computer Center is focused on two projects. One is the development of the JAMOL program system which was designed for molecular orbital calculations of large polyatomic systems. In this project new theoretical methods for the large scale computation are investigated. The JAMOL program will be registered as a library program of the Computer Center.

The other project is the theoretical investigation of metalloporphyrins. Metalloporphyrins are important polyatomic systems because of their roles in biological energy conversion processes.

VI-A Development of JAMOL Program System for Molecular Orbital Calculations

Hiroshi KASHIWAGI, Toshikazu TAKADA*, Fukashi SASAKI*, Shigeru OBARA*, and Eisaku MIYOSHI* (*Hokkaido Univ.)

A program system JAMOL 2[1] was written for LCAO SCF MO calculations with the basis of contracted Gaussian type orbitals (CGTO). Its flowchart is presented in Figure 1. One can use about 200 CGTO's for calculations on closed and open shell electronic states of polyatomic molecules. The input of nuclear coordinates and the symbol of the symmetry will automatically initiate calculations for molecules with C_1, C_s, C_i, C_2, D_2, D_4, C_{2v}, C_{4v}, C_{2h}, D_{2h}, D_{4h}, D_{2d}, and O_h symmetries.

The number of two electron integrals (TEI) required in ab initio MO calculations of large molecules is enormous, as it is proportional to the fourth power of the number of CGTO's. The most difficult problem in the design of a program system is how to calculate efficiently and save effectively these TEI's. The number of CGTO's and TEI's are listed in Table I for $C_{10}H_8$, CoF_6 and Co-porphine as well as the CPU time in JAMOL 2. A great economy is achieved by the ap-

1. Data imput
2. Calc. of symmetry orbitals
   3. Calc. of semiorthogonalized orbitals
4. Calc. of OEI's
5. List of necessary TEI's
6. Calc. of TEI's
7. Transformation of TEI's
8. Construction of supermatrices
9. SCF MO iteration
10. Population analysis
11. Calc. of moments, etc.

OEI: One electron integral
TEI: Two electron integral
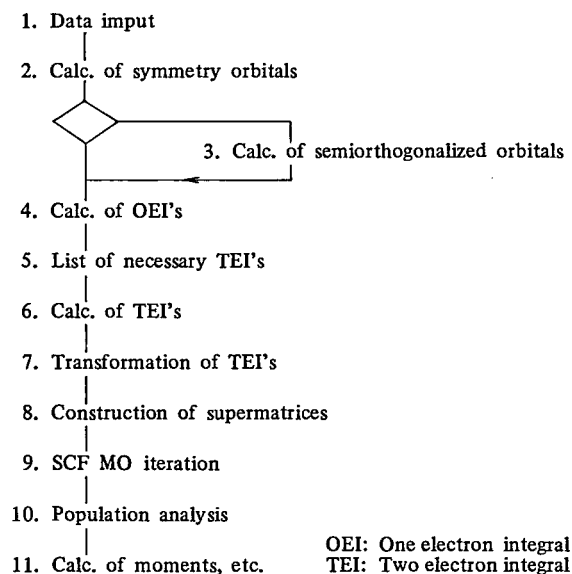
Table I. CPU Time by the Use of JAMOL 2 (FACOM 230–75 Computer)

molecule	$C_{10}H_8$[a]	CoF_6	Co-porphine[a]
number of GTO's	174	186	486
number of CGTO's (N)	58	128	187
number of TEI's ($\sim N^4/8$)	1,464,616	34,084,896	154,501,830
number of independent TEI's	291,484	820,567	10,096,264
number of calculated TEI's	102,600	820,567	2,284,595

step[b]	CPU time (hour)		
1~4	0.09	0.04	0.25
5	0.01	0.61	0.58
6	0.44	0.35	3.93
7	0.06	1.95	5.44
8	0.01	0.06	0.28
9	0.01	0.05	0.20
total	0.62	3.06	10.68

[a] Calculation based on semiorthgonalized orbitals.[3]   [b] See Figure 1.

plication of the group theory. The reduction rates of TEI's as shown in Table I, are roughly proportional to the inverse of the number of symmetry operations. Another method for reducing the number of TEI's is an integral approximation scheme based on semi-orthogonalized orbitals.[2,3] Its effectiveness is also shown in Table I. The error in the total energy of naphthalene with this approximation is only -0.0006 a.u.[3]

We are now developing a new version of the JAMOL program system with the following extensions and improvements.
a) Increasing the limit for the number of CGTO's.
b) Improvement of the semiorthogonalized orbital scheme.[4]
c) Speed-up of the molecular integral calculation.
d) Adoption of a new algorithm for the transformation of TEI's from the CGTO basis to the symmetry orbital basis.[5]

(In our new algorithm the CPU time is proportional to the fourth power of the size of a orbital set, while in the usual method it is proportional to the fifth power.)

The new version which is called JAMOL 3 will enable us to perform the same calculation as in Table I for Co-porphine within two hours. The JAMOL 3 system is expected to be a new powerful tool for molecular orbital calculations of large molecules.

References
1) H. Kashiwagi, T. Takada, E. Miyoshi, and S. Obara, *Library Program Manual of Hokkaido University Computing Center,* No. 1 and No. 2 (1977).
2) H. Kashiwagi, *Int. J. Quantum Chem.,* 10, 135 (1976).
3) H. Kashiwagi and T. Takada, *Int. J. Quantum Chem.,* 12, 449 (1977).
4) Y. Osanai and H. Kashiwagi, to be submitted.
5) T. Takada and F. Sasaki, to be submitted.

VI-B Ab Initio SCF MO CI Calculations of Metalloporphines

Hiroshi KASHIWAGI, Shigeru OBARA*, Toshikazu TAKADA*, and Nobumitsu HONJO* (*Hokkaido Univ.)

Ab initio LCAO SCF calculations including all 187 electrons of Co-porphine (CoP) have been carried out with the Roothaan SCF formulation for open-shells[1] on the basis of semiorthogonalized orbitals.[2,3] The molecule is assumed to be planar and to have the D_{4h} symmetry. SCF calculations are performed for various states of $[CoP]^-$, $[CoP]^0$, $[CoP]^+$, and $[CoP]^{2+}$ with a basis set of roughly double zeta quality for Co and N and of single zeta quality for C and H. The used program and the detail of the computation are shown in VI-A. Our investigation has been made extensively for the charge distribution, the character of ligand bonds, the d-d transition, the π-π* excitation, and the ionization. In this report the last two topics are presented briefly.

Ionization potentials (IP) are shown in Table I. The first two IP's of CoP correspond to removal of an electron from the two highest occupied orbitals $1a_{1u}$ and $5a_{2u}$. The calculated IP's are in good agreement with the IP's observed in the photoionization experiment for Co-octaethylporphyrin (CoOEP).[4] Other peaks were also observed at 7.48, 7.92, 8.16, 8.25, and 9.92 eV. These peaks can be assigned to ionizations from porphyrin π-orbitals, since their corresponding peaks were observed for free base OEP and MgOEP.[4] Configuration interaction (CI) calculations of $[CoP]^+$ are being performed in order to make these assignment more quantitative.

Excited states of porphine ring are investigated in π-π* CI calculations of CoP. Most of the singly-excited

Table II. Basis Functions for a π-π* CI Calculation of Co(II) Porphine ^2E_u States

$\Phi_1^{s,t}$:	$((1a_{1u},\ 5e_g)^{1,3}$	$14a_{1g})^2$
$\Phi_2^{s,t}$:	$((5a_{2u},\ 5e_g)^{1,3}$	$14a_{1g})^2$
$\Phi_3^{s,t}$:	$((2b_{2u},\ 5e_g)^{1,3}$	$14a_{1g})^2$
$\Phi_4^{s,t}$:	$((4a_{2u},\ 5e_g)^{1,3}$	$14a_{1g})^2$
$\Phi_5^{s,t}$:	$((1b_{1u},\ 5e_g)^{1,3}$	$14a_{1g})^2$

Table I. Ionization Potential (eV) of Co-Porphine $^2A_{1g}$ State

MO		orbital energy	IP calc.	reorganiza-tion energy	IP[4] obs.
π	$1a_{1u}$	-6.82	6.51	$(^3A_{1u})$	0.31	6.09
π	$5a_{2u}$	-7.12	6.77	$(^3A_{2u})$	0.34	6.58
d_π	$2e_g$	-14.37	7.47	(^3E_g)		
	$1e_g$	-16.21	8.92	(^1E_g)		
d_{xy}	$9b_{2g}$	-14.18	7.77	$(^3B_{2g})$		
	$8b_{2g}$	-15.76	10.05	$(^1B_{2g})$		
d_{z^2}	$14a_{1g}$	-15.31	9.06	$(^1A_{1g})$		6.25

Table III. Excitation Energies (eV) of Co(II)Porphine ^2E_u States

approximate form of solution	excitation energy calc.	obs.	
$\Phi_1^t\ -\ \Phi_2^t$	1.81	1.82[b]	
$\Phi_1^s\ -\ \Phi_2^s$	3.01	2.24[a]	Q
$(\Phi_1^s\ +\ \Phi_2^s)\ -\ (\Phi_3^s\ -\ \Phi_4^s)$	5.59	3.24[a]	B
$(\Phi_1^s\ +\ \Phi_2^s)\ +\ (\Phi_3^s\ -\ \Phi_4^s)$	5.85	3.84[a]	N
		4.59[a]	L
		5.98[a]	M

[a] CoOEP   [b] CuEtio

85

basis functions are included in the calculation. Important basis functions are presented in Table II, where the $5e_g$ orbital is the lowest unoccupied π-orbital and $14a_{1g}$ is the almost pure $3d_{z^2}$ orbital of Co. Results are shown in Table III. The agreement of calculated excitation energies with experiments is reasonable for lower states, but is poorer for higher states. This defect probably comes from the fact that diffuse π-orbitals are not included in the basis set. A more extensive SCF MO CI calculation, in which two sets of diffuse π-orbitals are included for C and N atoms, is being carried out for Cu-porphine. We expect to be able to describe excited states more accurately.

References

1. C. C. J. Roothaan, *Revs. Mod. Phys.*, **32**, 179 (1960).
2) H. Kashiwagi, *Int. Quant. Chem.*, **10**, 135 (1976).
3) H. Kashiwagi and T. Takada, *Int. J. Quant. Chem.*, **12**, 449 (1977).
4) S. Kitagawa and I. Morishima, private communication.

RESEARCH ACTIVITIES

VII. Instrument Center

We are studying with various instrumental techniques the reaction mechanism of hydrogenase which catalyzes the isotope exchange reaction between H_2 and D_2, the conversion of two modifications o-H_2 and p-H_2 and the reduction of cytochrome c_3. Chemical and biochemical methods are used to determine its reaction center. The magnetic susceptibility measurement and Mössbauer spectroscopy are applied to the study of magnetic properties of the hydrogenase reaction center. The Faraday magnetic balance with a superconducting magnet which is being built, will also be used.

The application of the enzyme fuel cell to the assay of enzyme activity is also studying. The mechanism of the enzyme fuel cell using hydrogenase are now carried out.

The electron transport phenomena in hemoproteins are also investigated by the use of the electrical conductivity measurement, the electrochemical method and the photoemission spectroscopy. Proteins investigated include horse heart cytochrome c, myoglobin and tetrahemoprotein, cytochrome c_3. Ionization potentials of hemoprotein and tetraphenylporphyrin are determined by means of the vacuum ultraviolet photoemission spectroscopy.

VII-A Reaction Mechanism of Hydrogenase

Hydrogenase, bacterial enzyme, is a bio-catalyst for the hydrogen cleavage reaction. Though its mechanism has been investigated kinetically by many workers, microscopical features are not clear yet. The first step of our research effort is to establish the reaction center of hydrogenase, and the next is the investigation of physical and chemical properties of the reaction center. It is also important to obtain phenomenological parameters in the course of the reaction. It has been found that a ferredoxin-type Fe-S cluster is a reaction center. Optical absorption and Mössbauer spectroscopies are applied to the study of the Fe-S cluster of hydrogenase. These spectra were found to be somewhat different from those of the clostridium 8Fe-8S cluster which did not catalyze the H_2-D_2 exchange reaction. These differences between hydrogenase and ferredoxin were related to their catalytic properties.

VII-A-1 Properties of Purified Hydrogenase from the Particulate Fraction of *Desulfovibrio vulgaris*, Miyazaki

Tatsuhiko YAGI*, Keisaku KIMURA, Hidehiro DAI-DOJI**, Fumiko SAKAI**, Shohei TAMURA**, and Hiroo INOKUCHI (*Shizuoka Univ., **Univ. of Tokyo)

Purified hydrogenase [EC 1.12. 2.1] solubilized from the particulate fraction of sonicated *Desulfovibrio vulgaris* cells is a brownish iron-sulfur protein of molecular weight 89,000, composed of two different subunits (mol. wt. 28,000 and 59,000), and conteins 7-9 iron and 7-8 labile sulfide atoms. The absorption spectrum of the enzyme was characteristic of iron-sulfur proteins. The millimolar absorbance coefficients of the enzyme were about 164 at 280 nm, and 47 at 400 nm. The absorption spectrum in the visible region changed upon incubating the enzyme under H_2 in the presence of cytochrome c_3, but not in its absence. This spectral change was due to the reduction of enzyme. The absorbance ratio at 400 nm of the reduced and the oxidized form of the enzyme was 0.66.

The activity of the enzyme was hardly affected by metal-complexing agents such as cyanide, azide, 1,10-phenanthroline, EDTA, Tiron, iodoacetamide, N-ethyl-maleimide and p-chloromercuribenzoate except for CO, which was a strong inhibitor of the enzyme. The activity was inhibited by SH-reagents such as p-chloromercuribenzenesulfonate. The enzyme was significantly resistant to urea, but susceptible to sodium dodecyl sulfate. These properties were very similar to those of clostridial hydrogenase [EC 1.12.7.1]. Several hydrogenase are compared in Table I.

References

1) L. E. Mortenson, R. C. Valentine, and J. E. Carnahan, *Biochem. Biophys. Res. Commun.*, 7, 448 (1962).
2) T. Yagi, and K. Maruyama, *Biochim. Biophys. Acta* 243, 214 (1971).
3) K. Kimura, H. Inokuchi, and T. Yagi, *Chem. Lett.* 693 (1972).
4) T. Yagi, M. Goto, K. Nakano, K. Kimura, and H. Inokuchi, *J. Biochem.* 78, 443 (1975).

Table I. Comparison of the Properties of Hydrogenase Preparations of Various Origins

| Source of hydrogenase	Hydrogenomonas H16[a]	Desulfovibrio vulgaris			Clostridium pasteurianum W5[a]	Chromatium[b]
		NCIB 8303[a]	Hildenborough[a]	Miyazaki[b]		
Electron acceptor	NAD^{+}	cytochrome c_3	cytochrome c_3	cytochrome c_3	ferredoxin	not NAD^{+}, nor ferredoxin
EC number	1.12.1.2	1.12.2.1	1.12.2.1	1.12.2.1	1.12.7.1	
Molecular weight		45,000	60,000	89,000	60,000	98,000
Subunits			30,000×2	59,000+28,000	monomer	50,000×2
Contents of						
Fe		0.72	3.5	7-9	12	4
Labile S^{2-}		0.35	3.2	7-8	12	4
Spectral properties						
Shoulder (small peak) at (in nm)	387, 411	408	near 400	near 400	near 400	410
Absorbance (mg/ml)	A_{400}=0.69 A_{280}=6.9	A_{408}=0.07 A_{277}=0.91	A_{400}=0.31 A_{280}=1.58	A_{400}=0.53 A_{280}=1.84	A_{400}=0.42 A_{280}=1.10	A_{410}=0.14 A_{280}=0.98
Absorbance (mM soln)		ϵ_{408}=3.1 ϵ_{277}=41	ϵ_{400}=17.7 ϵ_{280}=91	ϵ_{400}=47 ϵ_{280}=164	ϵ_{400}=25.3 ϵ_{280}=66	ϵ_{410}=14 ϵ_{280}=96
Absorbance ratio	A_{400}/A_{280}=0.10	A_{408}/A_{277}=0.08	A_{400}/A_{280}=0.20	A_{400}/A_{280}=0.29	A_{400}/A_{280}=0.38	A_{410}/A_{280}=0.15

[a] Soluble enzyme. [b] Solubilized enzyme from particulate fraction.

VII-A-2 Hydrogenase Activity in the Dry State. II. Isotope Exchange and Reversible Oxidoreduction of Cytochrome c_3

Keisaku KIMURA, Akira SUZUKI, Hiroo INOKUCHI, and Tatsuhiko YAGI (Shizuoka Univ.)

We observed that the purified desulfovibrio hydrogenase in the dry state could catalyze not only the conversion and exchange reactions but also the reversible oxidoreduction of the electron carrier, cytochrome c_3, with H_2. This behavior indicate that hydrogenase in the dry state retains all the catalytic functions observed in the aqueous medium. The rate of conversion was in the range of 0.1 to 0.65 molecule of H_2 converted per molecule of hydrogenase per second, and the ratio of the conversion rate to the exchange rate was near 5. The rate of oxidoreduction of cytochrome c_3 in the dry state was 0.015 molecule of H_2 uptaken in the forward reaction and 0.003 molecule of H_2 released in the reverse reaction per molecule of hydrogenase per second.

The process of these reaction could be explained by the observation that the hydrogenase molecule in the dry state has protons which are directly exchangeable with H_2 during the catalytic process. The reversible oxidoreduction of cytochrome c_3 in the dry state indicates that hydrogen is dissociated to provide electrons which are transferred to cytochrome c_3 molecules.

$$\text{cyt } c_3(Fe^{3+}) + H_2 \rightarrow \text{cyt } c_3(Fe^{2+}) + 2H^+$$
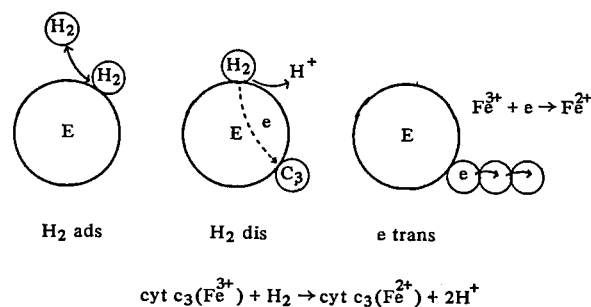
Since almost all cytochrome c_3 was reduced, it was suggested that cytochrome c_3 molecules not in direct contact with the hydrogenase molecule were reduced. We conclude that the rate determining step of the reduction of cytochrome c_3 in the dry state is the catalytic activity of hydrogenase itself, but not a diffusion-controlled process. The plausible electron transfer model in the dry state of cytochrome c_3 is given in Figure 1.

References

1) T. Yagi, M. Tsuda, Y. Mori, and H. Inokuchi, J. Amer. Chem. Soc. 91, 2801 (1969).
2) A. Couper, D. D. Eley, and A. Hayward, Disc. Faraday Soc. 20, 174 (1955).

VII-B Electron Transport Properties of Cytochrome

The electrical conduction of proteins in the solid state has been reported by numerous investigators with an interest in the carrier transport in biological systems. We have already examined a hypothesis of the mechanism of electron transport in respiratory proteins by means of the electrical conductivity measurement. The difference in the electrical conductivity was found between the film of hemoprotein and that of simple proteins with no heme as a prostheric group. The role of heme in the conduction mechanism in these complexes is being investigated. Electrochemical techniques are also being applied to cytochromes in order to clarify the electron transfer character of heme on the electrode surface.

VII-B-1 Electrical Conductivity of Cytochrome c Anhydrous Film

Yusuke NAKAHARA *(Tech. College of Miyakonojo)*, Keisaku KIMURA, and Hiroo INOKUCHI

[*Chem. Phys. Lett.*, **47**, 251 (1977)]

Electrical conductivities of both ferricytochrome c and ferrocytochrome c anhydrous films were measured at physiological temperatures. A film-casting method was used to prepare the film sample in order to avoid the effect of packing of molecules and to promote the removal of humidity of the sample. It was found that the V-I characteristics strongly depended on the amount of water absorbed in the sample. Decreasing the amount of water contained in the film, the V-I plots approach an ohmic limit. Since the deviation from Ohm's law results from the absorbed water in the film, the less deviation implies the less water contained in the sample.

Transient currents were observed after a step change of the applied voltage: the decay time $\tau_{1/2}$ for a wet sample was ten minutes or more but it was only a few seconds for a dry sample at the room temperature. A steady state current with an applied voltage of 500 V was held constant for 5 days for a dry sample. From these results, the conduction carriers in dry cytochrome c film are presumed to be electronic.

A comparison of the conductivity of ferricytochrome c with that of ferrocytochrome c was performed of the same sample. First, the temperature dependence of the conductivity was measured in the reduced sample. After full oxidation of the ferrocytochrome c, the oxidized form was used for the measurement. The linear relation of the logarithm of the conductivity against the reciprocal of the absolute temperature was reproducible in both species. We obtained rather low values of resistivities (55°C) of $6.5 \times 10^{10}\,\Omega$ cm for ferrocytochrome c and $6.5 \times 10^{8}\,\Omega$ cm for ferrocytochrome c, which can be compared with the previously reported value of $10^{11}\,\Omega$ cm (127°C). The apparent activation energy for the above conductivity, 0.6 eV, was the same in both samples.

The resistivities in our present work are very low, compared with those by Eley and Spivey, and Taylor who used dry powdered state samples. The difference

may have come from the sample preparation. An activation energy, 0.6 eV, both for ferrocytochrome c and ferricytochrome c is similar to Taylor's value at 40-70°C. As the activation energy is the same in the two redox states, it is expected that the conduction mechanism is also the same.

The turn-over number of cytochrome c (the number of electrons which is transported by cytochrome c per second) can be explained by the present results assuming a potential difference of 0.1 V was applied through the cytochrome molecule, the value being consistent with the difference in the redox potential between cytochrome $c_1(E_0' = 0.22$ V) and cytochrome oxidase ($E_0' = 0.29$ V).

References
1) P. H. Carnell, *J. Appl. Polym. Sci.*, **9**, 1863 (1965).
2) S. Hashimoto and H. Inokuchi, *Polym. J.*, **8**, 467 (1976).
3) D. Eley and D. Spivey, *Trans. Faraday Soc.*, **10**, 1432 (1960).
4) P. Taylor, *Discussion Faraday Soc.*, **27**, 239 (1959).

VII-B-2 Electrode Reaction of Cytochrome c_3 of *Desulfovibrio vulgaris*, Miyazaki

Katsumi NIKI *(Yokohama National Univ.)*, Tatsuhiko YAGI *(Shizuoka Univ.)*, and Hiroo INOKUCHI and Keisaku KIMURA

[*J. Electrochem. Soc.*, **124**, 1889 (1977)]

Cytochrome c_3 is an electron carrier present in the redox system of sulfate-reducing bacteria, *Desulfovibrio*. The molecular weight is nearly 14,000 and the heme content is four. It has been demonstrated by Yagi *et al.* that cytochrome c_3 is electrochemically active and interacts directly with a glassy carbon electrode. The electrochemical behavior of cytochrome c_3 on the mercury electrode has been studied by means of polarography, cyclic voltammetry and potentiometry.

A well-defined reduction wave of cytochrome c_3 was obtained in a polarogram. The small preceding wave at about -0.25 V vs. SCE is due to the trace of oxygen in the solution. The halfwave potential is -0.527 V, and the plot of log $[i/(i_d - i)]$ vs. the electrode potential produces a straight line with an inverse slope of 0.085 V

from which the apparent number of electrons involved in the electrode is calculated to be less than unity. For the mixed ferri- and ferrocytochrome c_3 system, the polarogram is symmetrical with respect to the current at $(i_{dc} + i_{da})/2$, where i_{dc} is the diffusion current for the reduction of the ferri-form and i_{da} is that for the oxidation of the ferro-form. The electrode potential corresponding to the current at $(i_{dc} + i_{da})/2$ is independent of the ratio of ferri-form to ferro-form and is equal to $E_{1/2} = -0.527$ V for the reduction of the ferri-form. From these results it may be concluded that the electrode reaction of cytochrome c_3 is reversible even in the presence of strong adsorption of cytochrome c_3 on the mercury electrode. This strong adsorption of the reactant is evidenced from the fact that the mercury drop formed in the cytochrome c_3 solution stayed on a mercury pool as a droplet at least for 30 min. The diffusion coefficient calculated from the pulse polarographic data was 1.2×10^{-6} cm^{2}s^{-1} for ferri- and ferrocytochrome c_3. This value corresponds to that of horse-heart ferricytochrome c (MW = 12,350) determined by hydrodynamic techniques, 0.95×10^{-6} cm^{2}s^{-1}.

The cyclic voltammograms of cytochrome c_3 with various scan rates are shown in Figure 1. The electrode potential at the current peak does not shift on the potential axis as a function of the scan rate. The current function $i_p v^{-1/2}$ is independent of the rate of voltage scan over a wide range, and the i_p vs. $v^{1/2}$ plot passes through the origin, where i_p is the peak current and v is the rate of voltage scan. The ratio of the cathodic to anodic peak current is almost unity. The difference between the peak potential, E_p, and the half-peak potential, $E_{p/2}$ was about 73 mV (the peak-to-peak separation is about 90 mV), which is much larger than 14.1 mV that is expected for the reversible four-electron electrode process.

The formal potential of the ferro- and ferricytochrome c_3 couple is -0.516 ± 0.001V (-0.270 ± 0.001V vs. NHE) and the Nernst slope of the plot of log (C$_o$/C$_r$) vs. the electrode potential is 88 mV. The apparent number of electrons involved in the electrode reaction
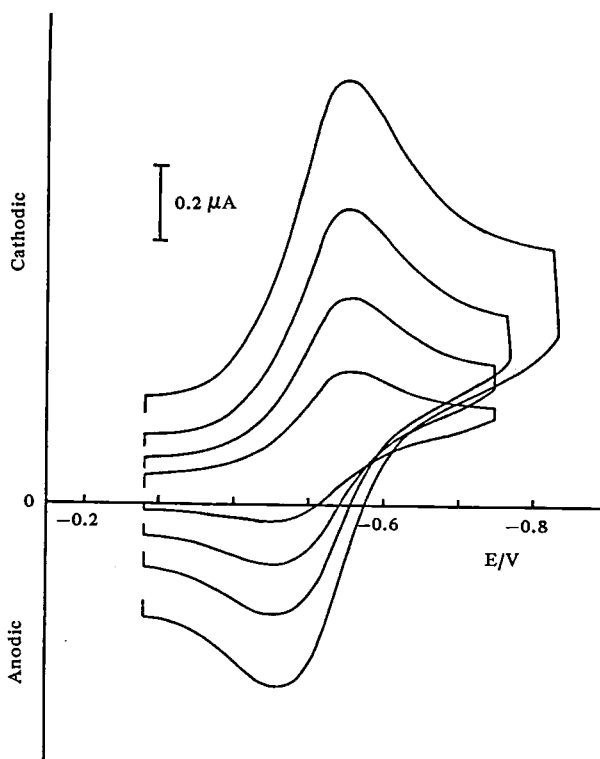
Figure 1. Cyclic voltammogram of cytochrome c_3 on HMDE. Scan rate, 30, 50, 100, and 200.mV sec^{-1}. Concentration of cytochrome c_3 is $5.2^4 \times 10^{-5}$ mole dm^{-3} in 0.03 M phosphate buffer at pH 7.0

calculated from the Nernst slope, therefore, is less than unity. The large Nernst slope, 88 mV, can be explained in terms of the combination of the Nernst plots for the multistep processes with a small difference in the formal potentials (the difference is at most 70 mV in the present case).

References

1) M. Ishimoto, J. Koyama, and Y. Nagai, *J. Biochem.* (Tokyo), 41, 763 (1954).
2) T. Yagi, M. Goto, K. Nakano, K. Kimura, and H. Inokuchi, *J. Biochem.* (Tokyo), 78, 443 (1975).

RESEARCH ACTIVITIES

VIII. Low Temperature Center

Low Temperature Center develops new cryogenic techniques in close cooperation with research divisions and other centers. In addition, we investigate the electrical, thermal, magnetical and other properties of one-dimensional metallic compounds with mixed valence states.

VIII-A Metallic Properties of One-dimensional Mixed Valence Compounds

Many studies have recently been carried out on the properties of one-dimensional metallic compounds, in connection with the existence of superconduction, and it has been revealed that they show such interesting phenomena as the Peierls transition and the Kohn anomaly. Among these compounds, there exist the compounds whose mixed valence state plays an important role in their metallic behaviours. The partially oxidized derivative of Magnus green salt with the formula $Pt_6(NH_3)_{10}Cl_{10}(HSO_4)_4$ is one of these mixed valence compounds originating from the coexistence of two valence states, Pt^{2+} and Pt^{4+}, and the averaged oxidation number of Pt in it is +2.33. We have been investigating this one-dimensional metallic compound by the measurements of electrical conductivity, magnetic susceptibility and heat capacity between liquid helium and room temperatures.

VIII-A-1 Electrical, Magnetical and Thermal Properties of the Partially Oxidized Derivative of Magnus Green Salt

Toshiaki ENOKI, Ikuji TSUJIKAWA *(Kyoto Univ.)*, Ryozo KUBOTA *(Kyoto Univ.)*, and Hanako KOBAYASHI *(Kyoto Univ.)*

The partially oxidized derivative of Magnus green salt (MGSPOS) is obtained from Magnus green salt $Pt(NH_3)_4 \cdot PtCl_4$, through the oxidation with H_2SO_4 and O_2. The powder sample of MGSPOS has been investigated as one-dimensional conductor with a mixed valence state.[1] Results of the X-ray powder pattern are consistent with a chain structure proposed by Gitzel *et al.*[2] The electrical conductivity shows a sharp peak between 190 and 220 K with the peak value extending over $10^{-1} \sim 10^{-4} \Omega^{-1} cm^{-1}$ depending on samples. The metal-semiconductor transition thus found is much less gradual than those in $K_2Pt(CN)_4Br_{0.33} \cdot nH_2O$ and NMP-TCNQ. The semiconducting phase below the temperature of conductivity peak has the gap energy $E_g \sim 0.03$ eV. In one of our samples, another transition from semiconductor to metal on cooling takes place at about 250 K. The thermal analysis shows that the transition at about 200 K from low temperature side is exothermic, while that at about 250 K is endothermic. This result suggests a thermally unstable state such as a glassy state below 200 K. The magnetic susceptibility indicates the absence of the Curie's behaviour. We are attempting to synthesize single crystals of MGSPOS with several methods of oxidation, with the purpose of understand-

ing its conductive property more clearly.

MGSPOS
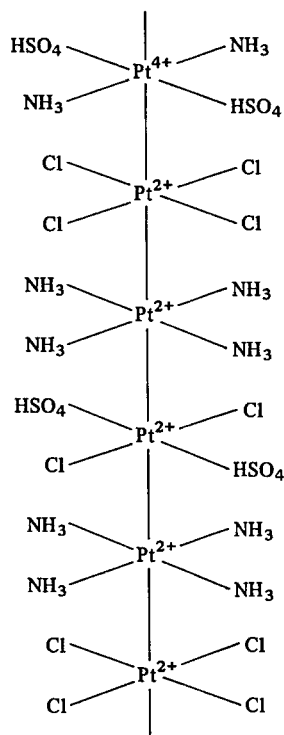
References

1) I. Tsujikawa, R. Kubota, T. Enoki, S. Miyajima, and H. Kobayashi, *J. Phys. Soc. Japan*, **43**, 1459 (1977).
2) W. Gitzel, H. J. Keller, H. H. Rupp, and K. Seibold, *Z. Naturforsch*, **27b**, 365 (1972).

RESEARCH ACTIVITIES

IX. Chemical Materials Center

We have carried out the synthesis of new chiral bisphosphines which are effective as ligands in metal catalyzed asymmetric organic reactions. We are also investigating the activation of strained carbon—carbon σ bonds by transition metal complexes. In the near future, we plan to initiate studies on infrared-laser induced organic reactions with the goal of developing new reactions with high selectivity.

IX-A Synthesis of a New Chiral Phosphine Ligand and its Use in Rh(I)—Catalyzed Asymmetric Hydrogenation of α-Amidoacrylic Acids

Hidemasa TAKAYA, Toshiaki SOUCHI *(Nagoya Univ.)*,[1] Arata
YASUDA, and Ryoji NOYORI *(Nagoya Univ.)*

Much effort has been made recently to develop new asymmetric reactions of high stereoselectivity. Asymmetric catalytic reactions are particularly noteworthy because of their high efficiency comparable to that of enzymes. The general methodology of the asymmetric catalytic reaction stems on the utilization of transition metal complexes bearing chiral organic ligands. The design and synthesis of new effective chiral ligands are, therefore, the most important requirements for developing new asymmetric syntheses. A variety of unique chiral ligands have so far been prepared and used successfully for many asymmetric catalytic transformations. However, most of the catalysts have the substrate specificity. We have to adopt catalytic systems most suitable to each reaction. Hence it is necessary to exert continuous efforts to develop new effective chiral ligands.

We have prepared 2,2'-bis(diphenylphosphino)-1,1'-binaphthyl (1) (hereafter abbreviated to BINAP), a new chiral bisphosphine ligand bearing only an axial element of chirality. Upon complexation, the chelate rings are variable in size depending on the bulkiness of metals and metal ions that form stable chelate complexes. The bulky binaphthyl group was expected to exert considerable steric restriction during catalytic reactions.

The racemic 1 was easily prepared by the route shown in Scheme I. Binaphthole 2, prepared easily from β-naphthole by the reported procedure, was converted to dibromide 3 by simply heating with triphenyldibromophosphorane in 26% yield. The dibromide 3 was treated with 4 equiv. of *tert*-butyllithium in THF at −95°C followed by addition of 4 equiv. of diphenylphosphinous chloride. Aqueous work-up and purification by column chromatography afforded d,l-1 in 30% yield as colorless crystals. Resolution of d,l-1 can easily be attained using chiral palladium complex 4. Addition of a solution of 1 in benzene to an equimolar amount of 4 in the same solvent followed by treatment with sodium tetraphenylborate yielded the complex 5 in 60 % yield, mp 155°C (dec), $[\alpha]_D^{23}$ +265° (c 0.19, acetonitrile). Fractional recrystallization afforded Pd(II) complex of (R)—(+)—1 [mp 162.5° (dec), $[\alpha]_D^{22}$ +374° (c 0.16, acetonitrile)] and that of (S)—(−)—1 [mp 161°C

Scheme I

(R)—(+)—1
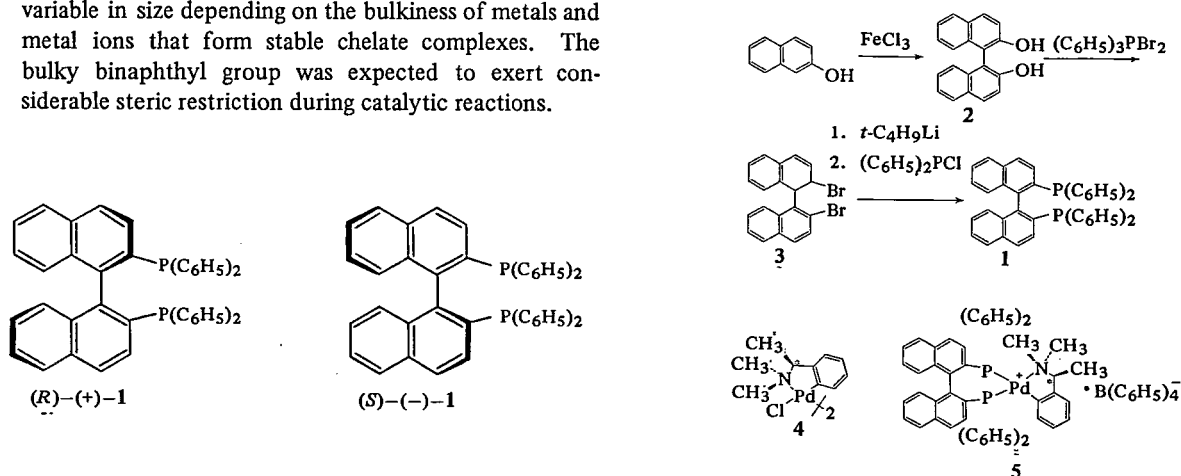
(S)—(−)—1

Substrate	Configuration of BINAP	Solvent	Yield, %	Product %ee	Configuration
H—C(COOH)=C(H)(NHCOCH$_3$)	R	A	92	16	S
	S	A	99	15	R
H—C(COOH)=C(C$_6$H$_5$)(NHCOCH$_3$)	R	A	98	39	S
	S	A	95	26	R
H—C(COOH)=C(C$_6$H$_5$)(NHCOC$_6$H$_5$)	R	B	99	38	S
	S	B	91	29	R
C$_6$H$_5$—C(COOH)=C(H)(NHCOC$_6$H$_5$)	R	B	94	83	R
H—C(COOH)=C(HO—C$_6$H$_4$—)(NHCOCH$_3$)	R	B	75	17	S
	S	B	71	20	R
H—C(COOH)=C(AcO—C$_6$H$_4$—)(NHCOCH$_3$)	R	A	91	31	S
	S	A	96	28	R
H—C(COOH)=C(CH$_3$O,AcO—C$_6$H$_3$—)(NHCOCH$_3$)	R	A	90	27	S
	S	A	93	21	R

(dec), [α]$_D^{22}$ −354° (c 0.12, acetonitrile)] in 39% and 36% based on the racemic 5, respectively. Reductive decomposition with LAH followed by recrystallization from benzene—ethanol (1:1) produced pure (R)—(+)-1 [mp 243—244°C, [α]$_D^{20}$ +220° (c 0.25, benzene) and (S)—(−)-1 [mp 242—243° C, [α]$_D^{25}$ −229°(c 0.31, benzene) in 78% and 67%, respectively.

Catalytic asymmetric hydrogenations of prochiral α-acylaminoacrylic acids were carried out in the presence of Rh(I) complex by the use of the bisphosphine 1 as the chiral ligand. The results are given in Table I.

Although (Z)-olefin did not give satisfactorily high stereoselectivity, (E)-isomer afforded high optical yield (83%). The correlation between the catalyst structure and the configuration of the products is under consideration. We are also making efforts to demonstrate the usefulness of this new chiral phosphine ligand for other kinds of asymmetric transformations.

Note
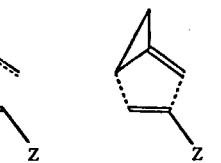
1) The graduate student of IMS, May 1977—March 1978.

IX-B Nickel(0) Catalyzed Reaction of Methylenecyclopropanes with Electron Deficient Olefins. Mechanistic Aspects
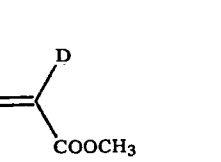
Ryoji NOYORI (Nagoya Univ.), Masashi YAMAKAWA (Nagoya Univ.), and Hidemasa TAKAYA

There has been considerable recent interest in transition metal promoted reactions of strained cyclic hydrocarbons. We have found that methylenecyclopropanes add to carbon—carbon double bonds in the presence of nickel(0) complexes giving methylenecylopentanes in good yields (eq. 1).[1] Four reaction modes A—D were possible candidates for the present catalytic transformations. Experiments employing alkyl-substituted methylenecyclopropanes (2 and 3) indicated that the cyclopropane rings suffer cleavage at C-2 and C-3 or C-1 and

(1)

1, R^1 = R^2 = H   Z = COOCH$_3$,
2, R^1 = H;   CN, COCH$_3$
  R^2 = CH$_3$
3, R^1 = CH$_3$;
  R^2 = H

C-3 σ bonds (mode A or mode D). Utilization of deuterium labeled methyl acrylate **4** afforded the product **5** which revealed that the reaction of **1** with methyl acrylate proceeds so that the vinylic bond of **1** is cleaved (mode D).[2]

6   **7**   **8**

A   **B**   **C**   **D**

4   **5**

The reaction of **1** with 1,2-disubstituted olefins such as dimethyl fumarate and maleate, however, afforded two kinds of products **6** and **7** (Z = COOCH₃). While the product **6** is apparently obtained by the mode D combination, the compound **7** can be produced by modes A–C. This time, we have disclosed that the compound **7** arises from the mechanism involving trimethylenemethane intermediate (mode A).

9   **10**   **11**

A mixture of deuterium-labeled methylenecyclopropane **8** and dimethyl fumarate in benzene was kept at 60°C for 2.5 h in the presence of bis(acrylonitrile) nickel(0) under argon. Usual work-up gave 1:1 adducts **9** and **10** in a ratio of 38:62 (Z = COOCH₃). NMR analysis of **10** showed that the deuterium atoms are located equally on the three carbon atoms, which indicates that trimethylenemethane–Ni(0) complex of type **11** is incorporated in the reaction forming **10** (mode A).

Now two types of ring opening (mode A and mode D) proved to occur in the nickel(0) catalyzed reactions of **1** with electron deficient olefins depending upon the olefins used. Details on the correlation between reaction modes and electronic properties of the olefins are under investigation.

References

1) R. Noyori, T. Odagi, and H. Takaya, *J. Am. Chem. Soc.,* 92, 5780 (1970).
2) R. Noyori, Y. Kumagai, I. Umeda, and H. Takaya, *J. Am. Chem. Soc.,* 94, 4018 (1972).

RESEARCH FACILITIES

Experimental and theoretical techniques in molecular science have been making so rapid a progress in recent years that molecular scientists need more and more supports from all fields of science and technology. In IMS, five research facilities, i.e., Computer Center, Low-Temperature Center, Instrument Center, Chemical Materials Center, and Development Workshop exist as supporting facilities for research activities in IMS. Associated to each research facility are technical associates and technicians as well as scientific staff. Keeping a close contact with the scientists of the corresponding facility and of research divisions, technical associates and technicians carry out works in their own specialized fields. These technical employees are organized in the Technical Section and supervised by a technical chief. Such an organization of technical employees as a group of technical experts is the first example among national institutes and universities in this country. The scientific staff associated with the research facilities also carry out their own scientific research in close cooperation with other scientific members of IMS.

Computer Center

The Computer Center is scheduled to introduce a large computer in January 1979 and will begin computational services soon after. The computer will be used not only by the research staff of IMS but also by scientists outside the Institute in the related fields. The Computer Center is to serve the following purposes:

1) Large scale computation in molecular science.
2) Collection and analysis of experimental data in molecular science.
3) Development and maintenance of the molecular science program library.
4) Computational services for the neighboring National Institute for Basic Biology and National Institute for Physiological Sciences.
5) Participation in the computer net work in Japan in the future.
6) Development of the quantum chemistry data base.
7) Administrative computation for the Institutes.

The Computer Center building with a $1000 \, m^2$ floor space is to be completed in December 1978.

The computer system to be introduced, shown diagramatically on the next page, consists of two HITAC M-180 computers with an overall processing capacity of over 6 million instructions per second. The processor uses 32 bit words and is essentially IBM-compatible at both the hardware and software levels. It will have 8 mega byte main memory and 7150 mega byte disk memory. It will also be equipped with magnetic tape drives, and an XY-plotter and a graphic display as well as usual input-output devices. The system is designed to work with no operator.

Low Temperature Center

Low Temperature Center supplies coolants such as liquid nitrogen and liquid helium. The staff of this center also develops new cryogenic techniques in close cooperation with research divisions and other centers.
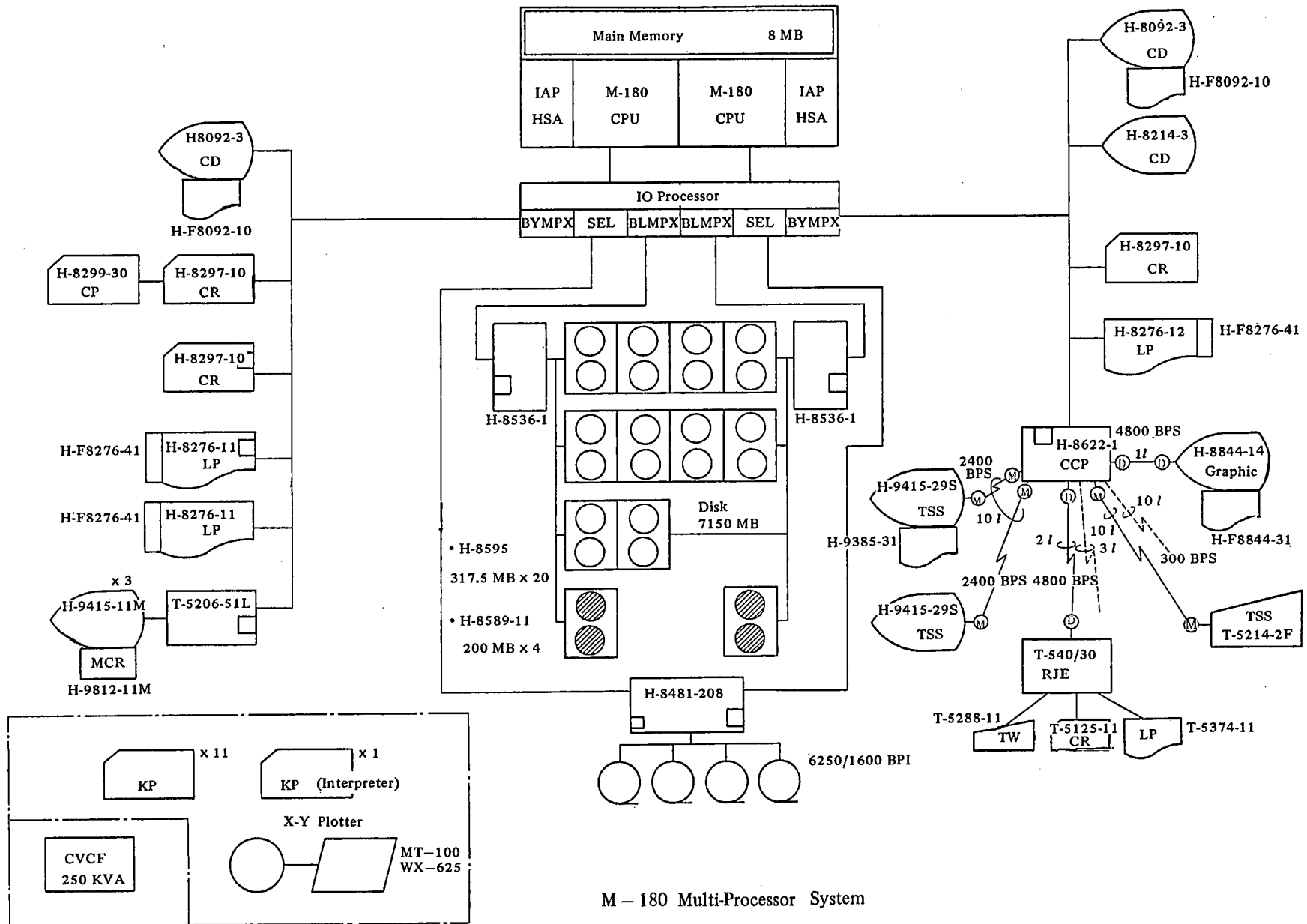
The center is still in the earlier stage of development, and, in this year, it supplies liquid nitrogen. The center building with three liquefaction machine rooms, ten laboratories and a machine shop will be completed in March 1979. The liquefaction of helium will be carried out with a machine of the 40 l/h capacity. A room is set aside for the future installation of a hydrogen liquefier. The floor and walls of the machine rooms are separated from the rest of the building to avoid the propagation of vibrations. The laboratories are to be equipped with spectroscopic, magnetic and calorimetric instruments for low temperature measurements. Seven laboratories are located at the basement in order to obtain a well regulated environment.

Major equipments are:

Helium liquefier	CTI-1400
Cold converter of liquid nitrogen	OSAKA SANSO CO-3
Helium leak detector	ULVAC DLMS-33

Instrument Center

The Instrument Center maintains and makes available instruments for general use, such as NMR, IR, visible-UV, vacuum UV, Raman, emission, and photoelectron spectrometers. Besides operating these equipments, its staff also

Main Memory 8 MB

| IAP HSA | M-180 CPU | M-180 CPU | IAP HSA |

IO Processor

BYMPX | SEL | BLMPX | BLMPX | SEL | BYMPX

H-8092-3 CD
H-F8092-10

H8092-3 CD
H-F8092-10

H-8214-3 CD

H-8299-30 CP
H-8297-10 CR

H-8297-10 CR

H-8297-10 CR

H-8276-12 LP
H-F8276-41

H-F8276-41
H-8276-11 LP

H-F8276-41
H-8276-11 LP

x 3
H-9415-11M
T-5206-51L
MCR
H-9812-11M

H-8536-1
H-8536-1

Disk 7150 MB

• H-8595
317.5 MB x 20

• H-8589-11
200 MB x 4

H-8481-208

6250/1600 BPI

4800 BPS
H-8622-1 CCP
H-8844-14 Graphic
H-F8844-31

2400 BPS
H-9415-29S TSS
H-9385-31

2400 BPS 4800 BPS
H-9415-29S TSS

T-540/30 RJE

TSS T-5214-2F

300 BPS

T-5288-11
TW
T-5125-11 CR
LP T-5374-11

KP x 11

KP x 1 (Interpreter)

X-Y Plotter

CVCF 250 KVA

MT–100 WX–625

M – 180 Multi-Processor System

carries out research on improving the existing instruments as well as developing know-hows of new experimental techniques or instruments. The Center lends out electronic instruments, such as oscilloscopes, lock-in amplifiers, integrators, ammeters, and high voltage supplies.

The Center building (1053 m², 2 stories) was completed in March 1978. It consists 3 rooms for material research (electric and magnetic properties), 4 rooms for spectroscopy, 2 rooms for laser research, 1 room each for magnetic resonance, X-ray diffraction, and electromagnetically shielding measurements. The floors of the laser rooms are separated from the walls in order to avoid vibrations from the building. The turbulence of air from the air conditioning system is minimized. The electromagnetic disturbance in the shielded room is -80 dB.

The major instruments installed at present are as follows:

Spectrophotometer	CARY 17
Dual-wavelength Spectrophotometer	HITACHI 556
Photoelectron Spectrometer	PERKIN ELMER PS-18
1-Meter VUV Scanning Monochromator	GCA MCPHERSON 225
1-Meter-Czerny-Turner Scanning Spectrometer	SPEX 1704
1-Meter-Double Monochromator	SPEX 14018
X-ray Diffractometer	RIGAKU DENKI GEIGER FLEX 2027
Surface Roughness Tester	DEKTAK
Fourier-Transform IR Spectrophotometer	JEOL JIR-10
Corrected Recording Spectrofluorophotometer	SHIMADZU RF-502
Fourier-Transform NMR Spectrometer	JEOL JNM-FX100
Thermal Analyzer	DUPONT 990
High Vacuum Evaporator	ULVAC EBH-6
Automatic Recording Spectropolarimeter	JASCO J-40C
Laser-Raman Spectrophotometer	JEOL JRS-400T
Scanning Electron Microscope	HITACHI S-450
Nanosecond Spectrometer	APPLIED PHOTOPHYSICS SP-3X+ORTEC
Argon Ion Laser	SPECTRA-PHYSICS 164-05
Nitrogen Laser-Tunable Dye Laser	MOLECTRON UV-24 + DL 14
High Speed Refrigerated Centrifuge	KUBOTA KR-180A
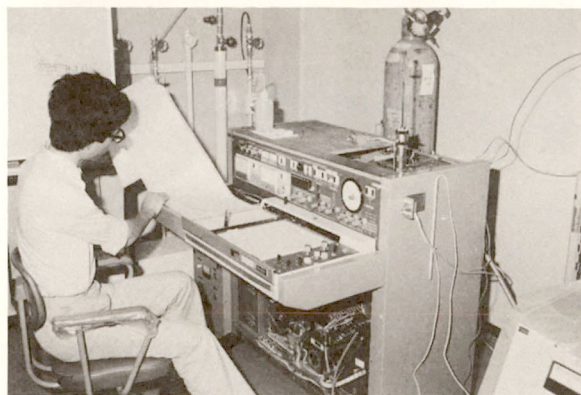
Photoelectron Spectrometer
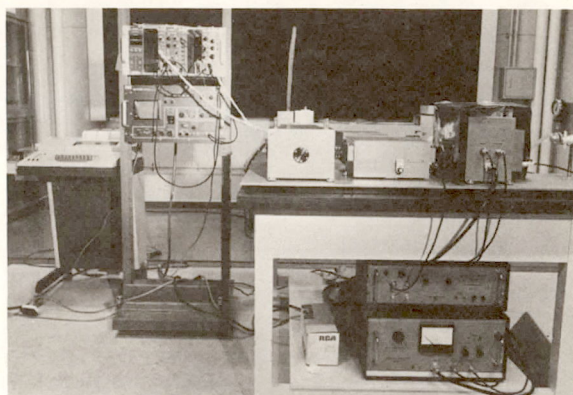
Nanosecond Spectrometer

Chemical Materials Center

The Chemical Materials Center is the preparation center of chemical substances. Upon requests by staffs of IMS, the scientists and technicians of this facility prepare organic and inorganic compounds by synthesis, purification, and crystallization. As the need arises, they develop new methods for preparing interesting chemicals in high purity and in large quantities. They also carry out research on development of new chemical reactions, elucidation of reaction mechanisms, and analysis of chemical substances. They also participate in disposition of waste chemicals and solvents.

The Center building was completed in March 1978. The two-storied building (1060 m²) consists of the following facilities: four laboratories for organic and inorganic synthesis, a laboratory for high-pressure experiments, four instrumentation rooms, two-clean rooms (class 100 and 10000), a laboratory for preparation of pure crystals, a stockroom of chemicals, and an electric gilding room. Each room is provided with tubing for cooling water, city gas, and special gases (argon, nitrogen, oxygen, compressed air, and vacuum pipes, and a recovery tube of helium),

distributing box (single- and three-phase current totaling 30 KW), and an emergency shower as standard equipments. About five hundred chemicals and solvents are stored in the stockroom. All hoods are equipped with scrubbers and chemicals can be safely handled in them. Solar energy collectors supply hot water necessary for experiments.

Major equipments are:

Gas Chromatograph-Mass Spectrometer	JEOL JMS D300 equipped with EI, CI, and FD ion sources, and JMA-2000 mass data analysis system
High Performance Liquid Chromatographs	JASCO TRI ROTAR and JASCO FAMILIC-100
Inert Atmosphere Glove Box	Vacuum/Atmospheres Co. MO-40-2V DRI-TRAIN
Infrared Spectrometer	Hitachi 295
Instrument for Crystal Growth	Assembled in IMS
Analytical Gaschromatograph	Ohkura 701
Preparative Gaschromatograph	Shimadzu GC-6A
Automatic Waste Fluid Disposition Apparatus	Yanaco YWT-1
Polarimeter	JASCO DIP-4
Zone Refiner	Shibayama SS-960
Freeze Dryer	RFS-5000
Autoclave	Nitto Koatsu (500 ml) equipped with automatic temperature controller
Automatic Laboratory Washer	Miele G-19LG
Ultrasonic Cleaner	Kokusai Denki UO600FA-UT50A
Bath Cooler	NESLAB CryoCool CC-100 equipped with temperature controller
Low Temperature Room	SANYO ($4°C$, 3.3 m^2)
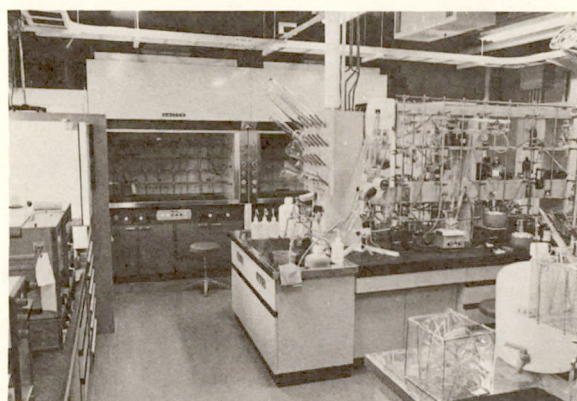
The Laboratory for Organic and Inorganic Synthesis
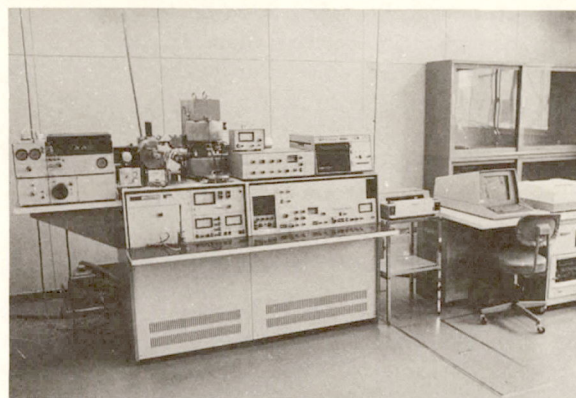
Gas Chromatograph—Mass Spectrometer

Development Workshop

Development Workshop consists of machine shop, electronic shop, and glass-blowing shop. The Workshop building completed in March 1978 has two stories with the floor space of 1260 m^2.

Development Workshop is expected to play a unique and important role in the research activities at IMS. It designs and constructs instruments based on IMS's own ideas. It also improves existing research equipments. Technicians are making an interplay with scientific staff members to support activities of the Workshop. Technical meetings are regularly held twice a year, which provide opportunities for the technicians to exchange information and to discuss technical problems with those from other institutes and universities.

1) Machine Shop

The facilities constructed or to be constructed at IMS include high-vacuum apparatus, lasers, microwave spectrometers as well as various types of equipments operated at the liquid-helium temperature. All these are of high performance and thus require a very fine engineering to prepare their parts. Therefore, in addition to lathes, fraises, drilling machines, and grinders of common use we have installed the following special machines:

(i) NC Lathe (OKUMA TEKKOSHO LS-N). This computer-controlled lathe has been used to prepare microwave lenses with spherical and/or paraboloidal surfaces, made of Teflon, TPX, or metals. It also prepared spherical collectors for electron spectroscopy. None of these parts can be constructed with a normal lathe. The electronic shop is developing microcomputer facilities to feed tapes in the NC lathe.

(ii) Spark erosion machine (MAKINO SODICK GP-20L). This has been used to make a 50 mm diameter stainless steel cylinder of 0.025 mm thick, which is to support an optical window in a low-temperature apparatus. It has also been used to drill a very fine slit (0.04 mm wide and 30 mm long).

(iii) Electron-beam welder (NEC EBW). This can weld tightly two different kinds of metals (e.g. copper and stainless steel). This welding eliminates a possible leakage in a vacuum apparatus operated at a very low temperature, especially in those parts that suffer from frequent changes of temperature. We can use a beam of 10 mA accelerated at a voltage of 150 kV under the pressure of 5×10^{-2} Pa or less. The maximum beam power is 1.5 kW.

(iv) Helium/nitrogen leak detector (ULVAC DLMS 33). This detects a leakage in an ultra-high vacuum apparatus as small as $3 \times 10^{-9} l$ Pa/s. It may even detect the nitrogen gas. This machine consists of a detector combined with a vacuum system designed by the Machine Shop. It is equipped with a microcomputer that automatically eliminates backgrounds and noise signals.
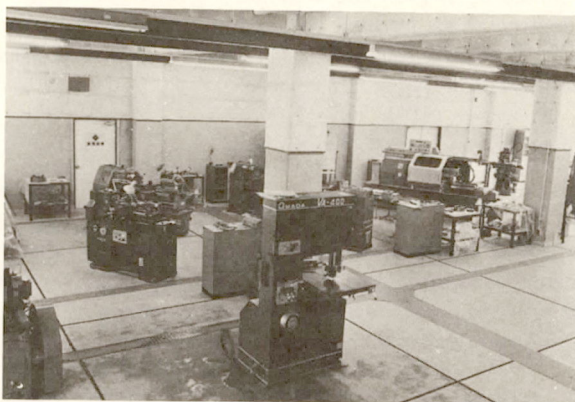
Machine Shop

2) Electronic Shop

The major instruments installed are:

Oscilloscope	TEKTRONICS 7904 (500 MHz)
Spectrum Analyzer	TAKEDA RIKEN 4110M (200 Hz–1.3 GHz)
Frequency Counter	TAKEDA RIKEN 5502C ($\leq$ 1.4 GHz)
Lock-in Amp	PAR 124
Boxcar Integrator	PAR 162
LCR Meter	HEWLETT-PACKARD 4262A
Teletype	CASIO 502

By the request of research Divisions, the Electronic Shop has designed and constructed the following devices:
  i) High voltage pulser to trigger a flash lamp.
  ii) Laser power peak detector.
  iii) Spectrum position sensor made of a photodiode array for a monochromator.

The Shop is developing hardwares as well as softwares for microcomputers which are to be used for automatic control and data processing in experimental apparatus.

It also stocks electronic parts and data handbooks for the convenience of researchers who design and build their own electric equipments.

3) Glass-blowing Shop

We have installed the following machines:

Glass Lathe	RIKEN SEIKO RGL-4DLH (max. diameter of the glass pipe 200 mm)
Stop Welder	NIPPON AVIOTRONICS NW-29 DS (100 W)
Water Welder	FUJI BUSSAN S51-4 (oxygen/hydrogen evolving rate 170 l/h)
Glass Grinder	SANWA DIAMOND SDK 20-B (diamond disk 300 mmϕ with an angle holder)
Ultrasonic Microboring Machine	CHO-OMPA KOGYO UM-2-7B
Ultrasonic Soldering Machine	ASAHI GLASS SUNBONDER USM-II

The Shop has constructed, among others, high vacuum glass apparatus and laser tubes.

LARGE SCALE RESEARCH EQUIPMENTS AND SPECIAL RESEARCH PROJECTS

I. Large Scale Research Equipments

Before the foundation of the Institute for Molecular Science a committee on research facilities (chairman: Professor I. Tanaka, Tokyo Institute of Technology) discussed the priority for large scale equipments to be installed in the Institute. These equipments should be of great and common use for researches in the field of molecular science, but were too expensive to install in other institutions. The equipments which the committee recommended to set up first are facilities (1) for time-resolved spectroscopy and (2) for high resolution spectroscopy. Both spectroscopic systems should have lasers as the main light sources.

1) Time-Resolved Spectroscopy

The system contains a repetitive picosecond Nd^{3+}: YAG laser and a high power nanosecond Nd^{3+}:YAG laser. Frequency conversions in both visible and near infra-red region are developed. An ultrafast streak camera was installed.

1-a) Time-Resolved Spectroscopy in the Picosecond Region

A passively mode-locked Nd^{3+}:YAG laser and amplifiers are developed. A single pulse is selected by Pockel's cell from the pulse trains of the oscillator output, and amplified by three stage amplifiers (6ϕ, 8ϕ, and 12.7ϕ rods). The characteristics of the output pulses are 100 mJ (nominal, 140 mJ maximum) output energy for a single pulse, ~15 picosecond pulse width (FWHM) obtained at the wavelength of the second harmonic (532 nm, 2ω), and 5Hz repetition rate. Figure 1 shows the overview of the laser system. Fiugre 2 shows the actual pulse shape observed by a streak camera. The second harmonic was obtained by a KDP crystal with 20 mJ output energy. The third harmonic (355 nm, 3ω) was produced by mixing of the fundamental and second harmonic with KDP crystal with an

efficiency of ~60 %. The fourth harmonic (266 nm, 4ω) had an output of ~3 mJ. The production of the fifth harmonic (213 nm, 5ω) by either mixing of ω and 4ω with KPB crystal or of 2ω and 3ω with ~90° phase matched deuterated KPB is under way.

The tunable wavelength conversion by an optical parametric oscillation (OPO) is developed with the cooperation of the Development Workshop (Dr. Y. Takagi). By tuning the temperature of an ADP crystal, 4ω gives the tunable picosecond output pulses between 420 and 720 nm. The pulses are amplified by a second crystal with a gain factor of ~10^2. The total output energy is about 20 μJ and the conversion efficiency is ~5%.
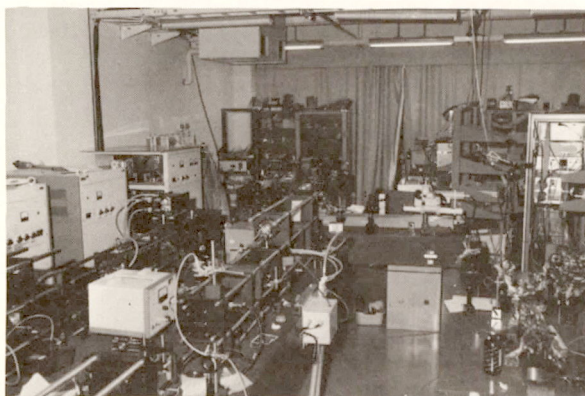

Figure 1. Overview of the repetitive ps laser system. A passively mode-locked Nd^{3+}:YAG laser, a single pulse selector, and amplifiers are shown.
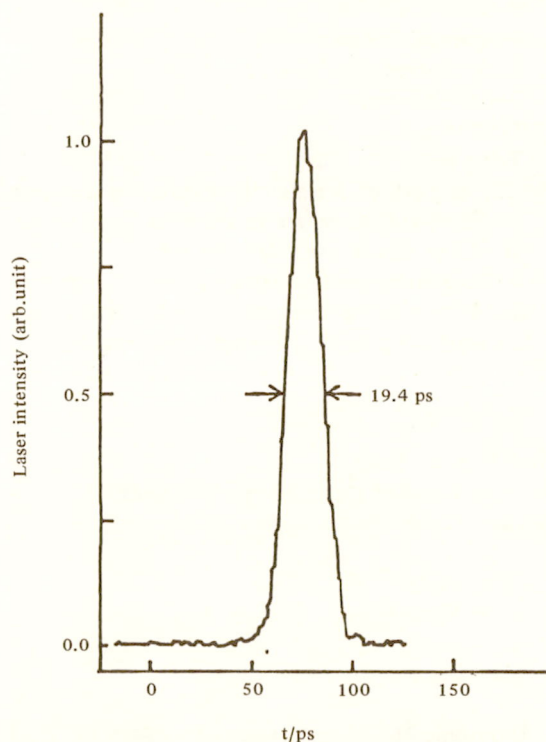

Figure 2. Observed laser pulse of the second harmonic (532 nm). The apparent pulse width of 19.4 ps corresponds to 14.4 ps after the correction of the slit width of a streak camera.
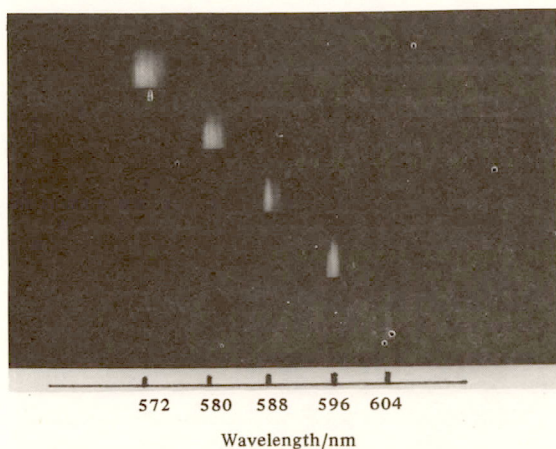
100

572   580   588   596   604

Wavelength/nm

Figure 3. Tunable picosecond pulses obtained by optical parametric oscillation without amplification. Photograph indicates 5 lines of 8 nm separation between 572 nm and 604 nm.

The amplification of the output pulse by passing together with the 2ω beam through a dye cell is now in progress. The spectral purity was $\lesssim 5A$. Figure 3 shows the obtained output at various wavelengths.

A streak camera (Hamamatsu C979) with UV optics was installed for the observation of transient phenomena in the picosecond region. The streak was digitized by a TV camera and microcomputer system (Hamamatsu C1000). The data are transferred to a NOVA3 mini computer. The distortion of the time base and vertical intensity of the camera are fully corrected. The observations of slower phenomena with a transient digitizer (Tektronix WP2000) and of the picosecond transient absorption with an optical multichannel analyser (PAR 1205) are also available (photo).

The following studies have been carried out with the equipments.

Dynamic behaviors of excited states in intra-molecular exciplexes by Prof. N. Mataga. (Osaka Univ.)

Fluorescence dynamics of concentrated reaction center of photosynthetic bacteria by Prof. S. Morita. (Univ. of Tokyo)

Fluorescence dynamics of concentrated reaction center of spinach chloroplast by Dr. I. Ikegami. (Teikyo Univ.)
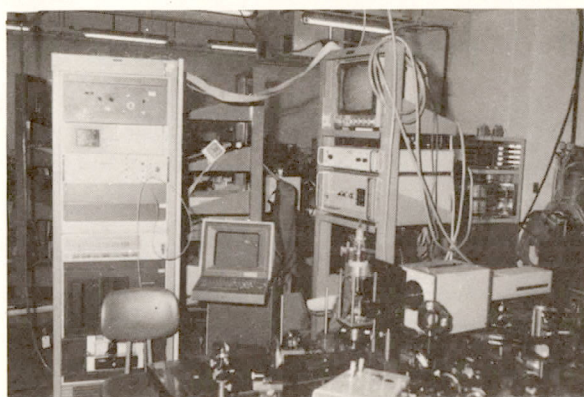
Streak camera and data processing systems.

Temperature dependence of fluorescence lifetimes of trans-stilbene. (IMS)

Electron transfer distances obtained by picosecond study of fluorescence dynamic quenching. (IMS)

Fluorescence dyanmic quenching in indole-chloromethane systems due to photoionization. (IMS)

Energy transfer in tetracene-doped anthracene single crystals by Dr. J. M. Morris. (Univ. of Melbourne and IMS)

Fluorescence dynamics of dye monolayer at the surface of a molecular crystal by Dr. F. Willig. (Fritz-Haber Inst. and IMS)

Ultrafast optical excitation and detection of ESR with paramagnetic materials. (IMS)

Picosecond analysis of the fluorescence lifetime of the coenzyme in D-amino acid oxidase; Evidence for the difference in the lifetime of the monomer and the dimer by Prof. F. Tanaka (Mie Nursing College), N. Nakashima and K. Yoshihara (IMS), and Prof. K. Yagi (Nagoya Univ.).

1-b) Time-Resolved Spectroscopy in the Nanosecond Region

Professor I. Hanazaki (Osaka Univ. and an adjunct associate professor for 1976 – 1978) developed a tunable near infra-red light source with a Q-switched Nd^{3+}:YAG laser (NEC). The Nd^{3+}:YAG laser has a two stage amplifier with a final output energy of 900 mJ and a pulse width of 30 ns. About 10 % conversion to the second harmonic (532 nm, 2ω) was obtained. The third harmonic was obtained with an RDP crystal with an efficiency of ~40 %. The second harmonic was then introduced to a temperature controlled $LiNbO_3$ crystal. The homogeneity of the temperature was kept below $\pm 0.02°$ and the temperature stability was less than $\pm 0.02°$. The tunable light of 600 ~ 690 nm and 2.3 ~ 4.6 μm was obtained with an output of 600 μJ. Improvement for a wider tunable range and a higher output is now in progress.

2) High Resolution Spectroscopy

The main parts of the apparatus are tunable cw lasers with high spectral purity.

2-a) Visible Region

Two dye lasers were installed:
i) Spectra Physics 580A (pumped by a Spectra Physics Ar^+ laser 171-05 with the output of 15W in the visible and 1.2W in the ultraviolet region),
ii) Coherent Radiation 599-21 (pumped by a Coherent Radiation Ar^+ laser CR-4SG with the output of 4W).
The SP laser is less stable (about $\pm 15MHz$) than the CR laser (a few MHz), because the latter may be locked to an external cavity of high stability by a feedback loop. On the other hand the SP machine is somewhat easier to operate in a wider wavelength region. Both lasers oscillate in the region of 550-630 nm by using Rhodamine 110, 6G, B, and 101 as lasing dyes. A typical output is 20-150 mW.

Professor F. Shimizu (Univ. of Tokyo, an adjunct

Associate Professor of IMS for 1976–1977) developed a wavelength meter consisting of four sets of etalons, with a single-frequency He-Ne laser (NEC GLG 2012, GLS 2012) as a standard. It measures the wavelength of a dye laser with a precision of 0.01 cm^{-1}. For a relative measurement of the laser frequency we may use the cavity mode of the dye laser and a spectrum analyzer (Tropel 240 with the free spectral range of 1.5 GHz).

Fluorescence spectroscopy is one of the most sensitive methods. Figure 4a shows a simple arrangement for laser-excited fluorescence spectroscopy; we monitor the fluorescence intensity by using a photomultiplier (Hamamatsu 1P28 or R666S) while we scan the frequency of a dye laser. The signal thus observed corresponds to the absorption spectrum with a linewidth of the Doppler limit. This technique has been applied not only to stable molecules ($^{14}NO_2$, $^{15}NO_2$) but also to transient species (NH_2, PH_2, HNO, HSO). When the reaction producing unstable species under consideration emits a strong chemiluminescence, we may chop the exciting laser light and use a lock-in detector to observe fluorescence. We eliminate the interferring light by using appropriate filters.

Two methods are available to achieve sub-Doppler spectroscopy. One was first invented by A. L. Schawlow and his coworkers; as shown in Figure 4b we split the laser beam into two and propagate them through a cell in the opposite directions. It is difficult to superpose the two beams completely because this may cause instability of the laser by feedback, but still two beams
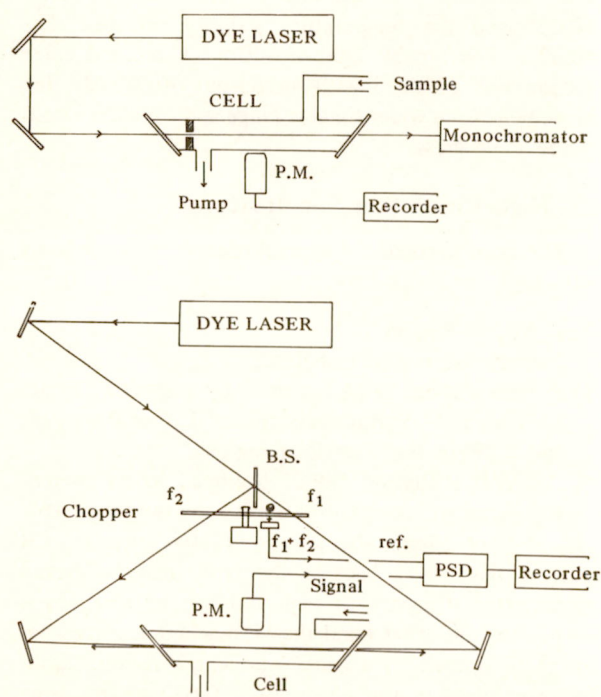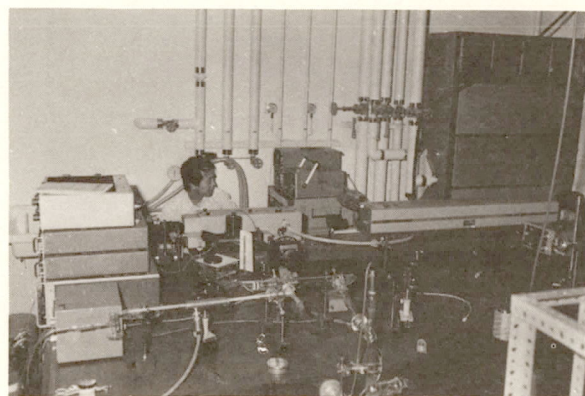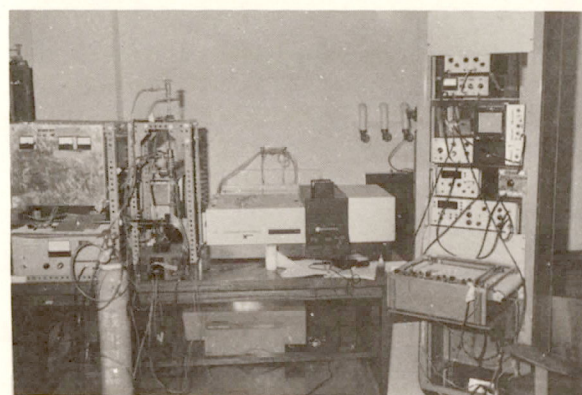

CR599 dye laser. Observing inter-modulated fluorescence.

may be overlapped in some length in the cell. Then the absorption by molecules moving perpendicularly to the laser may be saturated, and a Lamb dip will then be observed. When we chop the two beams at different frequencies, f_1 and f_2, we may take out only the saturation signals by using a phase sensitive detector operated at the sum frequency $f_1 + f_2$ (photo). This method was successfully applied to PH_2 and NO_2; the observed spectra were as narrow as 12 MHz. Most of the linewidths may be attributed to incomplete overlapping of the two beams. The other method is microwave-optical double resonance. Although we fed a microwave power of a few W to a fluorescence cell by using a traveling wave tube, we could so far observe the signals from $^{14}NO_2$ and $^{14}NH_2$.

2-b) Infrared Region

A Laser Analytics LS-3 spectrometer was installed (photo). The laser elements are made of the p-n junction of Pb-salt semiconductors. The laser wavelength may be scanned by changing either the supplied D.C. current (typically 0-2A) or the temperature of the diode. The diode is cooled by a closed cycle He refrigerator and works from 10K to a few ten K (sometimes up to 120K). One diode covers the wavelength region of $100 - 400$ cm^{-1} with many gaps. We have at present thirteen diodes for $876 - 2519$ cm^{-1}, but need to

Figure 4. (a) (upper trace) Laser excitation spectroscopy with a dye laser as a source,
(b) (lower trace) Intermodulated fluorescence spectroscopy.

Laser Analytics LS-3 diode laser spectrometer.

increase the number for a more complete coverage. According to the specifications of Laser Analytics the spectral purity is ±3 MHz or less and the stability is ±9 MHz in 30 sec or better. Although we have been unable to test these specifications of the diodes quantitatively, the spectra we observed indicated that most of our diodes satisfied these requirements; for example, the observed linewidth was near the Doppler limit for a pressure less than a few Torr. In most cases a diode oscillates in more than one mode. We use a monochromator to sort out an appropriate mode. Because the total output power is specified to be larger than 0.1 mW, the power of one mode may be as small as a few ten μW. It may thus be not possible to observe a saturation effect.

The simplest way of observing an absorption line is to chop the laser beam at 400 Hz (video dection). A more advantageous method is to modulate the diode (e.g. 5 kHz) and to detect the absorption line at twice the modulation frequency (10 kHz) by a phase sensitive detector. This technique makes the baseline flat (the mode curve is a smooth function of wavelength) and makes the sensitivity an order of magnitude higher than that of the video detection. For a strong band such as ν_1 of N_2O we could observe the spectra of a species with an abundance as small as 10^{-4}, by using a single-path cell of 15 cm long with a sample pressure of 1-2 Torr in it. The S/N ratio is limited neither by a detector noise nor by a source noise, but by Fabry-Perot type fringes produced by optical components. We may eliminate these fringes by applying the Stark or Zeeman modulation. A preliminary experiment we carried out indicates that the Zeeman modulation is particularly useful to observe the infrared spectra of paramagnetic species.

An important porblem with a tunable laser is how to measure the laser frequency precisely. We may use some appropriate gases as standards, for which high resolution infrared data were reported. It is, however, more desirable to construct a wavelength meter of high precision. Such a device is being designed.

The bands so far investigated with this spectrometer are listed below:

CF$_4$ ν_3 by Prof. T. Fujiyama (Tokyo Metropolitan Univ.)

ClO$_2$ ν_3 by Dr. Y. Hamada (Univ. of Tokyo)

NO$_2$, NO by Dr. N. Takeuchi (Natl. Inst. for Environmental Studies)

^{15}NH$_3$ ν_2, H$_2$O ν_2 by Prof. T. Shimizu et al. (Univ. of Tokyo)

N$_2$O ν_1, CH$_3$F ν_6, CS v = 1 ← 0, 2 ← 1, SO($^3\Sigma^-$) v = 1 ← 0, NS v = 1 ← 0 (IMS).

As an example Figure 5 shows the spectra of CS recorded by source modulation. A few lines of N$_2$O, which appeared simultaneously, served as wavelength standards.
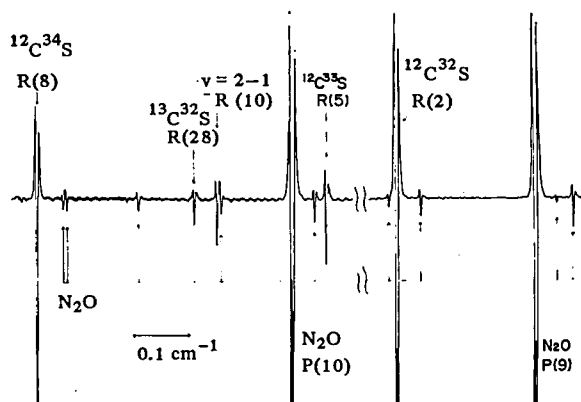

Figure 5. The v = 1 ← 0 and v = 2 ← 1 vibration-rotation transitions of CS, observed by a tunable infrared diode laser. A few lines of N$_2$O recorded simultaneously were used as frequency standards.

3) Picosecond Continuously Tunable Laser from UV to IR

The committee on the research facilities approved a project of developing a tunable picosecond laser in the entire ultra violet, visible, and infrared region. The project will be undertaken in the fiscal year of 1978.

The recent innovation of the high power laser technology and non-linear optics made it possible to develop a tunable laser for a wide wavelength region. Picosecond lasers are particularly suitable for this purpose since the peak damage thresholds of the non-linear materials are high for ps pulses. Among various methods of tuning the pumping laser, we apply the second harmonic generation, mixing of different wavelengths, and optical parametric oscillations (OPO) on non-linear crystals and the induced Raman scattering by a pressurized hydrogen gas.

The fundamental pumping source is the passively mode-locked Nd^{3+}:YAG laser and 6 stage amplifier systems. Spatial filters and soft apertures are set to maintain the proper quality of the laser beam during the
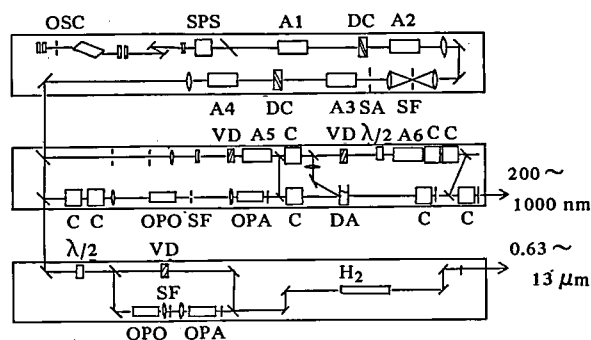
Figure 6. A block diagram of the picosecond continuously tunable laser from UV to IR. OSC: Nd^{3+}:YAG oscillator; SPS: single pulse selector; A 1 ～ 6: Nd^{3+}:YAG amplifiers; DC: dye cells; SF: spatial filters; SA: soft aperture; VD: variable delay prisms; C: non-linear crystals for frequency converstion; λ/2: halfwave rotator; OPO: optical parametric oscillator; OPA: optical parametric amplifier; DA: dye amplifier; H$_2$: induced Raman cell.

103

Figure 7. Estimated frequency and energy for the picosecond continuously tunable laser. a: OPO of 3ω or 4ω amplified by a dye laser; 2a: second harmonic of a; $2a + \omega$: mixing of 2a and ω; $a\pm\omega$: mixing of a and ω; $a-\omega+4\omega$: mixing of $a-\omega$ and 4ω; b: OPO of ω or 2ω; $b-H_2$: induced Raman scattering by hydrogen gas.

amplifications. A block diagram of the laser system is shown in Figure 6. The visible output will be obtained by OPO of the fourth harmonic $(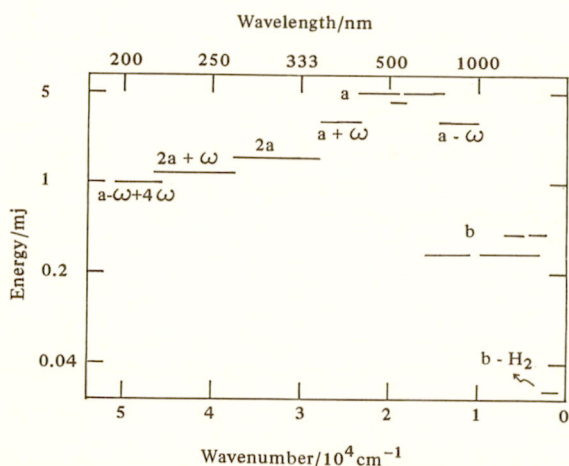4\omega)$ on an **ADP** crystal. A small portion of the output corn is selected and amplified by a second crystal. The spectral purity is improved by a selected amplification. The beam is led to a dye amplifier and ethalon system. The frequency is further converted as shown in Figure 7.

The tunable infra-red light is obtained by OPO of ω on a $LiNbO_3$ crystal and amplified by a second crystal. The tuning of the wavelength is made by tilting the oscillator and amplifier crystals which are controlled by a microcomputer. The beam is introduced to a pressurized hydrogen gas cell. A continuously tunable light up to $\sim 13\ \mu m$ will be obtained by coherent Raman mixing in H_2. Instruments for the spectroscopic studies will be provided.

A sub-picosecond dye laser which is excited by an Ar ion laser will also be planned.

II. Special Research Projects

In April 1975 the newly born Institute has initiated the Special Research Projects. Two projects presently in progress under the first five year plan are:
(1) Investigation of energy conversion processes at the molecular level.
(2) Molecular designing for interesting and useful materials.
The projects are being carried out in close collaboration of research divisions and facilities. Collaborators from outside also make important contributions.
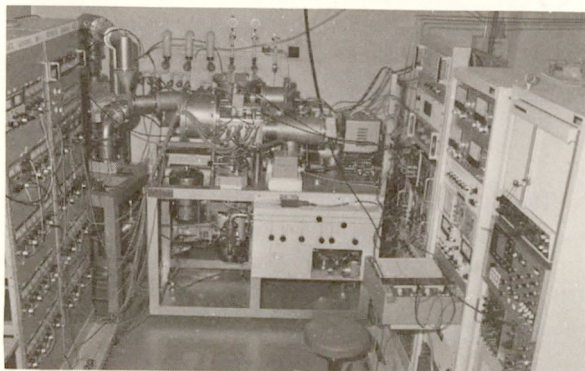
The Threshold Electron-Secondary Ion Coincidence Apparatus (TEPSICO).

Apparatus for Production of Highly Excited Atoms.

Fundamental and applied research of energy conversion is being undertaken by several groups. In the work on *the energy conversion in ion-molecule reactions* (See Research Activities IV - E) the photoionization processes and their application to ion-molecule reactions are investigated by the use of a threshold electron-photon-secondary ion coincidence technique (photo). A group initiated a study on *the structure and reactivity of highly excited molecules and molecular ions* (See II - D, photo). Another group worked on *the energy conversion in chemical reactions of molecules adsorbed on the solid surface* (photo). Photochemical cells which are made of metals or semiconductors coated with a thin organic film have been used for a study of the con-
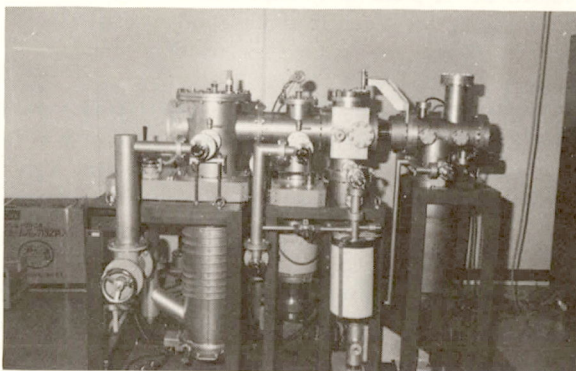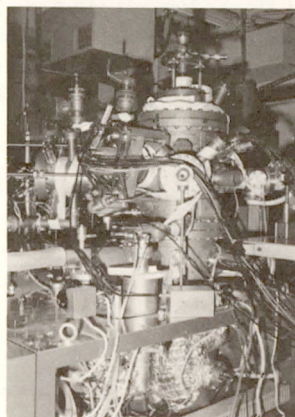
"Koku I", the UHV system for the study of well defined surface reaction.

version of photon energy to the electric energy. A theoretical group in collaborating with the Computer Center has been studying *potential energy surfaces and dynamics of simple elementary reactions* (See I - B).

In the project of the molecular design *the preparation of novel compounds having interesting properties* is in progress (See IV - B). In 1978 a study on *the new synthetic techniques by means of the laser light source* has been initiated. *The study of unstable molecules by the laser magnetic resonance* is also included in their project (See II - A). The theoretical study on *the structure of catalysis and the mechanism of catalytic reactions* uses Xα and molecular orbital methods to investigate the electronic structure of solid surfaces and chemisorbed molecules.

JOINT STUDIES PROGRAM

Study of Hyperfine Interactions in the Solid State Using Optical Excitation Techniques

Coordinators: Hideaki CHIHARA (Osaka Univ.)
Satoru SUGANO (Univ. of Tokyo)
Hiroo INOKUCHI (Division of Molecular Assemblies)

An attempt was made to study the hyperfine interactions in the excited electronic states of molecules in an otherwise inert matrix. Transition from a localized triplet state to an exciton state is expected to manifest itself in the experiments being planned. Optical excitation and magnetic resonance techniques were useful in elucidating the nature of the interactions. (1976–7)

Spectroscopic Studies on Unstable Molecules and Molecular Ions

Coordinators: Eizi HIROTA (Division of Molecular Structure)
Shuji SAITO (Division of Molecular Structure)

The joint research was initiated by discussing what sort of experimental apparatus was to be set up at IMS, to investigate the molecular structures of the transient species. A special emphasis was given to new techniques including the laser-microwave double resonance and the signal averaging by the computer control of spectrometers. A result on an unstable molecule HNO is worth mentioning; K. Takagi (Toyama Univ.) and S. Saito observed the fluorescence spectrum for the first time, by exciting $\tilde{A}^1A'' \leftarrow \tilde{X}^1A'$, the (100) ← (000) and (020) ← (000) bands at 620 nm with a dye laser. They could reduce chemi-luminescence by reacting the O atom with C_2H_4 and then the product (possibly HCO) with NO. (1976–7)

Hydrogen Dissociation Mechanism of Hydrogenase and its Application for Electrode Reaction

Coordinators: Hiroo INOKUCHI (Division of Molecular Assemblies)
Tatsuhiko YAGI (Shizuoka Univ.)
Katsumi NIKI (Yokohama National Univ.)
Kazuo OHNO (Univ. of Tokyo)
Shohei TAMURA (Univ. of Tokyo)

To analyse the hydrogen dissociation mechanism of hydrogenase, we observed its physico-chemical properties, catalytic activities in gaseous and solid states,

spectroscopical and electrochemical behaviors. We found that in cytochrome c_3, four-hemes linked with hydrogenase as an electron carrier showed physical and electrochemical properties unexpected as an molecule and also as an aggregate. In the study of electrode reaction of cytochrome c_3, a large Nernst slop and a broad voltammogram with small peak current suggested that the electrode reaction is a four one-electron process and the hemes in the molecule are nonequivalent and non-interacting. It was understood from the conductivity measurement that the electron transport in this heme compound was very easy at the reduced state. (1976–8)

Tunable Near UV Coherent Light Source

Coordinator: Fujio SHIMIZU (Univ. of Tokyo)

A technique to obtain a stable tunable coherent source in near uv region for high resolution spectroscopy was proposed. Some preliminary experiments were also done. Since it is not possible to obtain such a uv source directly from a tunable laser, the most promising method is to double the frequency of a stabilized dye laser in visible region by a nonlinear crystal. The problem in this technique is that the improvement on the stability reduces the output power of the laser below the required level (over 1W) for the doubling, because the thermal distortion of the active medium tends to lase in multimode. We proposed the optical cavity configuration for the dye laser, in which the laser beam is elliptically focused on the dye jet, thereby increasing the thermal distortion. We also performed experiemnts to improve the stability of the existing dye laser using new ideas in the dye jet system. (1977–8)

Solid State Chemistry of High-Photoconductive Compound: Tetrabenzo[a,cd,j,lm]-perylene (TBP)

Coordinators: Hiroo INOKUCHI (Division of Molecular Assemblies)
Junji AOKI (Toho Univ.)
Satoshi IWASHIMA (Meisei Univ.)

Among the number of aromatic hydrocarbons, tetrabenzo[a,cd,j,lm]-perylene (TBP), a nine benzene-ring compound, has peculiar characters, such as the non-coplanar molecular structure, a high-photoconductive response, and also a quick crystal-growth from the amorphous film at the room temperature. To study these characters extensively, a large amount of this hydrocarbon was synthesized from benzanthrone by

means of the alkali fusion method. To purify this hydrocarbon, we applied several methods including chromatography, the complex formation with alkali metal and also the treatment with maleic anhydride. After these treatments, about 30 g of TBP having very high-purity was prepared. Now, we are trying to make its single crystals with a size large enough for photo-conduction measurements. (1977—8)

Theory of Chemisorption on Solid Surfaces

Coordinators: Masaru TSUKADA (Division of Theoretical Studies)
Junjiro KANAMORI (Osaka Univ.)
Satoru SUGANO (Univ. of Tokyo)

The molecular orbital calculation of atomic clusters of moderate size is one of practical approaches to investigate the electronic structure of solid surfaces and the mechanism of chemisorption. The Hartree-Fock-Slater approximation utilizing the so-called $X\alpha$ potential provides us a powerful, reliable and nevertheless economical method to obtain the molecular orbitals of the cluster.

In this joint study, we performed an extension of the discrete-variational (DV)-$X\alpha$ method to the clusters on the surface of ionic crystals and metallic oxides. The essential point of the extension is the inclusion of the long-range Coulomb potential from the exterior of the cluster by the model of the uniformly charged ion spheres. A part of the results obtained by the method is reported in the section I-F in "Research Activities". (1977—8)

Synthesis of a New Chiral Phosphine Ligand and its Use for Stereoselective Organic Reactions

Coordinators: Hidemasa TAKAYA (Chemical Materials Center)
Ryoji NOYORI (Nagoya Univ.)
Yoshihiro HAYAKAWA (Nagoya Univ.)
Masaru YAMAKAWA (Nagoya Univ.)

Optically active 2,2'-Bis(diphenylphosphino)-1,1'-binaphthyl (BINAP), a new chiral bidentate phosphine ligand, was prepared. Racemic BINAP was first synthesized and then resolved by use of chiral palladium complex. Asymmetric hydrogenations of α-acylamino-acrylic acids were carried out in the presence of $[Rh(binap) (nbd)]^+ClO_4^-$ and optical yields up to 83% ee were attained. The correlation between the catalyst structure and the configuration of the products was discussed. For the details of the results, see section IX-A in "Research Activities". (1977—8)

A Theoretical Approach to the Dynamical Reaction Path

Coordinators: Tokio YAMABE (Kyoto Univ.)
Hiroshi FUJIMOTO (Kyoto Univ.)
Tsutomu MINATO (Kyoto Univ.)
Keiji MOROKUMA (Division of Theoretical Studies)
Shigeki KATO (Division of Theoretical Studies)

The energy gradient technique to locate the equilibrium and the transition states on the multi-dimensional potential surface was employed to CH_3CH_2F molecule. Reasonable vibrational structures and the geometry of the transition state were obtained for the fragmentation of HF from CH_3CH_2F. The same method was used for geometry optimization of the various types of the protonated thioformaldehyde. It is proposed that the C-protonated complex H_3CS^+ may be the most stable form. An energy decomposition analysis is carried out to elucidate the origin of this behavior of the C=S group. (1977—8)

Study of Electronic Correlation in Molecules with Newer Mathematical Techniques

Coordinators: Haruo HOSOYA (Ochanomizu Univ. and IMS)
Suehiro IWATA (Institute of Physical and Chemical Research)
Shigeyuki AONO (Kanazawa Univ.)
Hideo FUKUTOME (Kyoto Univ.)
Kichisuke NISHIMOTO (Osaka City Univ.)
Taiichi SHIBUYA (Shinshu Univ.)

In order to clarify the nature of the electronic correlation in the molecules, large or small, the mathematical structures of several newer techniques were reviewed, criticized, and discussed in detail.

Fukutome has developed a general theory of the collective motions of the Fermions in molecules based on the Lie algebra, in which the conventional electronic theories including the Hartree-Fock method and random phase approximations are included as special cases. Minoru Takahashi (College of General Education, Osaka Univ.) has developed the method for solving rigorously the two-dimensional Hubbard model. Iwata has studied the lowest electronic state of ethylene molecule skewed by 90 degrees by analyzing the model Hamiltonian and its eigenvalues and concluded that the above-mentioned state is a singlet contrary to the generally accepted assignment. (1977—8)

Future Plan for Time-Dependent Theories

Coordinators: Katsunori HIZIKATA (Univ. of Electro-Communications and IMS)
Keiji MOROKUMA (Division of Theoretical Studies)

We held a discussion meeting on the plan and discussed the following.

1) Non-perturbational Treatment of Time Dependent Problems.

The ordinary approach to the time dependent problem is to treat the time dependent part of the Hamiltonian as a perturbation. Search must be made, however, for the cases where exact time-dependent solutions might be possible and we can still extract a useful information for real systems.

Other topics discussed include

2) Non-adiabatic Processes in Chemical Reactions, and
3) Dynamical Processes in Laser Field.
   (1977—8)

OKAZAKI CONFERENCES

IMS conducts research conferences, called Okazaki conferences, on subjects related to the special research projects. mentioned before. These conferences are held usually two times a year with a moderate number of participants, around 40, including several invited foreign speakers. During a typical conference, ten or more talks and discussions, a reception, and a dinner party are scheduled.

In the past three years six Okazaki Conferences have already been held successfully. Outlines of these conferences are as follows.

The First Okazaki Conference

Photo-electrode Process
(January 14–16, 1976)

Organizer: H. Tsubomura *(Osaka Univ.)*
Invited Speakers: H. Gerischer *(Fritz-Haber Inst. and IMS)* and A. J. Bard *(Univ. of Texas)*

The photoelectrochemical method has been gaining in popularity as one of the most promising and attractive methods for the solar energy conversion, although it will need much effort for more than several decades before it becomes practical. The goal of this meeting was to throw light on the most important problems in this interdisciplinary field. Participants from various fields such as electrochemistry, molecular spectroscopy, semiconductor physics, and molecular biology made efforts to get a common basis for understanding through the discussion on the current topics such as the photovoltaic effect of semiconductor electrodes, the photogalvanic effect, the chlorophyll electrode, and the energy conversion by bilayer membranes.

The Second Okazaki Conference

Theoretical Chemistry, as the Foundation of Molecular Designing
(February 15–18, 1976)

Organizers: K. Hijikata *(Univ. of Electro-Communications and IMS)*, H. Hosoya *(Ochanomizu Univ.)*, S. Iwata *(Inst. of Phys. and Chem. Research)*, K. Kuchitsu *(Univ. of Tokyo)*, and K. Yoshihara *(IMS)*
Invited Speakers: P. W. Atkins *(Oxford Univ.)*, P. S. Bagus *(IBM Research Lab., San Jose)*, and C. Moser *(CECAM, Paris)*

In this conference Dr. Bagus talked on the recent results of his ab initio calculations: (i) X-ray photoelectron spectra of diatomic molecules, (ii) $Fe(C_5H_5)_2$ and its ion, (iii) molecular negative ions of CO_2, CS_2, etc., (iv) force constants in CH, OH, HCN, C_6H_6, etc., (v) chemisorption of an H-atom on a Be (001) surface. Through his works we understood the present status

of computer techniques and of computational chemistry.

Dr. Atkins gave a lecture on "Non-computational Quantum Chemistry", where he developed the conceptional structure of the whole field of theoretical chemistry we are facing to. His lecture was published as "IMS Leaflet No. 3".

After the introduction of a few important studies of Japanese participants, we spent a day and half for the free discussion on the future of theoretical chemistry and on our expectations for IMS. Aided by the guests' sensible humours, the sessions were greatly fruitful and pleasant. Our anticipation in the conference are being realized in the present activities of theoretical groups in IMS.

The Third Okazaki Conference

Molecular Freedom of Motion in Molecular Crystals
(December 5–8, 1976)

Organizers: H. Inokuchi *(IMS)* and H. Chihara *(Osaka Univ. and IMS)*
Invited Speakers: J. G. Powles *(Univ. of Kent)* and C. H. Wang *(Univ. of Utah and IMS)*

The Conference was designed to put together the research scientists in molecular dynamics in solids who work by using different experimental and theoretical approaches, thereby providing an effective interface for a common understanding of the status of the problem. This was because such understanding was believed necessary for developing research toward material design for interesting and useful physical and chemical properties.

Every presentation aroused heated discussions, centered on what is being looked at by a particular approach and on how to integrate the information gained by different approaches. The success of the meeting depended on the facts that most people talked about simple, fundamental substances and that speakers had a good understanding of the objectives of the Conference.

The Fourth Okazaki Conference

Resonance and Non-linear Raman Scattering
(January 18–20, 1977)

Organizers: E. Hirota *(IMS)*, M. Ito *(Tohoku Univ.)*, M. Tasumi *(Univ. of Tokyo)*, A. Y. Hirakawa *(Univ. of Tokyo)*, and M. Tsuboi *(Univ. of Tokyo)*
Invited Speakers: T. G. Spiro *(Princeton Univ.)*, F. A. Miller *(Univ. of Pittsburg)*, and W. Siebrand *(NRC, Ottawa and IMS)*

Raman scattering intensity depends not only on the frequency of the scattered light, but also on the frequency of the exciting light. When the exciting frequency is close to a vibronic transition frequency, the intensities of some of the Raman lines are enormously enhanced. Which lines? How strong are they? What are the mechanisms? These were the subjects of this conference.

Concentric discussions were made (1) on the mechanism of the appearance of antisymmetric elements in the Raman scattering tensor for metalloporphyrins and some other materials, (2) on the vibronic wavefunctions of states involved in a vibronic interaction, (3) on the damping constant which is required to keep the frequency denominator finite (not zero) in the expression of the Raman scattering factor, and (4) on the experiment of coherent anti-Stokes Raman scattering.
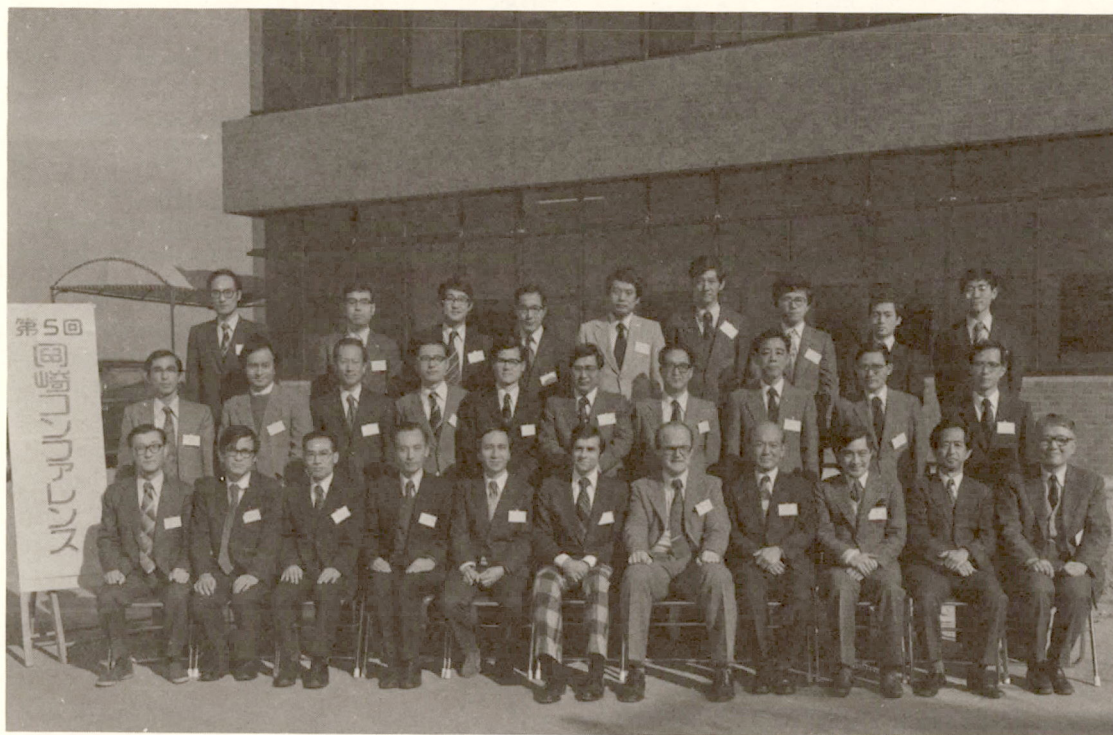
The Fifth Okazaki Conference

Higher Excited States of Molecules and Molecular Crystals
(December 4–7, 1977)

Organizers: J. Tanaka *(Nagoya Univ. and IMS)* and H. Inokuchi *(IMS)*
Invited Speakers: E. E. Koch *(DESY, Hamburg)*, M. Inokuti *(Argonne National Lab.)*, and G. E. Leroi *(Michigan State Univ.)*

As the title implies, the conference was intended to cover a wide range of subjects related to higher excited state physics and chemistry, regardless of whether the system concerned is a free molecule or a molecular assembly. An emphasis was placed on the studies using synchrotron radiation, as exemplified by the invited talk by Dr. Koch who presented extensive studies of vacuum ultraviolet spectroscopy and photoelectron spectroscopy at DESY. Studies using INS-SOR constituted another main topic, covering vacuum ultraviolet spectroscopy of both gases and condensed matter. Productions and subsequent dynamical behavior of highly excited states in the gas phase were also subjects of intensive discussion. The dynamical processes discussed include optical emission, unimolecular decomposition, autoionization, and several collisional processes, both electron and photon impact being used in such studies. Roles of higher excited states of molecules in radiation physics and chemistry were reviewed by Dr. Inokuti in another invited talk and were also discussed extensively.

The 5th Okazaki Conference 4–7/12/1977

The Sixth Okazaki Conference

Photoelectric Phenomena in Organic Solids
(February 13–15, 1978)

Organizers: M. Sano *(Univ. of Electro-Communications)*
and H. Inokuchi *(IMS)*
Invited Speakers: F. Willig *(Fritz-Haber Inst. and IMS)*
and L. B. Schein *(Xerox Co.)*

In this Conference, the fundamental electronic properties of photoconductive organic solids were discussed in relation to the mechanisms for charge carrier generation, carrier transport, and carrier-exciton interaction.

The contents discussed in the conference include the following. The carriers generated in the region of contact between a solid and an electrode were reported to move around about several hundreds Å two-dimensionally in parallel to the solid surface before they escaped into the solid interior.

The electron mobility in the c' direction of a naphthalene single crystal was found to be nearly independent of temperature in the region between 324 and 150 K, and to increase rapidly with decreasing temperature below 100 K. The temperature-independent mobility was interpreted in terms of the small polaron conduction under the condition that the energies for contributing lattice vibrations were much smaller than the total conduction-band width.

Long-chain hydrocarbons, *o*-terphenyl, perylene-TCNQ, anthracene-TCPA, $[(C_6H_5)_3PCH_3]^+_{1-x}$ $[(C_6H_5)_3AsCH_3]^+_x$ $(TCNQ)^-_2$ crystals, PVK-acceptor systems, and fatty acid salt monolayer films were found to be promising materials for the understanding of photoelectric phenomena in the organic solids.

RESEARCH SYMPOSIA

Future Patterns of Research Organization in Chemistry
May 18th, 1976 and Oct. 25th, 1976

> Organizer: Hiroo INOKUCHI (Division of Molecular Assemblies)

Structures and Characterization of TCNQ Complexes
July 7th–9th, 1976

> Organizers: Jiro TANAKA (Nagoya Univ.)
> Hiroo INOKUCHI (Division of Molecular Assemblies)

Activity of Technical Groups in Research Institution
July 20th, 1976 and Dec. 24th, 1976

> Organizers: Hiroo INOKUCHI (Division of Molecular Assemblies)
> Shigetoshi TAKAHASHI (Technical Department)

Laser Induced Chemical Reactions
Dec. 17th–18th, 1976

> Organizer: Soji TSUCHIYA (Univ. of Tokyo)

Generation and Application of Picosecond Pulses
Dec. 18th–19th, 1976

> Organizer: Keitaro YOSHIHARA (Division of Electronic Structure)

Stereochemistry of Coordination Compounds
Dec. 20th–22th, 1976

> Organizer: Hideo YAMATERA (Nagoya Univ.)

The Role of Applied Molecular Science in Basic Organic Chemistry
Jan. 30th–Feb. 1st, 1977

> Organizer: Hideki SAKURAI (Tohoku Univ.)

Studies on the Primary Reactions of Photosynthesis
Feb. 7th–8th, 1977

> Organizer: Sigehiro MORITA (Univ. of Tokyo)

Dynamical Processes in Excited Electronic States
Feb. 21th–22th, 1977

> Organizer: Eizi HIROTA (Division of Molecular Structure)

Continuum Light Sources of Extreme Ultra-violet Wavelength Region
Mar. 10th–11th, 1977

> Organizers: Inosuke KOYANO (Division of Molecular Assemblies)
> Hiroo INOKUCHI (Division of Molecular Assemblies)

Formations and Reactions of Highly Excited Atoms and Molecules
Mar. 25th—26th, 1977

Organizer: Kozo KUCHITSU (Univ. of Tokyo)

The Way to Interesting and Useful Novel Materials
July 15th—16th, 1977

Organizers: Koichi KOBAYASHI (Univ. of Tokyo)
Seiichi TANUMA (Univ. of Tokyo)
Hiroo INOKUCHI (Division of Molecular Assemblies)

Chemical Utilization of Solar Energy
Sept. 26th—27th, 1977

Organizer: Katsumi TOKUMARU (Univ. of Tsukuba)

Distribution of d-Electrons in Ionic Crystals and Transition-Metal Complexes
Nov. 11th—12th, 1977

Organizer: Fumiyuki MARUMO (Tokyo Institute of Technology)

High Resolution Spectroscopy of Free Radicals and Molecular Ions
Nov. 25th, 1977

Organizer: Eizi HIROTA (Division of Molecular Structure)

Topics in Applied Molecular Science and Dynamic Organic Chemistry
Jan. 19th—20th, 1978

Organizer: Aritsune KAJI (Kyoto Univ.)

Charge Transport Mechanism in Organic Solids
Feb. 3rd—4th, 1978

Organizers: Yusei MARUYAMA (Ochanomizu Univ.)
Hiroo INOKUCHI (Division of Molecular Assemblies)

What Can Be Done in Molecular Science with the Continuum Light Source of Extreme Ultra-violet
Wavelength Region?
Mar. 6th—7th, 1978

Organizers: Hiroo INOKUCHI (Division of Molecular Assemblies)
Inosuke KOYANO (Division of Molecular Assemblies)

Large Scale Calculations for Electronic States of Atoms and Molecules
Mar. 10th—11th, 1978

Organizer: Keiji MOROKUMA (Division of Theoretical Studies)

The Intercalation Compounds of Graphite — Their Solid State Physics and Chemistry
Mar. 16th, 1978

Organizer: Ikuji TSUJIKAWA (Kyoto Univ. and IMS)
Hiroo INOKUCHI (Division of Molecular Assemblies)

FOREIGN SCHOLARS

Visitors from abroad play an essential role in research activities and always welcome at IMS. The following is the list of foreign scientists who have visited IMS by the end of July 1978. The sign * indicates a visitor invited to attend an Okazaki Conference and † indicates a visitor on the Invited Foreign Scholars Program.

Prof. E. C. Lim†	Wayne State Univ.	(USA)	Aug.–Oct. 1975
Prof. H. Gerischer	Fritz-Haber Inst.	(Germany)	Jan. 1976
Prof. A. J. Bard*	Univ. of Texas	(USA)	Jan. 1976
Prof. J. O'M. Bockris	Finders Univ.	(Australia)	Jan. 1976
Dr. P. W. Atkins*	Oxford Univ.	(UK)	Feb. 1976
Dr. P. S. Bagus*	IBM	(USA)	Feb. 1976
Dr. C. Moser	CECAM	(France)	Feb. 1976
Dr. G. Herzberg	NRC	(Canada)	Mar. 1976
Prof. S. H. Bauer	Cornell Univ.	(USA)	Mar. 1976
Prof. J. I. Steinfeld	MIT	(USA)	Mar. 1976
Prof. J. G. Powles*	Univ. of Kent	(UK)	Dec. 1976
Dr. M. Inokuti	ANL	(USA)	Dec. 1976, Dec. 1977
Dr. W. Siebrand†	NRC	(Canada)	Dec. 1976 – Mar. 1977
Prof. C. H. Wang†	Univ. of Utah	(USA)	Dec. 1976 – Mar. 1977
Prof. T. G. Spiro*	Princeton Univ.	(USA)	Jan. 1977
Prof. F. A. Miller	Univ. of Pittsburg	(USA)	Jan. 1977
Dr. J. M. Morris†	Univ. of Melborne	(Australia)	Feb.–May 1977
Prof. R. F. Curl†	Rice Univ.	(USA)	May–Aug. 1977
Prof. T. Kuwana	Ohio State Univ.	(USA)	July 1977
Prof. J. B. Donnet	Univ. der Haut-Phin	(France)	Aug. 1977
Prof. G. Porter	Royal Inst.	(UK)	Sept. 1977
Prof. C. A. McDowell	Univ. of British Columbia	(Canada)	Sept. 1977
Prof. R. D. Brown	Manash Univ.	(Australia)	Sept. 1977
Dr. T. Oka	NRC	(Canada)	Sept. 1977

Professor Mulliken visited IMS (April, 1978).

Prof. W. Klemperer	Harvard Univ.	(USA)	Sept. 1977
Dr. H. Seki	IBM	(USA)	Sept. 1977
Dr. K. K. Kanazawa	IBM	(USA)	Sept. 1977
Dr. R. Zahradnik	Academy of Science	(Czechoslovakia)	Nov.–Dec. 1977
Prof. E. E. Koch*	DESY	(Germany)	Dec. 1977
Prof. G. E. Leroi	Michigan State Univ.	(USA)	Dec. 1977
Dr. F. Willig†	Fritz-Haber Inst.	(Germany)	Dec. 1977 – Mar. 1978
Dr. L. B. Schein*	Xerox	(USA)	Feb. 1978
Prof. J. Sheridan	Univ. of North Wales	(UK)	Mar. 1978
Dr. H. Tributsch†	Fritz-Haber Inst.	(Germany)	Mar.–June 1978
Dr. K. H. Grellmann	Max-Planck Inst.	(Germany)	Mar. 1978
Prof. R. S. Mulliken	Univ. of Chicago	(USA)	Apr. 1978
Dr. B. M. Rode	Univ. of Innsbruck	(Austria)	Apr. 1978
Dr. I. Botskor	Ulm Univ.	(Germany)	Apr. 1978
Prof. A. J. Yencha	State Univ. of New York	(USA)	May 1978
Prof. J. E. Boggs	Univ. of Texas	(USA)	May 1978
Prof. A. J. Heeger	Pennsylvania State Univ.	(USA)	May 1978
Prof. J. C. Baird†	Brown Univ.	(USA)	May–Oct. 1978
Dr. V. K. Kaushik	Indian Inst. of Tech.	(India)	May 1978
Prof. R. A. Caldwell	Univ. of Texas	(USA)	June 1978
Prof. D. H. Busch	Ohio State Univ.	(USA)	June 1978
Dr. W. A. Kreiner†	Ulm Univ.	(Germany)	July–Sept. 1978
Dr. J. T. Hougen	NBS	(USA)	July 1978 – Feb. 1979
Dr. M. Lücke	Tech. Univ. Munich	(Germany)	July 1978
Prof. B. C. Eu	McGill Univ.	(Canada)	July 1978

AWARDS

Prof. Hiroo Inokuchi received the Award of the Chemical Society of Japan in the spring meeting (1978) of the Society for his contribution to

"Studies on Solid State Chemistry of Aromatic Compounds".

Prof. Inokuchi's Scientific Achievement:

Establishment of Research Field of Organic Semiconductors. In 1950, Prof. H. Inokuchi found with Prof. H. Akamatu that violanthrone and its related organic solids possess a feeble electrical conduction, $10^{-9}-10^{-12}\mho$cm, with a positive temperature dependence. This finding was the first step for the establishment of a novel category of organic materials, organic semiconductros.

Finding of High Electrical Conduction of Charge-Transfer Complexes. In 1954, he also found with Professors Akamatu and Y. Matsunaga that the complexes between perylene and bromine have a very high electrical conduction, about $10^{-1}\mho$ cm. This was one of the first reports on the high conductivity measurement of charge-transfer complexes.

Observation of Photoemission from Organic Solid. He applied the photoelectron spectroscopical method to organic solids with his collaborators and observed the accurate values of their ionization potentials, work functions, energy gaps of band structure, polarization energies and also their electron depths. These studies have accelerated the analysis of the mechanism of electrical conduction in organic solids.

Measurement of Hydrogen Dissociation Activity of Charge Transfer Complexes and Preparation of Biocell. He found a hydrogen dissociation character on aromatics-alkali metal charge transfer complexes. Further, he and his co-workers prepared a bio-cell using a hydrogen dissociative enzyme, hydrogenase.

The 1978 Award of The International Academy of Quantum Molecular Science has been given to Prof. Keiji Morokuma for his contributions in the field of

"Excited States, Reaction Paths and Intermolecular Interactions".

Prof. Morokuma's Scientific Achievement:

Prof. Morokuma has made contributions in many fields of quantum chemistry. Those include the theory of rotational barrier, the electronic structure of polymers, theories of hyperfine coupling in free radicals, potential energy surfaces for chemical reactions including T+CH$_4$ and photodissociation of H$_2$CO. He has also published on the relationship between classical collision dynamics and the transition state theory, and on the semiclassical collision theory of electronic transitions.

He made an interesting contribution in the development of the molecular orbital theory in the complex plane of nuclear coordinates. He established the theoretical basis for the analytic continuation and subsequently calculated the potential energy surfaces in the complex plane for several reactive and non-reactive systems.

Prof. Morokuma's most important contribution is his studies of molecular interactions in the ground and excited states. He was the first to carry out an ab initio calculation for the water dimer, predicting an essentially correct geometry. By introducing a clearly defined energy decomposition scheme, he assessed contributions of energy components and explained the origins of various molecular complexes, including the hydrogen bonding, the electron donor-acceptor complexes, the protonation complex as well as the reaction intermediates and activated complexes.

He has recently led the use of the ab initio energy gradient technique to locate the transition state and the reaction coordinate for chemical reactions. The energy and force components along the reaction coordinate have also been analyzed for better understanding of the electronic basis of chemical reactions.

LIST OF PUBLICATIONS

Division of Theoretical Studies

1. K. MOROKUMA, "Why Do Molecules Interact?- - - The Origin of Electron Donor-Acceptor Interaction, Hydrogen Bonding and Proton Affinity", *Acc. Chem. Res.*, 10, 294 (1977).
2. J. O. NOELL and K. MOROKUMA, "The Hydrated Electron as Studied by the Fractional Charge MO Model", *J. Phys. Chem.*, 81, 2295 (1977).
3. B. D. JOSHI and K. MOROKUMA, "Force Decomposition Analysis along Reaction Coordinate", *J. Chem. Phys.*, 67, 4880 (1977).
4. S. NAGASE and K. MOROKUMA, "An ab initio MO Study of Organic Reactions. The Energy, Charge and Spin Decomposition Analyses at the Transition State and along the Reaction Pathway", *J. Am. Chem. Soc.*, 100, 1666 (1978).
5. S. NAGASE and K. MOROKUMA, "The Relative Stability of Planar and Perpendicular Olefins", *J. Am. Chem. Soc.*, 100, 1661 (1978).
6. M. TSUKADA, "Two-dimensional Wigner Crystal in MOS Structures under Strong Magnetic Field", Proc. 7th *Intern. Vac. Congr. & 3rd Intern. Conf. Solid Surfaces* (Vienna 1977).
7. H. ADACHI, S. IMOTO, T. TANABE and M. TSUKADA, "Cluster Calculations of the Electronic Structure of Interstitial Hydrogen in Titanium, Nickel and Palladium", *J. Phys. Soc. Japan*, 44, 1039 (1977).
8. M. TSUKADA, C. SATOKO and H. ADACHI, "Surface Electronic Structure of TiO_2 by the DV-Xα Cluster Calculation", *J. Phys. Soc. Japan*, 44, 1043 (1977).
9. A. MOTOYAMA and H. HOSOYA, "King and Domino Polynomials for Polyomino Graphs", *J. Math. Phys.*, 18, 1485 (1977).

Division of Molecular Structure

1. E. HIROTA, K. MATSUMURA, M. IMACHI, M. FUJIO, Y. TSUNO, and C. MATSUMURA, "Microwave Spectra of $^{13}CH_3{}^{12}CD_3$ and $^{12}CH_3{}^{13}CD_3$ and the C-C Bond Length of Ethane", *J. Chem. Phys.*, 66, 2660 (1977).
2. T. AMANO and E. HIROTA, "Microwave Spectrum of ^{35}ClO in the Excited Vibrational State and a Comment on the Centrifugal Distortion Constants", *J. Mol. Spectrosc.*, 66, 185 (1977).
3. R. F. CURL, Y. ENDO, M. KAKIMOTO, S. SAITO, and E. HIROTA, "Hyperfine Structure in the $\tilde{A}$ State of PH_2 Arising from the Fermi Interaction of ^{31}P", *Chem. Phys. Lett.*, 53, 536 (1978).
4. E. HIROTA, "Microwave Spectrum of Methylene Fluoride in Excited Vibrational States", *J. Mol. Spectrosc.*, 69, 409 (1978).

Review Articles and Textbooks

1. S. SAITO, "Laser Spectroscopy", *Kagaku* (in Japanese), 31, 692 (1976).
2. S. SAITO, "Recent Topics of Interstellar Molecules-Observations of Free Radicals and Molecular Ions", *Kagaku no Ryoiki* (in Japanese), 30, 1128 (1976).
3. E. HIROTA, "Potentials for Internal Rotation Measured by Rotational Spectroscopy", *Kagaku Sosetsu* (in Japanese), 10, 182 (1976).
4. E. HIROTA and C. MATSUMURA, "Generation and Utilization of Microwave", *Shinjikkenkagakukoza* (in Japanese), 5, Maruzen.
5. E. HIROTA, "Laser Chemistry of Free Radicals", *Kagaku* (in Japanese), 32, 66 (1977).
6. E. HIROTA, "Microwave Spectroscopy (as an Analytical Tool)", *Kagaku Kyoiku* (in Japanese), 25, 455 (1977).
7. E. HIROTA, "Laser Chemistry and Laser Spectroscopy", *Kagaku* (in Japanese), 33, 66 (1978).
8. S. SAITO, "Chemical Analysis by Microwave Spectroscopy", *Bunseki* (in Japanese), 1978, 246.
9. E. HIROTA, "Molecular Structure Determination", *Shinjikkenkagakukoza* (in Japanese), 17, Maruzen.

Division of Electronic Structure

1. M. SUMITANI, N. NAKASHIMA, K. YOSHIHARA and S. NAGAKURA, "Temperature Dependence of Fluorescence Lifetime of Trans-stilbene", *Chem. Phys. Lett.,* **51**, 183 (1977).
2. T. KAWAI, K. TANIMURA and T. SAKATA, "Mechanism of Photocurrent Generation at Zinc-Tetraphenyl-porphine/Metal Electrode", *Chem. Phys. Lett.,* **56**, 541 (1973).
3. A. NAMIKI, N. NAKASHIMA, K. YOSHIHARA, Y. ITO and T. HIGASHIMURA, "Transfer of Solvated Electrons to Some Aliphatic Halides in Ethanol at 77K; The Role of Franck-Condon Factors", *J. Phys. Chem.,* **82**, 1901 (1978).
4. N. NAKASHIMA, A. NAMIKI and K. YOSHIHARA, "Electron Transfer Distances Obtained by Picosecond Study of Fluorescence Dynamic Quenching", *J. Photochem.,* **9**, 230 (1078).

Review Articles and Textbooks

1. T. SAKATA, "Photoelectrochemistry and Energy Conversion", *Solid State Physics* (in Japanese), **12**, 779 (1977).

Division of Molecular Assemblies

1. T. YAGI, K. KIMURA, H. DAIDOJI, F. SAKAI, S. TAMURA, and INOKUCHI, "Properties of Purified Hydrogenase from the Particulate Fraction of Desulfovibrio vulgaris, Miyazaki", *J. Biochim.,* **79**, 661 (1976).
2. Y. NAKAHARA, K. KIMURA, and H. INOKUCHI, "Electrical Conductivity of Cytochrome *c* Anhydrous Film", *Chem. Phys. Letts.,* **47**, 251 (1977).
3. K. NIKI, R. YAGI, H. INOKUCHI, and K. KIMURA, "Electrode Reaction of Cytochrome c_3 of Desulfovibrio vulgaris, Miyazaki", *J. Electrochem. Soc.,* **124**, 1889 (1977).
4. K. SEKI, S. HASHIMOTO, N. SATO, Y. HARADA, K. ISHII, H. INOKUCHI, and J. KANBE, "Vacuum-ultraviolet photoelectron spectroscopy of hexatriacontane (n-$C_{36}H_{74}$) polycrystal: a model compound of polyethylene", *J. Chem. Phys.,* **66**, 3644 (1977).
5. S. HINO, N. SATO, and H. INOKUCHI, "Electron Escape Depths of Organic Solids", *J. Chem. Phys.,* **67**, 4139 (1977).
6. A. HASHIMOTO, K. SEKI, N. SATO, S. HINO, and H. INOKUCHI, "Anisotropic Photoemission from Oriented Polyethylene Film", *Rep. Progr. Polym. Phys. Jpn.,* **20**, 437 (1977).
7. S. HASHIMOTO, K. SEKI, N. SATO, and H. INOKUCHI, "Tailing of Photoemission from Polyethylene", *Rep. Progr. Polym. Phys. Jpn.,* **20**, 441 (1977).

Review Articles and Textbooks

1. H. INOKUCHI and K. SEKI, "Photoelectric Emission from Organic Solids", *Kagaku* (in Japanese), **31**, 635 (1976).
2. H. INOKUCHI, K. SEKI, S. HINO, and Y. HARADA, "The Photoelectron Spectroscopy of Ortanic Semi-conductors", *Kagaku no Ryoiki* (in Japanese), **31**, 495 (1977).

Chemical Materials Center

1. H. TAKAYA, M. YAMAKAWA, and R. NOYORI, "Nickel(0) Catalyzed Reaction of Bicyclo[1.1.0]butanes with Electron-Deficient Olefins", Fundamental Research in Homogeneous Catalysis, Vol. 2, M. Tsutsui and Y. Ishii Ed., Plenum Publishing Co. (1978), pp. 221–240.

Review Articles and Textbooks

1. H. TAKAYA and R. NOYORI, "Recent Progress in Organic Synthesis Using Iron Carbonyl Complexes", *J. Syn. Org. Chem. Jpn.* (in Japanese), **35**, 615 (1977).